Respiratory immunisation and mucosal immunity against influenza

Veronica Martini

Wolfson College

Thesis submitted for the degree of

Doctor of Philosophy in Interdisciplinary Bioscience BBSRC DTP

Supervisors:

Dr. Elma Tchilian

Professor Alain Townsend

Dr. Ronan MacLoughlin

Professor Alexander Drakesmith

Professor Simon Graham

Declaration of authorship

I declare that the work described in this thesis is my own, except where indicated below. Contributions by others are also acknowledged in the text and figure legends, where appropriate.

- Elma Tchilian, Alain Townsend and Ronan MacLoughlin helped with the research strategy for this project, providing guidance and supervision.

- Elma Tchilian and Mick Bailey conceived the influenza time course experiment held at the University of Bristol and Matthew Edmans and Adam McNee harvested the tissues.

- Matthew Edmans and Basu Paudyal designed the nucleoprotein peptide screening while Garry Dolton, Theo Morin and Andrew Sewell produced SLA-peptide monomers.

- Simon Gubbins contributed to the mathematical modelling and statistical analysis of influenza time-course experiments.

- Chris Chui and Katy Moffat offered support during the sorting experiment.

- Edinburgh Genomics performed cDNA library preparation and sequencing for the RNA sequencing experiment while Siddharth Jayaraman contributed to the bioinformatic analysis of the data.

- Ronan MacLoughlin supervised the *in vitro* aerosol characterization and helped, together with Michael Hinchcliffe, in the design of the scintigraphy study.

- Michael Hinchcliffe and Elaine Blackshaw contributed to the image analysis of the scintigraphy study.

- Alain Townsend conceived S-FLU and CLEARFLU vaccines, Holly Sadler characterised *in vitro* CLEARFLU and tested it in mice with the help of Pramila Rijal and Jack Tan.

- Matthew Edmans, Basu Paudyal, Adam McNee, Tiphany Chrun, Emmanuel Maze, Eleni Vatzia, Barbara Holzer and Sophie Morgan assisted with tissue processing during animal experiments.

The work presented in this thesis has been reproduced in part in the following scientific papers:

1. **Martini V.**, Edmans M., Gubbins S., Jayaraman S., Paudyal B., Morgan S., McNee A., Morin T., Rijal P., Gerner W., Sewell A. K., Inoue R., Bailey M., Connelley T., Charleston B., Townsend A., Beverley P. & Tchilian E. "Spatial, temporal and molecular dynamics of swine influenza virus-specific CD8 tissue resident memory T cells." bioRxiv (2021) https://doi.org/10.1101/2021.08.23.457377
2. **Martini, V.**, Paudyal, B., Chrun, T., McNee, A., Edmans, M., Atangana Maze, E., Clark, B., Nunez, A., Dolton, G., Sewell, A., Beverley, P., MacLoughlin, R., Townsend, A., & Tchilian, E. "Simultaneous Aerosol and Intramuscular Immunization with Influenza Vaccine Induces Powerful Protective Local T Cell and Systemic Antibody Immune Responses in Pigs." Journal of immunology (2021), 206(3), 652–663. https://doi.org/10.4049/jimmunol.2001086
3. **Martini, V.**, Hinchcliffe, M., Blackshaw, E., Joyce, M., McNee, A., Beverley, P., Townsend, A., MacLoughlin, R., & Tchilian, E. "Distribution of Droplets and Immune Responses After Aerosol and Intra-Nasal Delivery of Influenza Virus to the Respiratory Tract of Pigs." Frontiers in immunology (2020), 11, 594470. https://doi.org/10.3389/fimmu.2020.594470

I have also contributed to the following publications:

1. Vatzia, E., Allen, T., Manjegowda T., Morris S., McNee A., **Martini V.**, Kaliath R., Ulaszewska M., Boyd A., Paudyal B., Carr V., Chrun T., Maze E., MacLoughlin R., van Diemen P., Everett H., Lambe T., Gilbert S., & Tchilian E. "Respiratory and intramuscular immunization with

ChAdOx2 NPM1-NA induces distinct immune responses in H1N1pdm09 pre-exposed pigs." Research Square (2021) https://doi.org/10.21203/rs.3.rs-789957/v1

2. Chrun T., Maze E., Vatzia E., **Martini V.**, Paudyal B., Edmans M., McNee A., Manjegowda T., Salguero F., Wanasen N., Koonpaew S., Graham S. & Tchilian E. "Simultaneous infection with porcine reproductive and respiratory syndrome and influenza viruses abrogates clinical protection induced by live attenuated porcine reproductive and respiratory syndrome vaccination." bioRxiv (2021) https://doi.org/10.1101/2021.08.12.456007
3. Tan T.*, Rijal P.*, Rahikainen R., Keeble A.,Schimanski L., Hussain S., Harvey R., Hayes J., Edwards J., McLean R., **Martini V.**, Pedrera M., Thakur N., Conceicao C., Dietrich I., Shelton H., Ludi A., Wilsden G., Browning C., Zagrajek A., Bialy D., Bhat S., Stevenson-Leggett P., Hollinghurst P., Tully M., Moffat K., Chiu C., Waters R., Gray A., Azhar M., Mioulet V., Newman J., Asfor A., Burman A., Crossley S., Hammond J., Tchilian E., Charleston B., Bailey D., Tuthill T., Graham S., Duyvesteyn H., Malinauskas T., Huo J., Tree J., Buttigieg K., Owens R., Carroll M., Daniels R., McCauley J., Stuart D., Huang K., Howarth M. & Townsend A. "A COVID-19 vaccine candidate using SpyCatcher multimerization of the SARS-CoV-2 spike protein receptor-binding domain induces potent neutralising antibody responses" Nature Communications (2021) 12:542 https://doi.org/10.1038/s41467-020-20654-7
4. Edmans, M.*, McNee, A.*, Porter, E.*, Vatzia, E., Paudyal, B., **Martini, V**., Gubbins, S., Francis, O., Harley, R., Thomas, A., Burt, R., Morgan, S., Fuller, A., Sewell, A., Charleston, B., Bailey, M., & Tchilian, E. (* equal contribution) "Magnitude and Kinetics of T Cell and Antibody Responses During H1N1pdm09 Infection in Inbred Babraham Pigs and Outbred Pigs." Frontiers in immunology (2021), 11: 604913 https://doi.org/10.3389/fimmu.2020.604913

5. Holzer B.*, Rijal P.*, McNee A.*, Paudyal B., **Martini V.**, Clark B., Manjegowda T., Salguero F. J., Bessell E., Schwartz J. C., Moffat K., Pedrera M., Graham S. P., Noble A., Bonnet-Di Placido M., La Ragione R. M., Mwangi W., Beverley P., McCauley J. W., Daniels R. S., Hammond J. A., Townsend A. & Tchilian E. (* equal contribution) "Protective porcine influenza virus-specific monoclonal antibodies recognize similar haemagglutinin epitopes as humans." PLoS Pathogens (2021), 17(3), e1009330 https://doi.org/10.1371/journal.ppat.1009330
6. Graham S.*, McLean R.*, Spencer A.*, Belij-Rammerstorfer S., Wright D., Ulaszewska M., Edwards J., Hayes J., **Martini V.**, Thakur N., Conceicao C., Dietrich I., Shelton H., Waters R., Ludi A., Wilsden G., Browning C., Bialy D., Bhat S., Stevenson-Leggett P., Hollinghurst P., Gilbride C., Pulido D., Moffat K., Sharpe H., Allen E., Mioulet V., Chiu C., Newman J., Asfor A., Burman A., Crossley S., Huo J., Owens R., Carroll M., Hammond J., Tchilian E., Bailey D., Charleston B., Gilbert S., Tuthill T.* & Lambe T.* (* equal contribution) "Evaluation of the immunogenicity of prime-boost vaccination with the replication-deficient viral vectored COVID-19 vaccine candidate ChAdOx1 nCoV-19." npj Vaccines (2020) 5, 69 https://doi.org/10.1038/s41541-020-00221-3
7. McNee A.*, Smith T.*, Holzer B.*, Clark B., Bessell E., Guibinga G., Brown H., Schultheis K., Fisher P., Ramos S., Nunez A., Bernard M., Graham S., **Martini V.**, Chrun T., Xiao Y., Kash J. C., Taubenberger J. K., Elliott S., Patel A., Beverly P., Rijal P., Weiner D. B., Townsend A., Broderick K. E. & Tchilian E. (*equal contribution) "Establishment of a Pig Influenza Challenge Model for Evaluation of Monoclonal Antibody Delivery Platforms." Journal of immunology (2020), 205(3), 648–660 https://doi.org/10.4049/jimmunol.2000429
8. Holzer B.*, Morgan S.*, **Martini V.***, Sharma R., Clark B., Chiu C., Salguero F. & Tchilian E. (* equal contribution) "Immunogenicity and Protective Efficacy of Seasonal Human Live

Attenuated Cold-Adapted Influenza Virus Vaccine in Pigs" Frontiers in Immunology (2019) 10, 2625 https://doi.org/10.3389/fimmu.2019.02625

9. Holzer B., **Martini V.**, Edmans M. & Tchilian E. "T and B Cell Immune Responses to Influenza Viruses in Pigs" Frontiers in Immunology (2019) 10; 98 https://doi.org/10.3389/fimmu.2019.00098

Acknowledgment

I've been fortunate to have shared the joys and struggles of this D.Phil. with many great scientists and friends.

I would like to thank **Dr. Elma Tchilian**, **Prof. Alain Townsend**, and **Dr. Ronan MacLoughlin** for their guidance and for sharing their wisdom. Working with you has been truly inspirational, and your love and enthusiasm for science constantly moved me and pushed me to do my best.

I am also grateful to my co-supervisors, **Prof. Alexander Drakesmith** and **Prof. Simon Graham** for their patience and valuable advice in critical moments of my project. Thanks to **Dr. Sophie Morgan** and **Dr. Barbara Holzer**, who constantly and kindly helped day-to-day in the laboratory. A special thank you to **Prof. Peter Beverley** for the support and great scientific discussions in these years.

Thanks must also go to the incredible collaborators and their support. Thanks to **Dr. Michael Hinchcliffe** (Paracelsis ltd.) and **Elaine Blackshaw** (University of Nottingham) for the scintigraphy imaging and *in vivo* study. Thanks to **Mary Joyce** for the patience and guidance during my internship at Aerogen. I am grateful to **Dr. Pramila Rijal** and **Dr. Holly Sadler** for welcoming me to the Townsend lab and sharing their incredible knowledge with me. I want to thank **Prof. Andrew Sewell** for providing SLA monomer and **Dr. Ryo Inoue** for supplying CD69 antibodies. Thanks also to **Dr. Timothy Connelley** and **Dr. Siddharth Jayaraman**, who contributed to the bioinformatic analysis of RNA-sequencing data, and to **Dr. Simon Gubbins** for his insights in mathematical modelling.

Thank you to the BBSRC Doctoral Training Partnership for funding this project. In particular, thanks to **Prof. Gail Preston** for always being there for me. Thanks to a fantastic network of outstanding D.Phil students who I am fortunate to call friends (**Sofia**, **Anna**, **Lea**, **Signe**, **Angita**, **Martina**, **Riccardo**, **Nick**

and **Andreas**). A special thanks to **Ada** and **Carolina** for making me feel at home, loved and supported in these four years. I am also grateful to **Dr. Jia Chua** for hosting me while completing my research in Nottingham; you have been a great friend.

Thanks to all the students and staff of the Mucosal Immunology and PRRS Immunology groups over the years for their assistance. Particular thanks to **Dr. Matthew Edmans** and **Dr. Adam McNee** for sharing their knowledge on porcine immunology; **Dr. Eleni Vatzia** for the late nights on the Fortessa and great chats; **Dr. Tiphany Chrun**, **Dr. Emmanuel Maze** and **Dr. Basu Paudyal** for always showing up to support during long days: **Dr. Rebecca McLean** and **Dr. Jane Edwards** for taking me on board in their team during the COVID19 studies.

I am thankful to my family for always encouraging me to do my best, experience the world, and never give up. For the late-night phone calls of these past years and for sharing the best and worst days since I have memory, thanks to my fringue **Alice**, **Micaela** and **Martina**. Thanks to my number 1 supporter and the most patient boyfriend, **Rodolfo**, none of this work could have happened without you beside me.

I would like to dedicate this thesis to my grandparents **Bruno**, **Giuditta**, **Ernesto** and **Carla**, who financially and personally supported my University studies and scientific career. I wish I could share with you all this final achievement.

Table of Contents

List of Figures

List of Tables

Glossary and abbreviations

aa	amino acid
AAV	AAVKGVGTI epitope present in H1N1pdm09 NP at position 181–189, subsequentially loaded into SLA tetramer
Ab	antibodies
ADCP	antibody-dependent cell phagocytosis
aer.	aerosol delivery
AF	Alexa Fluor™
ASC	antibody secreting cells
BAL	bronchoalveolar lavage
BALT	bronchus-associated lymphoid tissue
BCG	Bacillus Calmette–Guérin vaccine
BCR	B cell receptor
BV	Brilliant Violet™
CB	carbonate bicarbonate
CD	cluster of differentiation
cDNA	complementary DNA
COVID-19	Coronavirus Disease 2019
DCs	dendritic cells
DFE	DFEREGYSL epitope present in PR8 NP at position 290–298, subsequentially loaded into SLA tetramer
dpc	days post-challenge

dpi	days post-infection
EFE	EFEDLTFLA epitope present in PR8 NP at position 252-260, subsequentially loaded into SLA monomer
eGFP	enhanced green fluorescent protein
ELISpot	enzyme-linked immune absorbent spot
ELLA	enzyme-linked lectin assay
Eomes	eomesodermin
FACS	fluorescence-activated cell sorting
FITC	fluorescein isothiocyanate
FSC	forward scatter
h	Hours
HA	haemagglutinin
HAI	haemagglutinin inhibition assay
HA0	precursor haemagglutinin that when cleaved in position 329 generate HA1 at the N-terminus and HA2 at the C terminus
HA1	HA subunit 1
HA2	HA subunit 2
HIV	human immunodeficiency virus
HPV	human papilloma virus
H1N1pdm09	A/swine/England/1353/2009
IAY	IAYERMCNI epitope present in PR8 NP at position 217–225 subsequentially loaded onto SLA monomer
IAV	influenza A virus
IBV	influenza B virus

ICV	influenza C virus
IC50	50% inhibitory concentration
IDV	influenza D virus
IFN	interferon
IHC	immunohistochemistry
IIV	inactivated influenza vaccines
IL	Interleukin
i.m.	intra-muscular
i.n.	intra-nasal
i.p.	intra-peritoneal
IRF	interferon regulatory transcription factor
i.t.	intra-tracheal
i.v.	intra-venous
jet-neb	jet nebuliser
LAIV	live attenuated influenza virus
LRT	lower respiratory tract
mAb	monoclonal antibody
MAD	mucosal atomisation device
MBq	mega becquerel
min	Minutes
MMAD	mass median aerodynamic diameter
MN	microneutralisation assay
MOI	multiplicity of infection

MSD	multidimensional scaling
M1	matrix protein 1
M2	matrix protein 2
NA	neuraminidase
NF-κB	nuclear factor κ-light-chain-enhancer of activated B cells
NGK	NGKWMRELI epitope present in PR8 NP at position 101-109 subsequentially loaded onto SLA monomer
NK	natural killer
NLRP3	nucleotide-binding oligomerization domain (NOD)-, leucine-rich repeat (LRR)- and pyrin domain-containing protein 3
NP	Nucleoprotein
NS-1	non-structural protein 1
NS-2	non-structural protein 2
PA	polymerase acid protein
PBMC	peripheral blood mononuclear cells
PB1	polymerase basic protein 1
PB2	polymerase basic protein 2
PPRs	pattern recognition receptor
PR8	A/Puerto Rico/8/1934
RIG-1	retinoic acid-inducible gene I
RNA-seq	RNA sequencing
ROI	region of interest
RT	respiratory tract
RT-qPCR	Real time quantitative polymerase chain reaction

SARS-CoV-2	severe acute respiratory syndrome coronavirus 2
SD	standard deviation
SFU	spot forming unit
SIM	simultaneous local and systemic administration
SLA	swine leukocyte antigen
SSC	side scatter
S1PR	sphingosine 1-phosphate receptors
Tb	Tuberculosis
TBLN	tracheobronchial lymph nodes
TCID50	50% tissue culture infectious dose
tetramer	assembly of SLA biotinylated monomer with loaded with the indicated epitope and fluorophored streptavidin
TCM	central memory T cells
TCR	T cell receptor
TEM	effector memory T cells
TGF	transforming growth factor
TLR	toll-like receptors
TNF	tumour necrosis factor α
TRM	tissue resident memory T cells
URT	upper respiratory tract
USA	United States of America
VAERD	Vaccine associate enhanced respiratory disease
VAY	VAYERMCNI epitope present in H1N1pdm09 NP at position 217–225 subsequentially loaded onto SLA monomer

VMD	volume mean diameter
VMN	vibrating mesh nebuliser
vs	Versus
50%IT	50% inhibition titre
^{99m}Tc-DTPA	technetium (^{99m}Tc) complexed with diethylenetriaminepentaacetic acid (DTPA)

Abstract

Influenza A virus (IAV) is a considerable threat to human and animal health. Current immunisation strategies rely primarily on inducing strain-specific neutralising antibodies with a limited breadth of protection. Increasing evidence indicates the importance of local immune responses and tissue resident memory T cells (TRM) for broad protection against respiratory infections, however, a vaccine that can be safely delivered to the lung is yet to be approved. In addition, there is little information on influenza A virus (IAV) specific TRM in the pig, a large animal model for IAV research, and a natural reservoir for the virus.

The first part of this thesis describes the characterisation of porcine CD8 TRM in the lungs and upper respiratory tract following H1N1pmd09 infection. The phenotype of CD8 T cells specific for three influenza nucleoprotein (NP) epitopes, detected using MHC class I tetramers, was determined. This analysis revealed that the hierarchy of response differed with time in different tissues. The frequency of NP-specific cells declined over 63 days in all tissues, but it was best maintained in the lung. Most tetramer^{+} CD8 T cells isolated from broncho-alveolar lavage (BAL) displayed a TRM phenotype, expressing CD69 and an effector memory phenotype. NP-specific T cells isolated from BAL presented genes characteristic of human TRM, but gene expression differed at 7, 21 and 63 days post-infection.

It is essential to assess vaccine deposition to provide optimal delivery of vaccines to the respiratory tract. The distribution of droplets generated by a commonly used intranasal device (MAD) and two commercially available vibrating mesh nebulizers (VMNs) was therefore compared. Droplets generated with the drug albuterol or a radiolabel (^{99m}Tc-DTPA), or a model vaccine (S-FLU) presented similar aerosol characteristics. A scintigraphic study using ^{99m}Tc-DTPA showed that VMNs uniformly distributed the radiolabel in the porcine lung and upper respiratory tract. The intranasal administration

of a large volume (1ml/nostril) by MAD also delivered a high proportion of the dose to the lungs, although in a concentrated and restricted area.

Recombinant single-cycle IAV viruses, such as S-FLU, may offer a promising solution to currently available vaccines as they can be delivered safely to the lung and elicit heterotypic immunity. However, previous studies in pigs showed a limited reduction in viral replication following challenge. In the last chapter, two strategies to improve S-FLU immunogenicity and protection are presented: 1) implementing a second-generation version of S-FLU expressing HA (CLEARFLU) and 2) administering S-FLU simultaneously by aerosol and intramuscular injection (SIM). CLEARFLU did not generate neutralising antibodies, however, S-FLU administered by SIM produced a high titer of neutralising antibody, robust local cellular responses and conferred protection against homologous challenge. On the other hand, intramuscular injection alone elicited humoral responses in the periphery, but failed to do so locally, and did not stimulate cellular responses. Aerosol S-FLU did not protect despite high T cell responses in the respiratory tract, probably due to the lack of neutralising antibody in the periphery.

These data showed for the first time that porcine TRM present similar properties to those of humans, further establishing the pig as a useful model for investigation of local memory responses following respiratory infection. In addition, aerosol delivery can uniformly target the lungs but only the SIM immunisation regime successfully protected pigs from challenge, warranting further studies of this immunisation strategy against IAV and other respiratory pathogens.

Chapter 1
Introduction

1.1 Influenza virus

Influenza viruses are zoonotic pathogens, infecting birds, humans and pigs (Figure 1.1) and many other species and a significant cause of morbidity and mortality in these species. In domesticated birds, influenza virus infects both the respiratory tract (RT) and intestine. Highly pathogenic avian influenza H5N1 have alone caused major economic losses (US$ 20 billion losses globally, since 2003), including the culling of 400 million birds (Food and Agriculture Organization of the United Nations (FAO) 2012). In humans and pigs, influenza virus infection is limited to the RT, and is spread by aerosolised droplets originating from saliva or nasal secretions (Torremorell et al. 2012). Each year between 290,000 and 650,000 people die from influenza-associated respiratory causes (Iuliano et al. 2018), while 10-20% of the world population contracts influenza (Peasah et al. 2013). Despite a low mortality rate, the seroprevalence in pigs is around 50%, with over 1.4 billion animals infected with influenza viruses in 2018 (Salvesen and Whitelaw 2021). Clinical manifestation of influenza virus infection in mammals includes fever, coughing, sore throat, and appetite loss. However, the clinical outcome of the disease is dependent on the host's immune responses, with hospitalisations and illness highest in children (<2 years old) and the elderly (> 65 years old) (Thompson, Comanor, and Shay 2006).

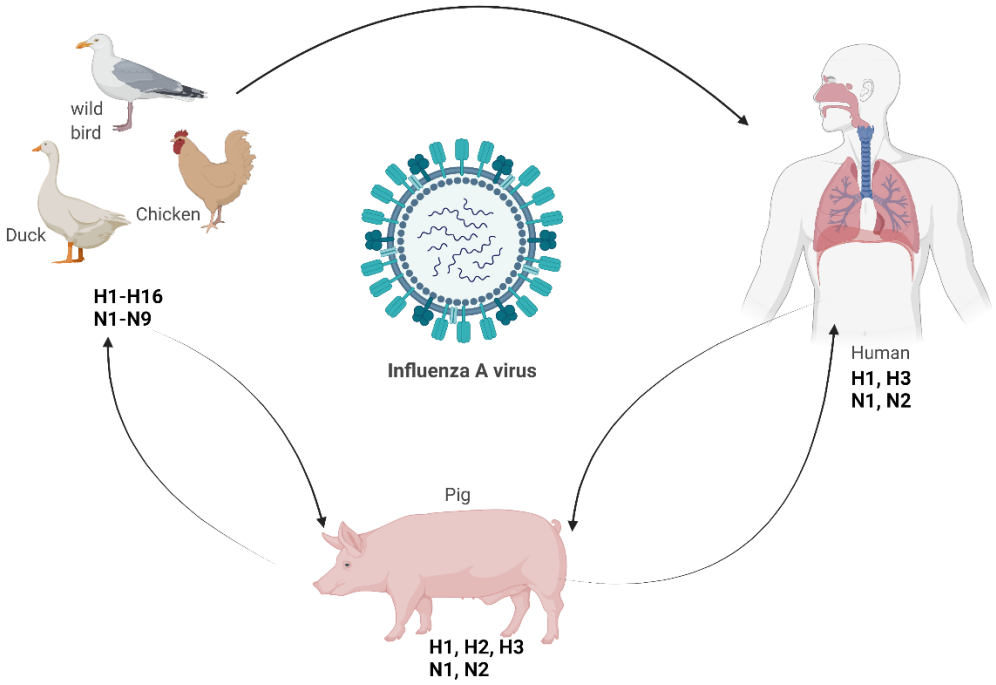

Figure 1.1 **Schematic representation of the zoonotic cycle of IAV within its main hosts.** H indicates haemagglutinin while N denotes neuraminidase circulating in each host. Figure created with ©BioRender.

Influenza viruses are part of the *Orthomyxoviridae* family. Influenza viruses are classified as Influenza A Virus (IAV), Influenza B Virus (IBV), Influenza C Virus (ICV) or Influenza D Virus (IDV). While IAV and IBV are responsible for seasonal epidemics in humans, domestic pigs are infected mainly by IAV, with few cases of IBV, ICV and IDV infection (Ran et al. 2015; Hause et al. 2013; Salvesen and Whitelaw 2021).

IAV virus, the focus of this thesis, presents an envelope that protects the single-stranded negative-sense RNA genome, organised in 8 segments encoding for 11 main proteins:

- Haemagglutinin (HA), present on the virus envelope, binds to sialic acids expressed on host cellular receptors. It is divided into two subunits (HA1 and HA2) after enzymatic cleavage by trypsin-rich environments in mammals. The consequent exposure of a fusion peptide present at the end of the (N)-terminal of HA2 allows the viral particle to fuse with the endosomal membrane of infected cells and release the viral genome and proteins in the cytoplasm.
- Neuraminidase (NA), also anchored to the envelope, is indispensable for releasing viral particles from the infected cells. NA removes sialic acids, present as part of the glycosylation process within the infected cells, from the cellular receptors and newly synthetised HA and NA, to avoid the formation of viral aggregates (Basak, Tomana, and Compans 1985).
- Matrix proteins 1 and 2 (M1 and M2) promote virion formation by interacting with the cytoplasmic component of HA and NA and the viral ribonucleoprotein.
- RNA-dependent RNA polymerase is a heterotrimeric complex of polymerase acidic (PA), polymerase basic 1 (PB1), and polymerase basic 2 (PB2). The polymerase transcribes viral RNA and replicates the IAV genome in the nucleus of infected cells.
- Nucleoprotein (NP) is the most abundant viral protein in infected cells and is fundamental for viral RNA packing, transcription and replication.
- Non-structural protein 1 (NS1) and PB-F2 display an immunomodulatory effect.
- Non-structural protein 2 (NS2), also known as nuclear export protein, is indispensable for trafficking viral RNA in the host cells.

IAVs are classified into subtypes based on the surface proteins HA and NA. To date, 18 HAs and 11 NAs have been identified but only H1, H2, H3 and N1, N2 serotypes normally circulate in mammals (Tong et al. 2013). In particular, H1N1, H1N2 and H3N2 are endemic in pigs (Baudon et al. 2017) and

H1N1 and H3N2 are responsible for seasonal epidemics in humans. More recently, outbreaks of H5, H7 and H9 from avian origin have been reported in humans (World Health Organisation 2021). HA is crucial in determining the host of influenza viruses. HA binds sialic acids attached to galactose via a α2-6 or α2-3 linkage, the latter mainly recognised by avian IAV (Rogers and Paulson 1983). In humans and pigs, the epithelial cells of the upper respiratory tract (URT) present sialic acid linked via a α2-6 bond while both linkages are present in the lower respiratory tract (LRT) (Nelli et al. 2010; Van Poucke et al. 2010).

Antigenically diverse strains can coinfect natural hosts and exchange viral gene segments within an infected cell. This phenomenon, known as antigenic shift, can lead to the generation of a new reassortant strain with pandemic potential, as occurred in 2009 with the emergence of the H1N1 pandemic virus (H1N1pdm09) (Vijaykrishna et al. 2010). In addition, the viral RNA-polymerase lacks proof-reading functions and is prone to error, leading to point mutations in the viral genes, an event referred to as antigenic drift. HA and NA are more susceptible to mutations due to the selective pressure of the immune system.

Innate immunity against IAV

Viral entry to epithelial cells is mediated by HA binding to the sialic acid, which causes endocytosis. When the virus reaches the endosome, the low pH of the environment triggers HA fusion to the endosomal membrane and activates the M2 ion channel. M2 acidifies the viral particle allowing the release of the packaged viral RNA into the cytosol. The host senses IAV by pattern recognition receptors (PRRs) (reviewed in (Iwasaki and Pillai 2014)). The uncapped single-stranded viral RNA is recognised by retinoic acid-inducible gene-1 (RIG-1) in all infected cells. In addition, B cells and dendritic cells

(DCs) recognise the single-stranded viral RNA via Toll-like receptor (TLR) 7, promoting interferon (IFN) responses to stop viral replication. TLR3 binds to double-stranded RNA in the endosome of macrophages, detecting phagocyted infected cells, stimulating an antiviral state. Myeloid cells can also form NLRP3 (NOD-, LRR- and pyrin domain-containing protein 3) inflammasome in response to stress and membrane damage and subsequently secrete cytokines to recruit leukocytes to the lung (Thomas et al. 2009).

After IAV recognition, PRRs initiate several signaling events and activate transcription factors such as NF-κB (nuclear factor κ-light-chain-enhancer of activated B cells) and interferon regulatory transcription factor (IRF) 3 and 7. These transcriptional factors promote the expression of IFNs and proinflammatory cytokines (tumor necrosis factor α (TNF), interleukin (IL) 6, IL-1β) related genes. Type I (e.g. IFNα and β) and III (IFNλ) IFN are autocrine and paracrine signals promoting an antiviral state and limiting viral replication. Type I IFN also enhance antigen presentation and phagocytosis (reviewed in (Lee and Ashkar 2018)). The major cellular components of innate immunity in the lung are natural killer (NK) cells, neutrophils, macrophages and DCs.

NK cells can be detected in the lung as early as 48 hours (h) post-infection with IAV (Stein-Streilein et al. 1983; Forberg et al. 2014). NKp44 and NKp46 receptors recognise HA expressed on the surface of infected cells and mediate their lysis (Mendelson et al. 2010).

Together with NK cells, neutrophils play a role in IAV clearance via the secretion of proinflammatory cytokines. Neutrophils exhibit Fc-mediated effector functions such as antibody-dependent cellular phagocytosis (ADCP), essential for viral clearance (Mullarkey et al. 2016). Recent studies in mice

highlighted the importance of neutrophils in the recruitment of CD8 T cells in the airways after IAV infection (Lim et al. 2015).

Alveolar macrophages are the primary phagocytic cells in the lung, limiting IAV spread by phagocytosis of infected cells (Tumpey et al. 2005). They also secrete proinflammatory cytokines such as TNF, IL-1, IL-6. Despite their essential role in limiting viral replication, macrophages were also associated with severe pneumonia after IAV infection (Hogner et al. 2016; Kobasa et al. 2007). Alveolar macrophages are also susceptible to IAV infection, although the shedding of infectious viruses from these cells is limited (Rodgers and Mims 1982).

DCs represent a bridge between innate immune responses and the adaptive immune system. Located underneath the URT epithelial cells and the lung parenchyma, DCs can also be found in the alveolar space (Holt et al. 2008). These cells are activated if directly infected by IAV or when acquiring viral antigen from infected apoptotic cells. DCs then migrate to the draining lymph nodes (LN), where they present antigenic peptides via the major histocompatibility complex (MHC) molecules. Viral epitopes (of 8-14 amino acid (aa) length) present in the cytosol are exposed on MHC class I on the surface of DCs, while epitopes processed in the endosome (12-16 aa) are presented on MHC class II molecules (Townsend, Gotch, and Davey 1985; Townsend, Bastin, et al. 1986). Epitope-MHC-I complexes are recognised by the T cell receptor (TCR) of CD8 T cells, while CD4's TCR binds to MHC-II complexes. Activated DCs provide costimulatory signals to T cells to enhance TCR signaling and promote T cell activation. CD28/B7 interaction represents the primary costimulatory signal during early responses and promotes the formation of effector CD8 T cells. A second costimulatory signal (4-1BB, also known as CD137) affects T cells numbers in the memory stage of the response (Bertram, Lau, and Watts 2002). DCs also secrete cytokines, a third signal for T cell activation, important in determining T cell

polarisation. In summary, DCs plays an essential role in the generation of optimal adaptive immune responses

Cellular immunity against IAV

In the LN, naïve T cells interact with activated DCs presenting IAV epitopes. This interaction activates T cells, which will then upregulate the activation markers CD69, described later, and CD25, receptor for IL-2, and start proliferating. Responding CD4 and CD8 T cells overexpress the transcription factor T-bet, involved in the production of T helper (Th) 1 characteristic cytokines IFNγ and TNF (Hao, Kim, and Braciale 2008). Activated effector T cells also downregulate CCR7 and CD62L, which allows them to migrate outside the LN, and home to the lung thanks to the expression of the receptor for the chemokines CXCR3, CXCR6 and CCR4 (Demi Brownlie 2021). In the lung, CD8 T cells target infected cells presenting IAV epitopes on MHC-I. Townsend et al. demonstrated that conserved viral antigens, mainly from IAV NP, were presented via the MHC-I molecule to cytotoxic T cells and could be defined by short synthetic overlapping peptides (Townsend, Rothbard, et al. 1986). More recent work defined the immunodominant epitopes recognised by CD8 T in the viral PA ($PA_{224-233}$), NP ($NP_{366-374}$) and PB1 ($PB1_{703-711}$) protein in B6 mice (Belz et al. 2000; La Gruta et al. 2008). Upon recognising the target antigen, CD8 T cells produce IFNγ, TNF and IL-2 and secrete granules containing perforin and granzymes to kill infected cells (Harty, Tvinnereim, and White 2000). Apoptosis of infected cells is also mediated by FAS ligand-induced caspase cascade.

CD4 T cells also play an essential role in the adaptive responses to IAV. IAV infections generate Th1 responses predominantly, producing mainly IFNγ. Th17 CD4 T cells are also generated during infection, although they can contribute to immunopathology (Crowe et al. 2009). The primary role of CD4 T helper

cells is to support the development of an optimal cytotoxic CD8 T cells response and tissue resident memory CD8 T cells (described later in this chapter).

Two other subsets of CD4 T cells are present at the late stage of the responses: cytotoxic CD4 T cells and follicular helper T cells (Tfh). Cytotoxic CD4 T cells can kill infected cells presenting viral epitope on MHC-II. Although at the steady-state MHC-II is restricted to antigen-presenting cells, it can be expressed by infected epithelial cells in the lung (Brown et al. 2012). Tfh cells reside in the germinal center of the LN, together with B cells. They contribute to optimal B cells responses by increasing B cell survival, class switching and somatic hypermutations (reviewed in (Crotty 2014)).

Following a peak expansion at 10 days post-infection (dpi) and subsequential pathogen clearance, 95% of activated IAV-specific T cells die while a small population of long-lived memory T cells persists, with higher frequencies maintained in the lung compared to the circulation (Flynn et al. 1998). The ontogeny of memory T cells has been debated and two mechanisms proposed: “one naïve T cell, one fate” or “one naïve T cell, multiple fates”. The first mechanism implies that a single naïve cell could give rise to effector or memory cells from the beginning of the immune response. The signal responsible for the fate of the naïve T cell could be generated during T cell priming by antigen-presenting cells, ahead of the first cellular division. In a “one naïve T cell, multiple fates” scenario, a single naïve cell precursor can generate both effector and memory T cells. In addition, not only naïve T cells but also their descending cells can subsequentially differentiate and contribute to the memory pool. An elegant study from Gerlach and colleagues demonstrated, using barcoded naïve T cells, that naïve T cells have multiple fates and nor the signals received during antigen presentation or T cells avidity influences their fate (Gerlach et al. 2010). The plasticity of T cells not only applies to circulating T cells, but recent

evidence suggests that T cells resident in at the mucosal site, such as the intestine, can recirculate and acquire new features in mice (Fonseca et al. 2020).

Because IAV-specific T cells mainly recognised epitopes of the more conserved internal protein, they are crucial for heterosubtypic protection. Heterosubtypic protection was first observed in Schulman's study, where mice infected with H1N1 recovered from a lethal dose of a different subtype (H2N2) IAV challenge (Schulman and Kilbourne 1965). In the 1970s, Braciale et al. demonstrated that CD8 T cells recognise epitopes conserved between different IAV viruses (Braciale 1977a, 1977b). Subsequent studies in mice revealed the role of CD8 T cells in protection by adoptive transfer experiments in both naïve and transgenic mice (Bender et al. 1992; Yap, Ada, and McKenzie 1978; Taylor and Askonas 1986). Pre-exposure with IAV enhanced viral clearance and limited lung pathology after heterosubtypic challenge, in the absence of crossreactive neutralising antibodies (Ab) (Graham and Braciale 1997; Flynn et al. 1998; Epstein et al. 1998). While the role of CD8 T cells in heterosubtypic protection is well established, it is less clear for CD4 T cells. Adoptive transfer experiment with physiological numbers of IAV-specific CD4 T cells resulted in weak protection after subsequent challenge (Thomas et al. 2010). However, their help for optimal CD8 T cells and B cells development is indispensable during heterotypic infections (McKinstry et al. 2012).

Demonstration of the role of T cells in heterotypic protection in humans requires documentation of previous IAV infections in the individual, which is challenging. However, several studies have taken advantage of the spread of new IAV strains. In1957, during the H2N2 pandemic, individuals recently exposed to the seasonal H1N1 strains were three times less likely to develop a symptomatic infection (Slepushkin 1959; Epstein 2006). Similar observations were reported in children during the H1N1 pandemic of 1977 and 2009 (Cowling et al. 2010; Sonoguchi et al. 1985). Early studies demonstrated

in vitro the crossreactivity of human CD8 T cells to different IAV strains (Biddison, Shaw, and Nelson 1979; McMichael and Askonas 1978). McMichael first reported the role of cross-reactive IAV-specific CD8 T cells in protection in an experimental challenge infection of humans (McMichael et al. 1983). During natural infection in 2009 H1N1 pandemic, preexisting cross-reactive CD8 T cells recognising PB1, M1, and NP epitopes and secreting IFNγ correlated with reduced viral shedding and milder symptoms (Sridhar et al. 2013). A parallel study confirmed that pre-existing NP-specific CD4 and CD8 T cells were associated with reduced nasal viral shedding but not with total symptom scores in patients infected during the 2009 pandemic (Hayward et al. 2015). Furthermore, IAV challenge studies correlated preexisting CD4 T cells with protection (Wilkinson et al. 2012). These data confirm the role of pre-existing T cell immunity in reducing viral shedding and the severity of the disease in humans and mice.

Antibody responses to IAV

Adaptive humoral responses promote the host defense to IAV infection via B cells' secretion of Ab. Protective Ab target HA and NA protein present on the viral envelope. Three classes of Ab are involved in IAV clearance: IgM, IgG and IgA.

IgM are the first line of Ab defence, as they are naturally present in circulation. IgM present a low affinity for viral antigens but contributes to the recruitment of viral antigens to the LN by forming large aggregates with the virus (immune complexes). However, optimal viral clearance requires high affinity, neutralising Ab.

IgG are generated by B cells after class switching and somatic hypermutations events. Naïve B cells express a B cell receptor (BCR, a IgM or IgD molecule anchored on the cell surface) which can directly recognise viral antigens or be stimulated by epitopes presented by antigen-presenting cells. Class switching and maturation of B cells takes place in the germinal centre of the LN, where activated B cells encounter Tfh. Thanks to the secretion of IL-4, IFNγ and transforming growth factor (TGF) β by Tfh and the binding with CD40L, B cells switch isotype from IgM to IgG or IgA (reviewed in (McHeyzer-Williams et al. 2011) and become antibody-secreting cells (ASCs). In humans, IgG ASCs are already detected 7 days post H1N1pdm09 infection (Wrammert et al. 2011). Once the infection is cleared, ASCs differentiate into long-lived plasma cells. IgG targeting the HA protein can neutralising viral entry by binding to the same site as sialic acid or more distal regions impairing viral entry by steric hindrance (Ekiert et al. 2012). Anti-HA Ab can also block viral fusion to the endosome (Brandenburg et al. 2013). Ab targeting NA have recently gained attention for their ability to inhibit viral exit from the infected cells, limiting virus spread and the fact that NA is more conserved than HA. Lower levels of Ab are also found to target the internal protein of IAV.

If IgG dominates the LRT (with IgG:IgA ratio of 2.5:1), IgA populates the URT (IgG:IgA 1:3) (reviewed in (Krammer 2019)). IgA are dimeric and produced locally by plasmacells and actively secreted in the mucosal sites. Although IgG and IgA may recognise similar epitopes, IgA are more broadly reactive, probably thanks to their higher avidity as a result of their multimeric form (Krammer 2019).

Ab responses generated after natural infection can be long-lived (Yu et al. 2008) but the high mutation rate of the virus generates variants (antigenic drift) that are poorly recognised by preexisting neutralising Ab, resulting in seasonal outbreaks and necessitating annual vaccines updates.

1.2 Animal models

Vaccine efficacy and immune responses to influenza viruses have been evaluated in several animal models, each presenting advantages and disadvantages (reviewed in (Rajao and Vincent 2015)).

Mouse models are inexpensive, and a wide range of immunological reagents are available for this species. However, human IAV can only cause disease in mice when the virus is adapted. For instance, A/Puerto Rico/8/1934 (PR8), commonly used to challenge mice, was generated after several passages in ferrets, mice, and fowl eggs. During the adaptation process, many mutations can arise therefore limiting the validity of the model. In addition, mice do not manifest typical clinical signs of IAV infection but weight loss and death are measured instead as an endpoint. Viral replication can only be assessed in the lung and even a small reduction in viral load can be associated with survival and positive outcome. Challenge experiments are generally performed under anaesthesia and, together with the volume of inoculation, it influences the viral distribution in the RT.

Ferrets are naturally susceptible to human IAV, with a similar sialic acid repertoire. After experimental infection, ferrets shed IAV from the URT similarly to humans, making them useful for studying viral transmission. In addition, ferrets develop typical clinical signs of influenza infection such as fever and sneezing. However, their special housing requirements, cost, limited commercial availability and lack of immunological reagents represent a challenge for studies in this animal model.

Guinea pigs have also been used as a model for IAV infection. They are relatively small, commercially available at a reduced cost and readily infected with human IAV. Experimental infection induces viral replication in the URT, but this is not generally associated with symptoms. A second limitation of this model is the scarce availability of immunological reagents.

The pig (*Sus scrofa*) can be a valuable model to study influenza infection, and its advantages and limitations are discussed in the next section.

Pig as a model for influenza research

The pig genome is more similar to human than the one of rodents (Rajao and Vincent 2015). Tracheobronchial structure, lung size, and submucosal glands in the porcine RT are closely related to humans (Judge et al. 2014). Like humans, the swine lung is lobulated with three lobes on the left and four on the right, although the porcine right apical lobe of the lung is directly connected with the trachea. The URT in pigs comprises tonsils and lymphoid structures similar to the humans Waldeyer's ring, which is absent in mice (Rothkotter 2009).

Pigs are a natural host for IAV and can be readily infected by some human IAV strains such as H1N1pdm09. Clinical manifestations of influenza are similar in both pigs and humans, with fever, anorexia, lethargy being the most common (Rajao and Vincent 2015). Porcine distribution of sialic acids shares similar patterns with human and both α2-3 and α2-6 linkages are present in the swine RT. In addition, human IAV strains replicate similarly in tissues extracted from porcine URT and LRT and several studies reported ongoing spillover events of seasonal human IAV into the swine population (Van Poucke et al. 2010) (reviewed in (Anderson et al. 2021)). Furthermore, innate and cellular responses observed in pigs after IAV infection resemble the humans, as discussed below.

Despite being closely related to humans in many aspects, pigs have some peculiar features. The swine LN present a so-called inverted structure with an outer medullary region and an inner cortex. This results in different lymphocyte migration patterns through the LNs with afferent lymph vessels and high endothelial venules conveying lymphocytes to the LN while their egress takes place in high endothelial

venules and not efferent lymph vessels as in humans (reviewed in (Rothkotter 2009)). Pigs also have high frequencies of γδ T cells in the circulation (Talker et al. 2013). They differ from circulating γδ in humans as a proportion of porcine γδ lack CD2 expression, and they do not respond to phosphorylated metabolites. However, their function in pigs is still unclear. Porcine CD4 T cells express CD8α after antigenic activation, a feature also present in SCID mice while rarely present in humans (reviewed in (Kaser 2021)).

Limitations to the use of pigs in IAV infections include high husbandry costs and the necessity of specialist facilities to house these large animals. In addition, limited immunological tools are available for this species. Aiming to define the specificity of the immune responses to infectious agents in more detail, several inbred minipig breeds have been developed, including NIH, Yucatan, and Gottingen with defined swine leukocyte antigens (SLA, the swine MHC) (Gutierrez et al. 2015). The inbred Babraham pig is the only full-size inbred pig closely related to commercially available breeds, for which immunological tools have been developed to study T cell responses to IAV and influenza vaccines (Tungatt et al. 2018).

1.3 Porcine adaptive immune responses to IAV

Although several studies in mice and humans demonstrated the protective role of cellular responses to influenza infection, few studies in pigs have analysed T cell immunity to IAV in depth.

After infection with H1N1 of swine-origin (Sw/OH/24366/07), Khatri et al. observed a decrease in the proportion of porcine CD4 cells in the trachea-bronchial lymph nodes (TBLN), peripheral blood

mononuclear cells (PBMC), lung and tonsils at 3 dpi (Khatri et al. 2010). In this experiment, CD4 T cells significantly increased in numbers in PBMC, compared to mock-infected animals, at 6 dpi. A more recent study investigated the dynamic of the responses to H1N2 virus at 2, 4, 6, 9, 12, 15 and 46 dpi (Talker et al. 2016). Proliferating $Ki67^+$ CD4 T cells were detected as early as 4 dpi in TBLN, with a smaller proportion present from 6 dpi in the lung (Talker et al. 2016). CD4 T cells secreted IFNγ, IL-2 and TNF in PBMC and TBLN with peak frequencies detected at 9 and 12 dpi. At 12 dpi time point, the IAV specific response included IFNγ single producing cells in the lung, TNF single producers in TBLN, and triple producers in the blood (Talker et al. 2016). CD4 cytokine-producing cells expressed CD27 and CD8α, defining a memory/activated CD4 phenotype in pigs. Intranasal (i.n.) challenge with H1N1pmd09 generated a high number of IFNγ and TNF secreting cells in BAL with a peak at 9 dpi while TNF producers dominated TBLN (Edmans et al. 2020).

CD8 T cells were significantly higher in lungs and BAL 6 days after Sw/OH/24366/07 challenge (Khatri et al. 2010). Similarly, in H1N2 infected pigs, activated $CD27^+Ki67^+$CD8 T cells peaked 6 dpi in the lung and were able to produce both IFNγ and TNF and express perforin up to 44 dpi (Talker et al. 2016). Edmans et al. reported high frequencies of cytokine secreting CD8 T cells in BAL, with an increased presence of IFNγ, TNF and IL-2 triple producer at 21 days post H1N1pdm09 challenge (Edmans et al. 2020). Similar kinetics were observed in the lung while the responses in PBMC waned at 21dpi.

The high heterogeneity of SLA molecules in pigs limited the study of the specificity of the T cell responses in this animal model. SLA comprises 3 clusters of high polymorphic genes: class I, class II and class III. SLA class I genes are expressed in most cells and include *SLA-1, SLA-2* and *SLA-3*, with 229 alleles (96 *SLA-1*, 90 *SLA-2*, 43 *SLA-3*). While SLA III is more conserved, class II presents 211

alleles (Maccari et al. 2017). The most common SLA in outbred pigs are SLA-1*0401 and SLA-1*0702, which were modelled *in silico* to identify IAV epitopes (Baratelli et al. 2017a; Pedersen et al. 2014a). Human and murine MHC-I molecules can present epitopes of 8–14 aa in length, the majority (>70%) of CD8 T cells recognise epitopes of 9 amino acids in length with a smaller proportion (~20%) able to bind to peptides of 10 aa (Ekeruche-Makinde et al. 2013). Similarly, porcine CD8 T cells recognise SLA-1 carrying 9-10 aa long peptides (Fan et al. 2016; Pedersen et al. 2013; Pedersen et al. 2014a). An immunoinformatic tool, PigMatrix, was also developed and used to predict SLA-I epitopes to seven IAV strains of swine-origin (Gutierrez et al. 2016). However, these predicted epitopes can only be used in individuals with matched SLA. Babraham pigs share identical SLA, overcoming this issue (Schwartz et al. 2018). These inbred pigs present SLA class I SLA-1*14:02; SLA-2*11:04 and SLA-3*04:03 and class II DRB1-*05:01, DQA-*01:03 and DQB1-*08:01. Four immunodominant epitopes in the NP protein of PR8 were recently identified after immunisation of Babraham pigs: DFEREGYSL (DFE), EFEDLTFLA (EFE), IAYERMCNI (IAY) and NGKWMRELI (NGK) (Tungatt et al. 2018). However, only one (DFE) of the four epitopes is conserved in H1N1pdm09. A timecourse study revealed that Babraham pigs infected with H1N1pdm09 had CD8 T cells specific for this epitope as early as 6 dpi, with the highest responses detected in the BAL until 21 dpi (Edmans et al. 2020). Studies in humans revealed that most immunodominant epitopes are present in the NP and M1 of H5N1 (Lee et al. 2008). A smaller study of only six individuals identified 54 dominant epitopes present in human and avian IAVs in the internal proteins NP, M1 and PB1 and recognised by both CD4 and CD8 (Assarsson et al. 2008). However, it is not clear if these porcine and the human immunodominant epitopes are protective.

Heterosubtypic protection was also assessed in pigs. Pre-exposure with H1N1 protected pigs from the subsequent infection with avian H5N1 and H5N2 strains (Van Reeth et al. 2009). This finding was

further corroborated with the use of H3N2 swine IAV for preexposure and avian H4N6, H5N2 or H7N1 as challenge viruses (De Vleeschauwer and Van Reeth 2010). However, the role of heterotypic protection in natural infections has not been studied.

Ab responses to IAV are less well defined in pigs compared to humans and mice. IgM binding to HA were present 3 days after exposure with the H1N1 (Lee et al. 1995). In contrast, HA-specific IgG increased in the serum after infection, starting from 6 dpi and reaching a peak at 14 dpi. Similar kinetics was also reported for IgA but with a lower magnitude in circulation compared to IgG. IgA but not IgG specific to HA were found at the mucosal sites in nasal washes while both isotypes were present in BAL. Similar findings were also reported after H1N1 challenge, with IgA ASC in the nasal tissues 6 fold higher than IgG (Larsen et al. 2000). More recently, Edmans and colleagues showed the presence of neutralising Ab (measured both by microneutralisation and hemagglutinin inhibition assay (HAI)) in circulation from 6 days post H1N1pdm09 challenge, with high Ab titres still detected at 21dpi (Edmans et al. 2020). In this study high number of HA-specific ASCs were present in TBLN and lung at 21dpi. In addition, mAbs isolated from lung LN of H1N1pdm09 infected pigs recognised the same epitopes on the HA as humans (Holzer et al. 2021). Furthermore, the prophylactic administration of a selected porcine mAb to pigs abolished lung viral load and greatly reduced lung pathology but did not eliminate nasal shedding of virus after H1N1pdm09 challenge (Holzer et al. 2021).

In humans, Ab responses to HA and NA correlated with protection to homologous IAV infection (reviewed in (Krammer 2019)). Similarly, neutralising Ab to HA protected pigs from clinical manifestations of the disease after homologous challenge (Bikour, Cornaglia, and Elazhary 1996). Vaccine-associated enhanced respiratory disease (VAERD) was reported in pigs immunised with whole inactivated virus followed by a heterologous IAV challenge (Khurana et al. 2013). High titre of non-

neutralising anti-HA stalk Ab resulted in enhanced *in vitro* membrane fusion of the virus and target cells (Khurana et al. 2013). Human studies have also reported exacerbation of the disease in adults during the 2009 pandemic in relation to low avidity cross-reactive Ab (Monsalvo et al. 2011). Mucosal Ab responses are also similar in humans and pigs. IgA levels in the porcine RT were associated with protection after challenge in the absence of a strong systemic Ab response (Loving et al. 2012). Vaccinees with high mucosal IgA were protected from IAV challenge and did not develop severe disease (Clements et al. 1986).

1.4 Current IAV immunisation strategies

Commercially available vaccines aim to generate high titres of serum Ab as these correlate with protection. HAI titres of immunised individuals and HA content of the vaccine preparation remain key measures of immunogenicity for regulators. HAI measures the titre of HA-specific Ab that block the virus from binding to sialic acid on red blood cells. This assay is quick and can be easily performed. However, increasing evidence shows the protective role of anti-HA stem antibodies (Ab), anti-NA Ab and T cell responses, not measured by this standard test but equally important. In addition, cross-protection is rarely obtained by Ab targeting the head of HA protein, as this region constantly mutates. Developing vaccines that rely on more conserved features of IAV, and can guarantee cross-protection, is a priority. Current immunisation strategies reduce morbidity and mortality but are only 10-60% effective in stopping viral shedding (Grohskopf et al. 2020). Vaccine's HA and NA are updated yearly to match the circulating viruses, typically deriving from 2 IAV and 1 or 2 IBV strains. The World Health

Organisation (WHO) decides biannually, once for the Northern hemisphere and once for the Southern, the vaccine composition, usually more 6 months in advance of the IAV season.

Two categories of vaccines are commercially available against IAV: inactivated influenza vaccines (IIV) or live attenuated influenza vaccines (LAIV).

Inactivated influenza vaccines

IIV are widely used in both humans and pigs and comprise whole virus particles, split virions and subunit vaccines. Whole virus particles are prepared from embryonated fowl egg grown (or less commonly cell culture grown) and purified IAV are subsequently inactivated chemically (with formaldehyde or β-propiolactone). In the production of split virions, the purified IAV is disrupted by detergent. Subunit vaccines are prepared from inactivated viruses with an extra purification step to obtain a formulation enriched in HA and NA proteins. In IIV, HA is the primary antigen in the vaccine formulation; while some vaccines also contain NA, this is not required. IIV are administered intramuscularly (i.m.) with or without adjuvant. IIV stimulate the generation of anti-HA Ab but are less efficient in promoting CD8 T cell responses. The vaccine production in embryonated eggs is cheap and guarantees a high yield but has the disadvantage of introducing egg-adapted mutations in the HA. To circumvent this limitation, cell culture-based vaccines have been licenced in many countries; however, they have high costs and a low production yield (Barr et al. 2018).

In the pig industry, whole inactivated virus is the most common vaccine platform, often administered with adjuvants, or in the form of autogenous vaccines. Autogenous vaccines contain an inactivated IAV isolated from the herd in which the vaccine is then administered. This immunisation platform is commonly used in the field (50% of the IAV vaccines administered in pigs in 2008) while other

commercially available IIV vaccines, such as Respiporc FLUpan, are less frequently purchased (5-25%) (reviewed in (Tchilian and Holzer 2017)). Sows are often immunised to ensure that piglets are protected by maternally derived antibodies (Vincent et al. 2008). A limitation of using IIV with an oil-in-water adjuvant is the development of VAERD in pigs infected with a mismatched strain (Gauger et al. 2011; Gauger et al. 2012; Kitikoon et al. 2012). In addition, vaccines for swine do not undergo periodic strains update, such as human, leaving the pigs at risk for novel IAV strain infections.

Live attenuated influenza vaccines

LAIV present a cold-adapted influenza virus backbone that can only replicate at temperatures lower than those found in the lung (35-37°C). Therefore, when the vaccine is administered i.n., it can replicate in the URT but not in the LRT. The temperature-sensitive backbone is complemented each year with the circulating HA and NA genes. More recently, a LAIV has become available for pigs in the United States of America (USA), with the commercial name of Ingelvac Provenza (Genzow et al. 2018). The swine LAIV backbone is the H3N2 A/swine/Texas/4199-2/98 virus, containing a deleted NS1 gene (Richt et al. 2006). Ingevac Provenza is a bivalent vaccine with HAs and NAs from old H3N2 (A/swine/Texas/4199-2/98) and H1N1 (A/swine/Minnesota/37866/1999) strains, which are not updated each year like humans vaccines. Many other experimental LAIVs were tested in pigs. For example, the porcine NS1 truncated LAIV elicited higher IgA responses in both BAL and nose than IIV. This vaccine also induced T cell responses that lasted 7-8 weeks post-administration (Kappes et al. 2012). In addition, LAIV partially protected pigs from H3N2 homologous and H1N1 heterologous challenge and prevented transmission (Loving et al. 2013; Kappes et al. 2012). In contrast to IIV, LAIVs did not develop signs of VEARD in vaccinated pigs (Vincent et al. 2012).

Mimicking natural infection, LAIV stimulate strong immune responses at the mucosal site of the URT. LAIV can induce mucosal IgA and systemic IgG and provide better cellular immunity than IIV in both humans and pigs (reviewed in (Mohn et al. 2018; Holzer, Martini, et al. 2019)). Infants immunised with LAIV, but not IIV, have high levels of IAV-specific CD4, CD8 and γδ T cells (Hoft et al. 2011). LAIV was also superior in reducing clinical signs in young children (Belshe et al. 2007). However, i.n. delivery of LAIV in adults failed to generate IFNγ secreting T cells (He et al. 2006). Compared to IIV, LAIV elicited a weaker Ab response to HA and NA in adults (Couch et al. 2012).

The disadvantage of LAIV is that it can be used only in children between 2-18 years old in Europe or up to 50 years-old in the US. The limited efficacy in adults, which limits its use in Europe to children, can be partly explained by the presence of preexisting immunity preventing vaccine replication in the nose and reducing its immunogenicity. Immunocompromised individuals cannot use LAIV as vaccine replication is more significant and may be harmful (Medical Advisory Committee of the Immune Deficiency et al. 2014). Reassortment with coinfecting IAV is a concern as this may allow the emergence of new pathogenic viruses (Zhou et al. 2016). This was observed in pigs in the US, where the Ingelvac Provenza LAIV reassorted with endemic viruses (Mancera Gracia et al. 2020).

Future vaccines against IAV

New influenza vaccine strategies are currently under pre-clinical and clinical development and include DNA-based vaccines, mRNA-based vaccines, viral vectors and virus-like particles (reviewed in (Wei et al. 2020)). Single-cycle vaccines, the focus of this thesis, have also been tested and offer several advantages. They lack a functional copy of a gene required for IAV replication, such as HA, M2, NA, or polymerases. Therefore, they can only grow when this protein is present in the environment, for

example, in cell lines expressing HA. Once delivered, they cannot replicate in the vaccinee, infecting the host's cells only once. Even if this process is limited, single-cycle vaccines can replicate their genome in the infected cells and express the vaccine's proteins in the host. Furthermore, single-cycle vaccines can generate strong T and B cell responses. With limited replication, this vaccine platform is safer than LAIV for immunocompromised individuals, and it has a lower risk of reassortment events.

S-FLU, a single-cycle vaccine candidate, is generated by suppressing the signal sequence of the HA by introducing a stop codon and deletion of a single base at position 83, impairing the expression of the protein (Powell et al. 2012). Early studies from Townsend et al. reported that lack of signal sequence of HA leads to rapid degradation of the protein, which could still be presented by MHC-I on the surface of infected cells (Townsend, Bastin, et al. 1986). A second version of S-FLU (used in this thesis) has a gene enconding eGFP in place of HA, to allow visualisation of the infected cells under UV light (Powell et al. 2012). Both versions required the presence of a cell line expressing functional HA to grow. The lack of HA did not affect the protein expression of other viral proteins such as NP and NA, expressed at similar level to wild-type PR8 virus (Powell et al. 2012). Both versions of S-FLU delivered i.n., protected mice from weight loss when challenged with homologous and heterologous viruses. S-FLU containing the HA sequence elicited HA-specific T cells, assayed by IFNγ ELISpot, but no difference in weight loss or T cells and Ab responses were presented between HA and eGFP version of S-FLU. Because HA S-FLU, despite the suppression of the signal sequence, can revert to its wild type form, eGFP S-FLU was used in subsequent studies.

S-FLU was designed to be safely delivered to the lung, because of its limited replication and lack of viable HA sequence. Lung delivery is associated with increased heterosubtypic immunity (Song et al. 2010). When LAIV was delivered to the lung, but not the URT, it effectively protected mice from

heterologous challenge (Lau, Wright, and Subbarao 2012). Nevertheless, the commercially available LAIV may be dangerous to be delivered to the LRT as viral replication may still occur. A second disadvantage that makes LAIV unsuitable for aerosol (aer). delivery is the risk of reassortment. Heterosubtypic immune responses are desirable, especially in a new pandemic, before a vaccine matched to the pandemic strain is available. LAIV induces strong cross-reactive T cell responses, but the presence of a functional HA increases the risk of reassortment and generation a potential new highly pathogenic IAV.

S-FLU, has been proven immunogenic in mice, ferrets and pigs (Holzer et al. 2018; Tungatt et al. 2018; Powell et al. 2012; Powell et al. 2019; Baz et al. 2015).

S-FLU given i.n. to mice generated a vigorous T cell response associated with markedly reduced viral titers and weight loss after homologous PR8 and heterologous H3N2 challenge. The mice developed cross-reactive T cell responses in the lung but lacked neutralising Ab in the serum (Powell et al. 2012). S-FLU coated with different H7 HAs conferred protection against heterosubtypic H3N2 infection but did not limit IBV replication (Powell et al. 2019). Neutralising Ab were only detected in the serum when S-FLU was administered i.p. (Powell et al. 2019).

S-FLU was compared to the cold-adapted LAIV in ferrets. I.n. delivery of H1 and H5 S-FLU in a prime and boost regime protected ferrets from homologous and heterologous lethal challenge, similarly to LAIV (Baz et al. 2015). In addition, ferrets immunised with a single dose of S-FLU or LAIV and challenged with homologous H1N1 virus, did not transmit the challenge virus to naïve individuals by the airborne route. Similar findings were also reported with S-FLU coated with H3 from

A/Switzerland/9725293/2013 after homologous and heterologous challenge with H1N1pmd09 (Holzer et al. 2018).

S-FLU is safe to be administered to the lung, and the pig model allowed evaluation of pulmonary delivery using a vibrating mesh nebuliser (VMN) commercially available for humans (SOLO, Aerogen ldt.). Pigs immunised by aerosol (aer.) with H1 S-FLU showed higher CD4 and CD8 responses in blood, BAL and TBLN compared to animals that received the vaccine intratracheally (i.t.) (Morgan et al. 2016). The presence of strong local T cell responses in BAL correlated with decreased nasal shedding and reduced lung pathology after homologous H1N1pdm09 challenge (Morgan et al. 2016). Pigs immunised by aer. with S-FLU did not develop neutralising Ab against the coated HA. Aer. delivery of H3 S-FLU to pigs reduced lung pathology following H1N1pdm09 challenge but, unlike ferrets, viral shedding was not reduced (Holzer et al. 2018).

These data show that the same vaccine has different protective efficacy in pigs and ferrets. In the absence of Ab, lung T cell immunity can consistently reduce disease severity but does not always abolish viral replication. It will be important to understand the reason for these differences between ferrets and pigs to determine which model is more predictive to humans. These data suggest that vaccines should be tested in more than one animal model and that the pig might be a more relevant large animal model because it is a natural host for influenza viruses and has very similar respiratory anatomy to humans.

1.5 Tissue resident memory T cells

The development of mucosal vaccines against influenza started in the 1950s. Nevertheless, their protective mechanism was elucidated only recently, when studies highlighted the distribution of T and B cells at mucosal sites (Masopust, Vezys, et al. 2001a; Reinhardt et al. 2000) Tissue resident memory

T cells (TRM) are generated at the site of pathogen entry after infection or immunisation. They originate from effector memory T cells (TEM) in circulation which enter but do not leave the mucosal sites (Masopust et al. 2010; Gebhardt et al. 2009; Teijaro et al. 2011). However, their migratory ability has been recently challenged by Fonseca (Fonseca et al. 2020). This study reported intestinal-derived TRM in circulation, that could differentiate into TCM or effector T cells upon recall, however it is not known if this migratory property is limited to a small subset of TRM. Because of their privileged location, TRM provide the first-line of defence to subsequent re-infections and conferred protection to lethal challenge in mice (Wu et al. 2014; Teijaro et al. 2011; Schenkel et al. 2013).

Identification and function of TRM

TRM have been identified in mice in lungs, nasal mucosa, salivary gland, tonsil, brain, intestine, skin and female reproductive tract (Masopust, Jiang, et al. 2001; Wakim, Woodward-Davis, and Bevan 2010; Casey et al. 2012; Thom et al. 2015; Cheuk et al. 2017). In most of the tissues above, TRM reside within the epithelial surface, patrolling the sites of pathogen entry. Their location constitutes a challenge for accurately studying the distribution and functions of this subset of T cells.

Several experimental techniques have been used to identify TRM and distinguish them from circulating T cells (Figure 1.2). Parabiotic surgery joins the blood circulation of two individuals, allowing equilibrium of lymphocytes in circulation but not of tissue resident cells (Teijaro et al. 2011; Klonowski et al. 2004; Takamura et al. 2016). A second approach uses *in vivo* labelling of circulating cells by intravenous (i.v.) infusion of a monoclonal antibody (mAb). Therefore, circulating T cells are labelled with the infused mAb, while cells that are resident in tissues outside the blood stream will not be labelled (Teijaro et al. 2011; Anderson et al. 2014; Turner et al. 2014). Another method distinguishing

circulating T cells from TRM aims to impair T cell migration pharmacologically or by antibody-mediated depletion. Administration of FTY720, an agonist of the sphingosine 1-phosphate receptors (S1PR), induces systemic lymphopenia and stops egress from the LN, therefore depleting T cells in circulation while not affecting number of TRM (Turner et al. 2014; Zens, Chen, and Farber 2016a). In humans, TRMs have also been identified after transplantation (Snyder et al. 2019).

TRM can be defined by their expression of different surface markers, although a definitive phenotype for all TRM is still debated. TRM present an effector memory phenotype ($CD45RA^{-}CCR7^{-}$ in humans or $CD44^{+}CCR7^{-}CD62L^{-}$ in mice) but can be discriminated from the circulating TEM by the expression of CD69, a marker of early activation and tissue retention, and CD103, also known as integrin αE (Steinert et al. 2015; Kumar et al. 2017). CD69 is a lectin binding to the S1PR-1; thus, it limits the responsiveness to the gradient of sphingosine 1-phosphate, a mediator of egress. Integrin αE is a receptor of E-cadherin, a tight junction protein present on epithelial cells, and it is responsible for tissue retention. However, resident CD4 and CD8 T cells, inaccessible to the bloodstream, were also reported to lack CD69 and CD103 in mice, highlighting the heterogeneity of this population (Turner et al. 2014). Other markers such as CD49a and chemokine receptor CXCR6 promote retention of TRM in tissues (Ray et al. 2004; Tse et al. 2014). In humans, programmed death (PD-1), a cell exhaustion marker, is expressed on lung, spleen, and liver TRM (Kumar et al. 2017). TRM also present a different transcriptional profile from TEM in the blood (Wakim et al. 2012; Mackay et al. 2013; Mackay et al. 2016).

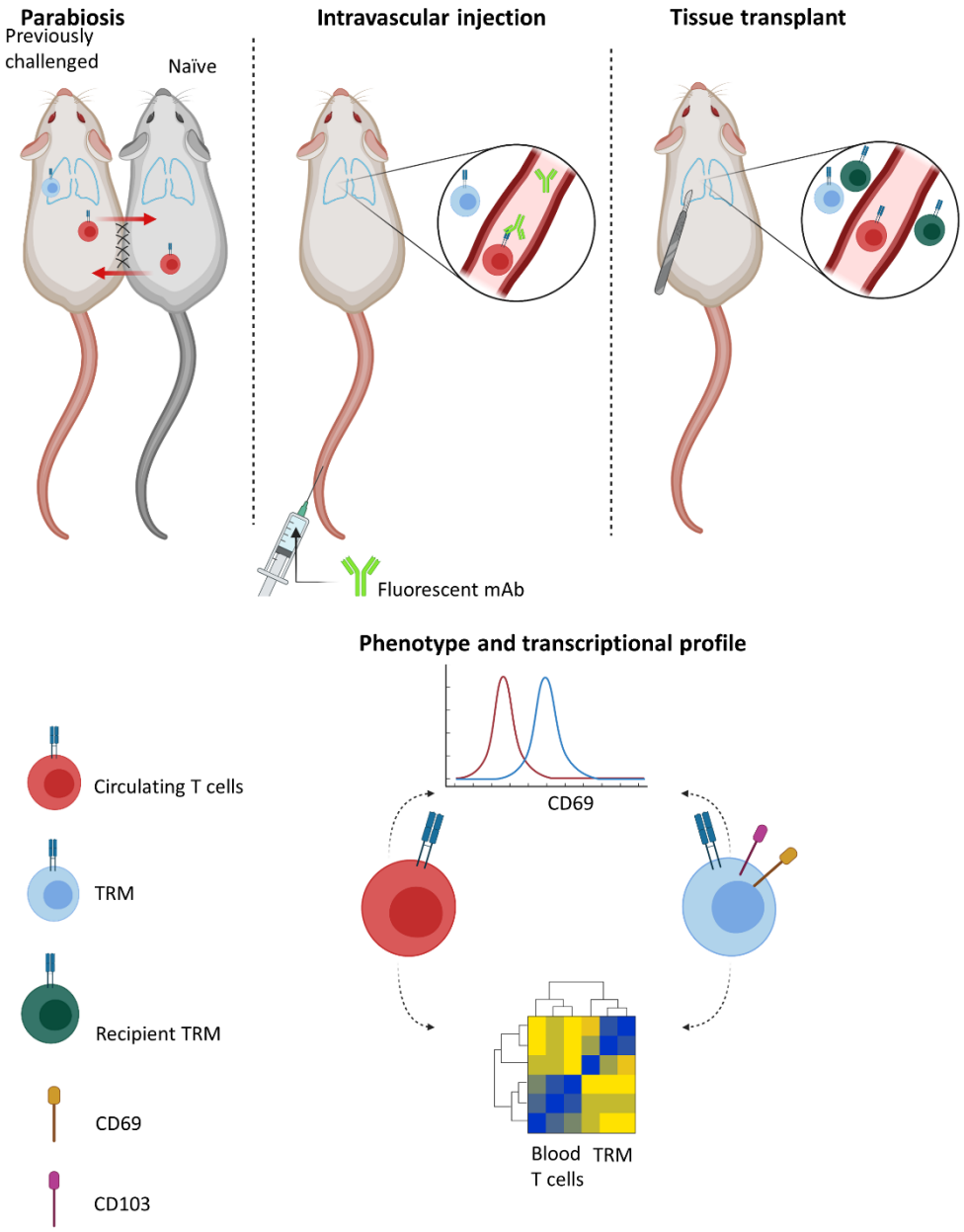

Figure 1.2 **Methods to identify tissue resident memory T cells.** Figure created with ©BioRender

Their unique localisation and functions contribute to the protective role of TRM. TRM are localised at the barrier sites, constantly exposed to pathogens, ensuring a rapid response. In the absence of TRM,

circulating memory T cells will encounter their cognate antigen in the draining LN and consecutively migrate to the site of infection, delaying the T cell response by days. In addition, TRM differ from memory T cells in circulation for their ability to rapidly secrete proinflammatory cytokines, such as IFNγ and TNF, and exhibits high expression levels of cytotoxicity-related genes (Schenkel et al. 2013; Mackay et al. 2016; Mackay et al. 2013; Kumar et al. 2017). TRM can also recruit circulating T and B cells and contribute to local DC maturation (Ariotti et al. 2014; Glennie et al. 2015; Schenkel et al. 2013).

TRM in the respiratory tract

TRM were identified in the nasal mucosa, lung airway and lung parenchyma, although their generation and maintenance differ in these tissues (Takamura et al. 2016; Pizzolla et al. 2017b) (Figure 1.3).

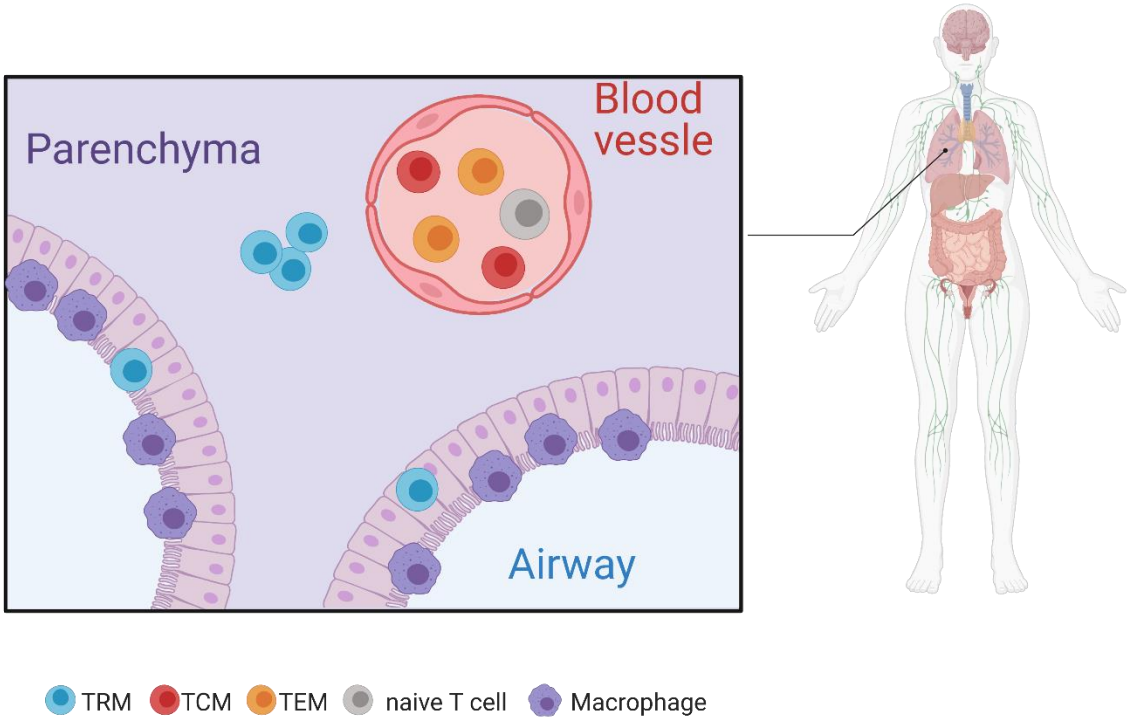

Figure 1.3 **Compartimentalisation of T cells in the lung.** Figure created with ©Biorender.

In the nasal epithelia, TRM can develop in the absence of local antigen recognition and their formation is not dependent on the TGFβ signalling pathway (Pizzolla et al. 2017b). In mice, TRM isolated from this tissue persist long after influenza infection (120 dpi) with minimal decay compared to the lung (Pizzolla et al. 2017b). In addition, this population conferred protection against rechallenge. Interestingly Pizzola and colleagues showed that nasal TRM display different immunodominance hierarchies compared to TRM isolated from the lung (Pizzolla et al. 2017b).

Generation of TRM in the lung is dependent upon the local environment and cognate antigen recognition. After initial priming in the local LN, antigen-experienced CD8 T cells migrate into the inflamed lung where they differentiate. TGFβ, secreted by epithelial cells and macrophages, is essential

for the establishment of lung TRM and their expression of CD103 (Yoshizawa et al. 2018). The persistent presence of the antigen in the lung is also required for optimal TRM formation in this organ as local inflammation alone fails to promote differentiation of circulating TEM into lung TRM (Takamura et al. 2016; McMaster et al. 2018).

TRM in the lung are localised in the airways and in the parenchyma. TRM in the airways are present in the bronchiole and alveolar space and can be isolated by broncho-alveolar lavage (BAL) with minimal blood contamination (Anderson et al. 2014). Airway TRM maintenance is dependent on T cell migration from the lung parenchyma (Ely et al. 2006). Airway TRM recovered in BAL suffer from constant exposure to oxygen, and amino acid starvation, promoting their apoptosis (Hayward et al. 2020). Nevertheless, these cells confer protection via rapid secretion of INFγ (McMaster et al. 2015).

TRM present in the lung parenchyma are more difficult to isolate as enzymatic digestion of the lung is required, but this method is not efficient in isolating all lymphocytes residing in the tissue. Due to the high vascularisation of the lung, cells isolated by digestion comprise TRM and T cells from circulation, therefore i.v. labelling of blood T cells is essential. The formation of TRM in the lung parenchyma has been the subject of several studies and two models have been postulated (Takamura et al. 2016). One model hypothesises that lung TRM are replenished by low-level migration to the lung of circulating TEM. The absence of antigen, cleared after infection, in addition to TEM differentiation into TCM, impairs homing of these cells to the lung in the long term (Ely et al. 2006; Slutter et al. 2017). A second model postulates that lung TRM are formed in the draining LN, and migrate to the site of lung damage and then the airways. Parabiosis studies corroborate this theory showing that TRM establishment in the lung occurs up to 10 days post IAV challenge, and cells recruited from the circulation failed to become TRM (Takamura et al. 2016).

The route of antigen administration and the presence of local inflammation is essential for lung TRM formation after immunisation. LAIV administered i.m. fails to generate TRM and equally i.n. administration of IIV does not elicit lung TRM formation (Zens, Chen, and Farber 2016a). Similarly, mucosal but not subcutaneous administration of Bacillus Calmette–Guérin vaccine (BCG) stimulated lung TRM development in mice (Perdomo et al. 2016). Nevertheless, Darrah and colleagues reported TRM formation in the lung of macaques after i.v. BCG vaccination (Darrah et al. 2020), most likely because BCG is a live vaccine and enters the lung. Moreover, the establishment of CD8 TRM in the airways is dependent on migratory $CD103^+$ DCs (Iborra et al. 2016). This antigen cross-presentation is best achieved with vaccines containing genetic materials, such as LAIV, DNA and mRNA vaccines, that stimulate the production of the vaccine proteins in host cells. Peptide or protein-based vaccines will require a mucosal adjuvant that enhances this process. If vaccines with genetic material delivered to the LRT can more easily generate TRM, the long-term maintenance of this population might require additional precautions. The initial number of TRM can influence the duration of the vaccine-induced protection (reviewed in (Schmidt and Lapuente 2021)). The addition of inflammatory agents, such as IL-1β, to the vaccine can increase the induction of TRM (Lapuente et al. 2018). A second strategy consists in repeated mucosal immunisations. Van Braeckel-Budimir demonstrated that CD8 TRM present in the lung of mice after four consecutive challenges with IAV survived for longer than CD8 TRM generated after a single exposure (Van Braeckel-Budimir et al. 2018). Repeated infections may also improve the ability of circulating T cells to reach the lung parenchyma and differentiate into TRM. A third approach utilises heterologous prime-boost or simultaneous parental and mucosal immunisation, previously reported to generate durable heterosubtypic protection (Uddback et al. 2016).

If the mechanisms of TRM entry and maintenance in the lung are still debated, their role in respiratory infection is well established. Adoptively transferred lung TRM isolated from previously exposed mice migrated back to the lung and improved survival after IAV challenge in recipient mice, while TEM isolated from the spleen failed to do so (Teijaro et al. 2011). Wu et al. demonstrated a correlation between the number of lung TRM and viral clearance during heterosubtypic infection (Wu et al. 2014). In addition, human challenge studies with respiratory syncytial virus (RSV) demonstrated a correlation between preexisting lung TRM and reduced symptoms and viral load however their longevity was not established (Guvenel et al. 2020; Jozwik et al. 2016). Nevertheless, their persistence is still questioned. Seven months after the first exposure with IAV, murine lung TRM declined significantly (Wu et al. 2014; Slutter et al. 2017) while repeated exposure improved their durability (Van Braeckel-Budimir et al. 2018). Takamura postulated that the presence of lung TRM in the parenchyma is associated with local inflammation and tissue regeneration, present only for a limited period (Takamura et al. 2016). In addition, TRM present in the alveolar space expressed a high level of annexin V, a marker of apoptosis (Hayward et al. 2020). In humans, the lifespan of lung TRM was evaluated after lung transplants (Snyder et al. 2019). TRM from the donor were isolated up to 15 months after transplant in the recipient, however, future studies will need to follow up lung TRM for longer. A recent study with lung tissues isolated from individuals ranging from 22-68 years of age reported the decline in the number of CD8 T cells with age (Nguyen et al. 2021). The TRM population appeared to be the most affected by the age-associated reduction. This resulted in a reduction of IFNγ secreting CD8 T cells after IAV infection of the lung tissue isolate. Lung TRM limited duration is probably a consequence of the harsh environment of the lung, although repeated antigen exposure could increase their lifespan (Van Braeckel-Budimir et al. 2018).

Murine CD4 and CD8 TRM in the lung confer protection against respiratory pathogens such as influenza virus, respiratory syncytial virus, *Mycobacterium tuberculosis* and *Bordetella pertussis* (Teijaro et al. 2011; Wu et al. 2014; Morabito et al. 2017; Sakai et al. 2014; Wilk et al. 2017). However, their role in large animal models such as the pig is less well understood. Identification of porcine TRM by an anti-CD3 mAb infusion confirmed that BAL T cells are TRM, while a smaller proportion (39%) of TRM was identified in the lung parenchyma of pigs immunised with S-FLU by aer. (Holzer et al. 2018). This study was limited to the detection of lung TRM but the specificity of CD3 i.v.$^{-}$ T cells was not investigated. In addition, the phenotype and functions of porcine TRM are yet to be established after influenza virus infection.

1.6 Respiratory immunisation

Despite an expanding knowledge on the role of mucosal immunity and TRM, only a few vaccines have been approved for delivery to the RT (reviewed in (Miquel-Clopes et al. 2019)). The majority of vaccines are delivered by injection with related safety and compliance issues, especially in developing countries. Logistics and cost of mass immunisations with injected vaccines are also challenges, as we have recently experienced during the COVID-19 pandemic. Vaccines targeting the RT can be delivered fast, safely and needle-free, efficiently stimulating local immune responses. Potential difficulties in the development of respiratory immunisation are the delivery system, deciding which part of the RT to target, and the limited availability of mucosal adjuvants.

Delivery systems

The delivery system needs to generate small liquid or solid particles of the vaccine formulation and ensure deposition in the RT. Aerosol can be generated from solid particles or liquid droplets in suspension in the air. Solutions can be administered by aerosol using nasal spray or nebulisers, while passive or active dispensers deliver dry powders. Solid aerosolised vaccines tested preclinically comprise inactivated viruses or subunit vaccines (reviewed in (Bahamondez-Canas and Cui 2018)). Liquid formulations can also deliver viruses and live attenuated vaccines, the focus of this thesis.

Nasal sprays are routinely used for influenza vaccination, where aer. is manually generated from a syringe attached to a conical nosepiece (Food and Drug Administration 2020; European Medical Agency 2013). A similar device, mucosal atomisation device (MAD), has been employed to administer LAIV and IAV to pigs (Holzer et al. 2018; Hemmink et al. 2016; Holzer, Morgan, et al. 2019). MAD can deliver a volume as small as 0.1ml, with droplets ranging from 30 to 100 μm in diameter (Teleflex) (Figure 1.4).

Nebulisers generate aer. by ultrasonic waves (ultrasonic nebulisers), rapid vibration of a mesh (VMN) or injection of compressed air in the liquid preparation (jet nebulisers (jet-neb)). The aer. generated from these devices contains mainly small droplets of 5-3 μm size (Arı 2014). The ultrasonic waves produced during aerosolisation cause protein aggregation and make ultrasonic nebulisers unsuitable for vaccine administration (Hertel, Winter, and Friess 2015). On the other hand, VMN and jet-neb have been used in vaccine efficacy clinical trials (Satti et al. 2014; Low et al. 2015) (Figure 1.4). Jet-neb requires a volume of 4-5ml for optimal delivery due to high residual volume (0.5-2 ml), under which aerosolisation is not possible (reviewed in (Arı 2014)). On the other hand, VMNs present minimal residual volume.

VMNs are also more time-efficient and can deliver a higher dose to the lung, although they are more expensive than jet-neb (ElHansy et al. 2017).

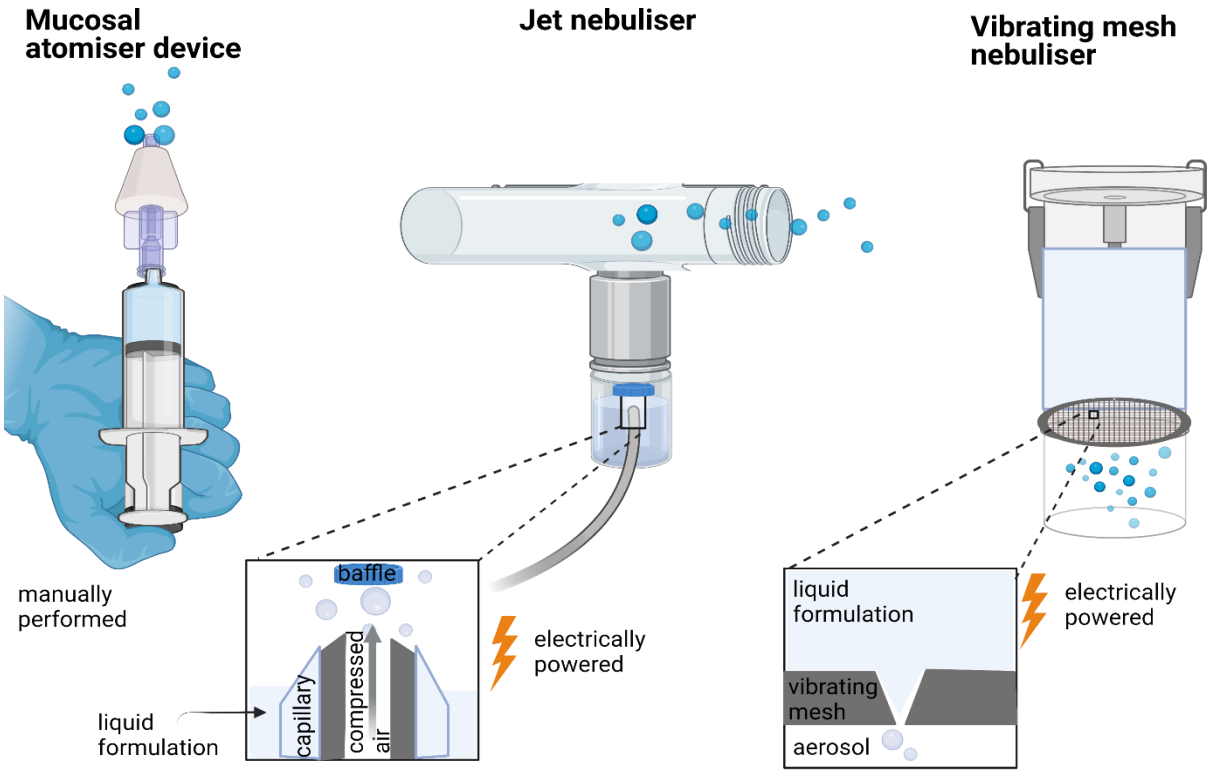

Figure 1.4 **Devices suitable for administration of liquid formulation vaccines to the respiratory tract.** On the left: the MAD device is activated by manual pressure at the bottom of the syringe, a soft conical plug is position in the nose of the vacinee while the liquid is aerosolised by a small atomizer at the top of the cone. In the centre: jet-nebuliser is activated by electric power. A flow of compressed air is put in contact with the vaccine forumation. A baffle ensure that only small dropelts can reach the tube connecting the device to the vacinee. On the right: vibrating mesh nebuliser (VMN). The VMN converts the electric power in vibration of a mesh positioned below the liquid formulation, generating an aerosol.

Currently, there are no commercially available devices designed to reliably target the LRT in livestock animals. Lung delivery is therefore achieved by i.t. or endobronchial instillation, both procedures require sedation or anaesthesia. Ideally, the device should be fast and practical for use by farmers.To limit the

dispersion of the aerosolised drug or vaccine, aer. devices for human use are attached to a mask. Masks for use in veterinary settings are commercially available for dry powder inhaled medications for feline, canine and equine (https://www.trudellanimalhealth.com/). The masks needs to provide correct fitting to the animal anatomy, therefore they will need to be adjusted according to the age. In addition, optimal aer. administration requires cooperation from the animals, a challenge considering the animal's stress when wearing a mask.

The success of vaccine delivery to the RT relies on an optimised combination of device and formulation. However, it is important to note that current regulations do not consider the vaccine and the delivery device as a whole entity. Aer. generating devices may deliver different doses to the vacinee's lung, limiting the efficacy if different "general purpose" nebulisers are used. This consideration is also crucial for preclinical studies, where devices and volume are often adjusted to the animal model without necessarily an understanding of the implications. Further, should an aerosolised vaccine be successfully developed, and commercially launched, it would be key that those administering the vaccine subsequently should adhere to protocols established in the Phase 3 trial. for consistency of dosing, post-aerosolisation compatibility, and compliance with how the Phase 3 trials were conducted, that this optimised combination be made available.

Targeting different regions of the RT

Particles size influences the delivery by aer. to the RT, with particles <5 μm reaching the lung, while bigger particles are trapped in the URT (nasal cavity, larynx and pharynx). To limit the deposition to the URT, nasal spray such as MAD device are used as their droplet size is > 5μm while nebulisers produce smaller particles that can reach the lung (Figure 1.5).

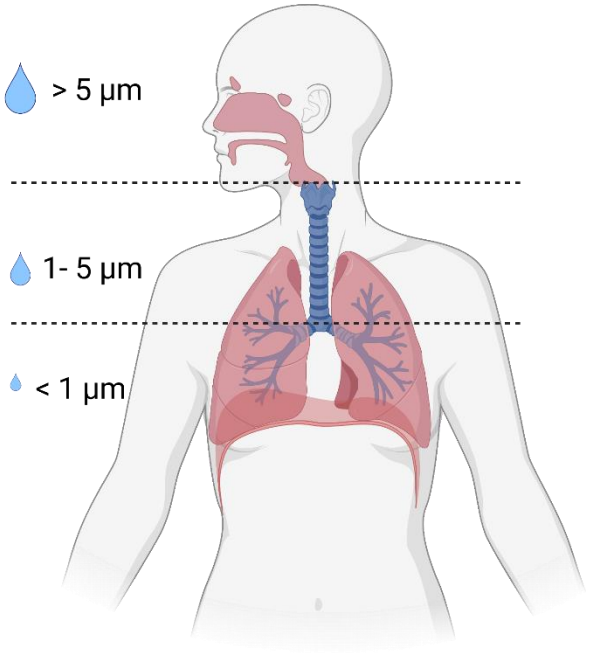

Figure 1.5 **Schematic representation of droplets deposition in different areas of the respiratory tract**

The different abundance of immune and epithelial cells in the different regions of the RT should also be taken into account when choosing a device. The upper bronchi are populated by both DCs and macrophages, while alveolar space contains predominantly macorphages (Holt 2000). DCs are fundamental in antigen presentation and the induction of adaptive immune responses, while macrophages are an essential first-line defence (Blank et al. 2011). The presence of cells expressing receptors for the virus also differs between URT and LRT. For instance, α2,3-linked sialic acids are abundant in the human lung, while α2,6 are more common in the URT. Due to its high vascularity, aerosol-delivery to the lung reaches the circulation. Therefore, aer. delivery induces much greater local and systemic immune responses than i.n. delivery (Song et al. 2010; Hemmink et al. 2016). In addition,

only LRT immunisation can generate lung TRM, protective against *M. tuberculosis* challenge (Ronan et al. 2009; Ronan et al. 2010).

I.n. delivered LAIVs vaccines are commercially available for humans, pigs and horses (Flu Avert, Merck Animal Health, US). Other i.n. delivered vaccines approved for animal use comprises a canine vaccine against *Bordetella bronchiseptica* and parainfluenza virus for use in dogs (Nobivac KC, MSD Animal Health) and two vaccines for use in cattle, one against infectious bovine rhinotracheitis virus (Tracherine, Zoetis UK Limited) and a second one for bovine parainfluenza and bovine respiratory syncytial virus (Rispoval RS + PI3, Zoetis UK Limited). However, aerosolised vaccines have yet to be approved. Sabin first proposed aer. immunisation in 1980s with two successful measle vaccine studies in children (Sabin 1983; Sabin et al. 1983; Sabin et al. 1984). Aer. vaccination is widely used in the livestock industry to immunise poultry against Newcastle disease by spraying the vaccine on the flocks (Villegas and Kleven 1976). Early studies in pigs delivered vaccines against *Mycoplasma hyopneumoniae*, *Actinobacillus pleuropneumoniae* by aer. using *ad hoc* generated systems (Hensel et al. 1996; Murphy et al. 1993). Recently VMN and jet-neb were tested in pigs, using a customised mask, to delivered influenza vaccine candidates (Morgan et al. 2016; Holzer et al. 2018). However, the distribution of particles in the porcine RT, which may be important for the induction of immune responses, remains unknown.

1.7 Aims of the thesis

Pigs are natural hosts of IAV and share physiological and immunological similarities with humans, making them an excellent model for studying immunity to IAV. However, the lack of tools to study

cellular responses is a challenge to fully understand the breadth, kinetics and functionality of responses. Porcine TRM have been identified in the lung, but their specificity or functions are yet to be established after IAV infection. It is also unclear if porcine TRM have a similar phenotype and transcriptome to those of mice and humans. Local immunisation is fundamental for the generation of TRM. However, antigen distribution in the RT of pigs following experimental challenge or mucosal immunisation has not been fully characterised. This thesis therefore aims to identify the phenotype and functional properties of porcine respiratory TRM, following IAV infection and to compare different means of respiratory delivery. Finally, this thesis investigates how optimally to immunise with novel single-cycle influenza vaccines.

In summary, the aims of thesis are:

- To characterise the phenotype, function, and gene expression of porcine TRM after IAV H1N1pdm09 challenge
- To evaluate deposition of particles after i.n. and aer. administration with MAD and VMNs.
- To compare the immunogenicity of novel single-cycle vaccine candidates and the role of the route of administration in protection against IAV infection.

Chapter 2
Materials and Methods

2.1 Reagents

Table 2.1 List of reagents

Reagents	Supplier/details
Cell culture	
DMEM high glucose	Sigma-Aldrich D5796
CD hybridoma media	Thermo Fisher 11279023
HT Supplement (100X)	Thermo Fisher 11067030
L-glutamine	Sigma-Aldrich G7513
Penicillin + Streptomycin (P/S)	Sigma-Aldrich P0781
1M HEPES Buffer	Sigma-Aldrich H0887
Foetal bovine serum (FBS)	Life Science Production S-001A-BR
Bovine serum albumin (BSA)	Sigma-Aldrich A7906
EDTA	Sigma-Aldrich E6758
Recombinant mouse IL-6	Thermo Fisher RMIL6I
Phosphate buffered saline (PBS)	Cell Culture Unit, The Pirbright Institute
DMSO	Sigma-Aldrich 276855
D10	DMEM + 10% heat-inactivated FBS + 10% HEPES + 10% P/S

Virus growth medium (VGM)	DMEM + 10% BSA + 10% HEPES + 10% P/S
Hybridoma media	CD media + 10% HT supplement + 20% L-Glut + mouse IL-6 + 10%P/S
Freezing media	DMSO + 10% heat-inactivated FBS
Tissue processing	
BAL collecting medium	PBS + 10% FBS (replaced by BSA if animals are infected)
RPMI-1640	Sigma-Aldrich R8758
R10	RPMI + 10% heat-inactivated FBS + 10% HEPES + 10% P/S
Blood collecting tubes – Vacutainer with heparin	Centaur Service 30236356
Serum collecting tubes – Vacutainer	Scientific Laboratory VC367895
Histopaque 1083	Sigma-Aldrich 1083
RBC lysis buffer (10X)	BioLegend 420301
Collagenase, type IV	Sigma-Aldrich C5138
DNase I	Sigma-Aldrich D5025
Dispase	Sigma-Aldrich D4693
Lung digestion medium	RPMI + 0.7mg/ml Collagenase + 0.05mg/ml DNAse
URT digestion medium	RMPI + 2mg/ml Collagenase + 0.1mg/ml DNase I + 0.1/mg/ml Dispase
Cell strainer 100 μm	Falcon 352360
Cell strainer 70 μm	Falcon 352350
Flow Cytometry	

FACS buffer	PBS + 2% heat-inactivated FBS + 2mM EDTA
Paraformaldehyde solution 4% in PBS	Santa Cruz 30525-89-4
1-step Fix/Lyse Solution (10X)	Thermo Fisher 00-5333-54
Cytofix/Cytoperm Fixation/Permeabilization Kit	BD Biosciences 554714
True-Nuclear™ Transcription Factor Buffer Set	Biolegend .424401
Mouse serum	
PMA Ionomycin - Cell Stimulation Cocktail (500X)	Thermo Fisher 00-4970-03
Protein kinase inhibitor (Dasatinib)	Axon Medchem BMS 354825
RNA-sequencing	
PicoPure RNA Isolation Kit	Thermo Fisher KIT0202
TURBO DNA-free Kit	Thermo Fisher AM1907
ELISpot	
MultiScreen-HA plates	Merk MAHAS4510
ConA	Thermo Fisher C860
Virus growth and serological assays	
Fetuin	Sigma-Aldrich F3385 (25 μg/ml solution in PBSA + 0.2% sodium azide)
PNA-HRP (peanut agglutinin conjugated to horseradish peroxidase)	Sigma-Aldrich L7759 (1 μg/ml solution in PBS + 0.1% BSA)
Carbonate-Bicarbonate (CB) Buffer	Sigma-Aldrich C3041
Trypsin, TPCK-Treated	Sigma-Aldrich 4370285

Sodium bicarbonate solution (7.5%)	Sigma-Aldrich S8761
Medium 199 (10x)	Sigma-Aldrich M0650
EMEM (10x)	Sigma-Aldrich M0275
DEAE-Dextran	Sigma-Aldrich 80881
Agarose	Sigma-Aldrich A9045
Nystatin	Sigma-Aldrich N9150
Plaque assay overlay media	10% EMEM(10x) + 10% P/S + 0.2%BSA + 10% HEPES + 0.5% dextran + sodium bicarbonate + 0.66% agarose + TPCK trypsin 2μg/ml in water
Virus transport media	10% Medium 199 + 10% HEPES + 10% P/S + 2.5% nystatin + 0.5% sodium bicarbonate +0.5% BSA in water

2.2 Animal experiments

Ethics statement

Animal experiments were conducted according to the UK Government Animal (Scientific Procedures) Act 1986 at the University of Bristol, The Pirbright Institute (TPI), the Animal and Plant Health Agency (APHA) and the University of Nottingham under project license P47CE0FF2, with approval from Animal Welfare and Ethical Review Bodies at each institute. All institutions conform to the Animal Research: Reporting of *In Vivo* Experiments (ARRIVE) guidelines. The inbred Babraham pigs (Signer et al. 1999; Schwartz et al. 2018) were bred at APHA following FELASA recommendations (Berset Convenor et al. 2021). Animals were pre-screened to ensure the absence of exposure to influenza viruses

(pandemic H1N1, H2N2, H3N2 and avian-line IAV strains) by haemagglutination inhibition test. The pigs (female and male) were randomised and acclimatised for at least 7 days before any procedures were carried out.

Influenza time course studies

Four influenza challenge experiments were performed: three took place at the University of Bristol (T1, T2 and T3), as previously reported (Edmans et al. 2020), while a more extended time-course study (T4) was performed at APHA (Figure 3.4). 38 Babraham inbred pigs (9.3 weeks old on average) were experimentally infected i.n., using a mucosal atomisation device (MAD) (MAD300, Wolfe-Tory Medical), with 1×10^7 PFU of H1N1 A/swine/England/1353/2009 (H1N1pdm09), 2ml per nostril. During T1 and T2, one infected pig was culled each day on days 1 to 7, 9, 11 and 13 post-challenge while uninfected control pigs were culled before infection (day -1, n=2) and at day 8 (n=2). In the T3 study, 3 challenged animals were culled at days 6, 7, 13, 14, 20 and 21 post-infection. Six control uninfected animals were included in T3: three culled on day -1 and the other three on the challenge day. In T4, 12 pigs (10.2 weeks old on average) were challenged as described above and four pigs were randomly culled at each of day 21, 42 and 63 post-infection.

FTY720 pilot study

The FTY720 study was performed at TPI. Eight weeks old Babraham pigs received 1mg/kg of FTY720 (Sigma-Aldrich, SML0700) in a capsule (n=2) or suspension with a juice (n=2). One animal was left untreated as a control. Blood samples were collected 0, 7, 24, 48, 72 and 96 h post-administration. Pigs were then culled four days after administration, and tissues were collected post-mortem.

Scintigraphic study

The scritingraphic study was conducted at the University of Nottigham under PPL 30/3350 as previously described (Martini et al. 2020). In brief, three Landrace x Hampshire cross female pigs were obtained from a commercial herd at six weeks of age. A cocktail of sedatives was used before administration of radioactive formulation (Zoletil at 4.4mg/kg, Tiletamine with Zolazepam; Virbac, UK and 0.044 mg/kg Domitor, Medetomidine, Orion Pharma, Finland). The sedated animals were positioned prone on a table during the administration, with a 40° angle between head and neck. The radioactive solution contained technetium (^{99m}Tc) complexed with diethylenetriaminepentaacetic acid (DTPA) (^{99m}Tc-DTPA) and was provided by the Radiopharmacy Unit, University of Nottingham. Animals received the radioactive material by aerosol using a small or medium droplet size VMNs or i.n. by MAD in a crossover design (Figure 4.3). One ml containing approximately 30 mega-becquerel (MBq) of ^{99m}Tc-DTPA in 0.9% saline was administered by aer. in 1 ml volume while a 1 ml solution containing 5 MBq was delivered i.n. in each nostril. Mediso X-ring gamma camera fitted with a Low Energy General Purpose collimator (Mediso Medical Imaging Systems, Hungary) was used to record the pigs' lateral, anterior and posterior images, right after the delivery. A four-day washout window between each experimental leg ensured the absence of residual radioactivity. Radioactive anatomical markers were applied to ensure optimal *post hoc* image reconstruction.

S-FLU and CLEARFLU studies

The pilot experiment comparing S-FLU and CLEARFLU (generated and kindly provided by Professor Alain Townsend) was performed at TPI. Two groups of three Babraham pigs of 5.5 weeks of age were sedated and immunized by aer. with H7N1 S-FLU [eGFP/N1(PR8)] H7t(Netherlands/219/2003) (2.4 ×

10^8 50% tissue culture infective dose (TCID50) or H7N1 CLEARFLU expressing H1 [(H1CFv2(England/195/2009)/N1(PR8)] with H7(Netherland/219/2003) as coating (1.3×10^8 TCID50). Two unimmunsed animals were used as control group. Immunised pigs were boosted after three weeks as described above and culled three weeks post boost. Ten minutes (min) before sacrifice, animals were infused intravenously (i.v.) with 1mg/kg of anti-CD3 monoclonal antibody (mAb) (clone PPT3), produced in house, to label circulating T cells.

A second pilot experiment tested S-FLU immunisation by intramuscular injection and was performed at APHA. Four Babraham pigs received H7N1 S-FLU [eGFP*/N1(Eng195)].H7(A/Neth/219/2003*t) (3×10^9 TCID50) in 4 ml delivered i.m. in the trapezius muscle behind the ear. The pigs were boosted three weeks post priming and culled three weeks later. Blood was collected weekly during the study.

A third study compared S-FLU i.m., aer. and simultaneous aer. and i.m. (SIM) immunisation (Martini et al. 2021). Babraham inbred female and male pigs were randomised and assigned to four groups of 6 animals as follows: 1) S-FLU by aer.; 2) S-FLU immunised i.m.; 3) a third group was immunised simultaneously i.m. and by aer. with S-FLU (SIM) and 4) unimmunized control group. Two pigs reached their humane end points due to heart conditions unrelated to the procedures, leaving control and i.m. group with five animals. All the animals were sedated prior immunisation with a cocktail of Zoletil (4.4mg/kg, Virbac) and Domitor (0.044mg/kg, Orion Pharma). Aer. administration was performed using a small droplet size VMN (Aerogen Solo, Aerogen Ltd.) attached to a custom-made veterinary mask (Holzer et al. 2018). Two ml of S-FLU containing 7×10^7 TCID50 S-FLU were administered by aer. I.m. pigs received the vaccine stock diluted to a final volume of 4 ml containing 7×10^7 TCID50 and 2 ml were administered as described above. SIM group received 2 ml containing 3.5×10^7 TCID50 S-FLU by aer. and 3.5×10^7 TCID50 S-FLU delivered in 4 ml i.m.. The animals were boosted similarly

three weeks later. All groups were challenged three weeks after the boost with 2.8×10^6 PFU of H1N1pdm09 i.n. with MAD (MAD300, Wolfe-Tory Medical). For logistical reasons, the challenge was performed in 2 different days so that half of the animal in each group were challenged on day 23 post-boost and the remaining half on day 25 post boost. Animals were culled at day 4 post-challenge. During the second cull, 1 mg/kg of anti CD3 purified mAb (PPT3 clone, produced at TPI (Section 2.4)) was infused i.v. to the pigs, 10 min prior to sacrifice. Since no difference was found in analyses of the samples challenged on different days, the results are presented together.

Gross and histopathological analysis were performed by Dr. Alejandro Nunez at APHA as previously described (Morgan et al. 2016; Holzer et al. 2018). Briefly, post mortem pictures of the lungs were taken and scored blindly by the pathologiest for macroscopic lesions (Halbur et al. 1995). The percentage of lung surface with lesions was calculated by digital image analysis (Nikon NIS-Ar software). Lung biopsys were subsequently taken from each lobe and stored in 10% formalin. Fixed samples were paraffin wax embedded, sectioned and stained with haematoxylin and eosin (H&E). 4 µm tissue sections were then stained for IAV NP as previously descibred (Vidana et al. 2014). The Iowa score, measuring histopathological changes, was blinded calculated by the pathologist following a method previously reported (Gauger et al. 2012).

2.3 Tissue sampling

PBMC and serum

Heparinised peripheral blood was diluted 1:1 in PBS. The diluted blood was then layered over histopaque and centrifuged at 800 × *g* for 25 min with the brake-off. Cells were collected at the interface, washed with 50 ml of PBS, and spun at 500 × *g* for 5 min (this step will be referred to as "washing step") before red blood cell lysis with 5ml of RBC lysis buffer. After two further washing steps, cells were re-suspended in R10 and counted with a hemocytometer. Cells were then centrifuged at 700g for 5 min, resuspended at a concentration of 2-4 × 10^7 cells/ml in freezing media, and stored in liquid nitrogen.

Serum was isolated from vacutainers by centrifugation at 2000 × *g* for 10 min and stored at -80° C.

BAL

BAL cells and fluid were isolated from the right lung lobes filled with 100 ml of BAL collecting medium, after massaging. This step was repeated twice so that the final volume used for the washing was 200 ml while the collected volume ~ 50 ml. BAL cells and fluid were then centrifuged at 500 × *g* for 5 mins. The supernatant was aliquoted and stored at -80° C while the cell pellets was washed, RBC lysed, and stored as described above.

Lung, nasal turbinates and trachea

A biopsy of the lung was taken and finely cut into pieces. The lung pieces were incubated with 7 ml of lung digestion medium for 2 h at 37° C in a shaking incubator. The digested lung was then placed in

R10 and mashed with the plunger of a syringe. Isolated cells were filtered through a 100 μm cell strainer and subsequentially centrifuged, layered on Histopaque, red blood cells lysed and stored as described above.

Trachea and NT were separated from cartilage with tweezers and digested for 2 h at 37°C in URT digestion medium. Tissues filaments were then processed as the lung.

Nasal swabs (one per nostril) were taken daily (up to 10 dpi in T1-T4 study, 5 dpi in the SIM study) following infection and placed in virus transport medium. Nasal samples were then vortexed, centrifuged at 700 × *g* for 5 min and aliquoted and stored at -80°C.

Spleen, tonsil and lymph nodes

A spleen biopsy was placed into gentleMACS™ Octo Dissociator, in C Tubes (both from Miltenyi Biotec) in R10 and disassociated. The dissociated tissue was filtered through a 100μm cell strainer, centrifuged, washed, layered on Histopaque and red blood cell lysed as described for PBMC isolation.

Tonsil and LN were finely cut into small pieces and mashed with the plunger of a syringe. The cells obtained were then processed as for spleen.

2.4 Production of anti-porcine CD3 mAb

PPT3 hybridomas (TPI) was cultured in hybridoma media. The supernatant was harvested every four days and diluted 1:2 with binding buffer (200mM sodium phosphate dibasic, 200mM sodium phosphate monobasic, 5M sodium chloride (all from Sigma-Aldrich) in water). The diluted supernatant was sterile filtered. An HiTrap Protein G HP antibody purification column (Cytival Life Science) was connected to a Model EP-1 Econo pump (Bio-Rad) and preconditioned with 50 ml of binding buffer at a selected

speed of 1.5 ml/min. The diluted hybridoma supernatant was then loaded onto the column. The column was then washed with 50 ml of binding buffer. The bound mAb was eluted with an acid glycin solution (0.1M glycine, pH 2.4-2.7) and collected in TRIS (pH8). The mAb solution was then dialysed (in a Slide-A-Lyzer™ Dialysis Cassettes, 10K MWCO, 12 ml, Thermo Fisher) in PBS with stirring overnight. The mAb solution in PBS was sterile filtered before the administration into the animals.

2.5 Flow cytometry

Tetramer staining

Biotinylated NP epitope-loaded SLA monomers (kindly provided by Professor Andrew Sewell), were freshly assembled into tetramer with streptavidin conjugated with PE, BV421 or BV650 (all from BioLegend) as previously described (Tungatt et al. 2018). The assembled tetramers were diluted in PBS and 0.05 μg/μl.

Frozen cells were thawed, washed in PBS and resuspended in R10. Two million cells were then seeded in a 96 well U bottom plate in duplicates (BAL, trachea, NT) or triplicates (lung, TBLN, tonsil) or quadruplicates (PBMC, spleen) according to the sample used. Cells were incubated with 50 μl of a 50 nM solution of protein kinase inhibitor in PBS and incubated at 37°C for 30 min. Tetramers (0.15 μg) were then added to the cells and incubated at 4°C for 30 min. Next, cells were washed with PBS and centrifuged for 2 mins at 700 × *g*. Surface or intracellular staining was then performed.

Surface staining

Two million cells were stained with 50 μl of fluorochrome-conjugated and unconjugated Ab mix (Table 2.2) at pre-determined optimal concentrations and LIVE/DEAD™ Fixable Near-IR (Thermo Fisher), an

amine-reactive dye that labels dead cells, diluted 1:500. When required fluorochrome-conjugated secondary Abs were used. Following this incubation the sedondary Ab binding sites were blocked with mouse serum (20% solution in PBS) prior to addition of other conjugated Ab. Staining steps were performed at 4°C for 20 mins, cells were then washed twice with 100 µl of PBS and centrifuged at 700 × *g* for 2 mins. Subsequently, the samples were fixed with 100 µl of a paraformaldehyde solution 4% in PBS at 4°C for 15 min. Cells were washed and resuspended in PBS for flow cytometer acquisition by LSRFortessa (BD Biosciences) or further intracellular staining. Data were analysed using FlowJo v10 (TreeStar).

Intracellular cytokine staining

Two million cells were seeded and stimulated with virus or vaccine at multiplicity of infection (MOI) of 1 in 200 µl of R10. Unstimulated wells were used as negative control and a phorbol 12-myristate 13-acetate (PMA)/Ionomycin cocktail was added as a positive control for the staining. The cells were stimulated with virus or vaccine overnight at 37°C or with PMA/Ionomycin was added for 6 h. Golgi Plug (BD) was then added at 1:1000 for the final 5 h of the stimulation before surface staining. Cells were stained for surface makers as described before. A fixations/permeabilisation step was then performed using Cytofix/Cytoperm (BD Biosciences) following manufacturer's instructions. Fixed cells were then stained with a 50 µl Ab mix (Table 2.2) in Permeabilisation Buffer (BD Biosciences) for 20 min at 4°C, cells were washed and resuspended with PBS for flow cytometer acquisition. Boolean gating in FlowJo v10 was used for data analysis.

Transcription factor staining

Transcription factors were stained using True-Nuclear™ Transcription Factor Buffer Set (BioLegend) as per manufacturer's instructions. Two million cells were surface stained as described above and fixed with Fixation/Permeabilisation Buffer for 60 minutes at room temperature. After washing with Permeabilisation Buffer, the cell suspension was further stained with 50 µl of Ab mix (Table 2.2) in Permeabilisation Buffer and incubated for 30 min at 4°C. The cells were then washed and resuspended in PBS prior to acquisition.

Cell sorting and depletion

To analyse the ability of different CD8 subpopulations to secrete cytokines, cryopreserved PBMC from naïve Babraham pigs were first stained for CD8β, CD45RA and CCR7 expression and sorted into 4 subpopulations ($CD45RA^{+}CCR7^{+}$, $CD45RA^{+}CCR7^{-}$, $CD45RA^{-}CCR7^{+}$, $CD45RA^{-}CCR7^{-}$) using the FACSAria™ III Sorter (BD Biosciences). Cells were then centrifuged at 500 × *g* for 5 min, re-suspended in R10 and incubated overnight at 37°C. On the following day, CD8 T cells were stimulated with PMA Ionomycin (BioLegend) for 2, 4 and 6 h, and cytokines detected by intracellular cytokine staining as described above, unstimulated cells were used as a control.

In order to isolate DFE^{+} CD8 T cells from different tissues, cryopreserved cells were first surface stained with anti-CD14 PE and anti-CD172a PE mAb in FACS buffer. The cell suspension was then washed and incubated with anti-PE beads (Miltenyi Biotec) for 15 min. PE labelled cells were then depleted using an LD magnetic column (Miltenyi Biotec) according to manufacturer's instructions. The remaining cell suspension was labelled with DFE tetramer and surface stained for CD3, CD8β, CD4

and Live/Dead. $DFE^{+}CD3^{+}CD8\beta^{+}$ cells were then sorted with FACSAria™ III Sorter (BD Biosciences) and processed for RNA-sequencing.

Table 2.2 List of mAbs used for flow cytometry

Antigen	Clone	Isotype	Fluorochrome	Source of primary Ab	Details of secondary Ab
CD3	PPT3	IgG1	PerCP Cy5.5	In house purified	Thermo Fisher
CD3	PPT3	IgG1	FITC	In house purified	Bio-Rad Laboratories
CD3	PPT3	IgG1	APC	Southern Biotech	
CD4	74-12-4	IgG2b	PerCP-Cy5.5	BD Biosciences	
CD8β	PPT23	IgG1	FITC	Bio-Rad Laboratories	
CD8β	PPT23	IgG1	PE	Bio-Rad Laboratories	
TNF	MAb11	IgG1	BV421	BioLegend	
IFNγ	P2G10	IgG1	APC	BD Biosciences	
IL-2	A150D 3F1 2H2	IgG2a	PE-Cy7	Thermo Fisher	rat-anti-mouse, IgG2a, BioLegend
CCR7	3D12	IgG2a	BV711	BD Biosciences	
CD45RA	MIL13	IgG1	FITC	Bio-Rad Laboratories	
CD69	01-14-22-51	IgG2b	PE Cy7	Kyoto Institute of Nutrition & Pathology (Hayashi et al. 2018)	Goat-anti-mouse, BioLegend
EOMES	WD1928	IgG1	PE	Thermo Fisher	

T-bet	eBio4B10	IgG1	PE Cy7	Thermo Fisher	
Ki67	B56	IgG1	BV650	BD Biosciences	
Perforin	δG9	IgG2b	Purified		Lightning-Linked PE-Cy7, antibody labelling kit, Novus Bio
CD27	B30C7	IgG1	APC	Bio-Rad Laboratories	
CD14	REA599	IgG1	PE	Miltenyi Biotec	
CD172a	BL1H7	IgG1	PE	Bio-Rad Laboratories	

2.6 RNA-sequencing

BAL DFE^{+} T cells were sorted (average of 4480 cells/sample) with FACSAria™ III Sorter (BD Biosciences) in PBS. Sorted samples were then centrifuged at 700 × *g* for 5 minutes and RNA was extracted using PicoPure RNA Isolation Kit (Thermo Fisher) as per the manufacturer's instructions. DNA was removed by DNase treatment (TURBO DNA-free™ Kit, Thermo Fisher). Isolated RNA was sent to Edinborough Genomics and used as input for SMARTer Stranded Total RNA-Seq Kit v3 - Pico Input Mammalian (Takara Bio) and PCR amplification performed. cDNA obtained was pooled and sequenced on NovaSeq using an S1 100 PE flow cell. Dr. Siddharth Jayaraman used raw fastq files for initial quality control using FastQC (https://www.bioinformatics.babraham.ac.uk/projects/fastqc/). Next, CogentAP (Cogent NGS Analysis Pipeline v1.0, Takara Bio) was applied to trim and add the sample barcodes to the fastq header for each sample. The reads were trimmed of Illumina and library

prep adapters using cutadapt (Martin 2011), and subsequentially aligned to *Sus scrofa* Sscrofa11.1 assembly (GCA_000003025.6) using STAR (Dobin et al. 2013) with default parameters. UMI-tools was used to discard duplicated reads (Smith, Heger, and Sudbery 2017) and featureCounts extracted the number of reads aligned to each gene feature (Liao, Smyth, and Shi 2014). Differential gene expression (DGE) analysis was carried out using TCC-GUI, which iterates DESeq2 for data normalisation, using the featureCounts output for pairwise comparisons (Su et al. 2019; Love, Huber, and Anders 2014). Pathway analysis was performed using Webgestalt online tool (Liao et al. 2019), selecting GSEA as comparison method and sscrofa as the reference genome. KEGG pathway database was used as reference and ensemble ID were uploaded together with ranked score ($-\log_{10}$(p value)*$\log_2$(fold change difference)) based on the results of DGE comparison. Other settings include: minimum number of IDs in the category (5), the maximum number of IDs in the category (2000), significance level (FDR < 0.05) and number of permutation (1000).

Raw data, meta data and differential gene expression analysis will be publically available, upon manuscript publication, at this link: https://www.ncbi.nlm.nih.gov/geo/query/acc.cgi?acc=GSE182645

2.7 ELISpot

IFNγ ELISpot

MultiScreen-HA ELISpot plates (Merck) were coated with 100 µl per well of primary anti-porcine IFNγ, clone P2G10 (BD Biosciences 0.5µg/ml in carbonate bicarbonate) and incubated at 4°C overnight. Plates were washed 5 times with PBS and blocked with R10 for 2 h. 0.2 million BAL cells or 0.25

million cells isolated from the other tissues were then incubated and simulated with H1N1pdm09 (MOI=1), peptides (see Table 7.1 for list of peptides), 4μg/ml ConA (Sigma-Aldrich) or media control at 37°C overnight. Each condition was present in duplicate. The plates were washed five times with PBS + 0.05% Tween20 before the incubation with a secondary biotinylated anti-porcine IFNγ detection Ab (clone P2C11, BD Pharmingen 0.25μg/ml in PBS). After 2 h of incubation at room temperature, the plates were then washed as before and streptavidin–alkaline phosphatase (Thermo Fisher) was added for 1 hour. Spots were developed by an alkaline phosphatase substrate kit (Bio-Rad) for 20 min, and the reaction stopped with tap water. Immunospots were detected using AID ELISPOT reader (AID Autoimmun Diagnostika). Results were calculated by subtracting from the average of experimental wells the average of medium control wells and expressed as the average of IFNγ producing cells per million cells in the virus or peptide stimulation.

B cells ELISpot

Cryopreserved PBMC, spleen and TBLN were seeded at a 10 million cells/well concentration in a 12 well plate and stimulated with the TLR7 agonist R484 (Miltenyi Biotec) at 1μg/ml in R10 supplemented with 0.1% β-mercaptoethanol (Thermo Fisher). After 48 h of stimulations, cells were washed twice with 50 ml of R10 and counted. 0.5 million cells were distributed in each well of ELISpot plates previously coated with anti-porcine IgG, clone MT421 (Mabtech), or anti-porcine IgA, clone A100-102A (Bethyl) in 1/500 dilution in CB buffer overnight at 4°C. Positive control wells, used to detect total IgG and IgA secreting cells, were incubated with 0.05 million cells. Each condition was tested in duplicate and plates were inclubated overnight at 37°C. Plates were then washed with PBS + 0.05% Tween20 five times and incubated with biotinylated HA (produced in house) for detection of HA specific B cells,

biotinylated keyhole limpet hemocyanin (KLH) (Sigma-Aldrich) as a negative control, both at 0.1 μg/ml in PBS, or biotinylated anti-porcine IgG (clone MT424, Mabtech) or anti-porcine IgA (clone A100-102-B, Bethyl) diluted 1/1000 in PBS to detect all Ig secreting B cells. After 2 h incubation, plates were washed and streptavidin alkaline phosphatase (Invitrogen, UK) added for another hour. The plates were then developed and read as described above. Spots detected in the KLH control wells were subtracted from the HA response and data presented as antibody-secreting cells (ASC) per million cells.

2.8 Virus growth and serological assays

Virus propagation

H1N1pdm09 virus inoculum (approximately 1000 PFU) in VGM was added to 80% confluent Madin-Darby Canine Kidney (MDCK) cells (Central Service Unit, TPI). One hour later, cells were washed with PBS and incubated in 30 ml of VGM + 2 μg/ml TPCK trypsin for 72 h to allow for viral growth. The supernatant was then collected and centrifuged at 500 × *g* for 5 min to pellet debris. The virus-containing supernatant was aliquoted and stored at -80°C.

Plaque assay

Viral titre in nasal swabs, BAL fluid and H1N1pdm09 MDCK grown virus was determined by plaque assay on MDCK cells. Samples were 10-fold serially diluted, starting at neat concentration, in DMEM and 100 μl overlayered on confluent MDCK cell monolayers in 12 well plates. After 1 hour, the plates were washed with PBS and overlayered with 2 ml of plaque assay overlay medium. Plates were

incubated at 37 °C for 72 h and plaques visualized by staining with a 0.1% crystal violet solution. Virus titre was expressed as plaque-forming units (PFU) per ml considering the initial dilution factor.

Microneutralisation assay

The titre of neutralising Ab titres was assessed in serum and BAL fluid samples by microneutralisation (MN). The samples were heat-inactivated for 30 min at 56 °C and diluted (starting at 1:20 for serum and 1:2 for BAL) in VGM. The diluted samples (50 µl) were incubated with 50 µl of S-FLU or H1N1pdm09 virus, at optimised concentration, in 96 well flat-bottomed plates and incubated for 2h at 37°C. MDCK-SIAT-1 cells, derived from MDCK transfected with the cDNA of human 2,6-sialyltransferase (SIAT1), were used in this assay for their ability to express two-fold higher amounts of α2-6-linked sialic acids than MDCK (Matrosovich et al. 2003). A cell suspension containing 3×10^4 cells in VGM was added to each well and the plates incubated overnight at 37°C. The supernatant was removed and cells fixed with 4% paraformaldehyde in PBS for 30 min at 4°C. If S-FLU was used, fluorescence from the eGFP was then detected. When using H1N1pdm09, the cells were washed twice with a glycine buffer (PBS, 20mM glycine) and permeabilised for 20 min with a solution of 20mM glycine + 0.5% tritonX100 in PBS. The plates were then washed twice with PBS and stained with 50µl/well anti-IAV NP mAb (Clone: AA5H, Bio-Rad) for 1 h at room temperature. After two washes with PBS, 50µl/well of goat anti-mouse IgG horseradish peroxidase (HRP) conjugated secondary Ab (Dako) was added and incubated for another hour at room temperature. The 3,3′,5,5′-tetramethylbenzidine (TMB) substrate was added to the plates, after two washes with PBS, and incubated for 5 minutes. A stop solution containing1M sulfuric acid was then added and absorbance measured at 450 nm and 630 nm (reference wavelength) on the Cytation3 Imaging Reader (Biotek). The

50% inhibitory titre was calculated as the midpoint between uninfected control wells and virus-infected positive controls.

ELLA

An enzyme-linked lectin assay (ELLA) was used to quantify the inhibitory enzymatic activity of NA by Ab present in serum or BAL. 96 well flat-bottom plates were coated overnight at 4°C with 25 μg/ml fetuin in PBS + 0.02% sodium azide. Heat-inactivated samples were serially diluted (starting 1:40 for sera and 1:4 for BAL) in VGM. An HA-mismatched S-FLU or IAV virus was used to minimise any potential steric effect of Ab binding to the vaccine's HA. An optimal S-FLU or IAV virus concentration was added to the diluted Ab for 20 min on a plate shaker. 100 μl of the solution containing virus and samples were then transferred to the coated plate, previously washed with PBS, and incubated overnight at 37°C. 100 μl of a 1 μg/ml solution of peanut agglutinin conjugated with HRP in PBS was added to each well and incubated at room temperature for 2 h. The plates were washed and developed as described above. The 50% inhibition titre was calculated as the highest dilution above the 50% inhibition line (midpoint between the signal generated by virus only and medium only wells).

HA-specific ELISA

Enzyme-linked immunosorbent assays (ELISA) was used to measure the titre of Ab recognising HA. 96 well microtiter plates were coated with either 1 μg/ml recombinant HA protein (provided by Prof. Alain Townsend) in CB buffer at 4°C overnight. Plates were blocked with a solution containing 4% milk powder + 0.05% Tween20 in PBS (blocking buffer) for 2 h at room temperature. Samples were serially diluted in the blocking buffer and added to the plates for 1 hour on a shaker. The plates were

washed three times with 0.05% Tween20 in PBS. HRP-conjugated secondary antibodies detecting porcine IgG or IgA (both from BioRad) were diluted in blocking buffer and added to the plates for 1 h at room temperature. TMB was used to develop the signal and plates measured as previously described.

The end-point titre was established using cut-off values (determined as average values for naïve pig samples plus three-fold standard deviation at the starting dilution).

2.9 Aerosol characterisation

Droplet size evaluation

Two VMNs producing different droplet size (3 – 5 μm) (Aerogen Solo, Aerogen ltd.) and the MAD were used for *in vitro* experiments. Albuterol sulphate (Ventolin, GSK) was used as a tracer solution for initial characterisation of the VMNs and MAD. Laser diffraction (Spraytec, Malvern Instruments) characterised the volumetric median diameter (VMD) of the aerosols generated by the devices after the delivery of 0.25ml of albuterol. The droplet size of the aer. generated by the devices was also measured using 0.25 ml of ^{99m}Tc-DTPA and S-FLU vaccine (3.5×10^7 TCID50). The and of the droplets generated A 2mg/ml albuterol sulphate solution was used to measure the fine particle fraction and the mass median aerodynamic diameter (MMAD) of the droplets generated by the VMNs using cascade impaction (Next Generation Impactor, Copley).

In vitro aerosol deposition in the pig model

A veterinary mask (Burtons Medical Equipment) was customised to include 1-way valves and absolute filters. A 3D printed pig head was connected to a breathing simulator (Dual Phase Control Respirator,

Harvard Apparatus) via an absolute filter positioned at the end of the throat, collecting inhaled drug. The breathing simulator was set to mimic the breathing parameters of a 15 kg (Tidal Volume (Vt) 115 ml, 25 breath per min (BPM), Inhalation:Exhalation (I:E) ratio 1:3) and a 20 kg (Vt 150 ml, 25 BPM, I:E ratio 1:3) pig. The VMNs were then attached to the mask and nebulised a nominal dose of 1 ml of 1mg/ml albuterol sulphate. The drug deposited on the filter was eluted by washes with water and quantified by UV spectrophotometry (Biochrom UV Vis, Cambridge) at 276 nm. The concentration of drug deposited was calculated by interpolation on a standard curve and expressed as a % of the nominal dose (amount in device before administration) delivered.

In vitro aerosol deposition in the human model

An adult head model (described in (Hibbitts et al. 2014)) was attached to the breathing simulator, mimicking the breathing pattern of a normal adult (Vt 500 ml, 15 BPM, I:E Ratio 1:1). The VMN was connected to an aerosol mask (I-Guard, Salter Labs) connected to an aerosol chamber (Aerogen Ultra, Aerogen) supplemented with a oxygen flow rate of 2 l/min. Two ml of 1 mg/ml albuterol was delivered and the drug deposited was calculated as above.

Scintigraphic image analysis

Hermes software (Hermes Medical Solutions) was used for image analysis. Three anatomical regions of interest (ROIs) were defined and analysed: the face area (nasal cavities and facial skin, was set as a circle of 10 cm diameter); the throat (set as a rectangle of length 17 cm); and lung (set as a trapezoid covering the whole lung area) (Figure 4.3). Radioactive material deposited in the area below the lung (stomach) was measured as a rectangle. Counts in the individual ROI were adjusted for background and

radioactive decay relative to the first image taken for each animal. Deposition in each specific ROI was then calculated relative to total adjusted counts as follows:

$$\frac{count\ in\ the\ specific\ ROI}{sum\ of\ count\ of\ face + throat + lung + stomach} * 100$$

2.10 Statistical analysis

Chapter 3

Dr. Simon Gubbins, Mathematical Biology Group, TPI, performed the mathematical analysis present in Chapter 3.

The changes over time in the proportion of tereamers$^+$ CD8$^+$ T cells were compared for each tetramer and tissue using the following curve, fitted to the data,

$$y(t) = y_0 + (y_{\max} - y_0)\left(\frac{t}{t_{\max}}\right)^6 \exp\left(-\frac{6(t - t_{\max})}{t_{\max}}\right),$$

where y represents the proportion at t days post-infection, y_0 the baseline proportion, y_{max} the peak proportion and t_{max} the time of peak proportion. This curve was selected as it gave an appropriate shape for the data without including too many parameters. Table 3.1 present the estimated parameters for each tetramer and tissue.

The changes with time in the proportion of tetramer$^+$ CD8 T cells expressing different phenotypic markers were compared fitting exponential curves to the data in each tissue,

$$y(t) = y_0 \exp(-dt),$$

(y = the proportion at t days post infection; y_0 = the initial proportion and d = the decay rate (/day)). Each marker was analysed independently.

In both analyses, the parameters (i.e. y_0, y_{max} and t_{max} or y_0 and d) were chosen amongst tissues and tetramers by fitting different models to the data by nonlinear least squares and the residual deviance for the models was compared using F-tests (Ross 1990). The analysis was implemented in Matlab (version R2020b; The Mathworks, Inc.).

Due to the limited data on $CD8^+$ T cells in the trachea, the proportion of cells specific for each tetramer were compared at each time point using a Kruskal-Wallis test followed by pairwise Wilcoxon rank-sum tests. This analysis was performed in R (version 4.0.5) (Team 2020).

The changes in the relative proportion of $CD8^+$ T cells specific for each tetramer was assessed with the following model in each tissue:

$$\begin{aligned}
y_{DFE}(t) &= K_1^{(DFE)} + \frac{K_2^{(DFE)} - K_1^{(DFE)}}{1+\exp(-b_{DFE}(t-d_{DFE}))}, \\
y_{VAY}(t) &= 1 - y_{DFE}(t) - y_{AAV}(t), \\
y_{AAV}(t) &= K_1^{(AAV)} + \frac{K_2^{(AAV)} - K_1^{(AAV)}}{1+\exp(-b_{AAV}(t-d_{AAV}))},
\end{aligned}$$

where y(t) is the proportion of the tetramer; t = days post infection; K_1 and K_2 are the minimum and maximum frequencies; b = the rate of change in frequency and d is the time of the maximum rate of change. This formula ensures the total proportion of cells is 100%. Changes in the parameters (i.e. K_1, K_2, b and d) in each tissue was assessed by fitting different models to the data as described above. This

analysis was implemented in Matlab (version R2020b; The Mathworks). This analysis was limited to samples for which the frequency of all tetramers was available.

The changes in the phenotype of tetramer^{+} CD8^{+} T cells in each tissue were assessed by linear models. The model variables included the proportion of cells in each subset (CD45RA$^{+/-}$ and CCR7$^{+/-}$), the tetramers and days post-infection, together with two- and three-way interactions between the variables. Model simplification proceeded by stepwise deletion of non-significant ($P>0.05$) terms (assessed by F-tests). This analysis was performed in R (version 4.0.5) (R Core Team 2021).

The frequencies of cytokine-producing cells in DFE^{+} and AAV^{+} populations over time were compared using two-way ANOVA in GraphPad Prism version 9.1.0.

Chapter 4

The counts obtained in the *in vivo* scintigraphy study amongst the different ROI were compared by two-way ANOVA. Unpaired *t*-test was chosen to compare the data from pig and human breathing simulator and the *in vitro* particle size characterisation experiments. Two-way ANOVA with Tukey post-hoc test was used to compare the droplet size of S-FLU and ^{99m}TC-DTPA generated by the two VMNs and the MAD. This statistical analysis was performed with GraphPad Prism (8.3.0)

Chapter 5

Kruskal-Wallis test was used for the comparison of viral load, pathology and adaptive responses between groups. Two-way ANOVA was selected to compare neutralising Ab responses and to analyse the hierarchy of the T cell responses in different tissues within the same group. GraphPad version 8.4.1 was used for this statistical analysis.

Chapter 3
Dynamics and phenotypic changes of influenza-specific CD8 T cells

3.1 Introduction

Cellular immunity against IAV plays a fundamental role in heterosubtypic protection, as previously described (Chapter 1). However, few studies have investigated in depth the T cells responses in pigs after IAV infection. These studies were limited to the enumeration of IAV responding cells or studied T cells after *ex vivo* restimulation with live virus, with consequent changes in phenotype (Khatri et al. 2010; Talker et al. 2016; Reutner et al. 2013; Edmans et al. 2020).

The lack of understanding of porcine cellular responses to IAV has been due, at least in part, to the scarcity of research tools to study T-cell responses in pigs. Immunological tools, such as defined T-cell epitopes and peptide-MHC multimer technology, have been recently developed in the context of IAV infection (Pedersen et al. 2014b; Baratelli et al. 2017b; Gutiérrez et al. 2016). The Babraham pig is a Large White inbred pig with an 85% identity between individuals (Schwartz et al. 2018). The SLA loci, equivalent to the murine MHC, are homozygous between individuals. This allowed the identification of four different IAV's NP immunodominant epitopes after aer. immunisation with the candidate single-cycle influenza vaccine S-FLU (Tungatt et al. 2018). However, only one of the four epitopes (DFE) is fully conserved between PR8 (the backbone of S-FLU) and H1N1pdm09. Our group has recently studied the kinetic of DFE^{+} CD8 T cells after H1N1pdm09 infection up to 21 dpi (Edmans et al. 2020).

Therefore, further identification of novel H1N1pdm09 influenza epitopes will be a useful step in determining the fine specificity of the cellular response in the Babraham pig.

Furthermore, while the phenotype of porcine CD4 helper T cells have been thoroughly analysed, CD8 T cells are less well characterised (Moreno et al. 2013; Talker et al. 2013; Reutner et al. 2013; Franzoni et al. 2013). In the blood of newly born pigs, CD8 T cells lacked perforin expression but were $CD27^{+}$, indicative of a naïve phenotype. In contrast, effector cells (identified as $CD27^{dim}perforin^{+}$) started appearing at seven weeks of age (Talker et al. 2013). Studies using a porcine CCR7 ligand (CCL19-human IgG1 fusion protein) attempted to describe the phenotype of CD8 T cells; however this characterisation was only performed in blood (Moreno et al. 2013). CCR7, essential for migration to lymphoid organs, and CD45RA, a known differentiation marker, are both widely used in human immunology, but they have never been studied in combination to define subsets of porcine CD8 T cells in tissues. In addition, phenotypic changes of IAV-specific T cells have not been explored before in the porcine model.

The recently discovered pulmonary TRM reside in the respiratory tract without recirculating, unlike central or effector memory T cells, constituting a first line of adaptive cellular defence (Masopust, Vezys, et al. 2001b). Several techniques have been adopted in mice to identify this population: parabiosis; *in vivo* labelling of leucoytes with mAbs; treatment with FTY720, an sphingosine 1-phosphate receptor (S1PR) agonist which causes peripheral lymphopenia and prevents tissue egress; transplantation or identification by transcriptional profiling (reviewed in (Szabo, Miron, and Farber 2019)). In mice, TRMs have been shown to exceed the number of T cells in the lymphoid system and play an essential role in maintaining local immune memory (Steinert et al. 2015). TRMs are the predominant population in human lungs and antigen-specific cells were found at stable frequencies years

after pathogen encounter, indicating their crucial role in respiratory infections (Kumar et al. 2017). Mouse and human TRM express CD69 and variably CD103, both essential for tissue retention (Teijaro et al. 2011; Masopust et al. 2006; Schenkel et al. 2013; Thome et al. 2014; Turner et al. 2014). However, the absence of monoclonal antibodies (mAbs) to porcine CD69 and CD103 has made studies of porcine TRMs challenging.

This chapter examines porcine CD8 T cells phenotype and their dynamics during IAV infection. The following specific aims are here addressed:

- To phenotype CD8 T cells using CD45RA and CCR7, together with the newly defined CD69 antibody (Hayashi et al. 2018) in different tissues at the steady-state.
- To identify novel CD8 epitopes in H1Npdm09 NP protein.
- To study the dynamics of CD8 T cells specific for three different NP epitopes.
- To phenotype NP-specific CD8 T cells.
- To analyse the transcriptional profile of NP-specific CD8 T cells at different times after infection.
- To study the differentiation state and functional profile of the different NP-specific CD8 T cells.
- To investigate the migration ability of leukocytes in different organs after treatment with FTY720.

3.2 The phenotype of CD8 T cells at steady-state

To define more thoroughly the phenotype of CD8 T cells in blood and different tissue, I first studied the expression of CD45RA and CCR7, known to identify four populations in humans: naïve

($CD45RA^{+}CCR7^{+}$), central memory T cells (TCM) ($CD45RA^{-}CCR7^{+}$), effector memory T cells (TEM) ($CD45RA^{-}CCR7^{-}$) and terminally differentiated effector (TDE) ($CD45RA^{+}CCR7^{-}$) (Romero et al. 2007). Because porcine T helper cells express CD8 as an α homodimer when activated (Reutner et al. 2013; Saalmuller, Werner, and Fachinger 2002), I used an antibody to CD8β combined with CD45RA and CCR7 Ab to identify and characterise CD8 T cells. At steady state in inbred Babraham pigs (10 weeks of age), TEM and naïve T cells are the predominant populations in blood (31.3% and 27.8% of CD8β respectively), followed by TCM (21.2%) and TDE (19.7%) (Figure 3.1 A and B). While a similar phenotype is present in the spleen, the TBLN is populated mainly by naïve (55.9%) and TCM (26.2%). Interestingly lung and BAL cells are more differentiated, exhibiting TEM (49.1% and 85.1% in lung and BAL respectively) and TDE (38.5% and 10.9%) phenotypes. I next investigated the expression of CD69, a known marker of activation and residency, in these different subsets (Farber, Yudanin, and Restifo 2014; Masopust and Schenkel 2013) using a newly defined anti-porcine CD69 mAb (Hayashi et al. 2018). Similar to humans, CD69 was absent in blood, while the highest expression was found in TCM and TEM in TBLN and in T cells isolated from the BAL (Figure 3.1 C).

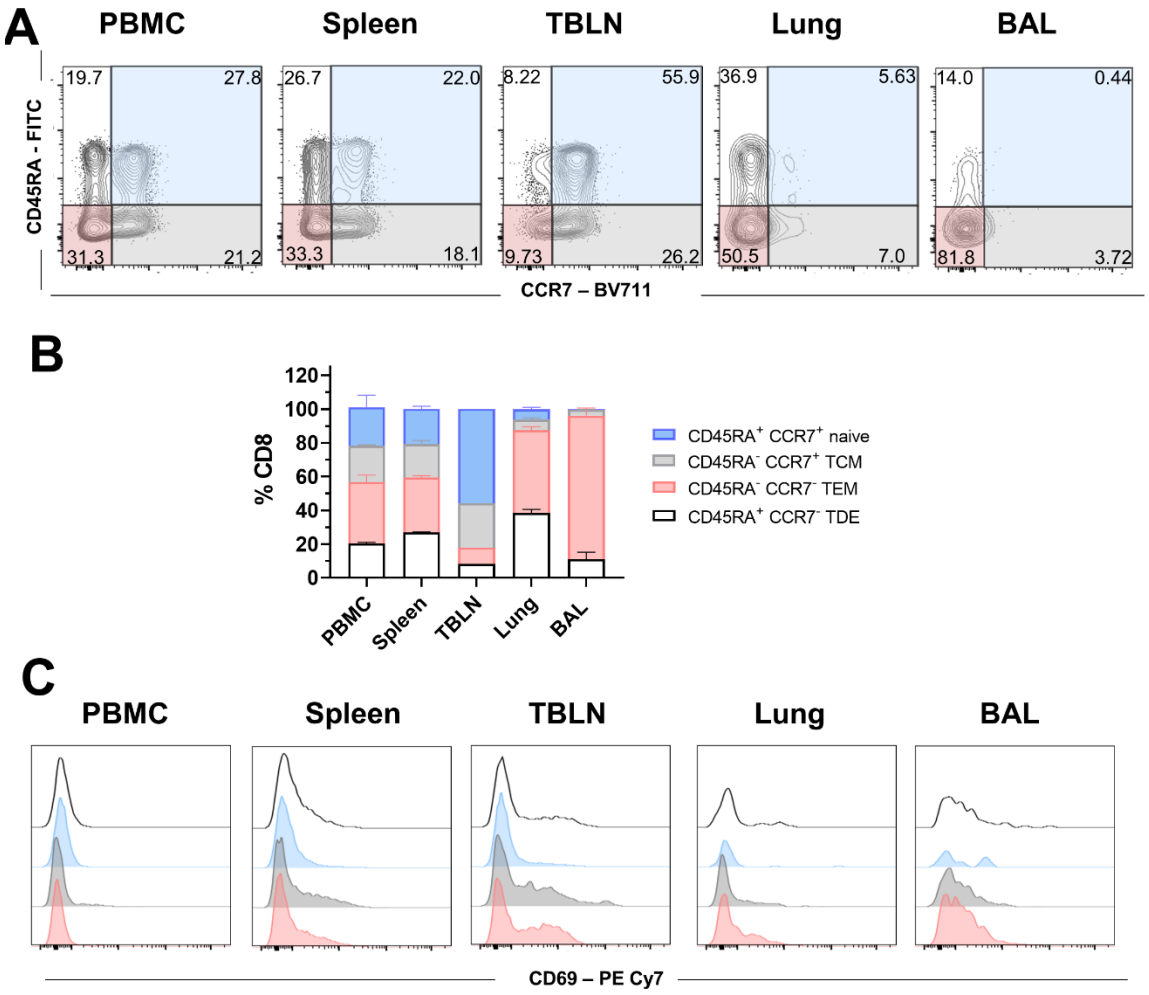

Figure 3.1 **Phenotype of porcine CD8 T cells across tissues. (A)** Expression of CD45RA and CCR7 by CD8 T cells isolated from the indicated tissues of naïve Babraham pigs. Quadrants show the proportion of each population. **(B)** Mean frequency (± SD) of TDE ($CD45RA^{+}CCR7^{-}$), naïve ($CD45RA^{+}CCR7^{+}$), TEM ($CD45RA^{-}CCR7^{+}$) and TCM ($CD45RA^{-}CCR7^{-}$) in CD8 from 3 animals. **(C)** CD69 expression in terminally differentiated effector (TDE, white), naïve (blue), central memory (TCM, grey) and effector memory (TEM, red) in CD8 T cells in the tissues analysed.

Porcine CD8 T cells subsets have been previously defined by the expression of CD27 and perforin (Talker et al. 2013). I therefore studied the expression of CD27 and perforin in combination with CD45RA and CCR7. Perforin was present only in TEM and TDE in all tissues, while naïve and TCM were predominantly $CD27^{+}perforin^{-}$, similarly to humans (Figure 3.2) (Vigano et al. 2014; Rufer et al. 2003; Romero et al. 2007). Perforin was constitutively expressed in TDE in all tissues studied, while TEM showed high levels of perforin in PBMC (53% of TEM), spleen (55.5%) and lung (57.9%) but not in BAL and TBLN (11.9% and 2.3% respectively). In contrast to previous studies (Talker et al. 2013), a $perforin^{+}CD27^{+}$ population was absent in all CD8 subsets studied.

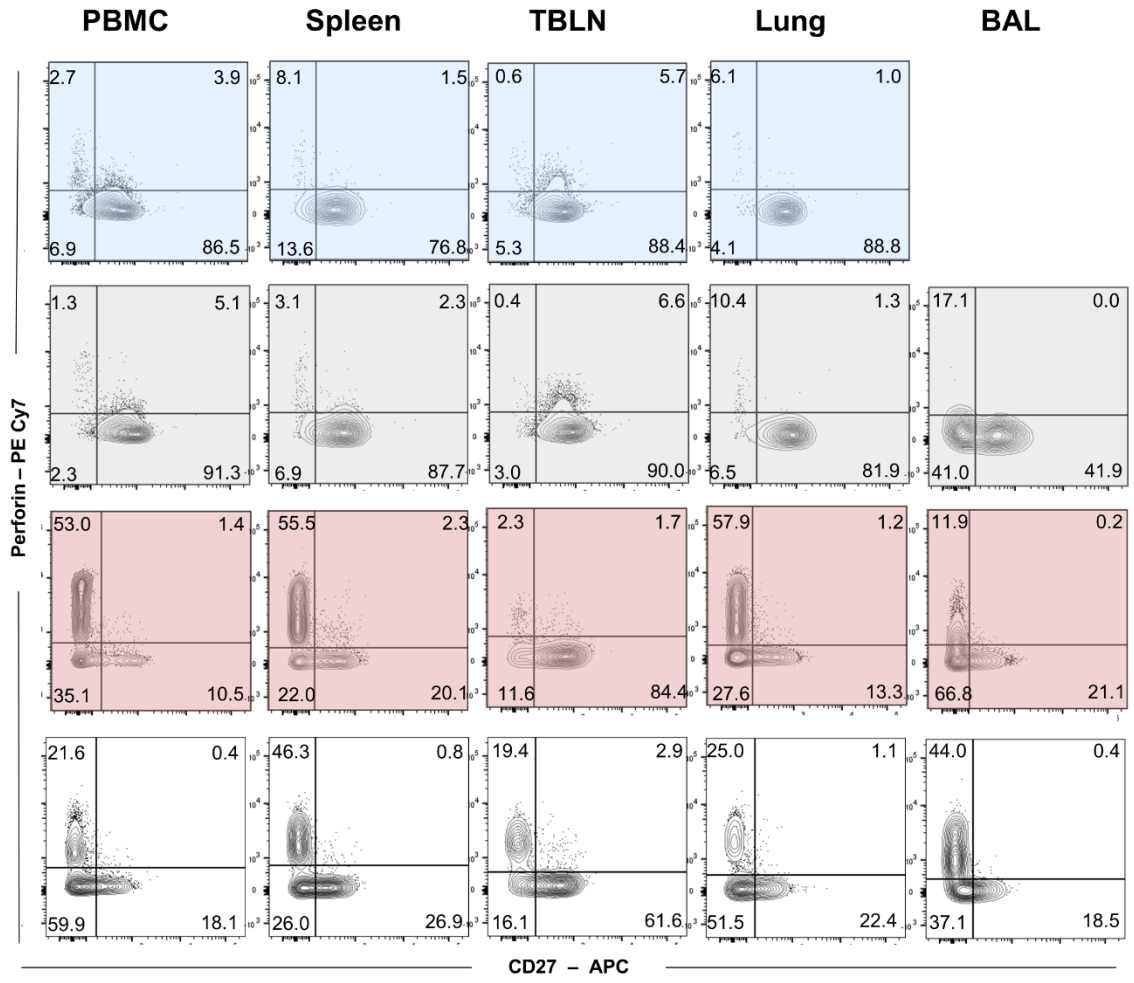

Figure 3.2 **Expression of perforin and CD27 in CD8 T cell subset** Representative plots showing perforin and CD27 expression in CD8 T lymphocyte subsets defined by CD45RA and CCR7 expression: naïve ($CD45RA^{+}CCR7^{+}$, blue), TCM ($CD45RA^{-}CCR7^{+}$, grey), TEM ($CD45RA^{-}CCR7^{-}$, red panels) and TDE ($CD45RA^{+}CCR7^{-}$, white panels). Each quadrant shows the mean percentage of 3 animals.

To investigate whether this classification of T cells reflected functional diversity, I sorted naïve, TCM, TEM and TDE CD8 T cells from PBMC and stimulated them with PMA and ionomycin. TEM responded rapidly, with 11,6% of cells secreting cytokines 2 h after stimulation (Figure 3.3 A). At the peak, 6 h post-activation, 28.1% of TEM were producing cytokines, while TDE and TCM exhibited a

moderate secretion (13.8% and 12.3% respectively) followed by naïve T cells (5.2%). The quality of the response was different with TCM and naïve T cells producing mainly TNF, TDE secreted more IFNγ (8%) with a smaller proportion secreting both IFNγ and TNF (4.9%) while TEM were mostly double producers ($IFN\gamma^{+}TNF^{+}$ 18.9%) at 6 h of stimulation (Figure 3.3 B and C).

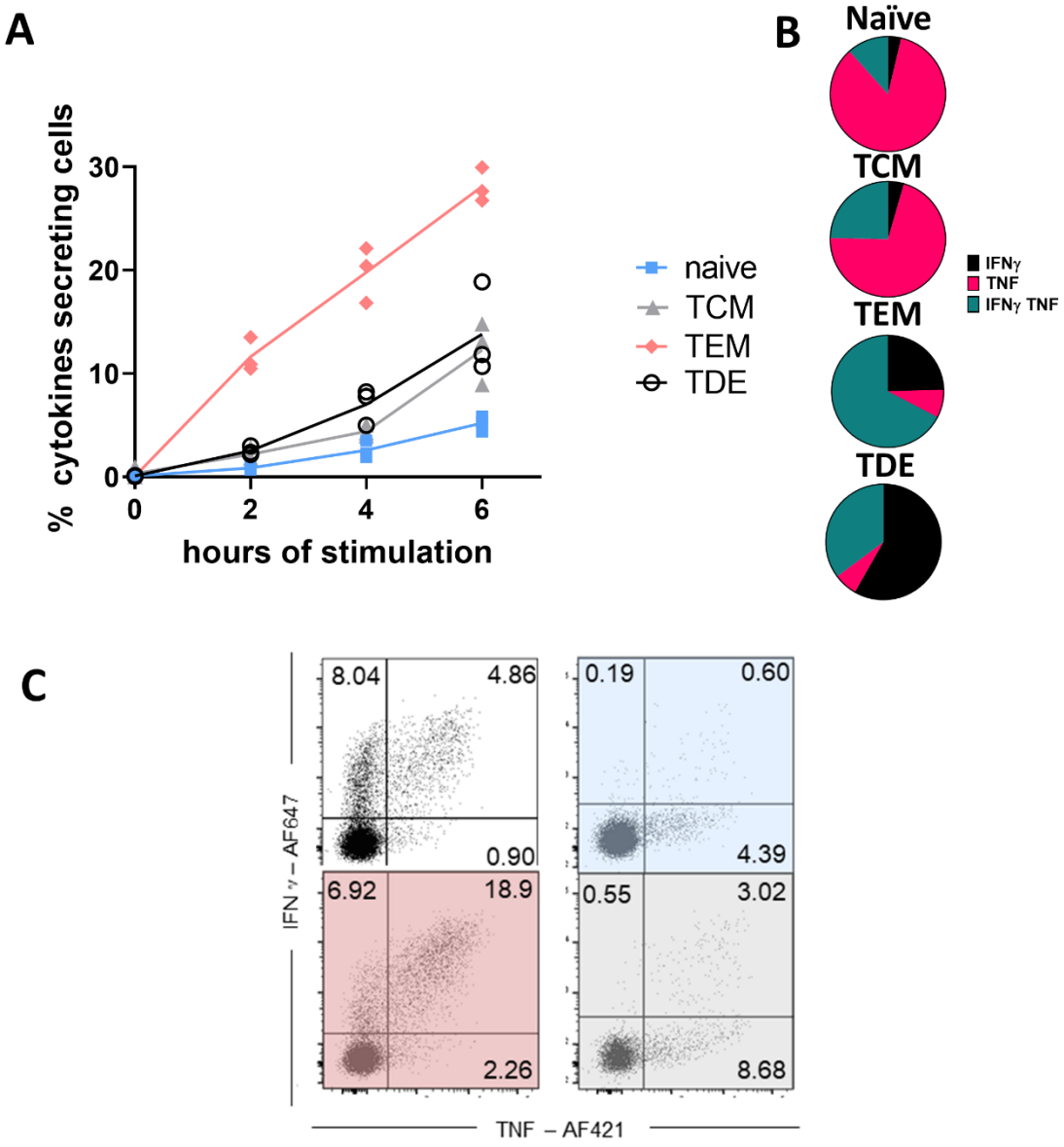

Figure 3.3 **Functional activity of CD8 T cell subsets. (A)** $CD8^+$ T cells from PBMC were sorted according to their expression of CD45RA and CCR7. The sorted cells were stimulated with PMA and ionomycin for 0, 2, 4 and 6 h and TNF and IFNγ secretion measured by intracellular cytokine staining. Each symbol represents one animal, this experiment was repeated twice. **(B)** The pie chart shows the proportion of single and double cytokine secreting CD8 T cells for IFNγ and TNF at 6 h of stimulation **(C)** Representative FACS plot showing the secretion of IFNγ and TNF after 6 h stimulation in TDE (white panel), naïve (blue panel), TCM (grey panel) and TEM (red). Mean proportion of IFNγ single (top left), double producer (top right) and single TNF (bottom right) T cells are reported.

Taken together, these data indicate that porcine CD8 T cells can be classified similarly to humans based on their expression of CD45RA and CCR7, and these markers identify functionally distinct populations. These subsets differ in their tissue distribution and expression of residency marker CD69. BAL CD8 cells are predominantly TEM phenotype with high expression of CD69 and, were not stained by intravenous CD3 mAb, in previous studies, indicating that they are TRM.

3.3 Influenza time course: experimental design

After studying the phenotype of CD8 T cells from unimmunised pigs, I wished to define how this might change during the immune response to IAV infection. Inbred Babraham pigs were infected i.n. with H1N1pdm09 in four experiments (referred to as T1-T4) (Figure 3.4). One pig was culled on each of days 1-7, 9 and 11 post-infection (dpi) in the first experiments (T1 and T2), three more at 6, 7, 13, 14, 20 and 21 dpi in experiment T3 and a further four at 21, 42 and 63 dpi in T4 (Edmans et al. 2020). Four uninfected pigs were sampled on the day of challenge and used as naïve controls. Viral load, determined in daily nasal swabs, was consistent between the experiments, with a peak at 5 dpi a complete resolution by 7 dpi in most pigs (Edmans et al. 2020).

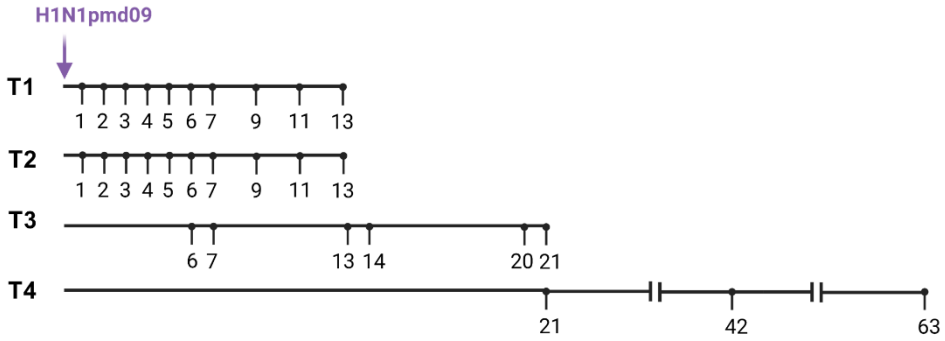

Figure 3.4 **Experimental design.** Babraham pigs were infected with H1N1pdm09 intranasally and culled on the indicated days post infection. Broncho-alveolar lavage (BAL), lung, tracheo-bronchial lymph nodes (TBLN), peripheral blood mononuclear cells (PBMC) and spleen were collected at all time points while nasal turbinates (NT) were isolated only in experiments T3 and 4**.**

3.4 Identification of new epitopes in H1N1pdm09 NP

To identify NP-derived epitopes for the H1N1pdm09 strain, peptides of 18 amino acids (aa) length, overlapping by 12 aa were screened by IFNγ ELISpot. The eight NP pools (81 peptides in total) (Table 7.1) were tested by IFNγ ELISpot on BAL, lung, TBLN and PBMC isolated at 13/14 dpi, at the peak of the response according to our previous findings (Edmans et al. 2020). Pools 3 and 4 consistently showed the greatest responses across tissues and were therefore broken down to identify antigenic peptides (Figure 3.5 A). Antigenic peptide identification was performed in TBLN, where the background was negligible and the responses high. Peptides 30 and 31 showed the highest response, followed by peptide 37 from pool 4 and were selected for minimal epitope identification (Figure 3.5 B). CD8 T cells commonly recognise peptides of 9 aa length, thus peptides 30, 31 and 37 were trimmed from either end down to 9aa (Figure 3.5 C). Two new epitopes were identified: $NP_{181\text{-}189}$ AAVKGVGTI (AAV) and $NP_{217\text{-}225}$ VAYERMCNI (VAY) (Figure 3.5 C), which were confirmed to be CD8 epitopes by IFNγ ELISpot (Figure 7.1) and loaded into SLA-2 molecules to generate tetramers.

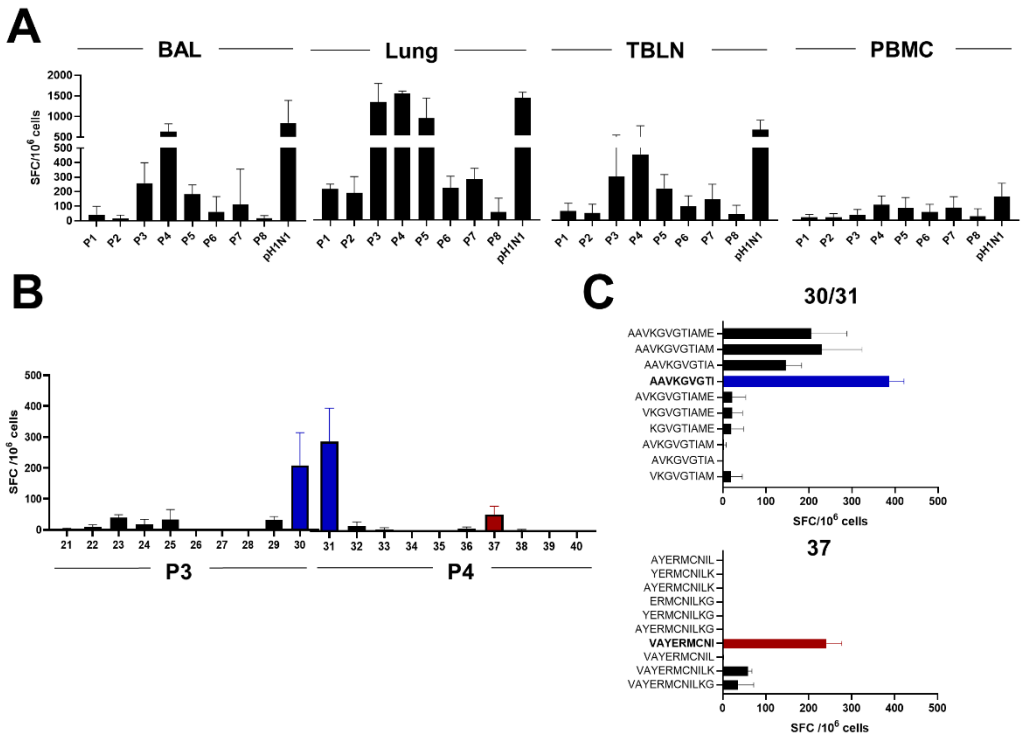

Figure 3.5 **Identification of NP epitopes AAV and VAY (A)** Pools of 10 peptides of 18 amino acids (aa) length from the NP of H1N1pdm09 were used for an initial screen to stimulate cells isolated from BAL, lung, TBLN and PBMC. Responses at 13/14 DPI were measured by IFNγ ELISpot and H1N1pdm09 (pH1N1) MOI = 1 was present as a positive control. **(B)** Spot forming cells (SFC) in TBLN after stimulation with individual peptides from pool 3 (p3) and pool 4 (p4), highlighted the peptides that subsequentially identified AAV epitope (in blue) and VAY (in red). **(C)** Minimal epitope identification (using peptides of 9 aa) from peptide 30/31 (top) and 37 (bottom) that lead to the identification of AAV (in blue) and VAY (in red) epitope. Mean and SEM of 3 animals. Credit to Matthew Edmans and Basu Paudyal for this work.

3.5 Dynamics of T cells responses

The kinetics of CD8 T cells specific for the three NP epitopes (DFE, VAY and AAV) were assessed in T1-T4 studies, starting from 6 dpi when a cellular response is first detectable (Edmans et al. 2020). The highest responses for all tetramers, as absolute counts, were found in the BAL and lung, followed by TBLN and NT (Figure 3.6).

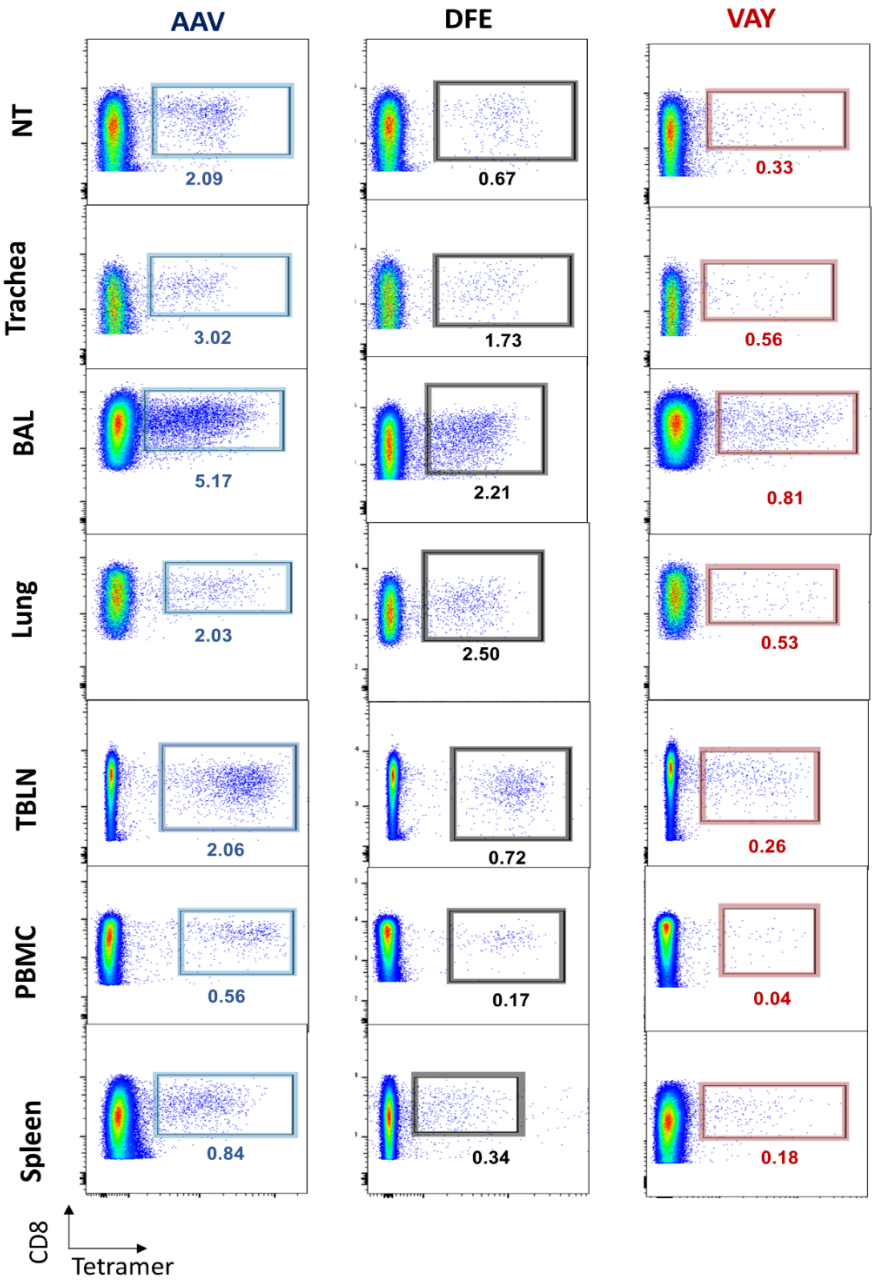

Figure 3.6 **Representative plots of tetramer^{+} cells at 21 dpi.** Numbers under the gated population indicate the % of tetramer+ CD8 T cells

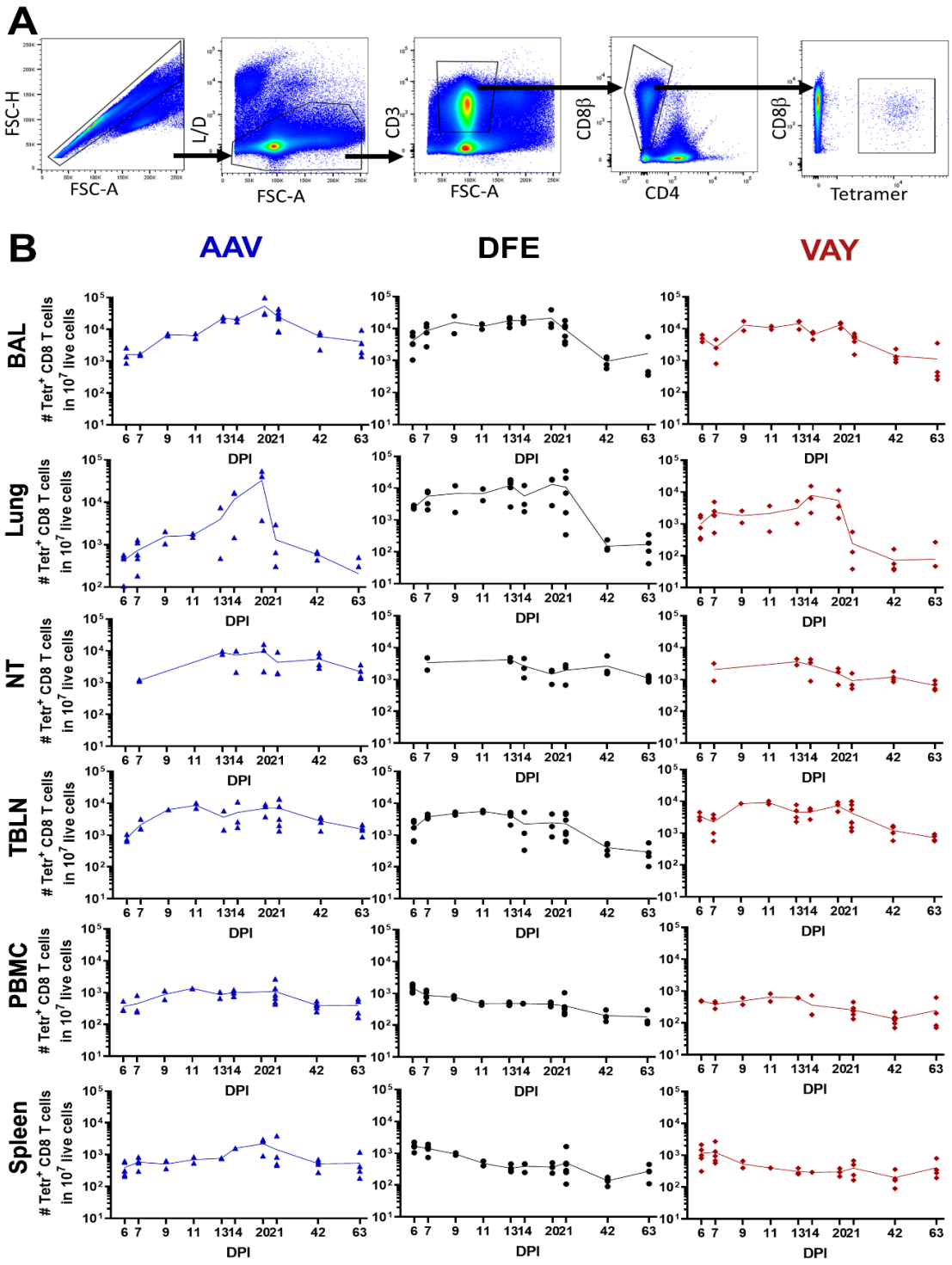
A
FSC-H
FSC-A
L/D
FSC-A
CD3
FSC-A
CD8β
CD4
CD8β
Tetramer
B
AAV
DFE
VAY
BAL
Lung
NT
TBLN
PBMC
Spleen
Tetr+ CD8 T cells in 10^7 live cells
DPI
6 7 9 11 1314 2021 42 63

Figure 3.8 **Counts of tetramer$^+$ cells in tissues. (A)** Tetramer+ CD8 T cells were identified with the following gating strategy: singlets, alive (Zombie NIR™), CD3, CD8β, and shown as number of tetramer$^+$ cells in 10 million alive cells. **(B)** Counts of tetramers$^+$ CD8 T cells in 10 million live cells isolated from each tissues. The symbols indicates individual animals while line connects the mean of each timepoint. DPI here indicates days post-infection

To assess changes over time, the proportions of tetramer$^+$ CD8 population were analysed for each tetramer (Figure 3.8). A mathematical model was developed in collaboration with Dr. Simon Gubbins (for equation, see Material and Methods).

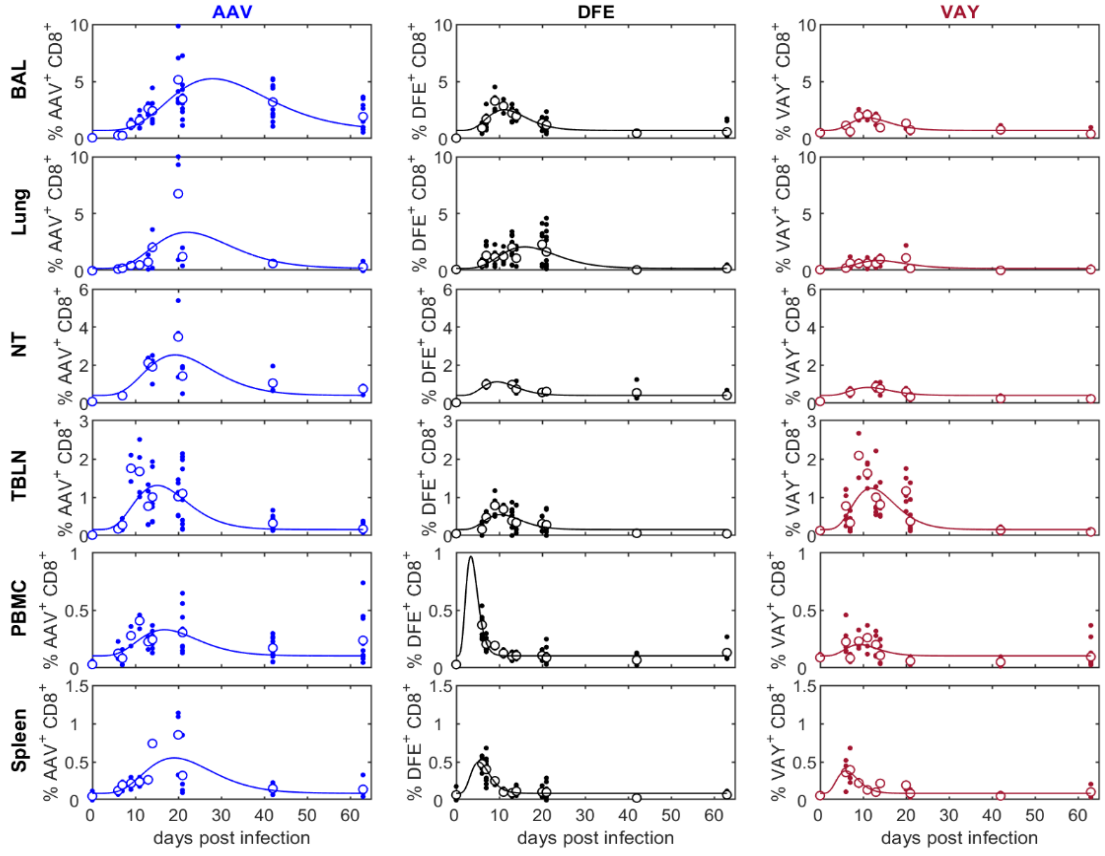

Figure 3.7 **Tetramer distribution in tissues**. Proportion (%) of CD8$^+$ T cells specific for AAV (left), DFE (middle) or VAY (right) in different tissues. In each plot the solid line is the fitted curve describing the dynamics, the large open circles are the mean % at each time point and the small filled circles are the observed % for individual pigs at each time point.

The model was chosen based on the best fit with the data: a curve that increases from the baseline (y_0) to a maximum (y_{max}) at the peak time (t_{max}) and then declines towards the baseline.

The fitted curves indicated that the peak proportion of CD8 T cells specific for each tetramer (y_{max}) and the timing of the peak (t_{max}) differed amongst tissues and between tetramers (Figure 3.7).

Interestingly, the modelled response in PBMC peaked earlier (16.8 dpi for AAV, 3.4 dpi for DFE and 9.1 dpi for VAY) compared to BAL, lung or NT (28.0 dpi, 11.2 dpi and 11.1 dpi respectively in BAL) (Table 3.1), in accord with the idea that cells generated in LN traffic to local tissues via the blood. AAV^+ CD8 T cells peaked 3 to 17 days later than the peak of DFE^+ or VAY^+ CD8 T cells in different tissues, while DFE and VAY responses shared similar kinetics in most tissues except PBMC, where DFE peaked earlier (Table 3.1 and Figure 3.7). The magnitude of AAV responses was greater than those to VAY and DFE in all tissues except PBMC, while DFE was higher than VAY in all tissues except for TBLN (Table 3.1 and Figure 3.7). Naïve animals showed minimal binding to all three tetramers (Figure 3.9 and Appendix Table7.1).

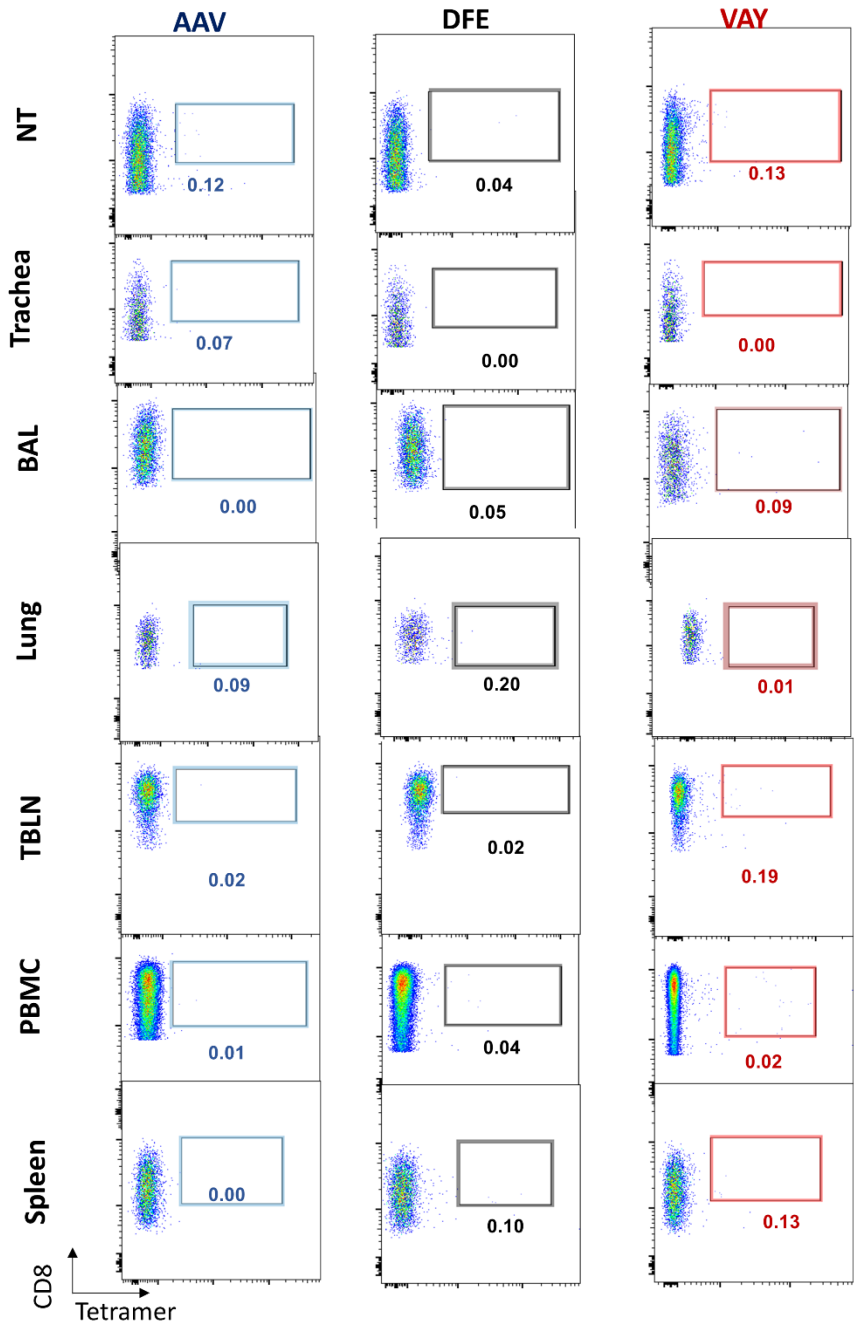

Figure 3.9 **Representative plots of tetramer^{+} cells at 0 dpi.** Numbers under the gated population indicate the % of tetramer+ CD8 T cells

Table 3.1 Estimated parameters describing the changes over time in the proportion of tetramer$^+$ CD8 T cells in different tissues.

Parameter	Tissue*	Tetramer		
		AAV	DFE	VAY
y_{max} - peak proportion (%)	BAL	5.23	2.52	1.80
	lung	3.37	2.10	0.90
	NT	2.53	1.12	0.83
	TBLN	1.31	0.55	1.23
	PBMC	0.33	0.97	0.20
	spleen	0.55	0.50	0.38
t_{max} - time of peak proportion (days post infection)	BAL	28.0	11.2	11.1
	lung	22.1	15.9	13.6
	NT	19.3	9.5	11.1
	TBLN	15.1	10.3	11.9
	PBMC	16.8	3.4	9.1
	spleen	19.1	5.3	6.0
y_0 - baseline proportion (%)†	BAL	0.71		
	lung	0.22		
	NT	0.41		
	TBLN	0.16		
	PBMC	0.10		
	spleen	0.09		

* BAL - broncho-alveolar lavage; NT - nasal turbinate; TBLN - tracheo-bronchial lymph node

† the baseline proportion is the same for each of the tetramers

Tracheal CD8 T cells were isolated only during experiment T4, at time points 21, 42 and 63 therefore it was impossible to model their kinetics. However, the AAV response was higher than that to DFE and VAY at 42 dpi (p=0.03), with DFE responses being significantly higher than VAY (p=0.03). AAV response remained higher than VAY at 63 dpi (p=0.03) (Figure 3.10).

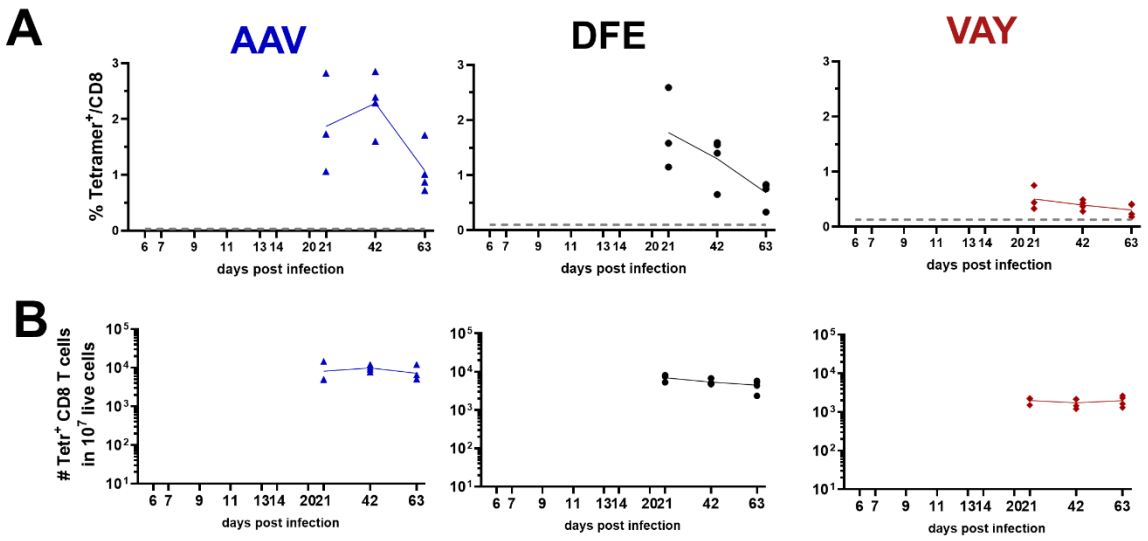

Figure 3.10 **Distribution of tetramer$^+$ cells in the trachea (A)** Percentages of DFE, VAY and AAV$^+$ within CD8 T cell population at day 21, 42 and 63 post infection **(B)** Number of tetramer$^+$ T cells in 10 million live cells. Each symbol represents an individual and the dotted line the average % of tetramer$^+$ T cells in naïve animals.

Changes in the proportions of different tetramer$^+$ cells in each tissue were modelled in relation to the total tetramers$^+$ population of CD8 T cells. BAL, lung and spleen presented similar changes in proportions of the different tetramer$^+$ populations. Despite being initially lower than VAY and DFE in all tissues, AAV was dominant by 30 dpi (60%), and in most tissues DFE and VAY declined (~20%) (Figure 3.11). However, in NT the frequency of cells specific for DFE remained constant (25%), while that for VAY decreased and that for AAV increased. In PBMC the proportions changed only gradually

(Figure 3.11), although the small number of PBMC data points mean that this observation should be interpreted with caution.

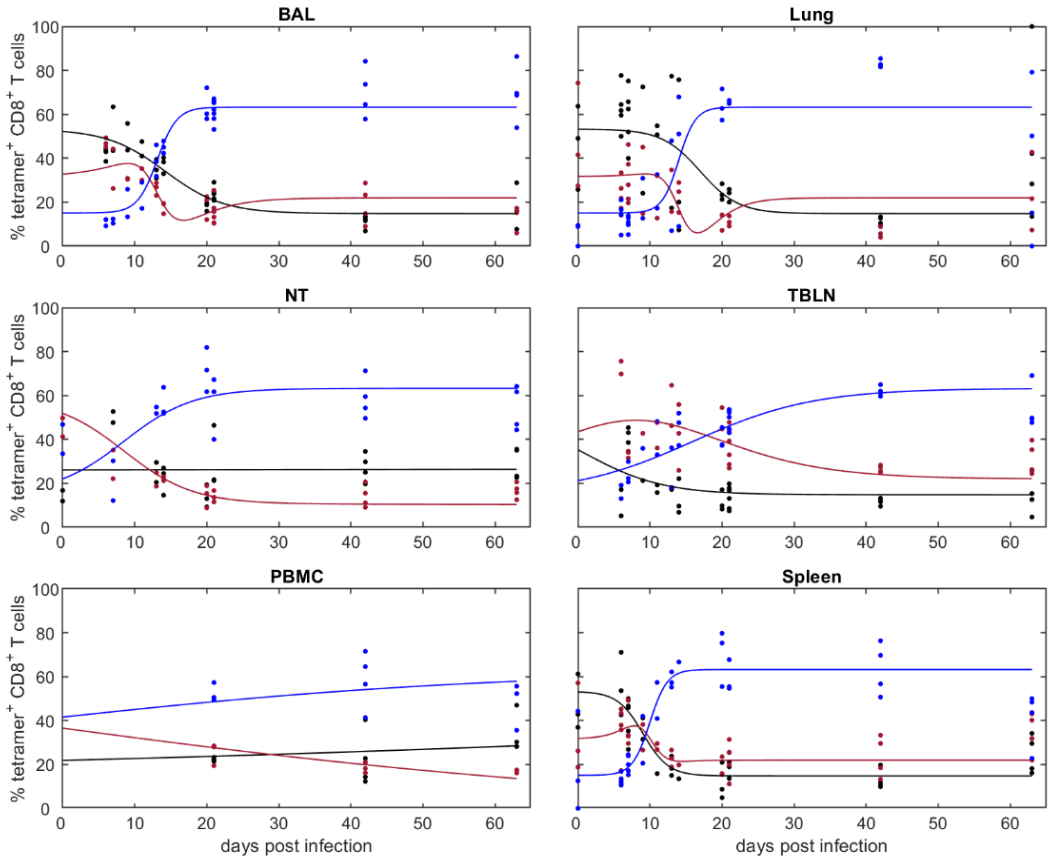

Figure 3.11 **Changes in the proportion of tetramer$^+$ CD8 T cells in different tissues** Relative proportion (%) of CD8$^+$ T cells specific staining with each tetramer (AAV blue; DFE black; VAY red) in the indicated tissues. In each plot the solid line is the fitted curve describing the dynamics and the points are the observed proportions for individual pigs at each time point

IAV-specific T cells in the nasal mucosa of mice are longer lived and showed a less rapid decline than those present in the harsh environment of the lung (Pizzolla et al. 2017b). I therefore investigated the decline of tetramer$^+$ T cells in all tissues after the peak response, using a mathematical model (Figure

3.12). AAV$^+$ CD8 T cells declined slower than cells specific for either DFE or VAY in all tissues. Furthermore, the proportion of cells specific for AAV decayed most slowly in BAL, indicating the importance of studying multiple antigen-specific T cells during infection.

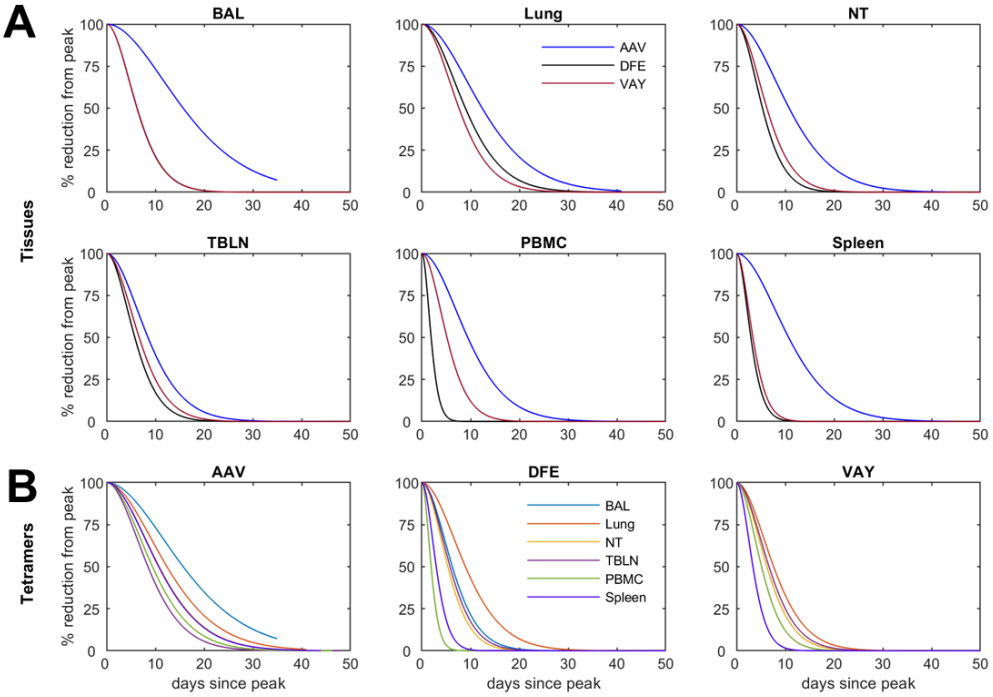

Figure 3.12 **Estimated decay over time (A)** Decay (% reduction from peak) of response within the indicated tissue. **(B)** Decay of tetramer$^+$ CD8 T cells in different tissues (as shown). Note: DFE and VAY share the same dynamics in BAL, VAY has the same dynamics in NT and PBMC while AAV has the same dynamics in NT and spleen so these decay curves overlap.

Collectively, these data show that the frequency of different tetramer$^+$ T cells varies between tissues, with the highest frequency in BAL. AAV tetramer$^+$ cells are dominant at later time points. In general, responses in PBMC peaked earlier compared to local tissues but waned more rapidly and did not reflect

the kinetic at the mucosal tissues. I did not observe a more rapid decay in lung and BAL than NT, as previously reported in mice (Pizzolla et al. 2017b).

3.6 Phenotype of NP-specific CD8 T cells over time

The phenotype of the NP-specific T cells present locally (in BAL and TBLN) and systemically (PBMC) was next analysed, using the newly established panel, and modelled (Figure 3.13 A and B). Due to limited sample availability, it was not possible to investigate the phenotype in NT, trachea, lung and spleen. Most tetramer^{+} cells exhibited TCM or TEM phenotypes throughout the time course in all tissues. Although the initial proportions differed amongst the tetramers (with AAV showing the highest percentage), a similar phenotype (TEM) was observed across tetramers with a slow but steady increase in TCM proportion in PBMC, reflecting the phenotype found most abundantly in TBLN (Figure 3.13 B). On average, more than 80% of NP-specific T cells in local LN expressed CCR7 and lacked CD45RA, while only a small proportion (8%) were negative for CCR7 (Figure 3.13). In contrast, in BAL the predominant phenotype was TEM (78.5%), with only a small percentage of cells expressing CCR7 (20.3% on average at 21dpi) which declined with time (Figure 3.13). TDE and naïve cells numbers were too small, so their analysis was not reliable.

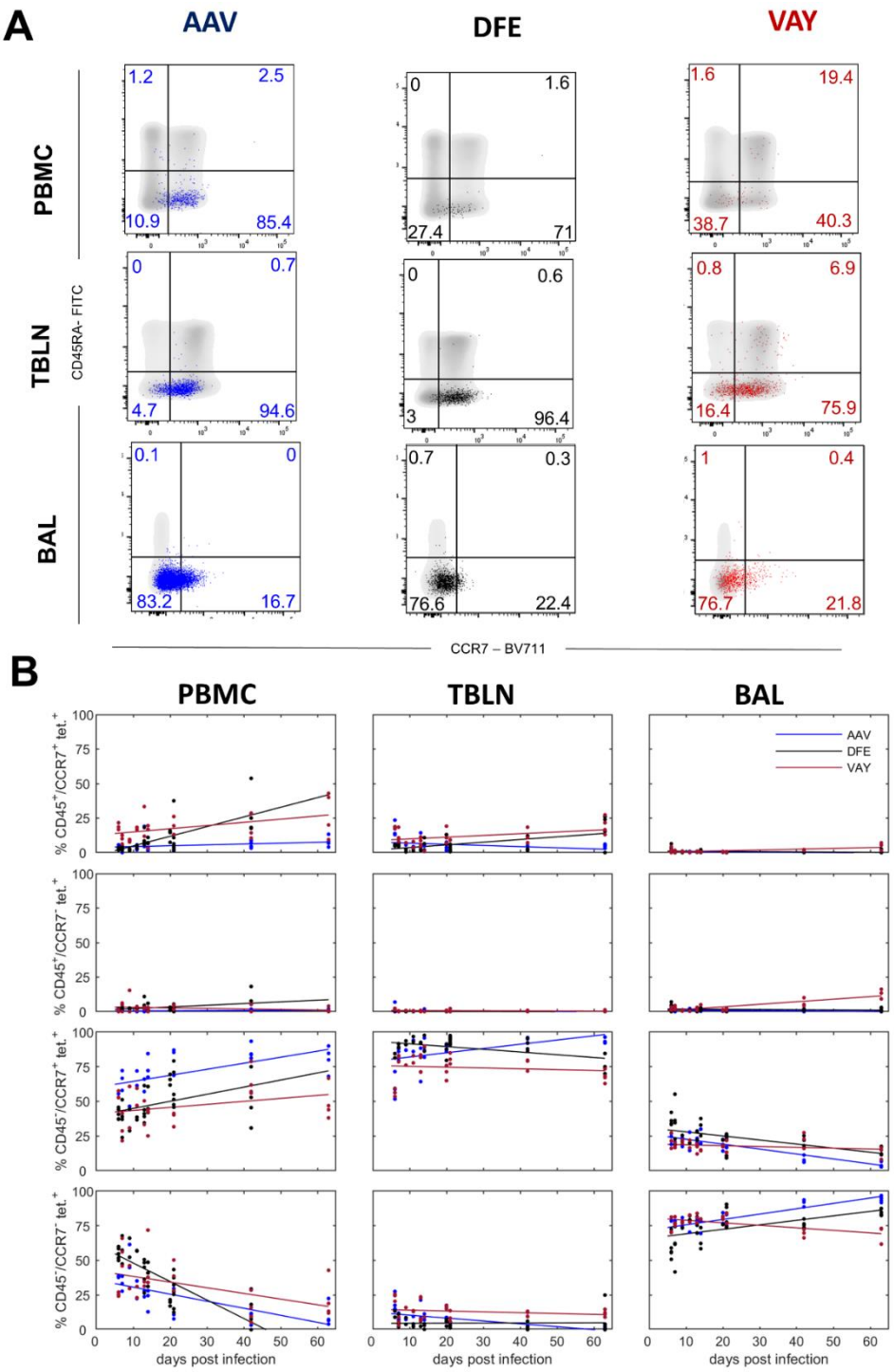
A
AAV
DFE
VAY
PBMC
TBLN
BAL
CD45RA- FITC
1.2
2.5
10.9
85.4
0
1.6
27.4
71
1.6
19.4
38.7
40.3
0
0.7
4.7
94.6
0
0.6
3
96.4
0.8
6.9
16.4
75.9
0.1
0
83.2
16.7
0.7
0.3
76.6
22.4
1
0.4
76.7
21.8
CCR7 – BV711
B
PBMC
TBLN
BAL
AAV
DFE
VAY
% CD45+/CCR7+ tet.+
% CD45+/CCR7- tet.+
% CD45-/CCR7+ tet.+
% CD45-/CCR7- tet.+
0
25
50
75
100
0
10
20
30
40
50
60
days post infection

Figure 3.13 **Phenotype of influenza-specific CD8 T cells in tissues and change over time (A)** Expression of CD45RA and CCR7 by AAV (left, blue), DFE (centre, black) and VAY (right, red) tetramer$^+$ (coloured dots) and total CD8 T cells (in grey) isolated at 21 dpi from PBMC (top), TBLN (middle) BAL (bottom), representative plots for one individual. **(B)** Proportion (%) of CD8$^+$ T cells staining with AAV (blue), DFE (black) and VAY (red) tetramer in different tissues. T cell populations are TEM (CD45RA$^-$/CCR7$^+$; top row) and TCM (CD45RA$^-$/CCR7$^-$; bottom row) in PBMC (left), TBLN (center) and BAL (right). In each plot the solid line is the fitted trend line and the points are the observed proportions for individual pigs at each time point.

3.7 Transcriptional changes of T cells in BAL after influenza infection

To better understand the differences between the tetramer$^+$ cells in the tissues studied, I next performed RNA sequencing (RNA-seq) on DFE$^+$ sorted cells. DFE was the tetramer of choice due to the limited availability of AAV and VAY tetramers at the time of the experiment.

Several studies in humans and mice showed that T cells isolated from lung and BAL highly expressed the core genes signature of TRM when compared to T cells in blood or spleen (Hayward et al. 2020; Sathaliyawala et al. 2013; Snyder et al. 2019; Kumar et al. 2017). Thus, I hypothesised that porcine BAL cells differentially expressed TRM genes compared to cells isolated from TBLN. The number of DFE$^+$ T cells in blood and spleen was too low to allow reliable RNA extraction, therefore, I used TBLN instead.

Secondly, I also wished to compare TRM gene expression in the upper and lower RT. After IAV infection in mice, these two compartments showed different dependencies on TGFβ signalling pathway and gene expression (Pizzolla et al. 2017b).

Finally, since the phenotype of tetramer$^+$ cells in BAL did not change significantly with time (Figure 3.13), a third aim was to investigate differences in the transcriptome of DFE$^+$ cells in BAL during infection (7 dpi) and at memory stages (21 dpi and 63 dpi).

RNA was isolated from DFE$^+$ cells sorted from BAL at 7, 21 and 63 dpi, TBLN and NT at 21 dpi, from the same animals. As a control, CD8 T cells from BAL of naïve animals were sorted (Table 3.2).

Table 3.2 **Summary of the sorted samples.** Sample identifier (ID) comprises the animal ID, day post-infection and tissue. Complementary DNA (cDNA) obtained after library preparation is reported in nanomolar concentration (nM).

sample ID	number of sorted cells	cDNA (nM)
0047 naïve BAL	64,646	9.82
R144 naïve BAL	82,773	143.81
G132 7dpi BAL	6,000	10.54
R140 7dpi BAL	11,000	29.82
P345 7dpi BAL	7,549	21.97
73 21dpi BAL	15,500	27.06
74 21dpi BAL	6,500	4.56
76 21dpi BAL	5,000	16.74
73 21dpi TBLN	1,650	1.43
74 21dpi TBLN	1,600	0.17
76 21dpi TBLN	600	0.98
73 21dpi NT	2,283	0.73
74 21dpi NT	1,077	0.24

76 21dpi NT	2,283	0.72
82 63dpi BAL	245	1.83
84 63dpi BAL	5,567	5.14
85 63dpi BAL	500	7.55

cDNA library preparation, sequencing and part of the RNA-seq analysis were conducted in collaboration with Prof, Timothy Connelley at the Roslin Institute and Edinburgh Genomics.

Unfortunately, a limited amount of cDNA was obtained from TBLN and NT, and therefore not sequenced, limiting the analysis to the BAL.

Multidimensional scaling (MSD) of 31,909 genes revealed that gene expression in DFE^{+} cells in BAL at 7 dpi was distinct from 21 dpi and 63 dpi, with the latter two time points being more closely related. Total CD8 T cells from BAL of the two naïve animals presented high variability due to small sample size, so were not taken forward in the analysis.

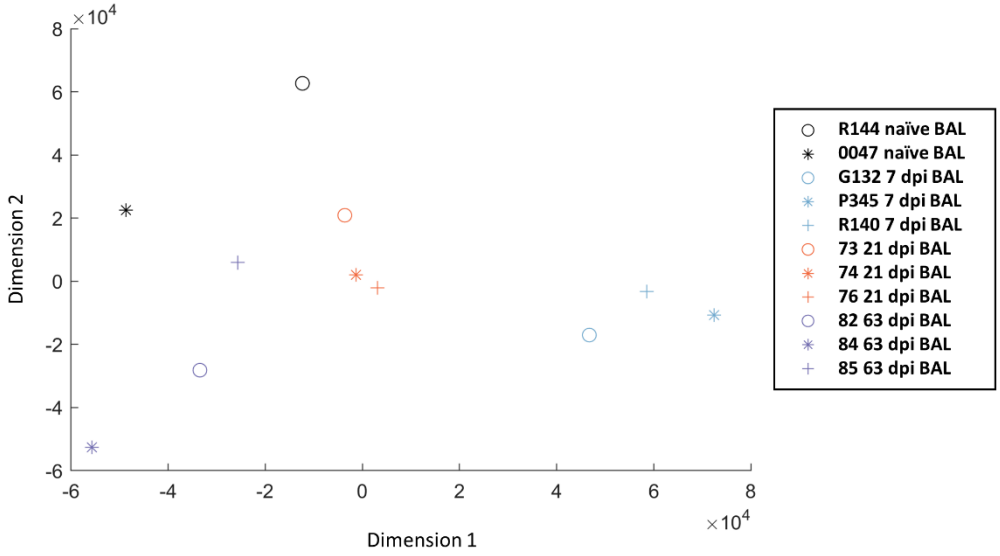

Figure 3.14 **Multidimensional representation of all genes in the sequenced samples**

Differential gene expression analysis was applied to compare 7, 21 and 63 dpi samples. We identified 4666 different genes significantly (p_{adj} value ≤ 0.05 and $|\log_2$ fold change$| > 1$) expressed in 7 dpi versus (vs) 21 dpi comparison while 1198 were differentially expressed in 7 dpi vs 63 dpi and only 560 in 21 dpi vs 63 dpi (Figure 3.15).

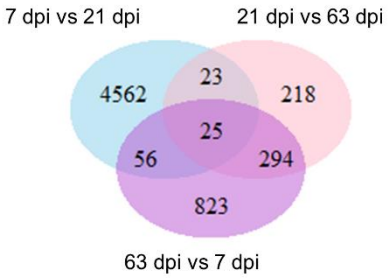

Figure 3.15 **Differential gene expression comparison.** Venn diagram shows the number of significant differentially expressed genes (q value ≤ 0.05 and $|\log_2$ fold change$| > 1$) between 7 dpi versus (vs) 21 dpi, 21 dpi vs 63 dpi, and 63 dpi vs 7 dpi comparison**.** The graph was generated using R.

At 7 dpi upregulated genes were involved in cell growth, movement (*Igfbp2*) and proliferation (*Ctla4, Kif11, Kif18a, Shmt1*) while at 21 dpi genes linked with T cell activation (*Tagap, IL2ra, Csf2, Dgkg*) and adhesion (*L1cam, Cass4*) were highly expressed (Figure 3.16 A). Interestingly, the comparison between 7 and 63 dpi revealed differential expression of genes involved in (*Jazf1, Atp8b4, Igf2bp3*), transcription factors (*Litaf*), T cell development and proliferation (*Ccnd3, Shcbp1*).

I then assessed differentially expressed genes in each pair-wise comparison for the enrichment of associated pathways. Upregulated pathways at 21 dpi, compared to 7 dpi, were linked to the control of Th1/Th2 differentiation, cytokines secretion, antigen processing, and presentation (Figure 3.16 B and Table 3.3). TGFβ signalling pathway, known to be involved in mucosal residency, was also upregulated at 21 dpi. No significantly regulated pathways were identified in the comparison between 63 dpi and the other time points.

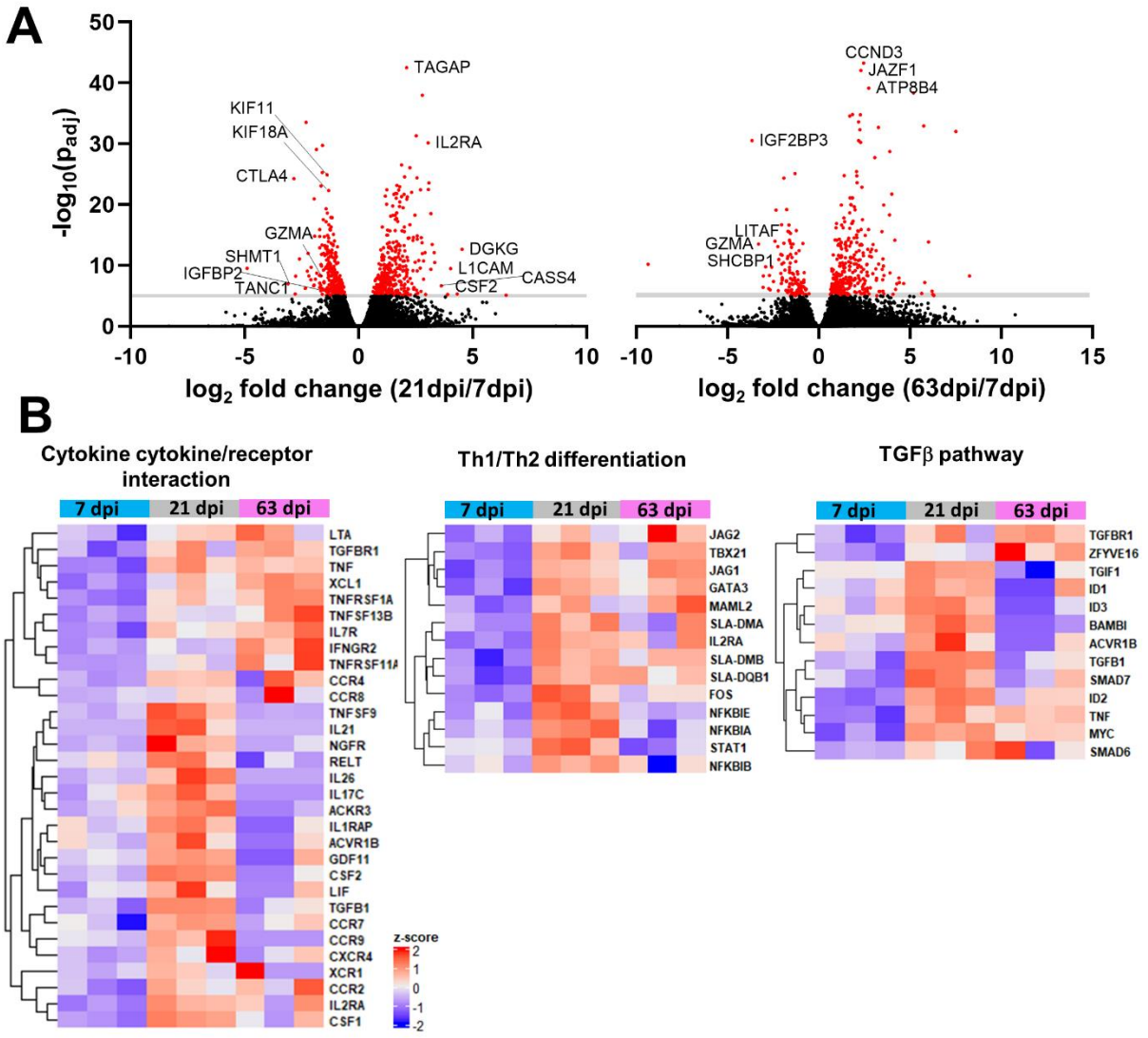

Figure 3.16 **Differentially expressed genes in DFE$^+$ cells in BAL at 7, 21 and 63 dpi. (A)** Volcano plot showing upregulated genes in 21 days post infection (dpi) vs 7 and 63 dpi vs 21 comparison. **(B)** Heatmap of selected genes from KEGG Pathway analysis related to cytokine production, T cell differentiation and TGFβ pathway (enrichment score of 0.76, 0.88 and 0.83 respectively).

Table 3.3 Relevant significant (FDR<0.05) KEGG pathways upregulated in 21 dpi vs 7 dpi comparison.

Gene Set	Pathway	Normalised enrichment score	P Value	FDR
ssc04640	Hematopoietic cell lineage	0.90817	0	0
ssc04010	MAPK signalling pathway	0.77936	0	0
ssc04658	Th1 and Th2 cell differentiation	0.88885	0	0
ssc05164	Influenza A	0.82988	0	0
ssc04668	TNF signalling pathway	0.85347	0.0014388	0.0014388
ssc04060	Cytokine-cytokine receptor interaction	0.75969	0	0
ssc04612	Antigen processing and presentation	0.88222	0	0
ssc04350	TGFβ signalling pathway	0.83065	0.0014925	0.0014925

I next examined the presence of gene expression features of tissue resident memory T cells (TRM), previously identified in the human lung, in these samples (Snyder et al. 2019; Kumar et al. 2017; Schoettler et al. 2019) (Figure 3.17). BAL cells from 63 dpi upregulated a gene related to integrins (*Itga1*), the TRM transcription regulator gene *Znf683* and downregulated genes involved in migration

(*Sell, S1pr1*) as in humans. In addition, at the earlier timepoint of 7 dpi DFE^{+} T cells expressed more cytotoxicity related genes (*GzmA, GzmH, Prf1 and Ccl5*) while starting from 21 dpi genes involved in cytokine signalling and secretion were upregulated (*Ifng, Tnf, Il13, Tgfb1* and *Tnfsf13b*) (Figure 3.17). Interestingly, *Cd69* expression changed with time and peaked at 21 dpi, similarly to CD103 gene (*Itgae*), which had its peak at 7 dpi.

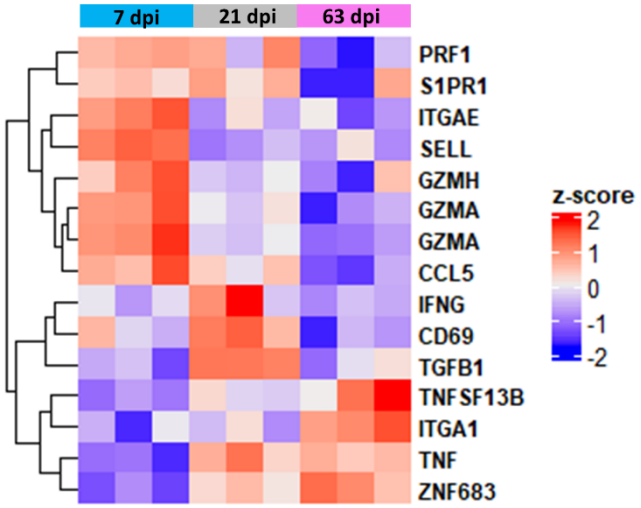

Figure 3.17 **Gene expression of tissue resident memory T cells features. (A)** Heatmap of selected genes related to tissue resident memory T cells.

Despite the similar phenotype, these data suggest that CD8 T cells at the site of infection change gene expression over time, with genes involved in proliferation and migration upregulated at 7 dpi while cytokine-related pathways are upregulated at 21 dpi.

3.8 Differentiation states and functions of influenza-specific T cells

RNA-seq analysis showed changes in CD69 gene expression with time, I, therefore, analysed and modelled CD69 protein expression in BAL, TBLN and PBMC (Figure 3.18 A) (for gating strategy, see Appendix Figure 7.2). CD69 protein levels decayed only slightly with time in BAL for all tetramers. This also applied to AAV and VAY labelled T cells in TBLN while it decayed in DFE^+ T cells at a higher rate (0.022/day for DFE, 0.003/day VAY and 0.001/day AAV) (Figure 3.18 A and Table 3.4). As reported above, PBMC expressed minimal CD69.

Pathway analyses revealed upregulation of Th1/Th2 differentiation-related genes in BAL T cells at 21 dpi compared to 7 dpi. I validated these findings by analysing and modelling the expression of the transcription factor T-bet, involved in Th1 differentiation and homing to inflammatory sites, and eomesodermin (Eomes), involved in the induction of memory and effector T-cell differentiation (Figure 3.18 B). Eomes was poorly expressed in BAL, only detectable at early time points and decayed rapidly in all $tetramer^+$ cells (0.33/day decay rate) (Figure 3.18 B and Table 3.4). AAV^+ CD8 T cells presented the highest expression of Eomes in TBLN (mean of 20.6%) followed by VAY and DFE while similar expression was present in PBMC for all tetramers, with no decay (Figure 3.18 B and Table 3.4). In contrast, T-bet expression differed significantly among tissues and tetramers. T-bet was highly expressed in TBLN and PBMC, where it decayed more slowly than in TBLN, for all tetramers. In TBLN T-bet decayed more slowly in AAV than DFE or VAY responding T cells (Figure 3.18 B and Table 3.4). Low levels of T-bet were present in BAL at early times in all tetramers, but its expression declined rapidly and was undetectable at later time points (Figure 3.18 B and Table 3.4).

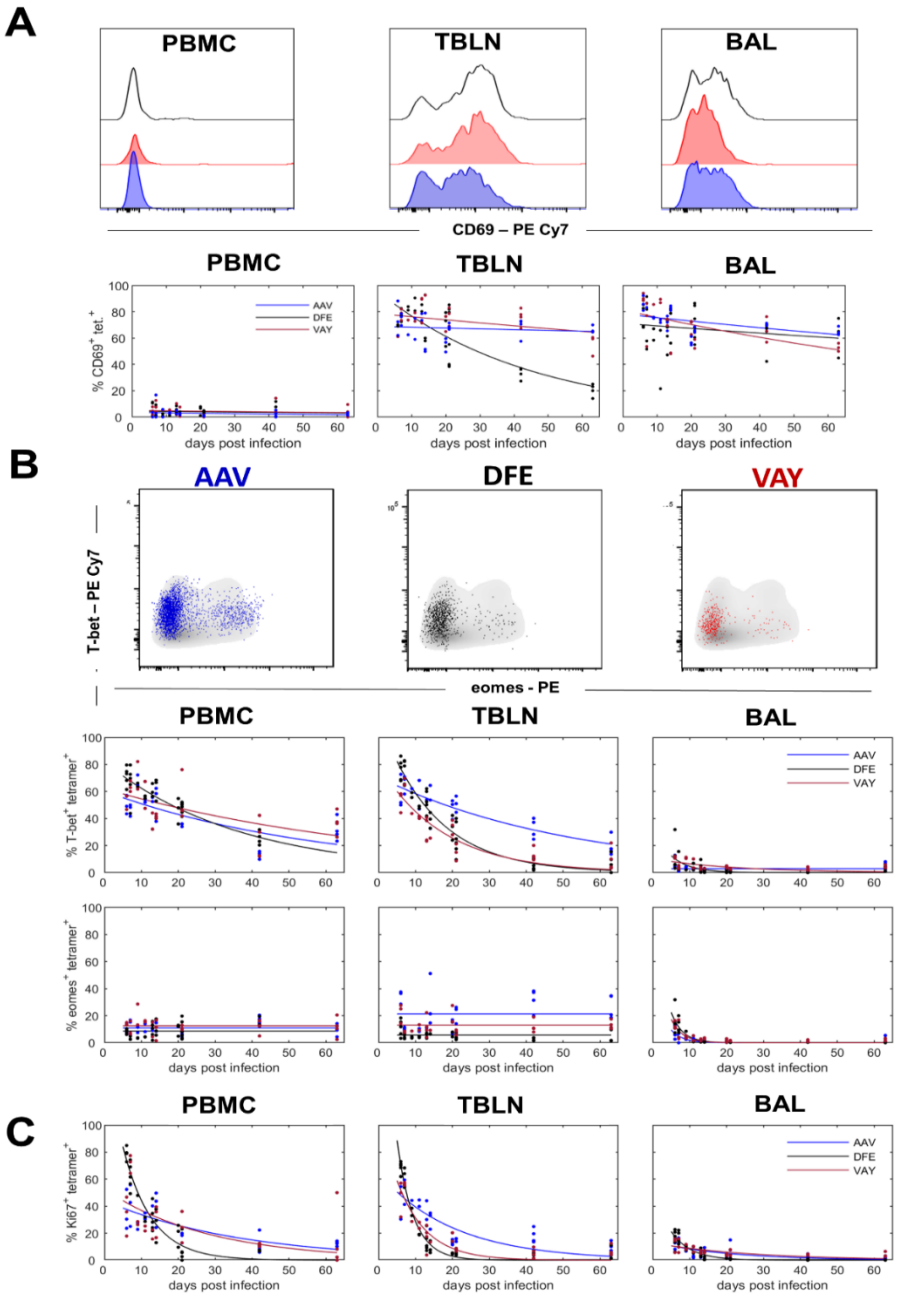

Figure 3.18 **Activation state and transcription factors expression in tetramer$^+$ CD8 T cells (A)** Top: Histograms show the expression of CD69 by DFE (black), VAY (red) and AAV (blue) tetramer$^+$ T cells in PBMC (left), TBLN (centre) and BAL (left) at 21 DPI. Bottom: Frequencies of tetramer+ cells expressing CD69 in PBMC, TBLN and BAL. **(B)** Top: Expression of T-bet and Eomes by AAV (left,

blue), DFE (centre, black) and VAY (right, red) tetramer$^+$ (coloured dots) and total CD8 T cells (in grey) isolated at 21 dpi from TBLN, representative plots for one individual. Bottom: Frequencies of tetramer+ cells expressing T-bet and Eomes in PBMC, TBLN and BAL. **(C)** Proportion of AAV, DFE and VAY tetramer $^+$ expressing Ki67 in PBMC, TBLN and BAL. In each plot the solid line is the fitted curve describing the dynamics and the points are the observed proportions for individual pigs at each time point

Table 3.4 Estimated decay rates (*d*; /day) in the proportion of tetramer specific T cells expressing different markers in different tissues.

Marker	**Tissue***	**Tetramer**		
		AAV	**DFE**	**VAY**
Ki67	PBMC	0.027	0.128	0.036
	TBLN	0.049	0.226	0.127
	BAL	0.050	0.186	0.038
T-bet	PBMC	0.017	0.027	0.013
	TBLN	0.019	0.067	0.057
	BAL	0	0.196	0.044
Eomes†	PBMC	0		
	TBLN	0		
	BAL	0.33		
CD69	PBMC	0.012	0.006	0.006
	TBLN	0.001	0.022	0.003
	BAL	0.004	0.003	0.007

* BAL - broncho-alveolar lavage; TBLN - tracheo-bronchial lymph node, † decay rate is the same for each of the tetramers

These data suggested that BAL TRM may have already switched off Eomes and T-bet protein expression and are no longer undergoing active Th1/Th2 differentiation.

Ki67 expression was analysed as a proxy for cell proliferation which is typically linked to differentiation. Whereas high frequencies of Ki67$^+$ tetramer binding cells were found in PBMC and

TBLN at early time points, only 14% of BAL cells were $Ki67^+$ at 6 dpi and Ki67 expression was barely detectable at 63 dpi (1.8%) (Figure 3.18 C).

The RNA-seq data showed changes in expression of genes related to cytokine production over time. Lymphocytes isolated from PBMC, TBLN and BAL were therefore stimulated with H1N1pdm09 and the production of IFNγ, TNF and IL-2 by tetramer binding cells was assayed by intracellular cytokine staining. I compared the responses of the dominant responding AAV population with DFE cells which decline more rapidly. Despite high expression of T-bet, PBMC $tetramer^+$ cells produced a limited amount of IFNγ (5.9% in DFE^+, 4,3% AAV^+ at 7 dpi), which was almost undetectable after 21 dpi (Figure 3.19). Similar kinetics were present in TBLN, with IFNγ and IFNγ/TNF co-producer being the most abundant in both DFE and AAV^+ CD8 T cells. The highest responses were detected in BAL, with consistent production of cytokines (predominately IFNγ and TNF) even at 63 dpi. No significant difference was observed between DFE^+ and AAV^+ populations, but there was a trend toward a higher proportion of triple producers ($INF\gamma^+TNF^+IL\text{-}2^+$) at later time points in AAV^+ cells compared to DFE^+ (Figure 3.19).

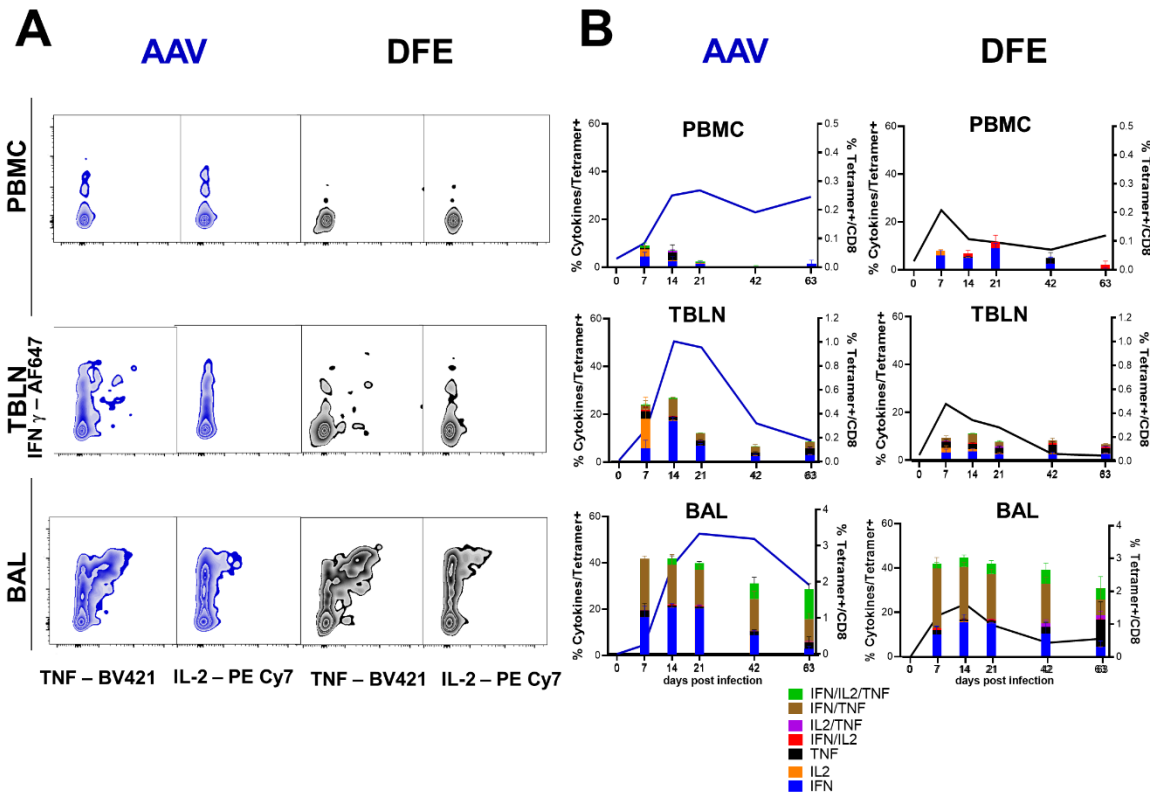

Figure 3.19 **Cytokine secretion after *ex vivo* virus stimulation of AAV and DFE tetramer$^+$ cells (A)** Lymphocytes isolated at different time points from blood, TBLN and BAL were stimulated with H1N1pdm09 MOI=1. Following 18 h of stimulation, cells were labelled using tetramers and cytokines quantified using intracellular cytokine staining. Representative plots of AAV$^+$ (on left) and DFE$^+$ (right) T cells secreting IFNγ, TNF and IL-2 cytokines, from lymphocytes isolated 14 DPI. **(B)** Mean frequency (± SEM) of tetramer$^+$ cells secreting IFNγ, TNF and IL-2 from PBMC (top panels), TBLN (in the middle) and BAL (bottom). On the right Y axes is reported the mean frequency of AAV$^+$ (in blue, left panels) and DFE$^+$ (in black, right panels) within CD8 T cells is reported. Data shown are mean of 3 / 4 individuals per timepoint. Two-way ANOVA was used for comparison of each cytokine population between DFE$^+$ and AAV$^+$ cells.

In conclusion, despite differences at the transcription level of CD69 and T cell differentiation genes, I did not find corresponding differences in their protein level expression in BAL, while TBLN and PBMC expressed T-bet and Ki67 at early time points, while Eomes up to 63 dpi. *Ex vivo* incubation with H1N1pdm09 resulted in IFNγ and TNF cytokine secretion by 7 dpi, despite upregulation of related genes

being highest at 21 dpi. These data suggest that BAL TRMs are a stable, largely non-dividing population able to produce abundant cytokines for at least 63 dpi.

3.9 Pilot study on T cell migration

TRM in mice are independently maintained from T cells in circulation and do not egress from mucosal sites (Turner et al. 2014) although this theory has been recently challenged (Fonseca et al. 2020).

In order to establish the methodology to determine whether circulating T cell contribute to protection or TRM are solely responsible for heterosubtypic protection, I tested FTY720 in pigs. FTY720 inhibits the recirculation of lymphocytes and monocytes from the LN by modulating sphingosine-1-phosphate-dependent lymphocyte egress (Brinkmann et al. 2002). Despite its wide use in human and mice, the drug was never administered to pigs. I therefore tested oral administration of FTY720 at 1mg/kg both as a solution and in the solid form of a capsule as a proof of concept (Figure 3.20).

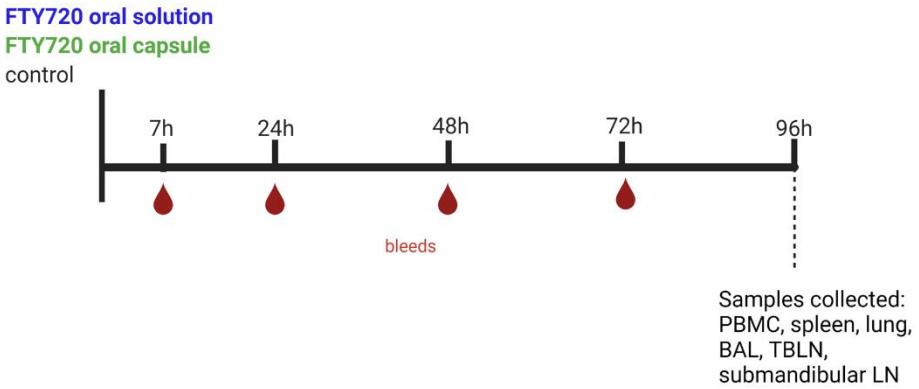

Figure 3.20 **FTY720 experimental design**. Babraham pigs were administered 1mg/kg of FTY720 in a capsule (n=2) or in a solution squirted into the mouth (n=2). A control pig was untreated. Pigs were bled

at: 7, 24, 48, 72 and 96 h post-administration. Five days after treatment (96h), all pigs were culled and PBMC, spleen, lung, TBLN and submandibular lymph nodes (LN) were collected.

Blood was monitored from 7 to 96 h post-administration for leukopenia. Level of granulocytes, monocytes, T cells, natural killer (NK) cells and mature B cells ($CD21^+$) were measured and compared to the baseline levels of each population prior to administration (Figure 3.21 A). At 7 h post-treatment, both FTY720 groups showed a marked reduction in T cells (to 13.1% and 15.23% of the baseline levels in the oral solution and oral capsule group, respectively), with naïve CD4 ($CD4^+CD8\alpha^-$) being the most affected population (Figure 3.21 B and C). B cells were also markedly reduced (to < 25% of the baseline in both groups) from 7 h while granulocytes and monocytes were at their lowest after 48 h. NK population was variable during all measurements so that no reliable conclusions can be drawn. From 48 h, pigs that received FTY720 by oral solution showed increased granulocyte and T cells levels compared to the oral capsule group, although their level did not reach baseline in blood (Figure 3.21 C). Five days post-administration (96 h), the lymphopenic effect persisted in the FTY720 oral capsule group. At the same time, most of the subsets studied reached around 50% of the baseline level in the oral solution group.

In BAL at 96h, I did not observe marked differences between the groups, suggesting that the cells isolated by lavage are resident. In the lung, γδ and CD8 T cells levels were more than fivefold lower in the oral capsule group compared to untreated control. On the other hand, leukocytes accumulated in LN. Monocytes and CD8 T cells were three times more abundant after FTY720 administration via capsule than oral solution or control, and overall leukocytes levels were increased by twofold in submandibular LN. A similar effect was observed in TBLN, while in the spleen the differences were marginal (Figure 3.22).

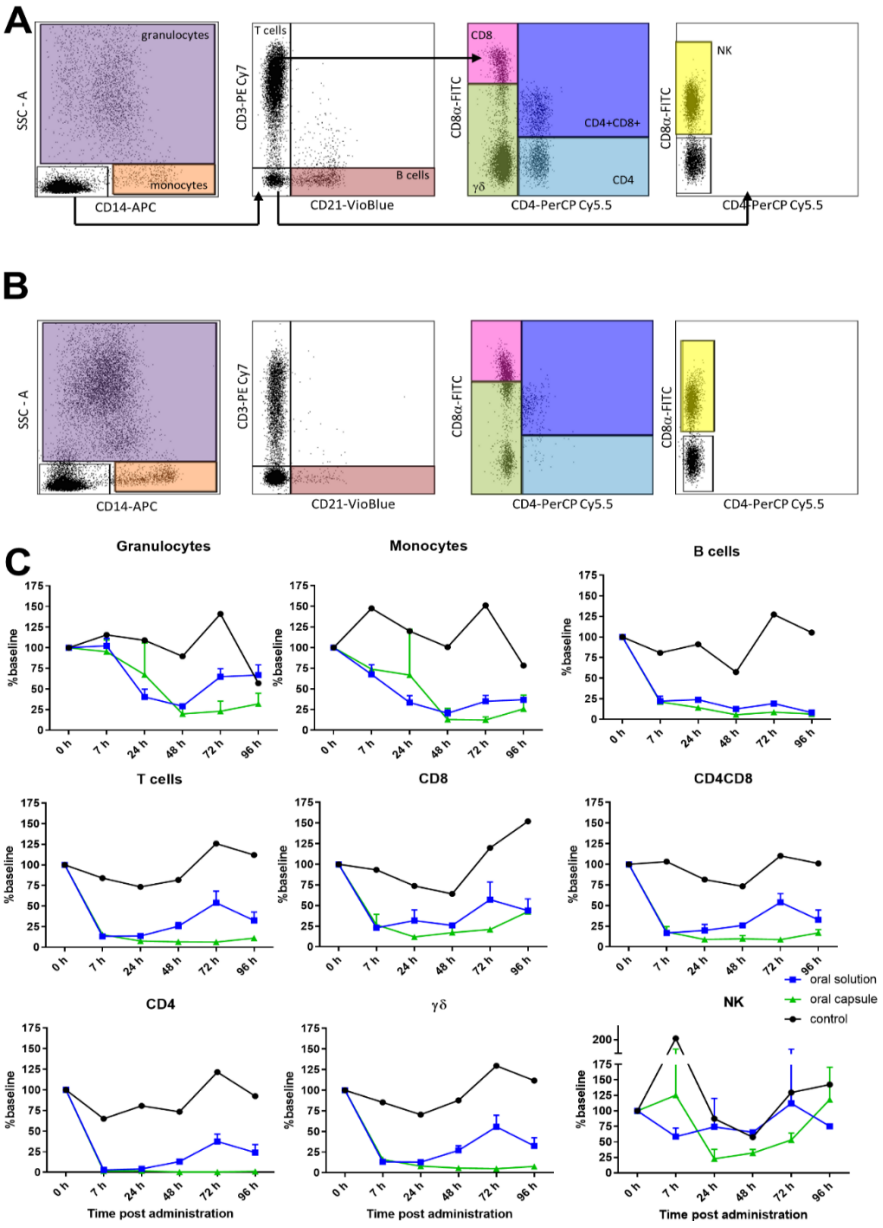

Figure 3.21 **Gating strategy and leukocytes levels in the blood. (A)** Gating strategy based on pre bleed sample. $CD21^{+}$ mature B cells are referred for convenience as B cells. **(B)** Representative blood sample after 96 h of FTY720 treatment by oral capsule. **(C)** Levels of different leukocytes were examined relative to their baseline level pre-treatment. Each symbol represents one animal, and the line connects the mean of each measurement.

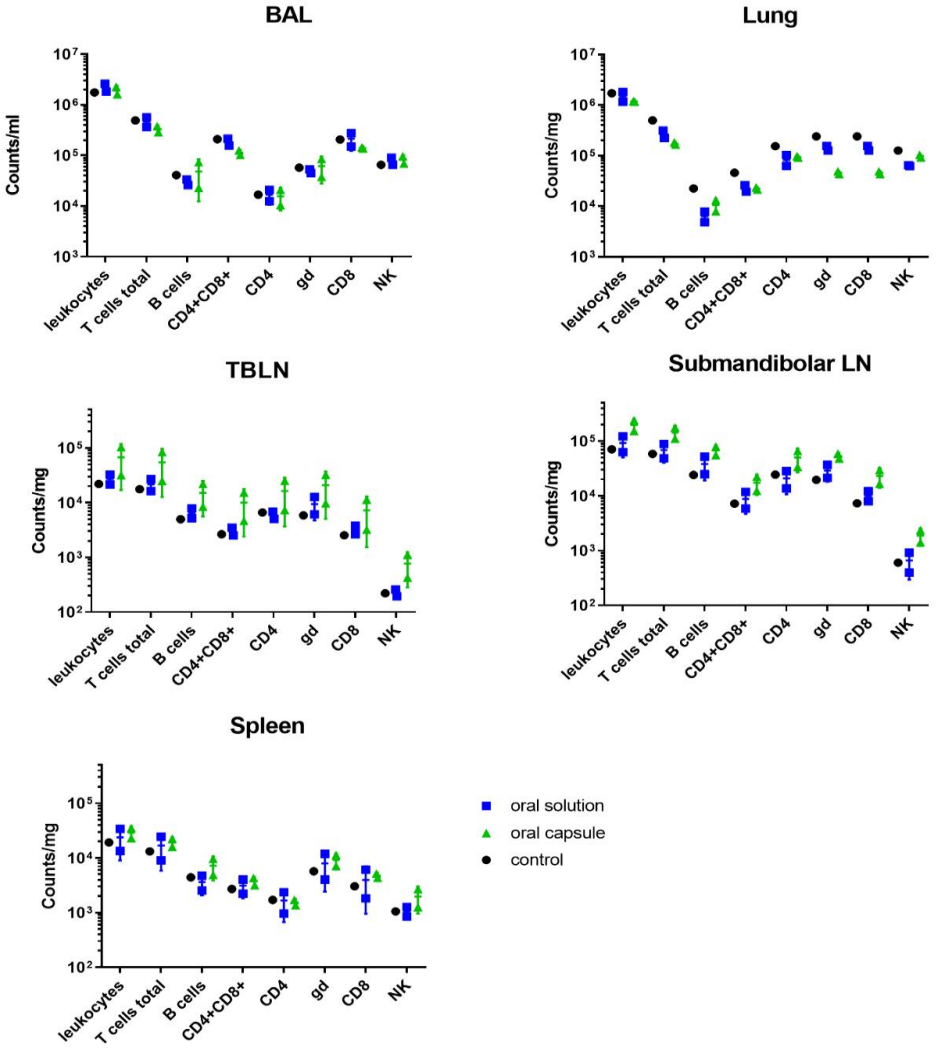

Figure 3.22 **Lymphocytes presence in tissues**. Tissues were weighed before lymphocytes isolation and counts adjusted per mg of tissue. BAL cells were isolated with 100ml of media and cell counts expressed per ml. gd indicates γδ T cells.

These data indicate that oral administration of FTY720 in capsule induced sustained leukopenia and can be used in the future experiments to establish the contribution of circulating T cells and TRM in protection.

3.10 Discussion

This chapter described the phenotype of porcine IAV-specific CD8 T cells in lymphoid and non-lymphoid tissues and showed that antibodies to CD45RA and CCR7 identify four subsets: naïve, TCM, TEM and TDE. The identity of these subsets was confirmed by additional staining for CD27 and perforin and by assessing their ability to secrete effector cytokines. As expected, in LN, the predominant population was naïve cells with few TEM and TDE. Like humans, most CD8 T cells in the lung were TEM and TDE (Snyder et al. 2019), while in BAL, TEMs predominate (~80%).

Previous studies in pigs showed that most TBLN, BAL, and, to a lesser extent, lung T cells are inaccessible to intravenous anti-CD3 mAb (Holzer et al. 2018; Martini et al. 2021); it was interesting to examine the expression of CD69, designated as a marker of early activation and tissue residence, on these cells. As in other species, CD69 was minimally expressed on blood T cells, although it can be upregulated upon activation with a mitogen (data not shown). In BAL, CD69 was present on a high proportion of cells, while a small proportion of $CD69^+$ T cells was found in the lung. CD8 T cells in TBLN and spleen also expressed this marker, perhaps reflecting that cells in these organs may have been recently activated. In the context of IAV infection, a high proportion of NP-specific T cells in TBLN expressed CD69 from 6 until 63 dpi, and $CD69^+tetramer^+$ cells in BAL reached 80% in all three $tetramer^+$ populations examined. Because CD69 is also a marker of early activation, future studies will be needed to investigate its coexpression with other activation markers such as CD25, CD38, and SLA-DR. In addition, the development of an anti-porcine CD103 will further confirm the role of CD69 as a residency marker in mucosal tissues.

This chapter compared the distribution, phenotype and gene expression of different antigen-specific cells during IAV infection. Intriguingly, the modelled kinetics of the responses to the three epitopes were very different, with DFE being the most abundant in PBMC and spleen early on but peaking in all other tissues at similar times to VAY. The response to the third epitope AAV appeared later, but by 20-30 dpi it was dominant in all tissues and persisted for longer. Others have reported marked differences in the hierarchy of the responses to immunodominant epitopes of IAV in mice (Wiley et al. 2001; Belz et al. 2000). Pizzolla and colleagues showed that T cells specific for immunodominant epitopes in NP, PA and PB proteins of IAV in the nasal mucosa shared a similar hierarchy with systemic responses, while in the lung all immunodominant epitopes were equally represented (Pizzolla et al. 2017b). In the present study, despite an initial peak of DFE^+ T cells, at the memory stage, the AAV epitope dominates in all tissues, with no marked difference between the organs. Furthermore, the response does not decline more rapidly in the lung or BAL than blood or spleen, although in mice both of these have been postulated to be hostile environments inducing transcriptional and epigenetic changes that promote apoptosis (Hayward et al. 2020). Further studies are required to understand why AAV responses are immunodominant compared to DFE and VAY. Immunodominance may be linked to peptide-MHC affinity and it has also been reported that early IFNγ production can provide an advantage to a given antigen-specific population (Jenkins et al. 2006; Liu, Whitton, and Slifka 2004). However, I did not observe significant differences in cytokine production between AAV^+ and DFE^+ CD8 T cells.

The reported results indicate that an airway population of TRM, recoverable by BAL, is established following IAV infections with a peak at 10-30 dpi. Early on, these cells were proliferative (5-22% $Ki67^+$ at 7 dpi), though Ki67 expression was much more prominent in tetramer binding cells in TBLN and PBMC, suggesting that the bulk of the BAL population arises by cell division before entry into the

airways. BAL Ki67 expression declined over time and, and so did the tetramer-binding population, indicating that cell division did not maintain this population. This finding is in line with recent studies on SARS-CoV-2 infection, revealing that despite a high number of lung resident T cells, these lacked Ki67 expression in humans (Szabo et al. 2021). Interestingly, the expression of the transcription factors T-bet and Eomes shared similar kinetics. In mice, T-box transcription factor downregulation and the consequent expression of CD103 on CD8 T cells are essential for TRM formation (Mackay et al 2015). In addition, DFE^+ T cells upregulated genes implicated in TGFβ pathway at 21 compared to 7 dpi. TGFβ plays a critical role in tissue retention and signaling differentiation into TRM (Zhang and Bevan 2013; Mohammed et al. 2016; Ma and Zhang 2015), suggesting that tetramer binding cells at 21 dpi already present TRM features. In addition, other genes characteristic of TRMs in humans were also upregulated at each of these time points.

Interestingly, *GzmA, GzmH, Prf1* genes were upregulated at 7 dpi, while *Ifn* and *Tnf* were highly expressed only at 21 dpi. A possible explanation for this difference lies in the kinetic of death mediated by these molecules. Cytotoxicity mediated by granzymes and perforin is a fast event, fundamental early on during infection when many infected cells are present. On the other hand, receptor-induced killing, such as the one promoted by TNF, is slow and could be beneficial at later time points, such as 21 dpi.

Others have reported marked differences in gene expression between CD8 T cells specific for different epitopes (Yoshizawa et al. 2018) which should be investigated in the future to understand the prevalence of AAV^+ CD8 T cells.

Treatment with FTY720, a drug that impairs leukocytes' egress from LN, and caused systemic leukopenia in pigs while the cells in the BAL were unaffected in this short-term experiment, confirming

that these are TRM. Future studies will investigate the protective role of pre-existing TRMs in the respiratory tract after heterotypic influenza challenge, post FTY720 treatment.

In summary, these data suggest that in this natural host model of IAV infection, CD8 TRM are established in the airways after clonal expansion in draining TBLN and migration to the lungs via the blood. Modelling of the kinetics of the responses to three different NP epitopes over time in different tissues highlights the importance of studying and modelling the response to different epitopes within the same protein, often oversimplified in mouse studies, where one immunodominant epitope is normally used. I demonstrate that antigen specific CD8 cells do not decline faster in the lung compared to other tissues, in contrast to previous literature. I demonstrate differences in gene expression over time in NP-specific TRM cells in BAL, linked to cytokine production and differentiation, indicating that TRM are not a completely stable population but continue to differentiate during their tissue residence. Nevertheless no difference in phenotype or functions between different tetramers-binding T cells was observed, so it remains unclear why AAV dominates over the other epitopes. This data revealed that although porcine TRM have a stable phenotype they exhibited major changes in gene expression.

Chapter 4
Distribution of droplets after aerosol and intranasal delivery to the porcine respiratory tract

4.1 Introduction

For decades, LRT infections have been in the top three causes of mortality in adults and children (Forum of International Respiratory Society 2017). Only a handful of pathogens are mainly responsible for these infections: influenza virus, respiratory syncytial virus, *M. tuberculosis*, and, more recently, SARS-CoV-2.

Vaccines are the most cost-efficient strategy to prevent infections, and much research aims to improve their efficacy against respiratory viruses. The effectiveness of a vaccines is measured by its ability to elicit good humoral and/or cellular responses in the periphery. The systemic immune responses were considered to mediate protection at the mucosal sites, where infections occur. Recently, several studies have shown that lung, skin, gut, and the reproductive tract's immune responses are distinct from those found in circulation and fundamental for protection (Beverley et al. 2014; Jin and Subbarao 2014; Jiang et al. 2012; Mueller et al. 2013). Despite evidence for the critical role of local immunity, only a handful of vaccines have been approved for mucosal delivery (Miquel-Clopes et al. 2019). Mucosal vaccination offers several advantages: it is needle-free, does not require trained personnel, delivers the antigens at the site of infection, eliciting mucosal immunity and can be an easy immunisation tool for a large population. Furthermore, mucosal immunisation is the most efficient way to elicit B and T tissue resident memory cells in the lung, as antigen encounter in the respiratory tract is thought to be important for their

formation (Pizzolla et al. 2017a; Allie et al. 2019). While systemic immunisation is characterised by serum IgG, IgA can only be generated at the immunisation site and in circulation when the vaccine is delivered locally. IgA are actively secreted across the epithelium in the RT as a dimer, a configuration shown to be more efficient in neutralising influenza, human immunodeficiency virus (HIV), and SARS-CoV-2 (Liew et al. 1984; Devito et al. 2000; Asahi-Ozaki et al. 2004; Sterlin et al. 2021). An advantage of respiratory immunisation is the enormous epithelial surface (more than 140 m^2) which facilitates absorption with its thin alveolar vasculature (Gehr, Bachofen, and Weibel 1978). Despite these advantages, only one vaccine (live attenuated influenza vaccine, LAIV) has been licensed to be delivered mucosally against respiratory infections in humans (Food and Drug Administration 2020; European Medical Agency 2013). Only seven of nearly 100 vaccine candidates in clinical trials against COVID19 are delivered intranasally (Lund and Randall 2021).

One obstacle in the preclinical development of respiratory vaccines is selecting which part of the respiratory tract to target: URT or LRT. Two different vaccination strategies have been tested: nasal spray (limited to URT) and small droplets aerosol (which also targets the lung). Both routes have been tested in humans, with aerosol measles vaccine delivered to children in Mexico in clinical trials and LAIV administered routinely i.n. in the US, UK and Europe (Jin and Subbarao 2014; Low et al. 2015). However, delivery to the nose or LRT may have significant immunological and safety consequences (Bolton et al. 2017). In fact, when comparing URT and lung targeting, different immune responses have been described for measles (de Swart et al. 2017), *Mycoplasma pulmonis* (Hodge and Simecka 2002), tuberculosis (Tb) (Ronan et al. 2010), and influenza (Lau et al. 2011; Smith et al. 2012; Hemmink et al. 2016; Minne et al. 2007). These findings suggest the need to study how to optimally deliver a new vaccine candidate to different RT areas.

A second challenge in developing mucosal vaccines against respiratory infections are the animal models available to study accurately vaccine delivery and immune responses. Rodents are widely used for preclinical vaccine evaluation; however, anaesthesia is often required for i.n. administration and challenge, changing their breathing pattern to deep and slow breaths that facilitate lung deposition. Therefore, immune responses obtained in these conditions may be misleading and reflect pulmonary delivery instead. This problem can be circumvented by limiting the administered volume to 10 μl in mice (Eyles et al. 1998). However, differences in the physiology of rodents, such as bronchus-associated lymphoid tissue (BALT) organisation and lack of tonsils in mice, may have an impact on the responses shown in these models (reviewed in (Davis 2001)). The pig is physiologically, immunologically, and anatomically more similar to humans and, therefore, an excellent model to study vaccine and immune responses in the RT (Rajao and Vincent 2015; Janke 2014). Porcine lung anatomy, epithelial structure, and submucosal glands resemble those in humans (Judge et al. 2014). In addition, pigs are a natural host for influenza, representing a great model to study immune responses to novel vaccines and influenza infection.

I.n. delivery by MAD, i.t. instillation and aer. delivery to the porcine RT using nebulisers have been previously tested to deliver vaccines or challenge with IAV (Vincent et al. 2012; Masic et al. 2013; Hemmink et al. 2016; Morgan et al. 2016; Holzer et al. 2018; Talker et al. 2016). While our group has routinely used both MAD and nebulisers, it is unclear where the delivered virus or vaccine is deposited. Different *in vitro* techniques have been used to address this question, such as measurement of vaccine-specific-RNA by RT-qPCR of the lung regions after delivery (Dr. Barbara Holzer, personal communication). To visually assess deposition, Evans Blue dye was aerosolised or delivered i.n. to pigs just before sacrifice (Hemmink et al. 2016). Unfortunately, none of these methods have provided a clear

characterisation or quantification of the distribution of the aerosol generated by the different delivery routes.

This chapter evaluates the properties of droplets and devices used to target the porcine RT. Here, I addressed the following primary objectives:

1. To compare *in vitro* the droplet size of aerosols generated by the MAD device and VMNs
2. To model *in vitro* the deposition of aerosols in the porcine RT using a breathing head model.
3. To assess *in vivo* the deposition following MAD or VMNs delivery by gamma scintigraphy.

The data presented in this chapter have been adapted from published work (Martini et al. 2020).

4.2 *In vitro* aerosol characterisation

A key aspect of targeted delivery to the RT is the device, which needs to reliably and reproducibly deliver the vaccine to the desired area. The deposition site is influenced by the droplet size of the aerosol, anatomy, and breathing rate. Large droplets (> 10 μm diameter) normally accumulate in the nose by inertial impaction, while small droplets (< 5 μm) can deposit in the trachea, bronchi, as well as alveoli (Québec 1994; Cheng 2014). It is unclear if, in pigs, very small aerosol (<3 μm) can deliver to the lung a higher dose, more successfully than aerosol with particles of 5 μm diameter. Two VMNs generating different droplet sizes were therefore compared. In order to do so, albuterol sulphate, a standard drug for aerosol studies, was used as a tracer. Two methods were used for the analysis of droplet size, in accordance with international regulatory standards: laser diffraction and cascade impaction (International Organization for Standardization 2013). During laser diffraction measurements, a collimated laser light illuminates the aerosol generated by the device. The scattered light is recorded by a series of detector lenses from which

the size of the droplets is estimated (named volume mean diameter (VMD)). Cascade impactors consist of several stages of different thicknesses placed in series. Aerosolised droplets with a small aerodynamic diameter will follow the flow of the air and reach the stages at the end of the series, while bigger droplets will be deposited on the first stages. Each stage is then washed, and the deposited droplets measured in each stage, allowing the calculation of the mass median aerodynamic diameter (MMAD).

The analysis of the two VMNs showed that one VMN, named "small VMN", produced droplets with a VMD of 3.5 µm and MMAD of 2.5 µm while the droplets of the second one, termed "medium VMN", had VMD of 4.5 µm and MMAD 3.5 µm (Figure 4.1 A). These are two fundamentally different techniques used in the measurement of droplet diameter, and a difference in readings is expected. The fine particle fraction, droplets of less than 5 µm, was greater in the small VMN compared to the medium one (Figure 4.1 B).

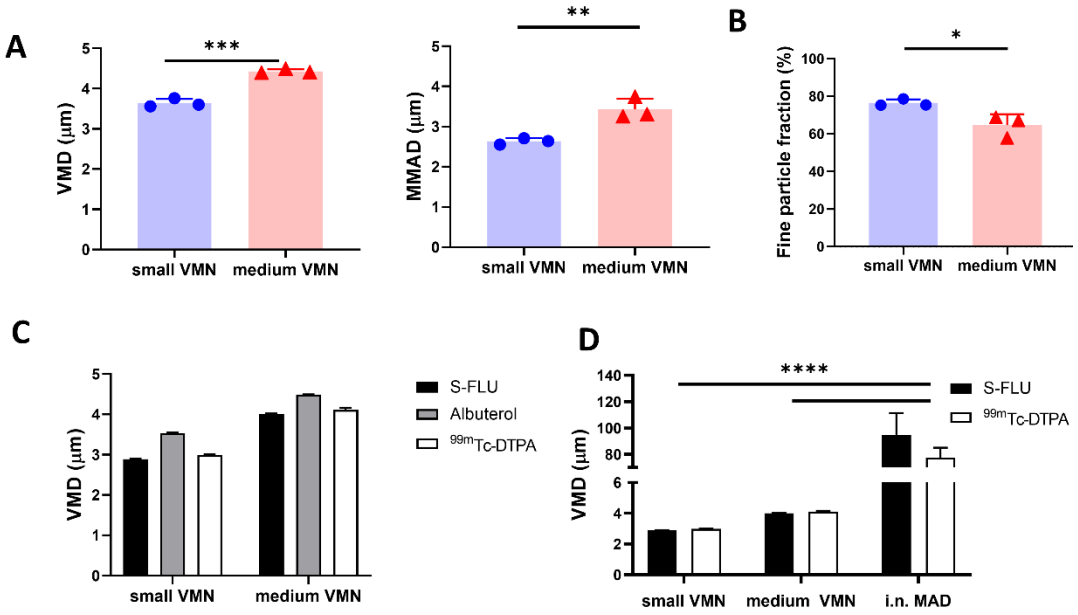

Figure 4.1 ***In vitro* aerosol characterization**. **(A)** The volume median diameter (VMD) and mass median aerodynamic diameter (MMAD) were measured for aerosols generated by small VMN and medium VMN using albuterol. **(B)** The fine particle fraction (droplets with diameter smaller than 5 µm) of the two VMNs. **(C)** The VMDs of aerosols generated using small and medium VMNs with albuterol, S-FLU and ^{99m}Tc-DTPA were compared. **(D)** The VMDs of aerosols generated using small and medium VMNs and i.n. MAD with S-FLU and ^{99m}Tc-DTPA were analysed. Here are presented the mean of three different experiments. Unpaired t-test was used for VMD, MMAD, fine particle fraction comparisons. Two-way ANOVA with Tukey post hoc test was used to compare small and medium VMNs and i.n. MAD with S-FLU and ^{99m}Tc-DTPA. Asterisks denote *$p \leq 0.05$, **$p \leq 0.01$, ***$p \leq 0.001$ and ****$p \leq 0.0001$.

In order to assess *in vivo* the distribution of droplets generated by the two nebulisers or the MAD device, I performed a scintigraphy study using the radionuclide technetium (^{99m}Tc) complexed with diethylenetriaminepentaacetic acid (DTPA) (^{99m}Tc-DTPA). This complex was chosen as it is routinely used in lung scintigraphy studies in humans. I then tested if ^{99m}Tc-DTPA could be used as a surrogate of both albuterol and influenza virus particles by analysing the droplet size of the aerosol generated by these three different preparations (Figure 4.1 C). S-FLU is an attenuated influenza virus vaccine, with a

single replication cycle, making it safer than influenza virus to use in these experiments. It is identical in structure to wild-type influenza and, therefore, a useful surrogate for studying its aerosolization properties (Powell et al. 2012). The VMD of droplets produced by the two VMNs, determined by laser diffraction, was comparable for albuterol, S-FLU and ^{99m}Tc-DTPA, with minimal differences (±0.4 µm) acceptable for the methodology (Figure 4.1 C).

The droplets of S-FLU and ^{99m}Tc-DTPA, generated using the MAD device, were then characterised. In the MAD, a syringe containing the preparation is fitted to a nozzle, which atomises the formulation. Both S-FLU and ^{99m}Tc-DTPA formulations generated a much larger droplet size with the MAD (average of 86 µm) compared to the VMNs. In addition, there was higher variability with the MAD (SD =10) compared to 0.02 for the nebulizers (Figure 4.1 D).

In conclusion, small and medium VMNs produced aerosols with different size distributions. In addition, these data indicated that aerosol of ^{99m}Tc-DTPA albuterol and S-FLU shared similar droplet sizes, therefore both albuterol and ^{99m}Tc-DTPA can be used as a surrogate to study the deposition of influenza virus particles. MAD generated a larger droplet compared to the VMNs, which could influence the distribution in the porcine airways.

4.3 *In vitro* aerosol deposition in a 3D printed pig head model

I next developed an *in vitro* model with the aim to quantify the dose delivered to the lung. These studies were performed at Aerogen ltd. as part of my industrial placement. The model aimed to reflect the breathing rate and anatomical features of the porcine URT and trachea. A 3D printed pig head was

connected to a breathing simulator via a collection filter positioned at the end of the trachea. Albuterol was delivered using a custom-made mask, similar to the one used for the *in vivo* study, and the drug collected in the filter was measured as an estimate of lung deposition. Body weights greatly influence lung volume in mammals, I here modelled the breathing patterns of 15 kg and 20 kg pigs, weight range of the pigs used in the scintigraphy study described below. I used a 7.7 ml/kg body weight to tidal volume (amount of air inhaled and exhaled in each respiratory cycle) conversion, therefore using 115ml and 150 ml to mimic the breath of a 15kg and 20kg pig (Stahl 1967). The small VMN was superior in the deposition of albuterol on the filter (18.1% for 15 kg and 22.3% for 20 kg pigs) compared to medium VMN (15.9% and 20.5%, respectively) (Figure 4.2 A).

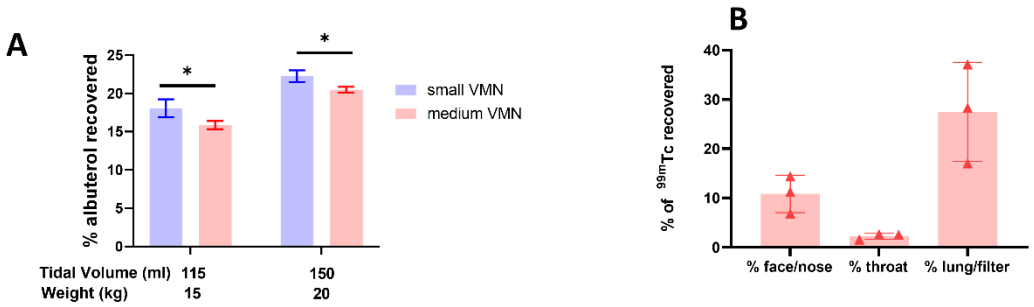

Figure 4.2 **3D printed pig head model (A)** A 3D printed pig head was used to assess potential lung deposition *in vitro*. Settings of the breathing simulator mimicked a 15 kg pig (115 ml tidal volume (Vt), 25 breaths per min (BPM), Inhale/Exhale ratio (I/E) 1/3) or a 20 kg pig (150 ml Vt, 25 BMP, I/E ratio=1/3). Drug deposition on a filter, interposed between the trachea and breathing simulator, is expressed as a % of the nominal dose (dose in the device before administration). **(B)** ^{99m}Tc-DTPA was delivered to the pig head using a medium VMN and images recorded under gamma camera. Counts recorded in the face area, throat and lung filter were then calculated as a % of counts delivered. This experiment was repeat three time with 4 days interval as washout period. Two-way ANOVA with Sidak post hoc test was used to compare albuterol aerosol deposition. Asterisks denote *$p \leq 0.05$.

I next adopted this model to quantify by scintigraphy the deposition of ^{99m}Tc-DTPA in the different areas of the 3D pig head model: face/nose, throat, and lung/filter. 115 ml tidal volume was chosed as it was the closest to that of the pigs used for the *in vivo* experiment. Due to the half-life of ^{99m}Tc-DTPA, I could test its delivery at four days interval to allow all remaining radioactivity in the model to fully decay, thus limiting the study to only the medium VMN, with three replicate experiments. The nebuliser delivered 10.8% of the counts to the face, 2.2 % to the throat and 27.5% to the filter/lung, while the majority was deposited in the mask or exhaled (Figure 4.2 B). This slightly higher deposition measured by gamma camera compared to the one obtained with albuterol (15.9%) might be explained by the difference in the quantification techniques used.

These data indicate that small VMN has the potential to deliver a higher dose to the lung compared to medium VMN.

4.4 Scintigraphy study

Experimental design

I next administered ^{99m}Tc-DTPA to three sedated pigs by aer., using small and medium VMNs, or i.n., using MAD, in a randomised crossover experimental design (Figure 4.3 A). A four days interval between each administration allowed complete radioactive decay of the previous dose of ^{99m}Tc-DTPA, while sedation was required for optimal image recording and it is routinely used when administering aer. to pigs. The total dose delivered i.n. was 10 mega becquerel (MBq), divided equally between both nostrils (1ml per nostril). A higher dose was administered via aer. (30MBq dose in 1 ml). This different dose was chosen to account for a bigger dispersion of the radioactivity in the entire lung when using VMNs, which could otherwise limit the detection of small quantities of radioactive material. Instantly

after ^{99m}Tc-DTPA administration, scintigraphic images of the animals were recorded, allowing visualisation and quantification of the delivered dose. Three regions of interest (ROIs) were investigated: face area (including both nasal cavities and facial skin), throat (comprising both trachea and oesophagus), and lung (Figure 4.3 B). A fourth region, the stomach, was included to detect any radioactivity present below the lung. Deposition in the stomach was recorded in 2 animals after MAD administration, probably because of swallowing nasal aspirate. The quantification in each ROI was

corrected for background and radioactive decay (see Chapter 2). The devices were imaged, using a gamma camera, before and after administration to quantify any residual ^{99m}Tc-DTPA (Figure 4.3 C).

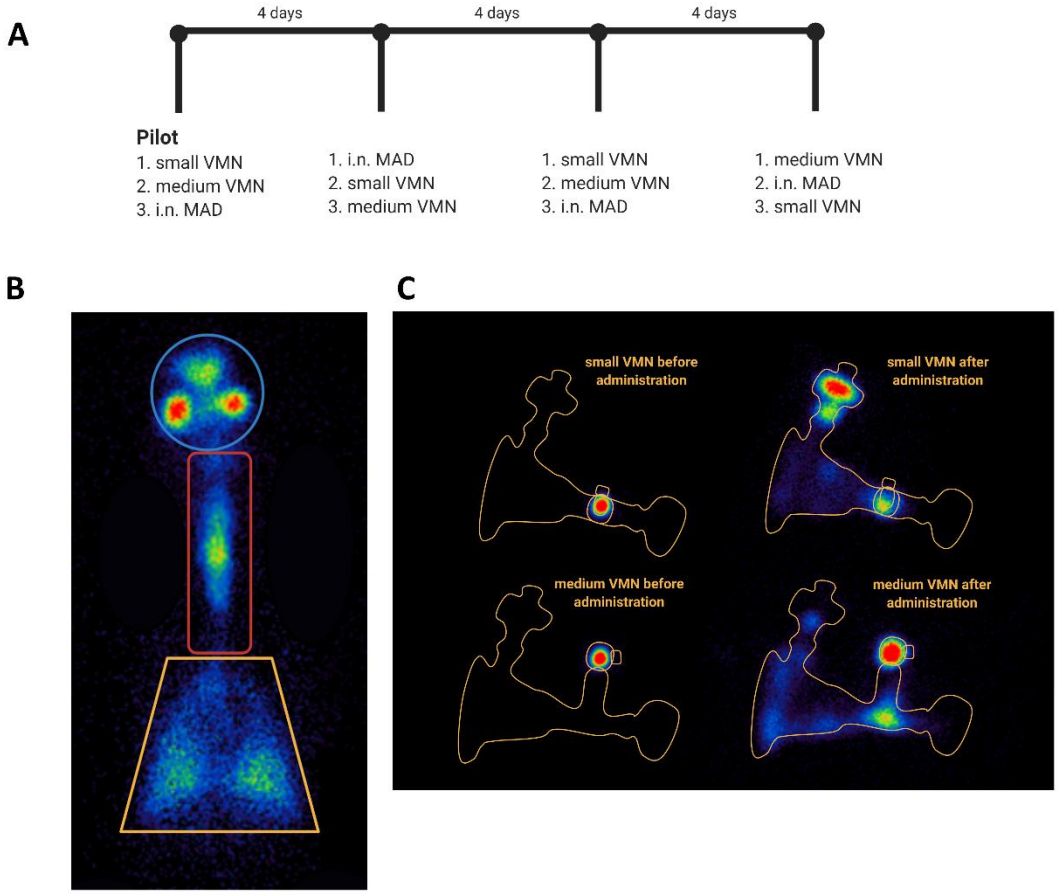

Figure 4.3 **Experimental design (A)** Schematic representation of the cross over experimental design for the *in vivo* scintigraphy study. ^{99m} Tc-DTPA was administered to three sedated pigs (indicated with numbers 1,2 and 3) using small and medium VMNs nebulisers or intranasally with the MAD (i.n. MAD). Each pig received the three different treatments sequentially at 4 days intervals, after the pilot study, conducted to test dose and equipment. **(B)** Diagram indicating the regions of interest analysed – face, throat, and lung. **(C)** Images of VMN devices before and after administration.

Deposition in the respiratory tract after aerosol and intranasal delivery

Images of the devices before and after delivery to the pigs showed a residual dose of 11% in the MAD compared to approximately 50% present in the nebulisers attached to the mask, concentrated mainly in the filter present on the masks designed to capture exhaled air for small VMN (Figure 4.3). As standard practice in scintigraphy investigations, I calculated the deposited radioactivity in each ROI as a percentage of the total amount of radioactivity detected in the animal, rather than as a fraction of the nominal dose. As reported in Table 4.1, a greater proportion was recovered in pigs after aer. administration with the VMNs (79.5% and 83.1%) compared to i.n. MAD delivery (62.1%) representing 37.8% and 55.1% of the dose present in the devices.

Table 4.1 Dose administered and recovered in pigs (mean ± SD)

Device	Dose of radioactivity administered as % of dose loaded into the device	Amount of radioactivity detected in the pig as % of dose administered	Amount of radioactivity detected in the pig as % of dose loaded into device
Small VMN	49.2 ± 5.8	79.5 ± 23.3	37.8 ± 6.3
Medium VMN	52.4 ± 10.5	83.1 ± 14.0	42.0 ± 2.5
i.n. MAD	88.8 ± 0.5	64.3 ± 2.4	57.1 ± 2.4

In the face area, I recorded a significantly higher amount of ^{99m}Tc-DTPA using medium VMN (56%) compared to MAD device (31.2%) (Figure 4.4 and Figure 4.5). The proportion of ^{99m}Tc-DTPA in the throat were slightly higher when using MAD (35.9%) or small VMN (31.5%) than medium VMN (18.7%) although this difference did not reach significance. MAD was significantly more efficient than

medium VMN in delivery to the lung, with 51.9% of the administered dose present in this ROI compared to 25.4% of medium VMN. Small VMN delivered a slightly higher dose to the lung (32.8%) compared to the medium VMN, but this difference was not significant ($p=0.16$). In the stomach of two of the pigs dosed with MAD, I recorded a small proportion of the radioactivity (7 and 10.1%), more obvious from lateral images (Figure 4.5 A).

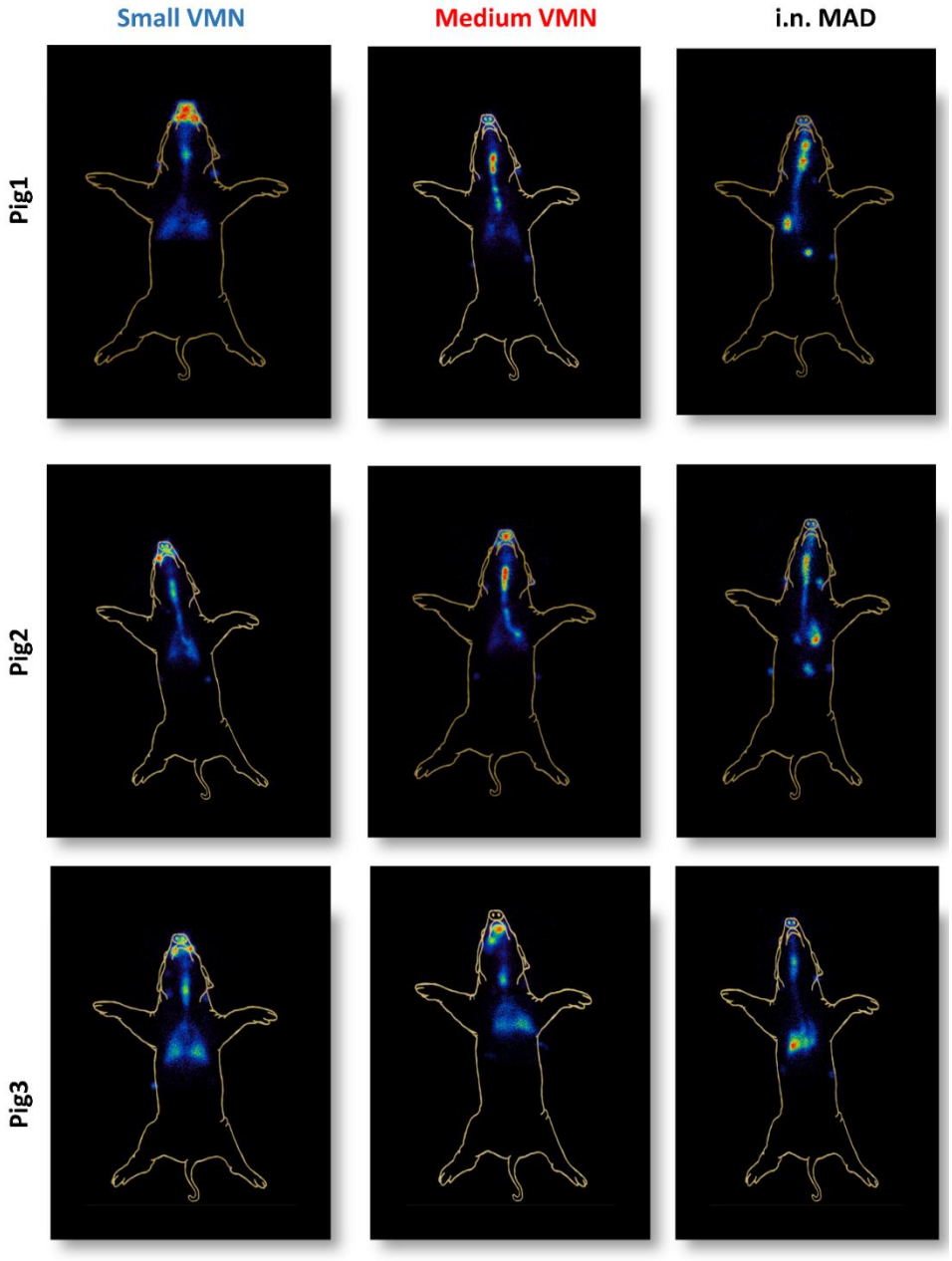

Figure 4.4 ***In vivo* scintigraphy images**. Superimposed frontal scintigraphic images of each pig after aer. delivery with small and medium VMN and i.n. MAD delivery. Radioactive anatomical markers (visible as a circle in the two images) were positioned around the ears and thorax of the pig to enable *post hoc* image reconstruction.

Gamma camera images of the three modalities indicated that a high proportion of the VMN delivered counts remained in the face area, which includes both nasal cavities and facial skin. In an attempt to estimate the deposited dose on the skin, I used skin wipes to try to remove the radioactivity deposited there. Although wipes might not recover 100% of the radioactivity, this showed a great proportion of technetium present on the facial skin, more so for the VMNs than after i.n. delivery (Figure 4.5). On the other hand, MAD's deposition appeared more distal and associated with the nasal cavities.

In the lung, the distribution was substantially different between the devices. I.n. MAD delivery concentrated ^{99m}Tc-DTPA in a small area. This relatively small area was found in 2 of the three pigs in the right lung, probably due to the asymmetrical bifurcation of the trachea, which favours the right lung. In contrast, the radioactivity was homogeneously distributed in the entire area of the lung with VMNs (Figure 4.4 and Figure 4.5).

Together these results suggest that MAD delivers a higher but variable dose to both URT and the lung, although in 2/3 animals I detected radioactivity also in the stomach. Despite a smaller proportion of the label reached the lung, VMNs homogenously target the lung with high deposition also recorded in the nose and trachea.

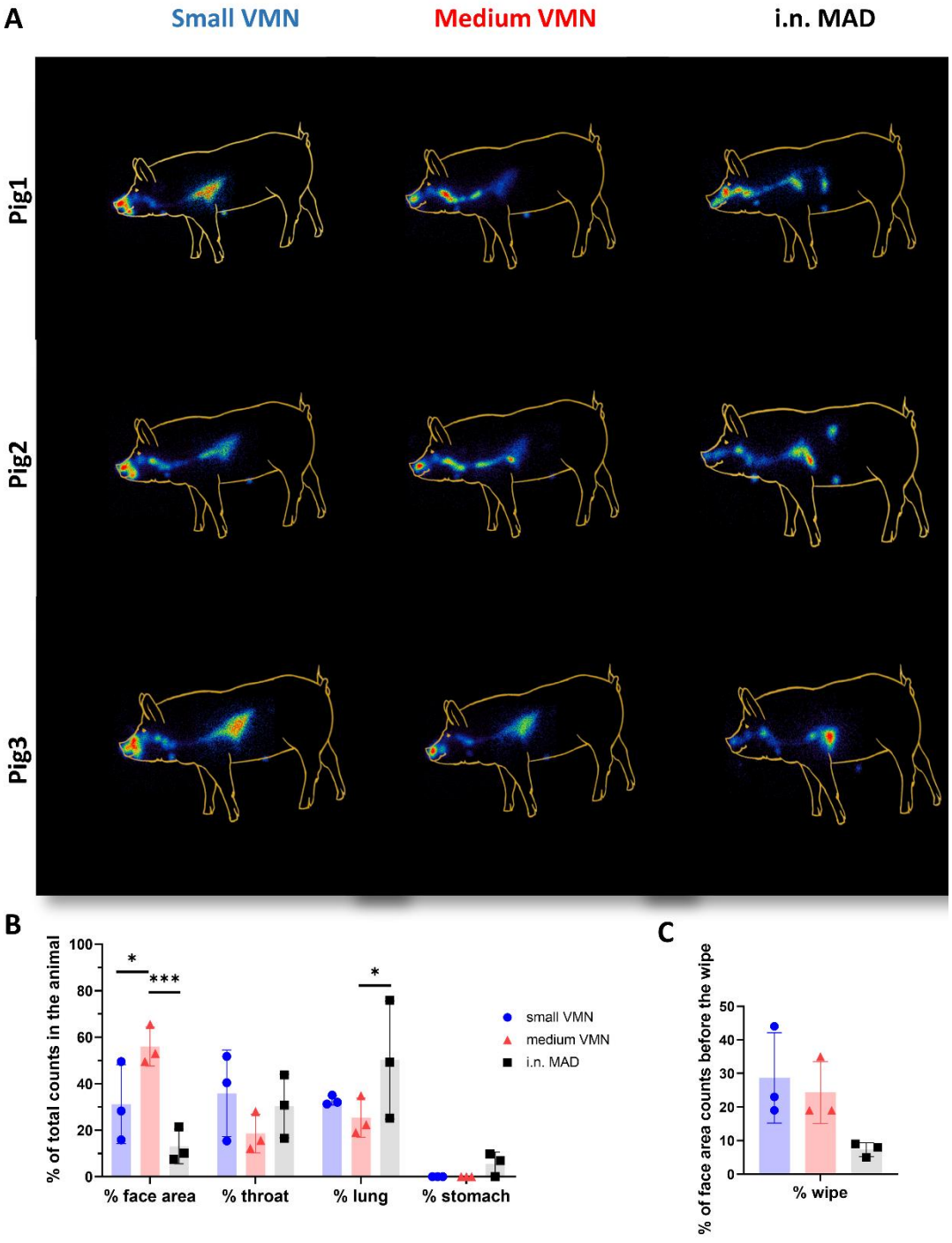
A
Small VMN
Medium VMN
i.n. MAD
Pig1
Pig2
Pig3
B
% of total counts in the animal
100
80
60
40
20
0
*
***
*
% face area
% throat
% lung
% stomach
small VMN
medium VMN
i.n. MAD
C
% of face area counts before the wipe
50
40
30
20
10
0
% wipe

Figure 4.5 **Deposition and quantification of ^{99m}Tc-DTPA. (A)** Lateral images taken after dosing. **(B)** The counts in each region of interest were expressed as percent of total counts in the animal. **(C)** After recording of all images, the face area of the pigs was wiped. Images of the pig face area and wipe were then recorded. Background corrected wipe counts were expressed as a % of the counts present in the face area before it was wiped. Two-way ANOVA was used for statistical analysis of the deposition in the different region of interest. Kruskal-Wallis test was conducted for the comparison of the face wipes' radioactivity, using GraphPad Prism (8.3.0). *p≤0.05, and *** p≤0.001.

Reproducibility

To assess the reproducibility of scintigraphy, counts from the pilot study were compared to those from the second leg study, where the same animals were dosed with the same devices. Although this comparison included only one animal per device, MAD showed high variability. Aer. administration was instead more reproducible, with consistent deposition in the lung for both small and medium VMN (Figure 4.6).

These data indicate that VMNs are reproducible, while MAD showed a greater degree of variability in lung deposition.

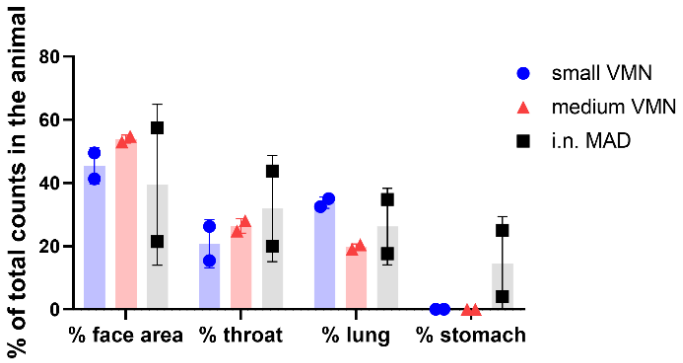

Figure 4.6 **Reproducibility.** The reproducibility of scintigraphy was assessed by comparing the pilot study with the second leg where each animal had the same treatment as in the pilot. Counts in each region of interest for the two experiments are represented as % of total counts in the animal.

4.5 Potential translation to human

To translate our findings in pigs to humans, I tested *in vitro* the delivery of albuterol to a human phantom. The human head was connected to a breathing simulator via a collection filter, simulating the deposition to the lung. The aerosol produced by VMNs was delivered to the phantom using the Ultra facemask (Aerogen). Similarly to the pig head model, small VMN was superior to medium VMN in delivering albuterol to the 'lung' (34.3% versus 26.8%) (Figure 4.7).

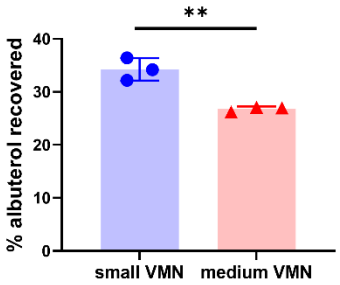

Figure 4.7 ***In vitro* human model.** An adult human phantom was connected to medium and small VMNs using Ultra (Aerogen), a human aerosol mask, with 2 L/min oxygen flow. The phantom human head was attached to a respiratory pump using a lung/filter and the amount of albuterol delivered was quantified. The symbols represent a replicate of the test. Unpaired t-test was used for statistical analysis. Asterisks denote **p≤0.01.

These results are in line with previous work in a human model (Bennett et al. 2019). VMNs' deposition has been recently tested in humans with a similar setup as our human phantom. VMNs deposited 34.1% in the LRT with 39.7% loss in the mask and device (Dugernier et al. 2017). A smaller tidal volume and a more complicated anatomy of the URT may explain the lower deposition in pigs compared to humans.

4.6 Discussion

This chapter presented the *in vitro* and *in vivo* deposition of droplets generated by three different devices: MAD, small VMN and medium VMN. Small VMN generated the smallest droplet (3.5 μm VMD) followed by medium VMN (4.5 μm), with MAD generating the largest droplets (86 μm).

In vivo, MAD delivered a consistently high percentage of the loaded dose (88.8%, SD 0.5). A relatively low proportion (mean ± SD: 13 ± 6%) of the administered dose was observed in the nasal cavities while MAD was superior to medium VMN in lung deposition. However, the MAD deposition in the LRT showed a very uneven distribution, localised in one region of the lung. I also observed a small fraction of the dose in the stomach (mean ± SD: 6 ± 5%), probably due to drainage from the nasal cavities, via the oesophagus. This deposition pattern is most probably a consequence of the large volume administered i.n. (1 ml) and the sedation process. Unfortunately, sedation was required for optimal imaging and can be avoided during vaccination or challenge experiments. In this study I delivered 1 ml per nostril, in an attempt to compensate for the larger swine nasal cavities. Adjusting the volume to 200μl (volume used for the FluMist, the commercially available human LAIV) could limit the deposition of the formulation to the URT, although studies will need to confirm this (Food and Drug Administration 2020; European Medical Agency 2013).

Dose administration via the nebulisers was more variable; a SD of 10.5 was obtained for the medium VMN compared to 5.8 for small VMN. These differences are probably related to the method of administration and in particular the effect that the animal's breathing pattern (i.e. rate and depth of breathing) has on the administration method. I.n. delivery is an active process (the solution is sprayed into the nasal cavity) occurring over a relatively short period (several seconds). Thus, is less prone to be

influenced by the animal's breathing pattern. In contrast, aer. administration using VMNs is a passive process and takes several minutes, therefore it is more dependent on the animals' breath rate.

After aerosolisation, I detected differences in the residual dose present in the mask and the counts recorded on the facial skins of the pigs. Approximately 3% of the residual dose after medium VMN administration was on the mask's top filter, intent to confine any exhaled particles (Figure 4.3). On the other hand, around 70% of the residual dose in the small VMN apparatus was found on the filter. In addition, medium VMN delivered a significantly higher proportion of the dose in the face area compared to small VMN (Figure 4.5). Thus, small droplets are more easily delivered to the porcine airways but can also be exhaled and deposited in the mask filter while bigger droplets of 4.5 μm, generated by medium VMN, are found in the face area as surface contamination of the skin.

Aer. administration with small VMN was highly reproducible (mean ± SD: 32.9 ± 1.60%). Deposition in the lung using the medium VMN 4.5 μm was somewhat more variable (mean ± SD: 25.4 ± 6.83%). As mentioned above, these differences could perhaps be attributed to the different particle size distribution between the two nebulisers with the smaller particle size promoting better delivery and more consistent lung deposition. However, there was no significant difference in terms of total lung deposition between the two nebulisers. Although VMNs delivered a lower proportion of the dose to the lung, this was much more evenly distributed compared to MAD. VMNs were also superior to MAD for reproducibility within the same animal.

Two-dimensional planar scintigraphy enabled us for the first time to quantify the delivered dose to the different areas of the RT, but it has some limitations. Due to its two-dimensional nature, the distinction of anatomical structures of interest, such as lateral wall and septum of the nasal cavity or different parts

of the LRT, cannot be made. Also, the technique is not fully quantitative since radioactivity scatter, the distance of the radioactive source from the camera head and tissue attenuation will affect the data. However, planar scintigraphy is a widely accepted method for investigating the regional deposition of pharmaceutical dosage forms especially following administration to the respiratory tract.

Whether the differences in deposition between MAD and VMNs will influence the immune responses to vaccines remains to be investigated. Our group has recently compared MAD delivery of an influenza vaccine candidate (ChAdOx NPM1 NA) with VMN, in a pre-exposure model (Vatzia et al. 2021). Thanks to the findings presented in this chapter, i.n. vaccination volume was adjusted to 300 μl to limit the delivery to the URT. Pigs were first challenged with H1N1pdm09 and 4 weeks later were immunised by aer. or i.n.. A third group received the vaccine i.m. while the control group was not vaccinated. Aer. immunised pigs showed a significantly higher level of IgG and IgA in the BAL and increased systemic humoral response compared to the i.n. group. Local T cell responses were also superior in this group. These results indicate that targeting the lung with VMNs elicits strong T cell and B cell responses even in animals previously infected locally. Future studies will need to confirm these findings in naïve animals and test whether aer. immunisation is superior to MAD delivery in generating TRMs. The homogenous aerosol deposition in the lung would, in theory, translate into homogenous TRM distribution and patrolling of the entire LRT, thus better protection. Although this hypothesis needs validation, one can speculate that a localised vaccine deposition, such as the one obtained with MAD, supports antigen-specific T cells' migration to a small area, where local inflammation occurred. Takamura and colleagues confirmed that local pulmonary inflammation drives T cell migration and differentiation into TRM via Repair-Associated Memory Depots (RAMD), populated by antigen-presenting cells (Takamura et al. 2016). The absence of RAMD in areas of the RT might imply limited

T cell recruitment right where viral particles will replicate in subsequent infection. Therefore, a homogeneous vaccine distribution, such as the one obtained with VMN, may be preferable.

Studies in mice and ferrets showed that optimal heterotypic protection is achieved when the LRT is targeted (Powell et al. 2012; Lau et al. 2011; Tannock, Paul, and Barry 1984). However, LAIV retains some potential for replication and it includes a viable HA, with risk for recombination in case of a concurrent infection, therefore it is not safe for pulmonary delivery (Ambrose and Coelingh 2012). On the other hand, novel vaccine candidates, such as S-FLU (see Chapter 5), single-cycle influenza vaccine lacking a functional HA gene, can be delivered safely to the LRT. Therefore, the findings here illustrated are invaluable for pre-clinical vaccine testing of such vaccine candidates.

This chapter illustrates the *in vitro* properties and *in vivo* deposition of the aerosols obtained using small VMN, medium VMN and the MAD device. Despite the fact that MAD showed a higher lung deposition, VMNs offered homogenous distribution in the porcine RT, which could be important for vaccination.

Chapter 5
New influenza vaccine candidates and the effect of route of administration on immune responses and protection

5.1 Introduction

S-FLU is a candidate IAV vaccine obtained by deleting the signal sequence of HA, therefore limiting its replication to a single cycle (Powell et al. 2012). The functional HA, necessary for the entry of the virus into the cells, is provided by pseudotyping. This vaccine has been tested in IAV challenge experiments in mice, ferrets, and pigs previously, with different degrees of protection. In the mouse model, S-FLU delivered i.n. was protective against lethal heterotypic challenge, thanks to the generation of cross-reactive CD8 T cells in the lung, while Ab responses against HA were detected only when the vaccine was given i.p (Powell et al. 2012; Powell et al. 2019). I.n. S-FLU protected ferrets from homologous and heterologous challenges, similarly to cold-adapted LAIV, and prevented transmission (Baz et al. 2015; Holzer et al. 2018). The pig is anatomically more similar to humans and offers the advantage of testing different routes of respiratory administration, such as i.n., i.t. and aer., more easily than in mice and ferrets. S-FLU i.n., i.t. and aer. administration routes were compared in pigs with aer. administration showing consistently reduced viral load in the nose and lung when partially matched to the challenge virus, correlating with a local lung T cell immune response (Morgan et al. 2016). In a heterologous challenge experiment, S-FLU by aer. reduced pathology but failed to stop viral replication in the porcine URT (Holzer et al. 2018). These findings are in contrast to what was demonstrated by Baz et al. in ferrets, the gold standard model for IAV research, where S-FLU stopped transmission and

reduced viral load (Baz et al. 2015). Consistent with studies in mice (after i.n. delivery) and ferrets, pigs immunised by aer. failed to generate neutralising antibodies against HA.

These data showed the importance of testing influenza vaccine candidates in pigs, a natural host of IAV and with a similar distribution of sialic acid receptors to humans (Trebbien, Larsen, and Viuff 2011). Aiming to improve the efficacy of S-FLU vaccine in pigs, two different strategies have been tested and described in this chapter:

1. Insertion of an HA expression cassette in S-FLU, generating the so-called CLEARFLU vaccine.
2. Administration of S-FLU by different routes: i.m. and a combination of aer. and i.m.

CLEARFLU

This second generation of S-FLU vaccine was designed by Alain Townsend and Holly Sadler (Figure 5.1). In CLEARFLU, the HA signal sequence is still present therefore the protein can be expressed in infected cells. However, its sequence contains several independent inactivating mutations. CLEARFLU was designed with the following 8 characteristics:

Cleavage resistance
Locked by inter-monomer disulphide bonds
Egg adaptations avoided
Antigenicity maintained
Receptor binding abolished
Fusion peptide inhibited
Loop inactivation by proline residues (not present in CLEARFLU's version tested in pigs)
Universal platform for all strains

Individual mutations and rationale are indicated in Table 5.1.CLEARFLU inactivating mutations in different locations of the HA ensure that compensatory mutations, able to re-generate a functional HA, will be unlikely but antigenic activity is conserved. Similarly to S-FLU, the functioning HA, indispensable for vaccine entry into target cells, is provided by pseudotyping. The presence of HA gene in CLEARFLU enables infected cells to express this protein on the surface, with the aim of improving neutralising Ab responses and immunogenicity. When tested i.n. in mice, H1 CLEARFLU generated strong neutralizing antibodies towards H1 in the sera (50% neutralisation titre of ~1:2000) (H. Sadler, thesis, 2021).

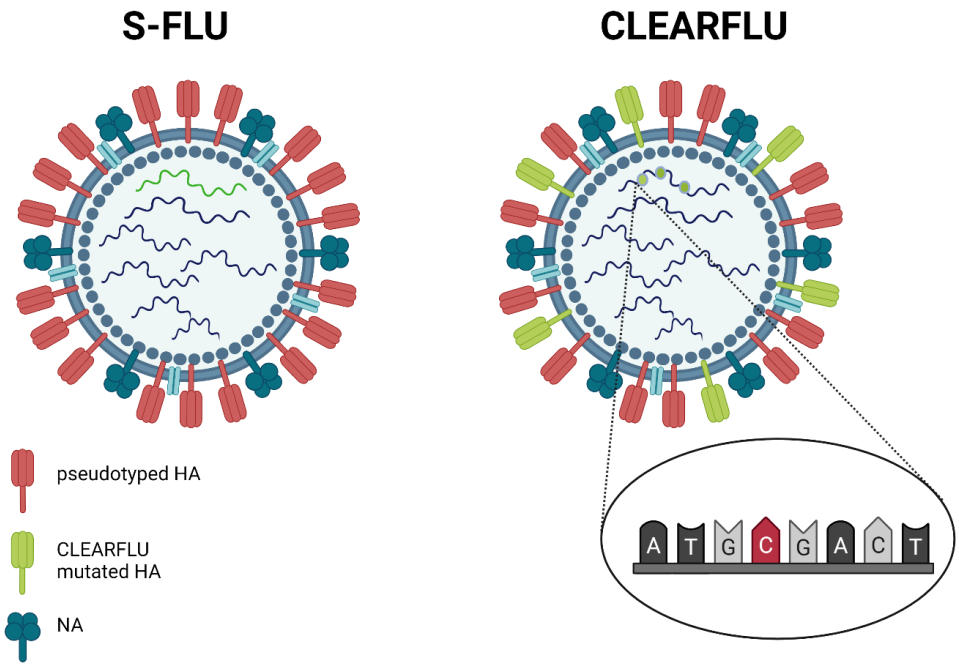

Figure 5.1 **S-FLU and CLEARFLU**. Representative diagram of S-FLU vaccine (on the left) and CLEARFLU (on the right). HA gene in S-FLU is coloured in green as an indication of the presence of eGFP sequence instead of HA. Mutations in the HA sequence of CLEARFLU are indicated with a green circle and exampled mutations are reported in the zoomed oval.

Table 5.1 Mutations in HA protein in CLEARFLU vaccine candidate (credit to Dr. Holly Sadler)

Mutation type	**Mutation Position** (H3 numbering system- see Burke & Smith, 2014)	**Rationale**
Cleavage resistance	HA1–R329Q	Cleavage of the precursor HA0 into HA1and HA2 by trypsin is necessary for conformational changes required for cell entry. Viruses with mutations at the cleavage site cannot replicate due to changes in protease sensitivity.
Locked by inter-monomer disulphidebonds	Head: HA1–212C & HA1–216C	The introduction of inter-chain disulphide bridges between head regions prevents membrane fusion for cell entry.
	Stem: HA1–30C & HA2-47C	Disulphide bridges between stem regions increase the stability of the HA trimer and may prevent fusion.
Receptor binding abolished	HA1–Y98F	The change from tyrosine to phenylalanine prevents the formation of a hydrogen bond with sialic acid residues necessary, for the binding, and attenuatates IAV in mice, but has a high rate of back mutation
Fusion peptide inhibited	HA2–G1Q, HA2-L2G	Mutations in the fusion peptide abolishfusion. The residues which are most highly conserved are most likely toblock function when mutated.
	HA2-I6G, HA2-G8A	

Different routes of administration

Studies in mice showed that S-FLU delivered i.p. generated the highest neutralising Ab titre in blood, suggesting that systemic administration can lead to higher Ab responses compare to local delivery (Powell et al. 2019). On the other hand, local immune responses are fundamental for heterotypic protection (reviewed in (Sridhar 2016)). Strategies that combine both local and systemic immunisation have been explored in Tb. Parenteral BCG priming and a subsequent i.n. boost with an adenovirus vectored vaccine expressing antigen 85A (Ad85A) improved protection in mice (Santosuosso et al. 2006). BCG alone or in combination with Ad85A enhanced protection when administered simultaneously systemically and to the respiratory tract in mice and cattle (Dean et al. 2015; Tchilian et al. 2011). Uddback et al. have adapted this strategy using an adenoviral vector expressing influenza nucleoprotein (NP) and demonstrated greatly improved efficacy and long-lasting protection against heterosubtypic influenza challenge in the mouse model (Uddback et al. 2020; Uddback et al. 2016).

This chapter describes immune responses after administration of CLEARFLU and S-FLU using different administration routes, and it addresses the following specific aims:

1. Comparison of cellular and humoral responses after S-FLU and CLEARFLU aer. immunisation
2. Evaluation of systemic immune responses following S-FLU i.m. administration
3. Comparison of protection induced by i.m., aer. and SIM regimes, using S-FLU. The work presented in this section has been adapted from a published manuscript (Martini et al. 2021).

5.2 Pilot study: S-FLU and CLEARFLU immunisation by aerosol

In mice, CLEARFLU expressing H1 (A/England/195/2009) and H3 (A/Hong Kong/5738/2014), delivered i.n., induced neutralising Ab responses against the expressed HA (1:2000 dilution of pooled sera) (Figure 5.2 and Figure 5.3). In contrast, sera of mice immunised i.n. with S-FLU, pseudotyped with H1/PR8 or H3 (A/Hong Kong/5738/2014), were not neutralising. Both vaccines generated inhibitory Ab against NA.

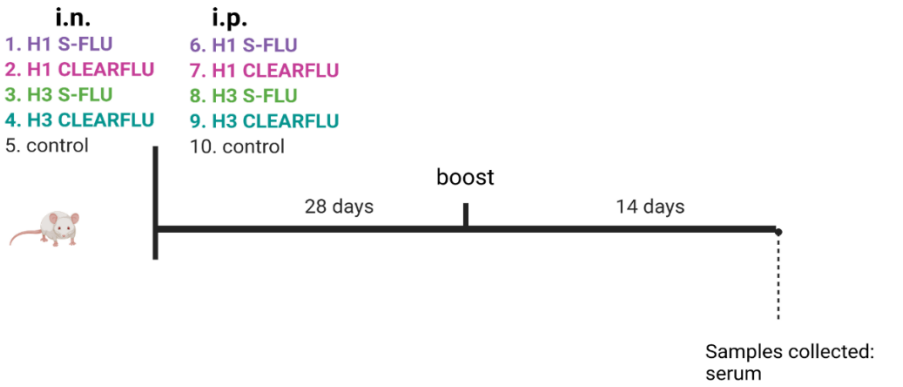

Group	Route of administration	Number of animals	Vaccine used	Titre (TCID50)
1. H1 S-FLU	Intranasal	5	[eGFP/N1(A/England/195/2009)] coatingH1 (A/England/195/2009)	N/A
2. H1 CLEARFLU	Intranasal	5	[H1CFv2(A/England/195/2009)/ N1(PR8)] coating H1(PR8)	$<3. \times 10^4$
3. H3 S-FLU	Intranasal	5	[S-eGFP/N2(NYMC X-217)] coating H3(A/Hong Kong/5738/2014)	1.2×10^6
4. H3 CLEARFLU	Intranasal	5	[H3CFv2(A/Hong Kong/5738/2014)/N1(PR8)] coating H1(PR8)	6.9×10^5
5. Medium Control	Intranasal	4	Unimmunised	N/A
6. H1 S-FLU	Intraperitoneal	5	[eGFP/N1(A/England/195/2009)] coatingH1 (A/England/195/2009)	N/A
7. H1 CLEARFLU	Intraperitoneal	5	[H1CFv2(A/England/195/2009)/ N1(PR8)] coating H1(PR8)	$<3. \times 10^4$
8. H3 S-FLU	Intraperitoneal	5	[S-eGFP/N2(NYMC X-217)] coating H3(A/Hong Kong/5738/2014)	1.2×10^6
9. H3 CLEARFLU	Intraperitoneal	5	[H3CFv2(A/Hong Kong/5738/2014)/N1(PR8)] coating H1(PR8)	6.9×10^5
10. Medium Control	Intraperitoneal	4	Unimmunised	N/A

Figure 5.2 **CLEARFLU and S-FLU experimental design in mice.** 6-8 weeks old BALB/c female mice were immunised as indicated using CLEARFLU or S-FLU or media, as a control, and sera collected 14 days post boost. The table reports the details of the immunisation regimes of this study. Holly Sadler and Alain Townsend performed this experiment.

A

	Assay	Samples used	Viruses used
Humoral responses	MN	Pooled serum	1. [eGFP/N1(PR8)] coating H1(PR8) S-FLU 2. [eGFP/N1(A/England/195/2009)] coating H1(England/195/2009) S-FLU 3. [eGFP/N2(NYMC X-217)] coating H3(A/Hong Kong/5738/2014) S-FLU 4. [eGFP/N2(NYMC X-217)] coating H3(X-31) S-FLU
	ELLA	Pooled serum	1. [eGFP/N2(NYMC X-217)] coating H3(A/Switzerland/9715293/2013) S-FLU 2. [eGFP/N1(A/Puerto Rico/8/1934)] coating H7(A/Netherlands/219/2003) S-FLU 3. [S-eGFP/N1(A/England/195/2009)] coating H7(A/Netherlands/219/2003) S-FLU

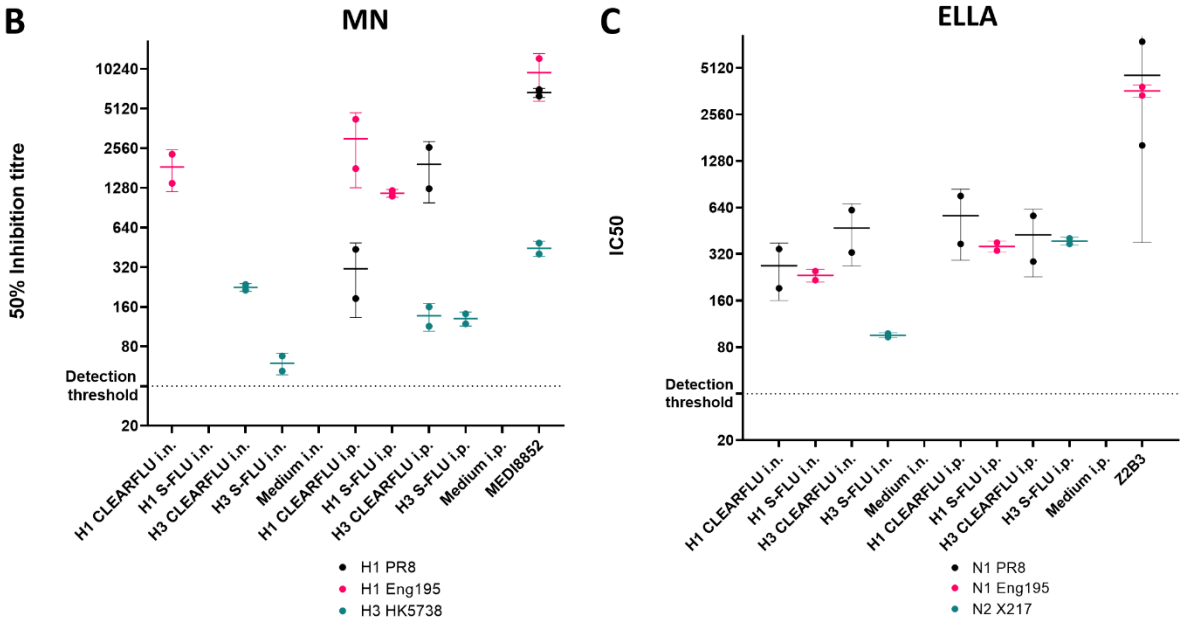

Figure 5.3 **Ab responses after CLEARFLU and S-FLU immunisation in mice. (A)** The table details the viruses used for the assays in B and C. Pooled sera of four/five animals were used for MN assay against H1 and H3 viruses **(B)** or inhibitory assay against the vaccines' neuraminidases N1 and N2 NAs (ELLA) **(C)** (starting dilution 1:40, viruses used are reported in the table). MEDI8852 and Z2B3 mAbs were used as positive controls for MN and ELLA assays respectively. The assays were repeated twice and the mean is shown. Credit to Holly Sadler for this work.

Because of these promising results, I tested CLEARFLU in pigs and compared it with S-FLU. Babraham pigs were chosen for this study as they share identical SLA, allowing the study of CD8 T cell responses using previously identified immunodominant epitopes in the NP protein of the PR8 backbone of both S-FLU and CLEARFLU (Tungatt et al. 2018). H7 (A/Netherlands/219/2003) S-FLU was administered by aer. to 5-6 weeks old pigs (n=3) (Figure 5.4). A second group of three pigs received CLEARFLU, coated with the same H7 and expressing the pandemic H1 (A/England/195/2009), by aer.. Three unimmunised pigs were used as a control, but unfortunately, prior to the start of the study, one pig died, reducing the number of control animals to two. Three weeks post priming, immunised animals received a second dose of the vaccines by aer.. All animals were culled 21 days post boost, 10 min after receiving i.v. 1mg/kg of purified mouse anti porcine CD3 mAb (clone PPT3, produced in house). The administration of anti CD3 mAbs aimed to distinguish between resident T cells in the RT (TRM, CD3 i.v.$^{-}$) from T cells in circulation (CD3 i.v.$^{+}$), as previously described (Holzer et al. 2018). Humoral responses against H7 and H1 HAs were then assessed: no neutralising antibodies were detected (starting serum dilution 1:20) in any of the groups (Figure 5.5). As in serum, no neutralising antibodies were found in BAL (starting dilution 1:2, data not shown).

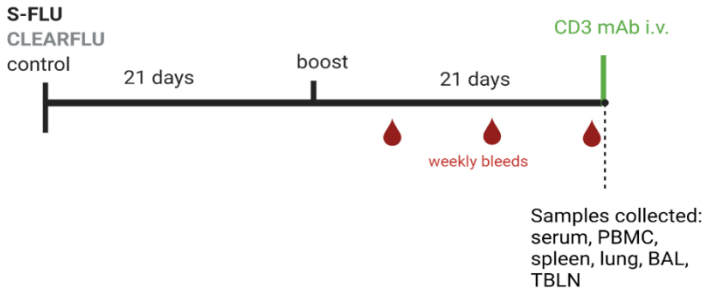

Group	Route of administration	Number of animals	Vaccine used	Titre (TCID50)
S-FLU	Aerosol	3	[eGFP/N1(PR8)] coating H7(Netherlands/219/2003)	2.4. x 10^8
CLEARFLU	Aerosol	3	[H1CFv2(England/195/2009)/N1(PR8] coating H7t(Netherlands/219/2003)	1.3. x 10^8
Control	N/A	2	Unimmunised	N/A

	Assay	Samples used	Viruses used
Humoral responses	ELLA	serum	[eGFP/N1 (PR8)] coating H5(A/Vietnam/1203/2004) S-FLU
	MN	serum	1. [eGFP/N1(PR8)] coating H7(Netherlands/219/2003) S-FLU 2. H1N1 (A/swine/England/1353/2009)
Cellular responses	ELISpot	PBMC, spleen, BAL	1. [eGFP/N1(PR8)] coating H7(Netherlands/219/2003) S-FLU 2. H1N1 (A/swine/England/1353/2009)
	Tetramer staining: enumeration and phenotyping	PBMC, spleen, BAL, lung, TBLN	N/A

Figure 5.4 **CLEARFLU and SFLU comparison: experimental design and assays performed**. 5–6-week-old Babraham pigs were immunised as indicated using CLEARFLU or S-FLU or left untreated, and blood samples collected every week after boost. The tables show the details of the immunisation regimes and the assays performed.

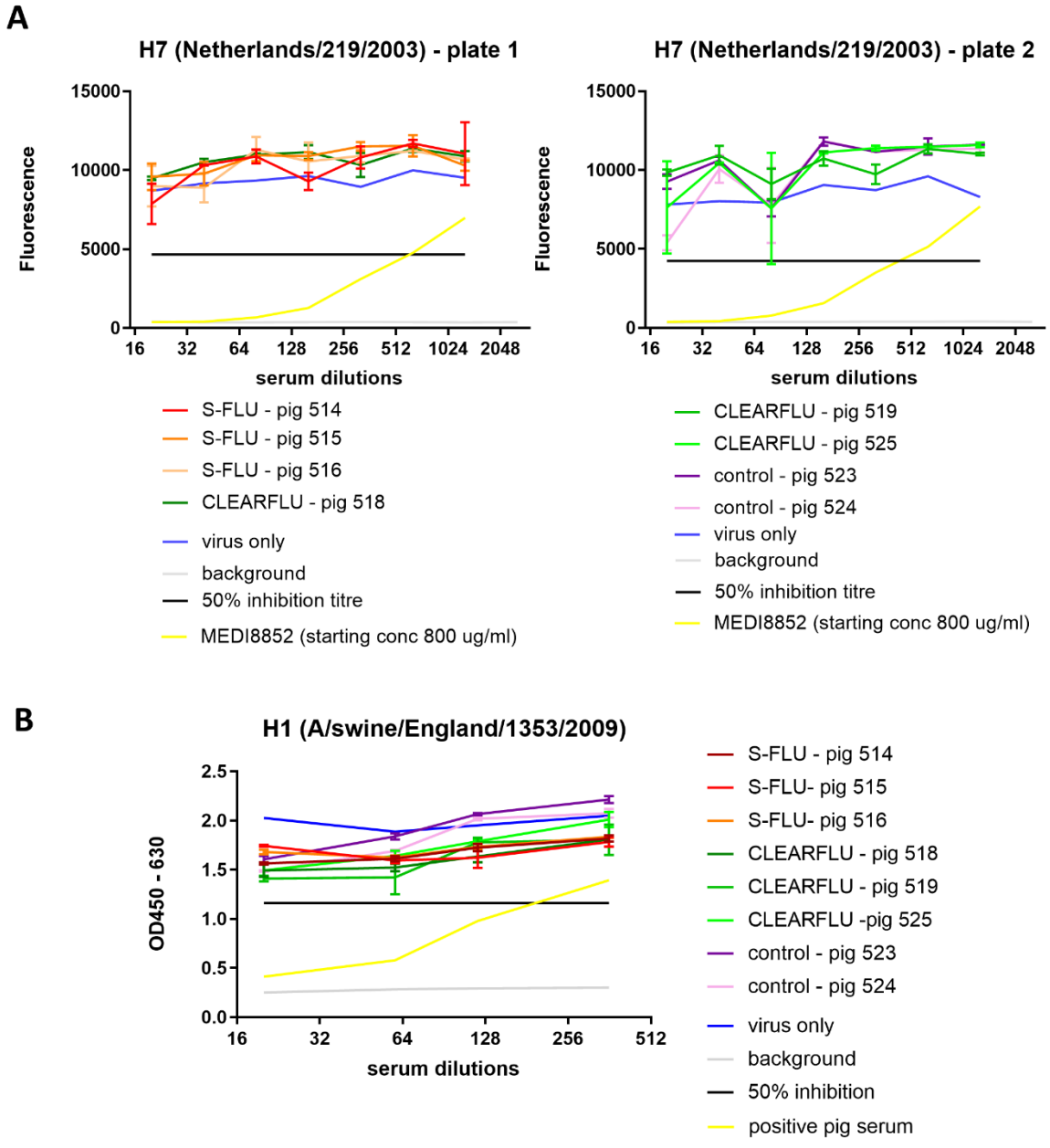

Figure 5.5 **CLEARFLU and S-FLU comparison: neutralising antibodies against viruses.** (A) Serum from 7 days post-boost was tested for its ability to neutralise H7 (A/Netherlands/219/2003) using MN assay. S-FLU expressing eGFP was used and fluorence measured as readout. MEDI8852 mAb is a positive control. (B) MN of sera at 7 days post boost with H1N1pdm09 virus. Viral NP protein was

detected using AAH5 mAb and serum from a pig infected with H1N1pdm09 was used as positive control.

Anti-NA activity was present in sera of 2/3 S-FLU immunised animals at all days after boost (peak response at 7 days post-boost (dpb), 161 mean inhibitory concentration 50 (IC50)) while CLEARFLU did not generate an anti-NA responses measured by ELLA (Figure 5.6). As for HA, BAL failed to neutralise N1 from PR8 (data not shown).

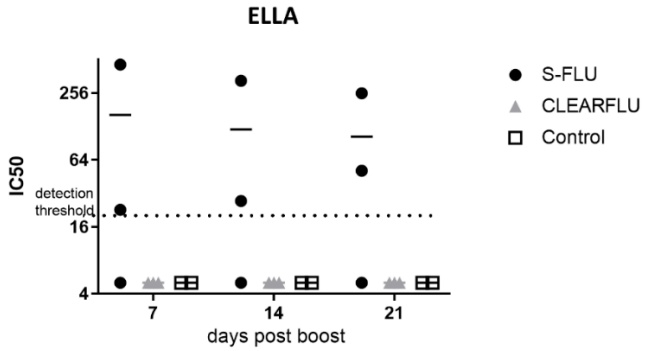

Figure 5.6 **CLEARFLU and S-FLU comparison: inhibitory antibodies against NA**. serum neuraminidase inhibitory Ab concentration (IC50) was measured weekly post boost. Symbols represent each animal and the mean is shown as line.

Cellular responses were assayed using IFNγ ELISpot. *Ex vivo* stimulation with S-FLU, CLEARFLU and H1N1pdm09, revealed low number of IFNγ secreting cells in PBMC and spleen. In contrast, I detected 2,165 and 2,170 SFU/10^6 cells against H1N1pdm09 in BAL of immunised animals with S-FLU and CLEARFLU respectively, and similar responses towards their respective vaccine viruses (Figure 5.7 A). Next, I evaluted CD8 T cells response using the four NP tetramers: DFE, EFE, IAY and NGK (Tungatt et al. 2018). Tetramer staining confirmed that the highest responses were in BAL, where almost 50% of CD8 T cells were specific for NP (22.6% DFE^+, 0.11% EFE^+, 10.7%NGK^+ and 21.3%IAY^+ in S-FLU group) (Figure 5.7 B and C).

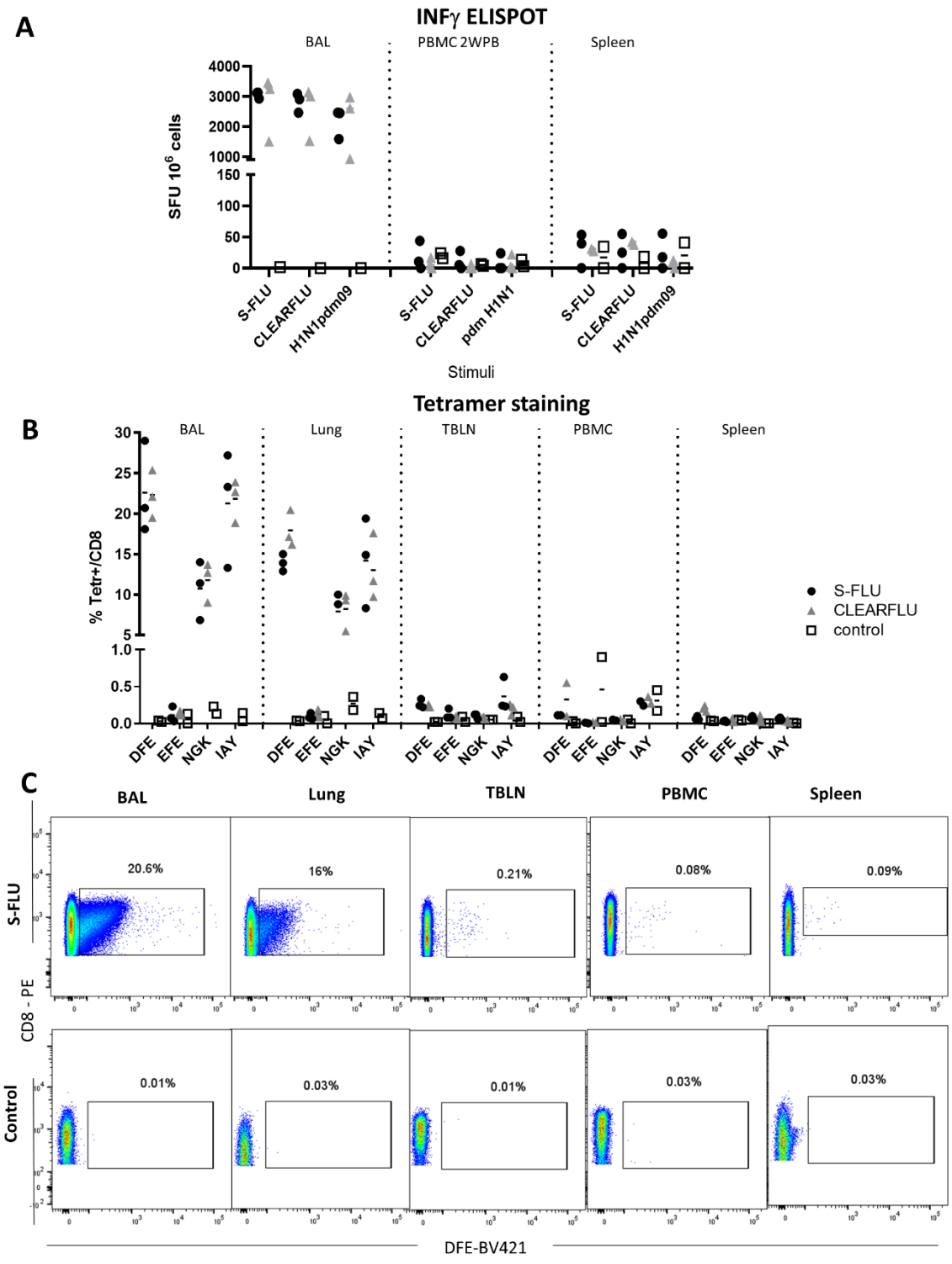
A
INFγ ELISPOT
BAL
PBMC 2WPB
Spleen
SFU 10^6 cells
4000
3000
2000
1000
150
100
50
0
S-FLU
CLEARFLU
H1N1pdm09
S-FLU
CLEARFLU
pdm H1N1
S-FLU
CLEARFLU
H1N1pdm09
Stimuli
B
Tetramer staining
BAL
Lung
TBLN
PBMC
Spleen
% Tetr+/CD8
30
25
20
15
10
5
1.0
0.5
0.0
DFE
EFE
NGK
IAY
S-FLU
CLEARFLU
control
C
BAL
Lung
TBLN
PBMC
Spleen
S-FLU
Control
CD8 - PE
20.6%
16%
0.21%
0.08%
0.09%
0.01%
0.03%
0.01%
0.03%
0.03%
DFE-BV421

Figure 5.7 **T cell responses. (A)** IFNγ secretion measured by ELISpot of lymphocytes isolated from BAL, PBMC 2 weeks post boost and spleen postmortem. Cells were stimulated with S-FLU, CLEARFLU or H1N1pdm09 (MOI=1) in triplicate wells. Here is shown the mean subtracted from the medium control. Spot forming units (SFU) were then scaled to 10^6 cells **(B)** Cyropreserved lymphocytes postmortem were stained with live/dead marker, CD3 and CD8β as well as SLA tetramers specific for the epitopes DFE, EFE, NGK and IAY. Percentages of tetramer$^+$ cells relative to CD8β are here shown, each symbol represents one animal and line indicates the mean. **(C)** Representative plots for S-FLU immunised (top) and control pig (bottom) of DFE$^+$ CD8 T cells in each tissue analysed.

The responses in lung mirrored the one in BAL, with DFE being the highest responding tetramer, followed by IAY, NGK and only marginal responses were detected against EFE. Three weeks post boost, CD8 T cells specific for the vaccines were present in the local LN at low frequencies and were mainly specific for DFE (0.27% in S-FLU group and 0.24% in CLEARFLU) and IAY (0.37% and 0.20% respectively). In the periphery, I could not detect significant numbers of tetramers$^+$ cells compared to control group.

I next investigated whether tetramer$^+$ cells present at the mucosal sites were resident or present in circulation with the infusion of an anti-porcine CD3 mAb prior to sacrifice. The inability to saturate all CD3 molecules on the surface of T cells with the infused Ab means that circulating CD3$^+$ cells were labeled with both *ex vivo* and i.v. mAb. Cells isolated from BAL and many in lung were inaccessible to the infused Ab and therefore resident (Figure 5.8 A). On the other hand, the majority of cells in spleen were labeled with both the infused and the *ex vivo* anti CD3 mAb, indicating that these cells were in circulation. I then studied the phenotype of DFE$^+$ cells isolated from various organs of S-FLU immunised animals. As for DFE$^+$ cells generated after H1N1pdm09 infection, tetramer$^+$ cells in BAL shared a TEM (CD45RA$^-$ CCR7$^-$) phenotype. The majority of DFE$^+$ cells in TBLN, spleen and blood also lacked CD45RA and CCR7, while a small proportion presented a TCM phenotype. Due to very small frequencies of tetramer$^+$ cells in circulation, their phenotype was less certain and I detected a low

proportion of DFE^+ cells with naïve phenotype (Figure 5.8 B). To study the proliferative and differentiation state of TRM, I investigated the expression of Ki67, T-Bet and Eomes. In all tissues analysed, DFE^+ cells were not proliferative. T-Bet, which promotes Th1 differentiation, was detected only in PBMC and Eomes, was downregulated in all tissues (Figure 5.8 C).

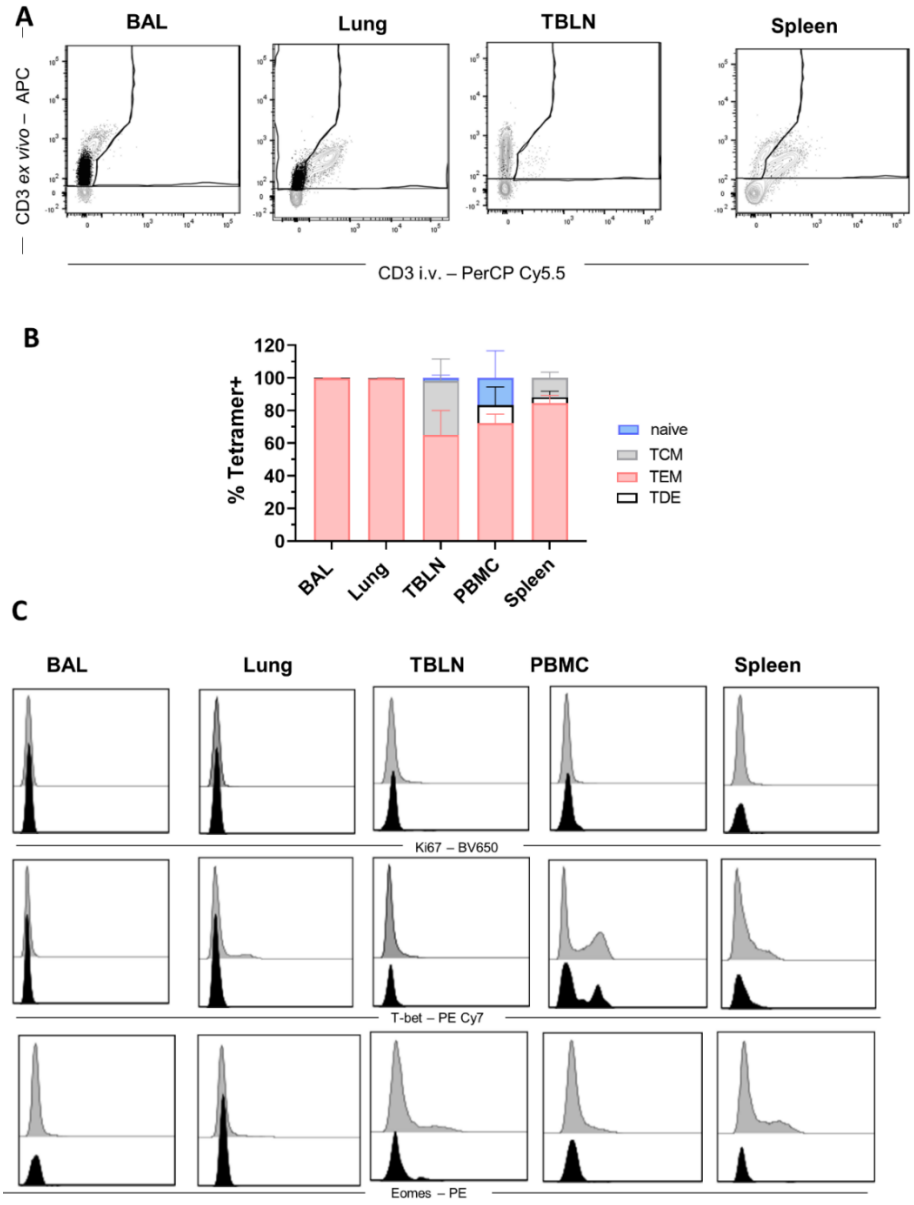

Figure 5.8 **Localisation and phenotype of DFE$^+$ T cells. (A)** Pigs were infused i.v. a mouse anti-porcine CD3 mAb (clone PPT3) 10 mins prior to sacrifice. Isolated lymphocytes were then labeled with anti-mouse IgG1 Ab linked to PerCP Cy5.5 and, after blocking with mouse serum, with anti-porcine CD3 mAb (clone PPT3) conjugated with APC. In gray is reported the staining of all lymphocytes while black dots indicate DFE$^+$ cells. **(B)** CD45RA and CCR7 expression of DFE$^+$ CD8 T cells in tissues **(C)**

Expression of Ki67 (top), T-Bet (center) and Eomes (bottom) of total CD8 (gray) and tetramer^{+} T cells (black).

Overall, these results indicate that CLEARFLU i.n. immunisation in mice generated neutralising Ab against HA and NA. However, when tested by aer. in the pig model, CLEARFLU failed to elicit strong Ab response. Both S-FLU and CLEARFLU recruited T cells in lung and BAL, with up to 50% of CD8 T cells specific for the vaccine's NP and they presented a TRM phenotype. At three-weeks post boost the response in the blood was barely detectable above the background staining, as previously reported (Tungatt et al. 2018).

5.3 Pilot experiment: S-FLU intramuscular immunisation

Although the sample size was small and results should be confirmed with more animals, the lack of Ab response after CLEARFLU immunisation led us to investigate a different strategy for vaccine administration in pigs: i.m. injection of S-FLU vaccine. As previously shown in mice, systemic administration of the vaccine induced a high level of neutralising Ab in blood at 14 days post boost (Figure 5.3). I therefore tested whether the same was true in pigs. Five to eight weeks old Babraham pigs (n=4) were immunised i.m. with [eGFP/N1(Eng195/2009)] S-FLU pseudotyped with H7(A/Netherland/219/2003). Three weeks later, pigs recieved a second injection of the vaccine and the animals were culled at 21 days post boost (Figure 5.9). For this study, sample collection was limited to blood samples prior to immunisation and each week post boost.

To determine the breadth of the humoral response within subtype, I studied neutralisation of different H7 HAs and inhibition of N1 NAs as indicated in Figure 5.9. Serum from 7 days post boost has a high

titre of neutralising antibodies against the vaccine HA (A/Neth/219/2003 1:2,880 mean 50% inhibition titre (50%IT)) (Figure 5.10). I next assessed neutralising responses to other low or high pathogenic H7 avian IAV responsible for several outbreaks in humans. With only 82% protein identity to the vaccine HA and A/New York/107/2003, sera from 7 days post boost showed a reduced mean 50%IT of 664 (Figure 5.10 A) towards this HA. Since the outbreak of H7N9 avian influenza A virus in China in spring 2013 (Gao et al. 2013), the virus has been responsable for five outbreak waves, infecting more than 1,500 people (Wang et al. 2017). A/Anhui/1/2013 was the predominant virus present during the first wave outbreak in China, in the spring of 2013, and, with 97% protein sequence identity with the HA of A/Netherland/219/2003, was well neutralised by the porcine sera (1:2279 mean 50%IT). Similalry to A/Anhui/1/2013, A/Shangai/1/2013, also isolated during the first wave, is a low pathogenic virus and was strongly neutralised (1:4795). After the first wave, surface genes of H7N9 viruses have developed into two linages, distinguished by the region of outbreak, either the Yangtze River Delta or the Pearl River Delta (Wang et al. 2016). I next studied the serum neutralisation against the high pathogenic viruses of the Yangtze River Delta lineage, which arose during the fifth and most contagious wave: A/Guangdong/17SF003/2016, A/Guangdong/TH005/2017, A/Guangdong/8H324/2017, A/Hong Kong/125/2017 and A/Taiwan/1/2017. While for A/Guangdong/17SF003/2016 the neutralising titre was comparable to the vaccine's HA one (1:2819), more recent viruses were less neutralised (A/Guangdong/TH005/2017 1:993, A/Hong Kong/125/2017 1:643, A/Taiwan/1/2017 1:125 and A/Guangdong/8H324/2017 1:111 50%IT) (Figure 5.10 A).

Inhibition of the NA was measured by ELLA assay. The high inhibition titre against the vaccine's N1 A/England/195/2009 (1:8,577) was mantained against the closely related A/Bayern/69/2009 and the

more recent A/Michigan/45/2015. However, serum of immunised pigs failed to inhibit the NA of A/Puerto Rico/8/1934, probably because they share only 80% protein identity (Figure 5.10 B).

I next evaluated systemic cellular responses using tetramers (Tungatt et al. 2018). At 21 days post boost NGK^+ CD8 T cells of all animals were higher than their level pre immunisation (0.92% of CD8 at 21 days post boost, 0.16% pre immunisation) while DFE^+ and EFE^+ percentages were not altered after immunisation (Figure 5.10 C). CD8 T cells specific for IAY were detected at high levels at the beginning of the study (0.73% of CD8) and only one outlier pig presented increased number of IAY^+ cells (Figure 5.10 C).

A

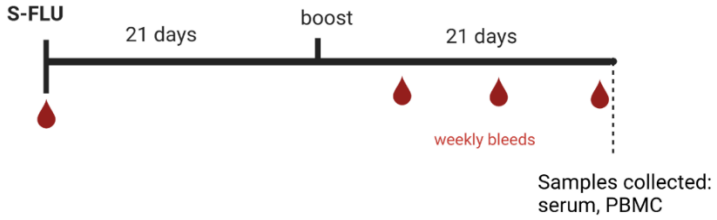

Group	Route of administration	Number of animals	Vaccine used	Titre (TCID50)
S-FLU	Intramuscular	4	[eGFP/N1(Eng195/2009)] coating H7(A/Neth/219/2003)	3×10^9

	Assay	Samples used	Viruses used
Humoral responses	ELLA	serum	1. [eGFP/N1(Eng/195/09)] coating H1 (Eng/195/09) S-FLU 2. [eGFP/N1(PR8)] coating H5(A/Vietnam/1203/2004) S-FLU 3. H1N1 (A/Michigan/45/2015) 4. H1N1 (A/Bayern/69/2009)
	MN	serum	1. [eGFP/N1(Eng/195/09)] coating H7(A/Neth/219/2003) S-FLU 2. [eGFP/N1(PR8)] coating H7 (A/NY/107/2003) S-FLU 3. [eGFP/N1(PR8)] coating H7 (A/Shanghai/1/2013) S-FLU 4. [eGFP/N1(PR8)] coating H7(A/Anhui/1/2013) S-FLU 5. [eGFP/N1(PR8)] coating H7 (/Guangdong/17SF003/2016) S-FLU 6. [eGFP/N1(PR8)] coating H7 (A/HongKong/125/2017) S-FLU 7. [eGFP/N1(PR8)] coating H7 (A/Guangdong/TH005/2017) S-FLU 8. [eGFP/N1(PR8)] coating H7 (A/Guangdong/8H324/2017) S-FLU 9. [eGFP/N2] coating H7(A/Taiwan/1/2017) S-FLU
Cellular responses	Tetramer staining: enumeration	PBMC	N/A

Figure 5.9 **S-FLU i.m.: experimental design and assays performed. (A)** Four 5-8 weeks old Babraham pigs were immunized intramuscularly with S-FLU (details in the table below), boosted 3 weeks apart and sacrifice 3 weeks after. **(B)** The tables summarise the assays performed and the viruses used for these tests.

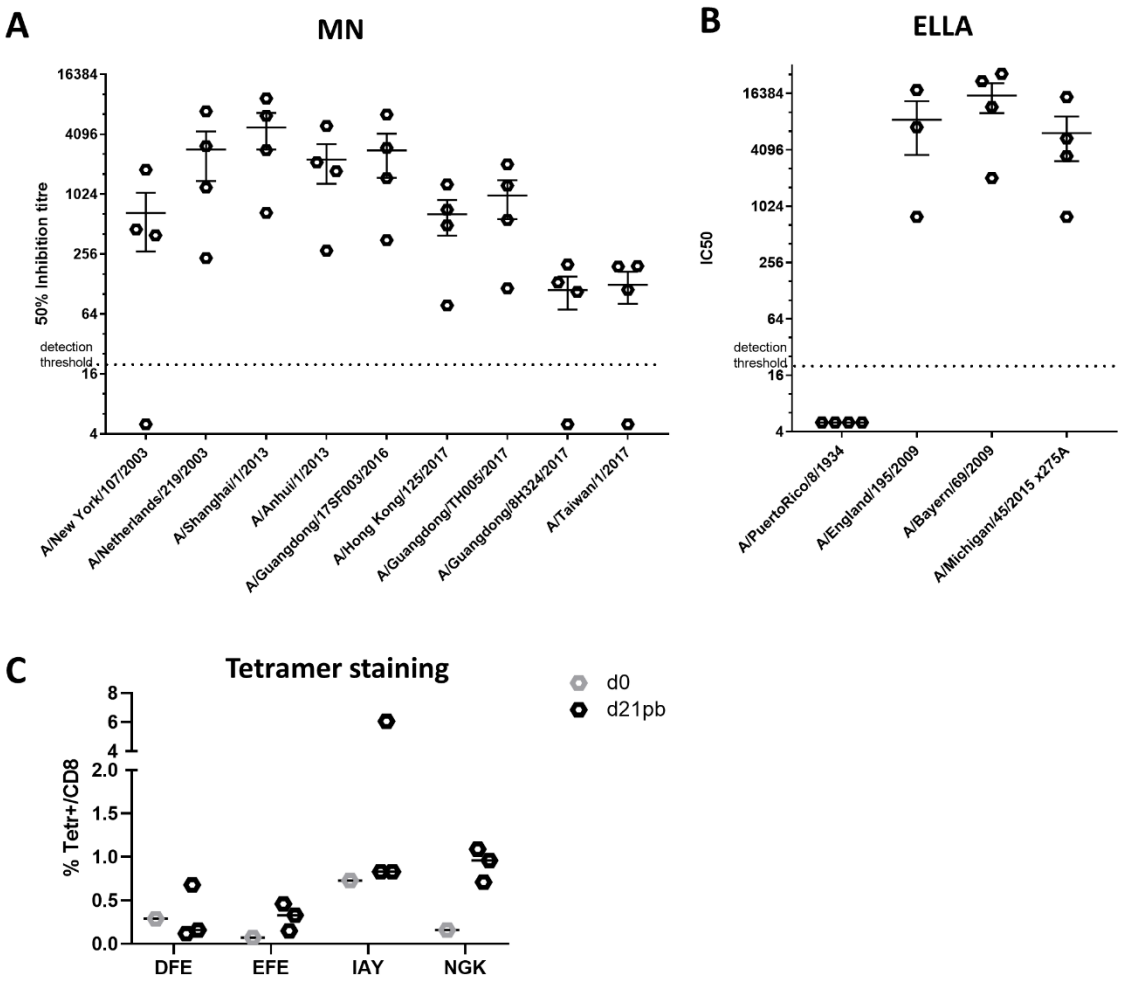

Figure 5.10 **S-FLU i.m.: humoral and cellular responses in blood (A)** Virus microneutralisation titre in sera at 7 days post boost against different H7 subtypes **(B)** Neuraminidase inhibitory Ab concentration (IC50) was measured 7 days post boost and cross reactivity tested to different N1 NAs **(C)** Enumeration of tetramer^{+} CD8 T cells in PBMC 21 days post boost (dpb). Each symbol represents one animal and the mean is shown as a bar. Pre-immunisation serum and PBMC were used as controls for the assays.

In summary, S-FLU delivered i.m. induced high level of neutralising Ab to HAs and inhibitory Ab to NAs of the same sub-type. CD8 T cells responses, identified by tetramer staining, were detected consistently against the NGK epitope.

Whether these levels of neutralising Ab are sufficient to provide protection was not investigated. This study was limited to the evaluation of the immune responses in the periphery, but it is not known whether neutralising antibodies were also present at mucosal sites or whether tissue resident memory T cells were generated.

5.4 Simultaneous aerosol and intramuscular S-FLU immunisation and challenge

Previous studies had demonstrated that S-FLU delivered by aer. reduces pathology and viral load in the lung and this was associated with a high level of local vaccine specific T cells (Morgan et al. 2016; Holzer et al. 2018; Morgan 2016). However, this vaccination regime did not consistently limit shedding from the URT, probably due to lack of neutralising Ab. I have shown that S-FLU delivered i.m. elicits high level of neutralising Ab in the serum but whether this is sufficient to confer protection is yet to be established. Uddback and colleagues tested an adenovirus vector expressing influenza NP systemically, locally and delivered with both routes simultaneously in mice and shown greatly improved and durable protection only when the vaccine was administered simultaneously (Uddback et al. 2016; Uddback et al. 2020). S-FLU vaccine was therefore tested by Alain Townsend's group in mice, comparing the immune responses generated after systemic administration, local delivery and a combination of the two (simultaneous i.n. and i.m., SIM) (Figure 5.11 A and B). 68 dpb, SIM immunised mice strongly

neutralised the vaccine HA, slightly lower titres were found in serum of mice immunised i.m. while i.n. delivery failed to produce neutralising Ab (Figure 5.11 C).

Taken together all these data prompted me to compare S-FLU SIM and i.m. (alongside aer. only) in pigs and study their protective potential in a challenge experiment. Three groups of 6 inbred Babraham pigs were immunised with H1N1 S-FLU (S-FLU) expressing HA and NA from A/England/295/2009 (H1N1pmd09): i.m. alone or by aer. alone or simultaneously by aer. and i.m. (SIM). The SIM group received the same total dose of the vaccine as the other groups but divided between the two sites. A fourth group of control animals was left untreated. The vaccinated groups were boosted three weeks later and all pigs were challenged i.n. with H1N1pdm09 four days prior to the end of the study (Figure 5.12). Before the end of the experiment two animals were culled due to underlying health conditions, leaving 5 pigs in the i.m. and control groups.

A

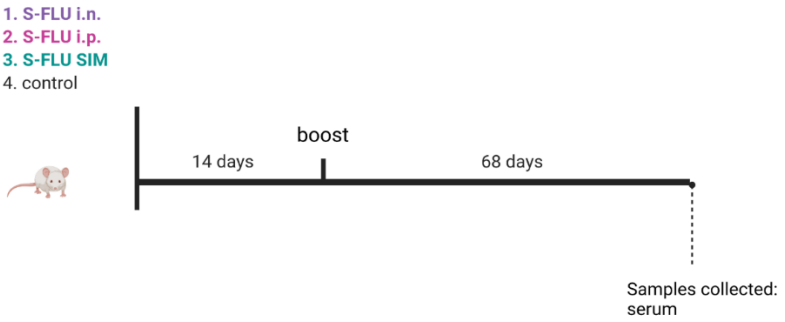

Group	Route of administration	Number of animals	Vaccine used	Titre (TCID50)
1. S-FLU i.n.	Intranasal	4	[eGFP/N1(PR8] coating H7(A/Hong Kong/125/2017)	10^5
2. S-FLU i.p.	Intraperitoneal	4	[eGFP/N1(PR8] coating H7(A/Hong Kong/125/2017)	10^6
3. S-FLU SIM	Intranasal and intraperitoneal	4	[eGFP/N1(PR8] coating H7(A/Hong Kong/125/2017)	i.n. 10^5 i.p. 10^6
4. Media Control	Intra nasal and Intraperitoneal	4	Unimmunised	N/A

	Assay	Samples used	Viruses used
Humoral response	MN	Serum	[eGFP/N1(PR8)] coating H7(A/Hong Kong/125/2017)

B

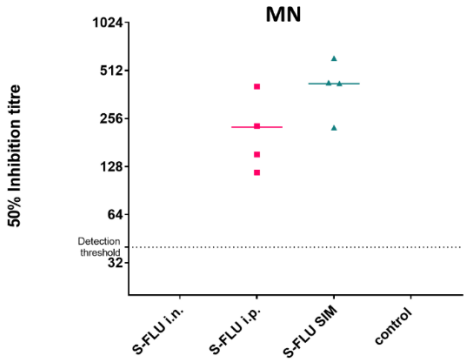

Figure 5.11 **S-FLU SIM in mice. (A)** 6-8 weeks old BALB/c female mice were immunised as indicated using S-FLU or medium, as a control, and sera collected 68 days post boost. **(B)** The table shows the

details of the immunisation regimes. **(C)** Neutralisation titre against H7 (A/Hong Kong/125/2017) obtained from sera at 68 days post boost. Holly Sadler and Alain Townsend performed this experiment.

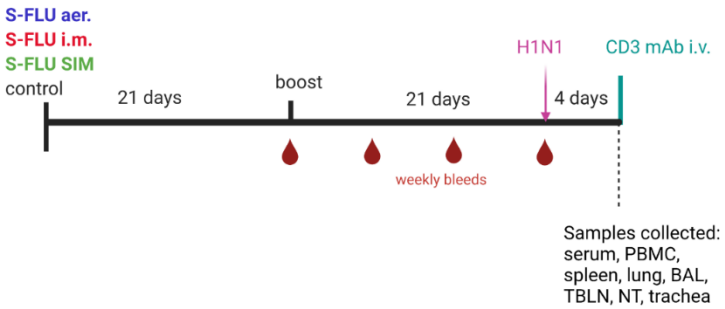

Group	Route of administration	Number of animals	Vaccine used	Titre (TCID50)
1. S-FLU Aer.	Aerosol	6	[eGFP/N1(A/Eng/195/2009)] coating H1(A/Eng/195/2009)	7×10^7
2. S-FLU i.m.	Intramuscular	5	[eGFP/N1(A/Eng/195/2009)] coating H1(A/Eng/195/2009)	7×10^7
3. S-FLU SIM	Aerosol and intramuscular	6	[eGFP/N1(A/Eng/195/2009)] coating H1(A/Eng/195/2009)	3.5×10^7 via aer. 3.5×10^7 via i.m.
4. Control	N/A	5	Unimmunised	N/A

	Assay	Samples used	Viruses used
Humoral responses	ELLA	serum	[eGFP/N1 (PR8)] coating H5(A/Vietnam/1203/2004) S-FLU
	MN	serum	1. [eGFP/N1(PR8)] coating H7(Netherlands/219/2003) S-FLU 2. H1N1 (A/swine/England/1353/2009)
Cellular responses	ELISpot	PBMC, spleen, BAL	1. [eGFP/N1(PR8)] coating H7(Netherlands/219/2003) S-FLU 2. H1N1 (A/swine/England/1353/2009)
	Tetramer staining: enumeration and phenotyping	PBMC, spleen, BAL, lung, TBLN	N/A

Figure 5.12 **S-FLU SIM in pigs: experimental design and assays performed.** Babraham pigs were immunized with S-FLU by aerosol (aer.), intramuscularly (i.m.) or simultaneously by Aer and IM (SIM) and boosted 3 weeks later while a fourth group of control animals was left untreated. All groups were then challenged with H1N1pdm09. Swabs were taken daily post challenge and all pigs were culled 4

days post challenge. Half of the pigs were infused intravenously with anti-porcine CD3 mAb 10 min prior to sacrifice. Tables shows the details of the immunisation (top) and the assays performed to evaluate the immune responses (bottom)

Protection

To assess protection, viral load in nasal swabs and BAL was measured and pathology in the lung evaluated. The viral load in the nasal swabs was significantly reduced in the SIM group on all days post challenge (dpc), except for 3dpc Figure 5.13 A).

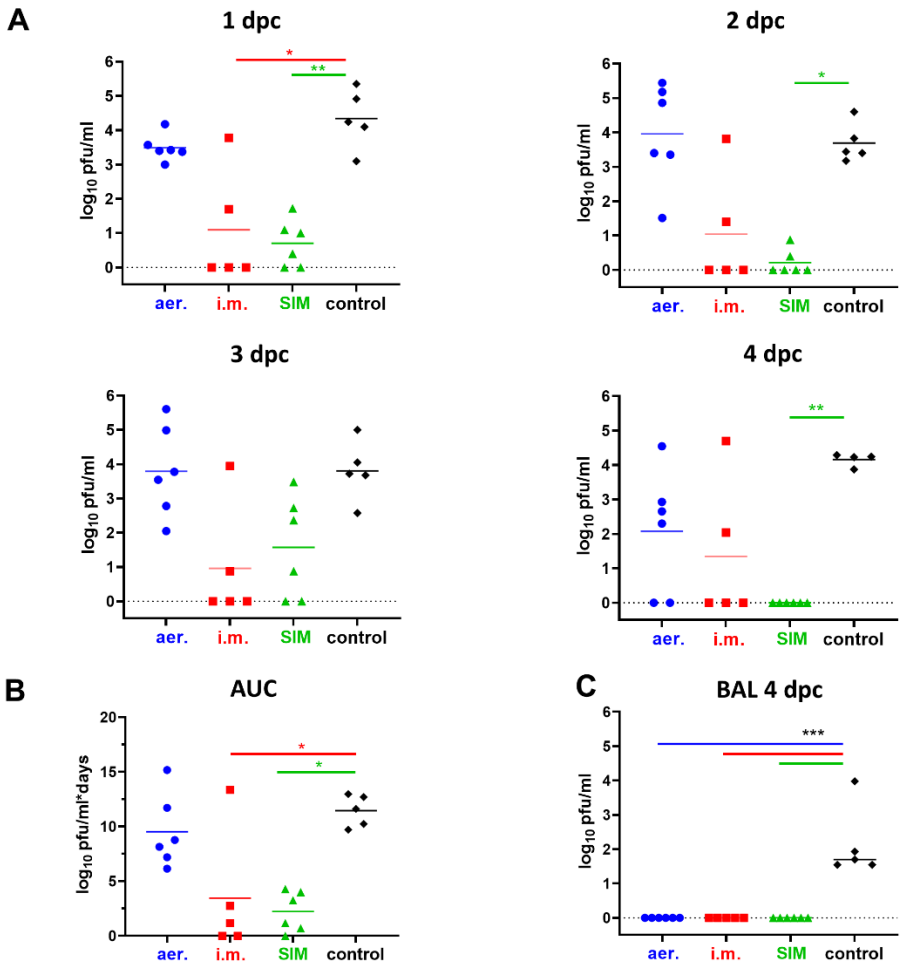

Figure 5.13 **S-FLU SIM viral shedding. (A)** Virus titre in nasal swabs measured by plaque assay at 1, 2, 3 and 4 dpc. **(B)** Area under the curve (AUC) of viral titre in the nasal swabs over time. **(C)** Viral titre in the broncho-alveolar lavage (BAL) 4 dpc. The data are the average of 2 separate assays, each symbol indicates an individual animal and the horizontal line the mean of the group. Data were analysed using the Kruskal-Wallis test. Asterisks indicate significant difference from the control group *$p<0.05$, **$p<0.01$ *** $p<0.001$.

In i.m. group viral load was significantly reduced only on 1 dpc, with two individuals consistently shedding virus throughout the experiment. Aer. did not stop viral replication in the nose, showing only a trend towards reduced viral shedding on 4 dpc (Figure 5.13 A). Overall, i.m. and SIM reduced significantly the viral replication in the nose, with an area under the viral load/time curve of 3.46 and 2.23, while the aer. and control groups showed greater shedding for longer (9.53 and 11.46 area under the curve respectively) (Figure 5.13 B). No virus was detected in BAL at 4 dpc in any immunised animals (Figure 5.13 C).

These results indicate that simultaneous SIM regime conferred protection with significant reduction in virus shedding. I.m. immunisation impaired viral replication in the nose in half of the animals, while aer. alone only showed a trend in reducing viral replication by 4 dpc.

Pathology

Bronchial and alveolar exudation with lymphoplasmatic infiltration, typical of influenza infection, was present in naïve animals and slightly reduced in the aer. group but almost absent in i.m. and SIM (Figure 5.14 A). In particular, a significant reduction in the severity of the lesions was observed in the i.m. and SIM groups ($p=0.02$ and $p=0.005$ respectively). IAV NP immunohistochemistry (NP-IHC) detection revealed a lower, although not significant ($p=0.55$), reduction in infected cells in the aer. compared to unimmunised animals, which showed abundant labelling (Figure 5.14 B). In the i.m. and SIM vaccinated group viral NP was detected in only one and two animals, respectively. Despite a reduction in gross

pathology and labelling of virus infected cells, no significant difference was found when histopathology and NP-IHC were combined (Iowa score) in all three vaccination regimes compared to control (Figure 5.14 B). In conclusion, despite absent viral load in the lung in all immunised animals, only pigs that received the vaccine both by both routes showed significantly lower lung gross lesions and NP-IHC.

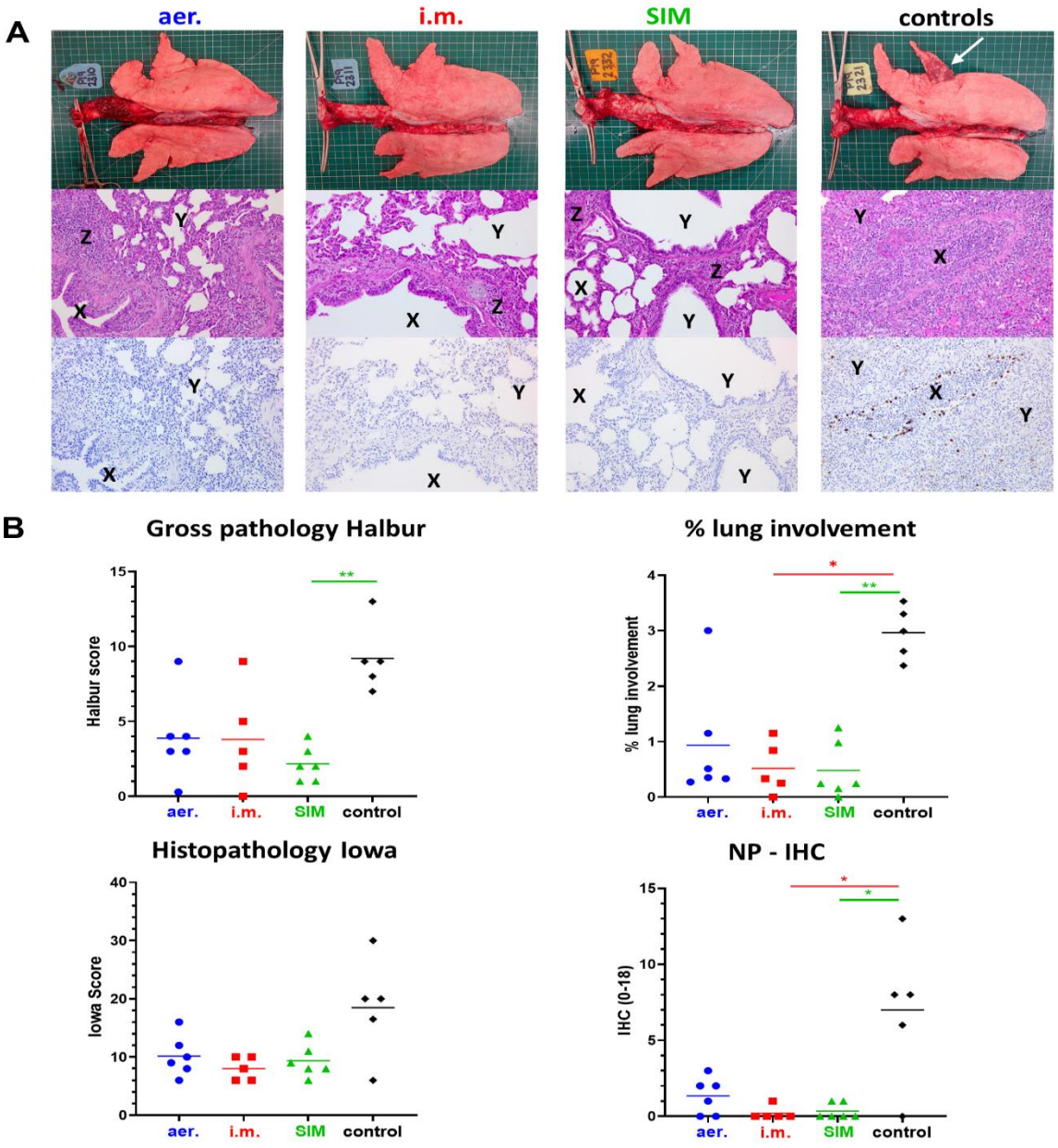

Figure 5.14 **S-FLU SIM: Pathology (A)** Representative lung gross pathology, histopathology (Hematoxylin and eosin (H&E) staining; original magnification x100), and immunohistochemical NP staining (original magnification x200) for each group are shown. Mild lymphoplasmacytic infiltration in peribronchiolar areas and expansion of alveolar septa are present in groups aer., i.m., and SIM (Z),

whereas bronchioles (X) and alveolar spaces (Y) remain free of cellular exudation (white spaces). There is a marked virus replication (brown labelling) in bronchiolar epithelial cells. **(B)** The gross and histopathological scores for each animal in a group and the group means are shown, including the percentage of lung surface with lesions, the lesion scores, and the histopathological scores (Iowa includes the NP staining). Pathology scores were analysed using one-way nonparametric ANOVA with the Kruskal–Wallis test. Asterisks denote significant differences: *p < 0.05, **p < 0.01, compared with control.

Ab responses

I next evaluated the Ab responses generated by the different immunisation regimes. Pre boost, both i.m. and SIM group already had low levels of neutralising Ab in the sera (average of 44 and 20.4 50%IT respectively) (Figure 5.15 A). At 7 dpb, the neutralising Ab titre increased 50-fold in both groups (average 50%IT of 1,920 for i.m. and 1,088 for aer.), levels which were maintained pre-challenge (832 and 413.3, respectively). For the first time I could detect neutralising Ab after aer. immunisation, although at very low level, with a peak at 14 dpb of 53.5 (50%IT) which rapidly decreased to an average of 7.3 pre-challenge. ELLA was then used to detect inhibitory antibodies to NA present at 4 dpc. I.m. immunised pigs developed the highest IC50 of 1,408 followed by SIM (453.3 IC50) while aer. showed minimal inhibition (average 14.2 IC50) (Figure 5.15 A). In contrast to what was observed in the serum, the neutralising Ab response in the lung was highest in the aer. group (13.3 50%IT) and detectable only in 3 out of 6 SIM animals while absent in i.m. group (Figure 5.15). As neutralising Ab could not be detected locally in the i.m. group, I asked whether we could detect any anti HA Ab in the BAL 4 dpc. A significantly high level of anti-HA IgG was found in both i.m. and SIM group (119.2 and 167 respectively) while IgA were significantly higher only when the vaccine was delivered locally (18.6 for aer. group and 46.6 for SIM) (Figure 5.15 B). Inhibitory activity towards NA was much lower in the BAL compared to serum and only significantly different from the control in the SIM animals (Figure 5.15 B). I next evaluated the number of HA-specific IgG and IgA B cells, in blood pre-challenge and in

spleen and TBLN 4 dpc. Despite the high neutralising titre in the serum of both i.m. and SIM pigs, no significant difference in Ab secreting cells (ASC) was found in blood and spleen (Figure 5.15 C). A significant number of HA-specific IgG secreting B cells were found in TBLN in the aer. group (mean 47.6 ASC/10^6) with a lower number in the SIM group (25.1 ASC/10^6). A similar trend was found for IgA HA-specific B cells, with aer. showing the highest proportion (22,8 ASC/10^6) followed by SIM (8.5 ASC/10^6). Only 2 out of 5 i.m. pigs showed HA-specific IgG and IgA ASC in TBLN (Figure 5.15 C).

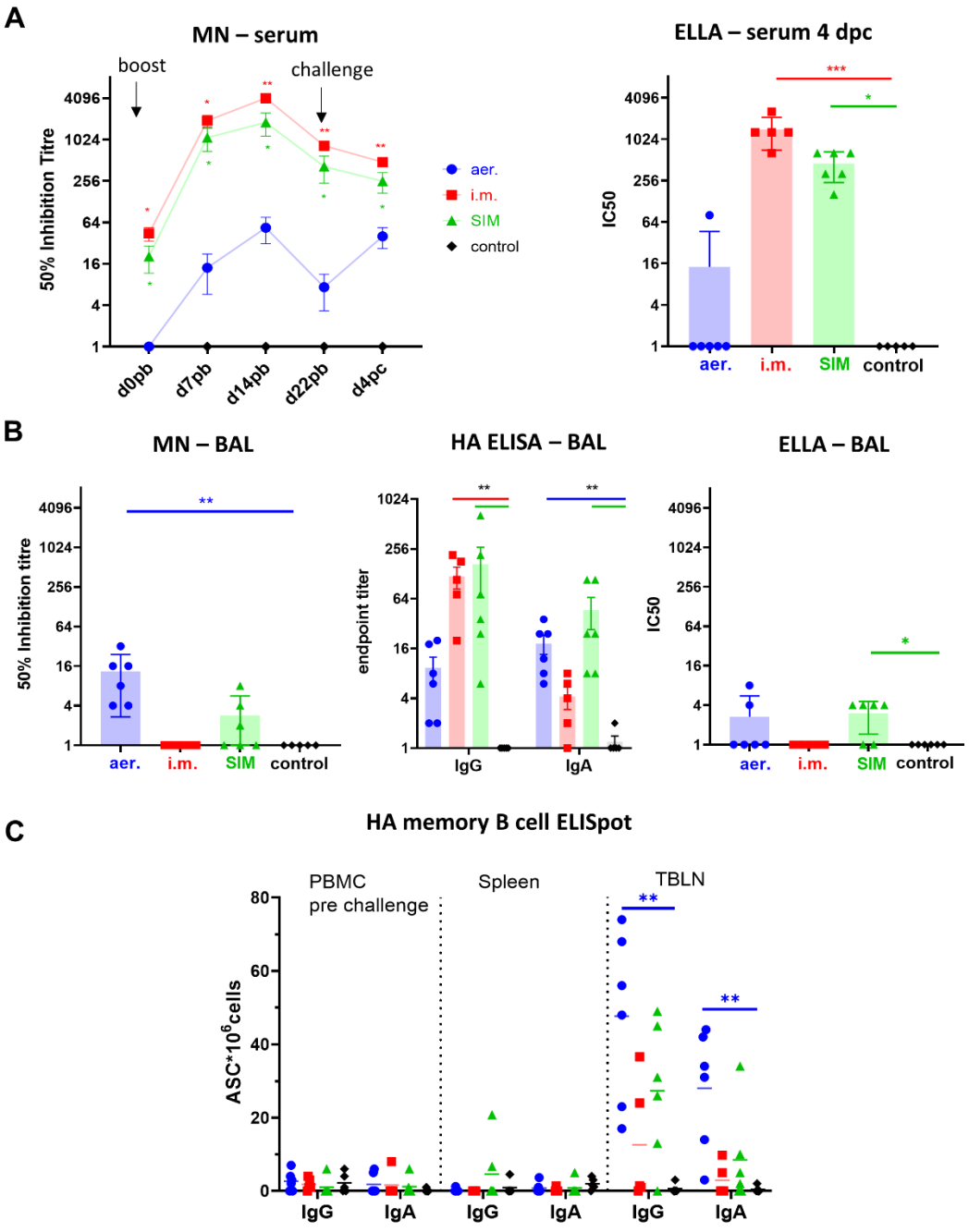

Figure 5.15 **S-FLU SIM: Systemic and local Ab responses. (A)** MN assay was used to determine serum-neutralising titres over time (shown as mean and SEM of two independent assays). NA inhibition activity was assessed in sera by ELLA at 4 dpc. **(B)** BAL at 4 dpc was

tested for its ability to neutralise (MN, left). ELISA titre of HA-specific IgG and IgA (centre), and NA inhibitory activity by ELLA (right) were assayed at 4 dpc in BAL. **(C)** HA-specific memory B cells were detected by ELISpot in PBMC (pre-challenge), spleen, and TBLN 4 dpc. Each animal is represented by a symbol, and the mean is shown as a bar. Serum neutralization was analysed with two-way ANOVA, whereas Kruskal–Wallis test was used for the analysis of NA inhibition in serum, BAL samples, and ELISpot data. Asterisks denote significance compared with control group (*$p < 0.05$, **$p < 0.01$, ***$p < 0.001$).

In summary, i.m. immunisation generated high neutralising Ab titre in blood but a limited Ab response in BAL. In contrast, aer. delivery generated the highest response in the local tissues (BAL and TBLN). The SIM grouped showed a one-fold decrease in virus neutralising activity compared to the i.m. group at all time points. In addition, SIM pig had half the number of HA-specific B cells in the TBLN compared to aer., showing the potential benefit of combining both immunisation strategies.

T cell responses in BAL

T cell responses in BAL were measured by intracellular cytokine staining. Following *ex vivo* stimulation with H1N1pdm09, no T cells responses were detected in the i.m. group (Figure 5.16). In contrast, aer. and SIM generated strong local T cell responses. CD8 T cells of aer. immunised pigs secreted mainly IFNγ (7.2% of CD8) followed by TNF (3.6%) and a similar trend was seen for the SIM group (4.5% IFNγ and 2.8% TNF) (Figure 5.16 A).

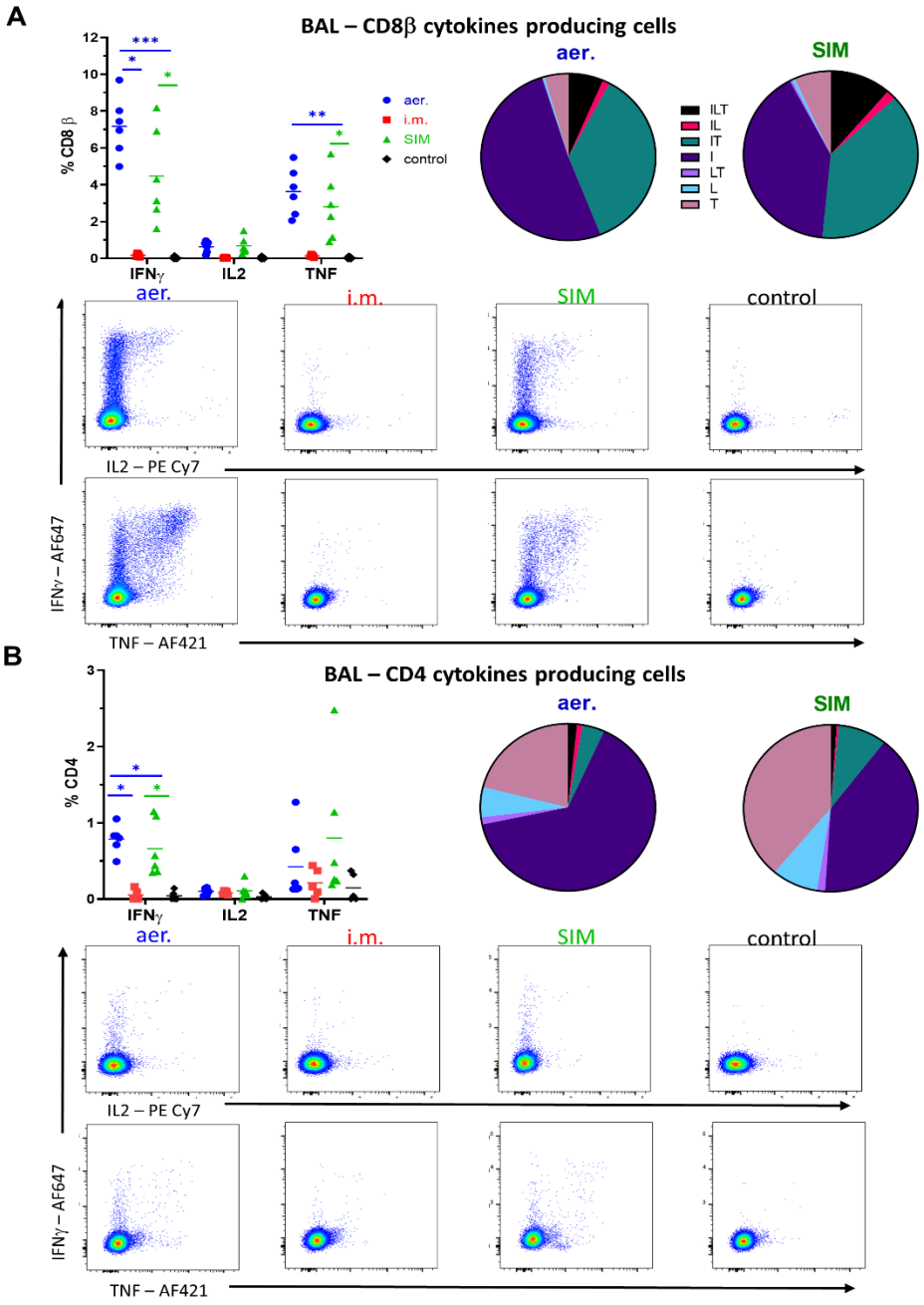

Figure 5.16 **S-FLU SIM: Cytokine secretion in BAL.** BAL was stimulated with H1N1pdm09 (MOI = 1) and IFNγ, and IL-2 and TNF production was measured in CD8 **(A)** and CD4 **(B)** cells by intracellular staining. Each symbol represents an individual animal, and the mean is

shown as a bar. The pie chart shows the mean proportion of single, double, and triple cytokine-secreting CD8 T cells for IFNγ (I), TNF (T), and IL-2 (L). Representative plots show the cytokine-secreting cells within the CD8 (A) and CD4 (B) populations. Kruskal–Wallis test was used to compare responses between groups, and asterisks indicate significant differences (*$p < 0.05$, **$p < 0.01$, ***$p < 0.001$).

The CD8 response in both groups was dominated by single producer IFNγ (51.1% of total cytokine secreting cells) followed by double producing IFNγ-TNF (36.2%) and a smaller proportion of triple secreting IFNγ-TNF-IL-2 cells (6.5%) (Figure 5.16 A). The CD4 response in the aer. and SIM group consisted mainly of IFNγ secreting cells (0.80% and 0.66% of CD4, respectively) with few double and triple cytokine producers (Figure 5.16 B).

Overall, aer. produced the strongest T cell response, followed by SIM, with a high proportion of IFNγ secreting cells. I.m. did not generate virus-specific T cells in the BAL.

Specificity of systemic and local CD8 T cell responses

I next sought to enumerate the S-FLU-specific CD8 T cells present in the local tissues as well as in circulation, using four different NP CD8 tetramers (Tungatt et al. 2018). As shown earlier in this chapter, responses to EFE were negligible with only CD8 cells in TBLN of aer. immunised animals showing a statistically significant difference from the control (Figure 5.17). In the NT, IAY^+ cells were the most abundant (4.95% of CD8 in aer., 1.36% in i.m., and 3.36% in SIM) followed by DFE^+ and NGK^+ (DFE: 2.45% aer., 0.66% i.m., 1.36% SIM; NGK: 2.19% aer., 0.18% i.m., 1.46% SIM) (Figure 5.18). The trachea showed similar specificity. The strongest response was observed in BAL for aer. and SIM groups while no response was detected in the i.m. group, supporting the results obtained by intracellular cytokine staining. Interestingly in BAL the hierarchy of the response differed from that in the NT. In particular, NGK dominated (13.38% aer., 13.81% SIM) followed by IAY (12.71% aer., 9.36% SIM)

and a smaller DFE response was found (5.96% and 4.70%). In the lung, I detected similar but lower responses (Figure 5.18).

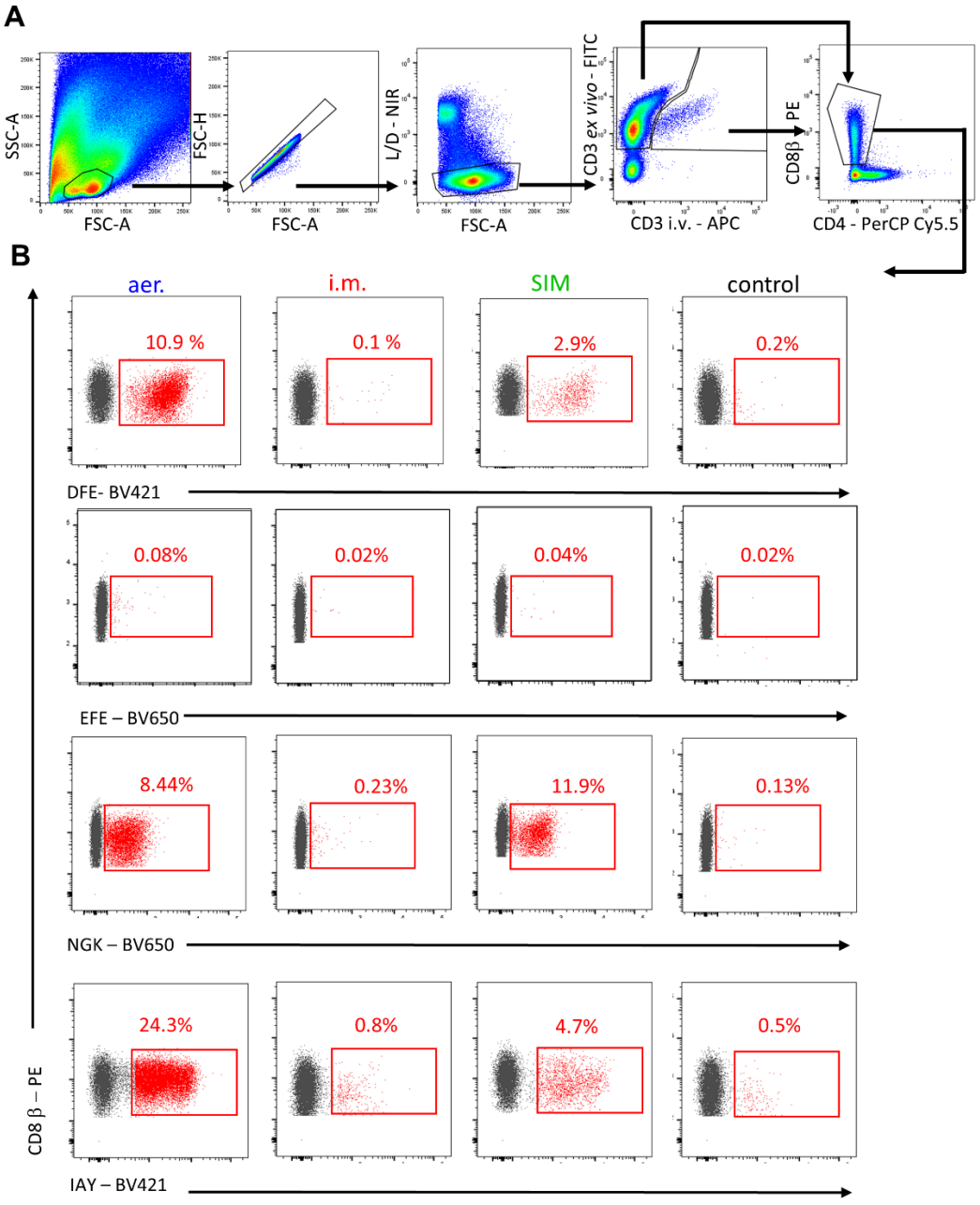

Figure 5.17 **S-FLU SIM: tetramer staining. (A)** Gating strategy for tetramer staining of BAL cells. (B) Representative FACS plots showing DFE, NGK, EFE and IAY tetramers binding cells (in red) among the CD8 T cells in BAL in the different groups.

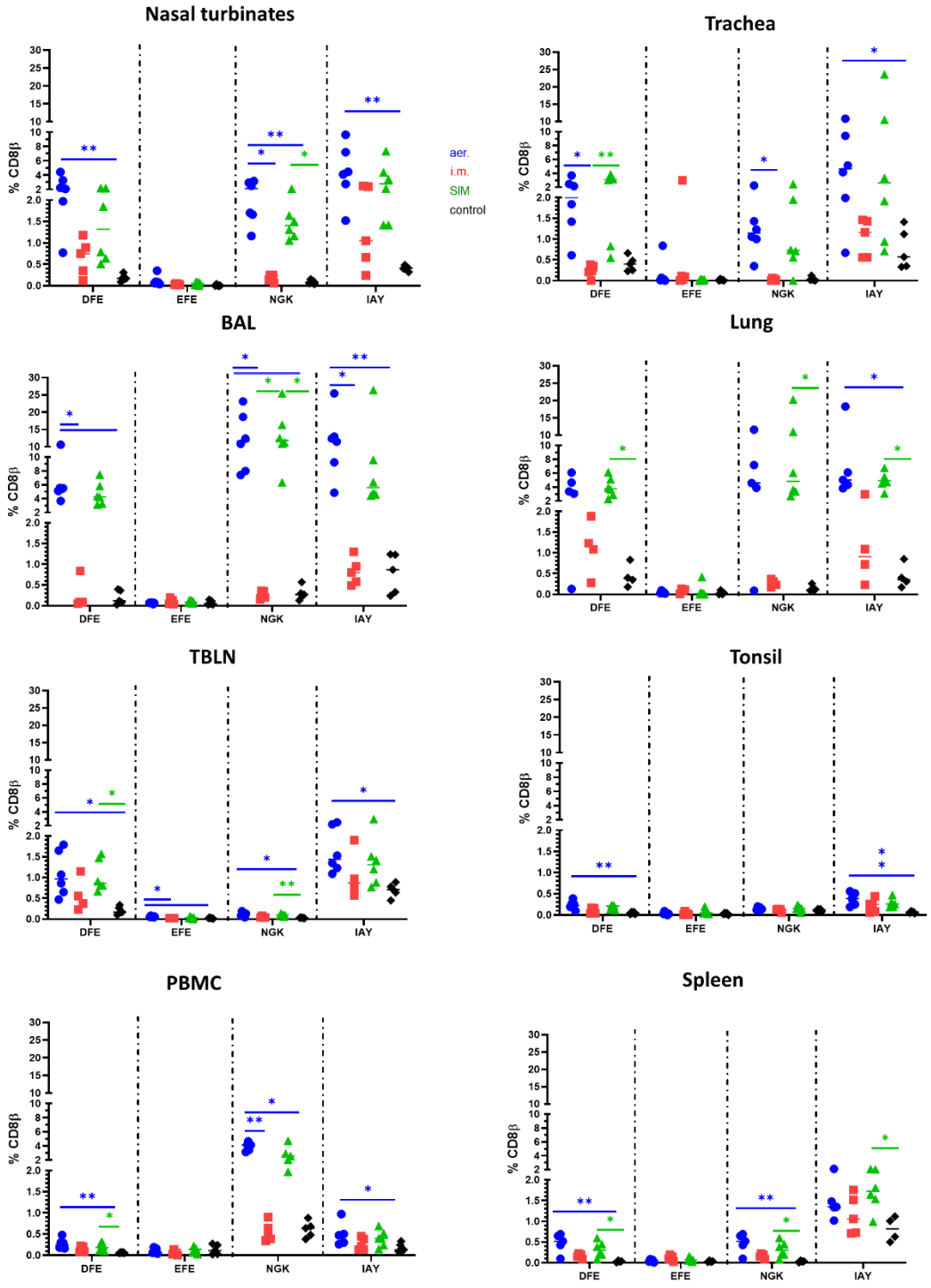
Nasal turbinates
Trachea
BAL
Lung
TBLN
Tonsil
PBMC
Spleen
% CD8β
DFE
EFE
NGK
IAY
aer.
i.m.
SIM
control

Figure 5.18 **S-FLU SIM: Percentages of DFE, EFE, NGK, IAY tetramer+ CD8 T cells in the respiratory tract and PBMC.** Each symbol represents an individual animal, and the mean is shown as a bar. Kruskal–Wallis test was used to compare responses between groups (*p < 0.05, **p < 0.01).

Surprisingly, in TBLN, I detected a limited number of NGK^+ cells (0.11% in aer.) while the majority of $tetramer^+$ cells recognised DFE (1.08% aer.) and IAY (1.64% aer.). Tonsil presented a similar trend although the responses were much lower (Figure 5.18). On the other hand, the biggest population found in the circulation at 4 dpc recognised NGK (3.91% aer. and 2.85% SIM) although there was still a significant presence of DFE and IAY^+ cells. Strikingly, no significant difference from the control group was found in the PBMC for the i.m. group. The dominance of NGK found in PBMC was not present in spleen, however due to high background staining in the control group, it is not clear which tetramer is dominant.

In order to understand the hierarchy of the tetramers in different tissues, I calculated the proportion of each tetramer in the totality of $tetramer^+$ CD8 T. A significantly higher proportion of DFE was found in NT ($p=0.01$) and trachea ($p=0.005$) compared to PBMC in the aer. group. In addition, throughout the entire RT, the proportion of IAY was significantly higher than in the blood ($p \leq 0.002$). NGK showed a opposite trend, with 84.22% of the total $tetramers^+$ cells in PBMC recognising this epitope while in the local tissue the proportion was significantly lower. These trends were also observed for the SIM group but where less pronounced in the i.m. animals, where the response was overall much lower.

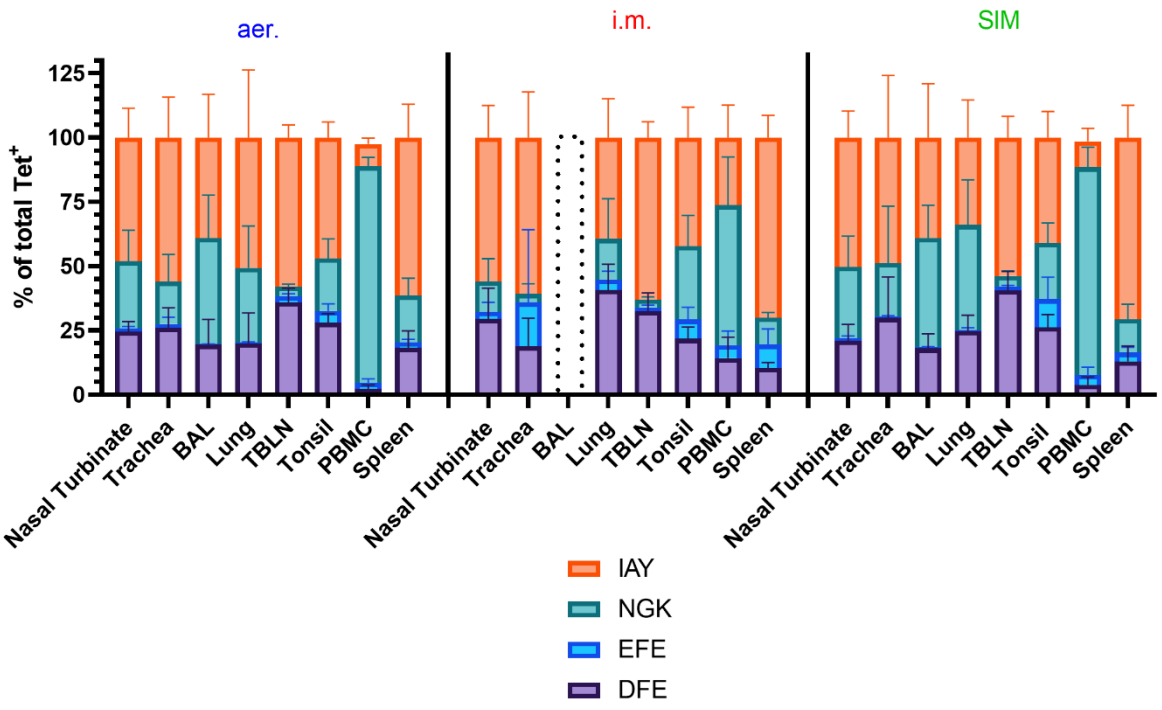

Figure 5.19 **S-FLU SIM: proportion of each tetramer among total tetramer$^+$ CD8 T cells in different tissues.** A dotted histogram for BAL of the i.m. group indicates the absence of response. The data represent the average of two separate assays. Two-way ANOVA to compare the proportions of tetramers in the different tissues of each group of animals.

Next, I evaluated the numbers of TRM in the RT identified by i.v. infusion of anti-porcine CD3 mAb (Figure 5.20 A). Most BAL cells were tissues resident and inaccessible to the influsued mAb (82.4% CD3 i.v.$^-$). In the URT a smaller porportion of cells were not bound by the i.v. mAb (11.6 and 38.8% in NT and trachea respectively), whereas 95% of lung T cells were positive for the infused and *ex vivo* CD3 mAbs, as a consequence of the known difficulties in isolating TRM and high blood contamination (Steinert et al. 2015). Tetramer$^+$ cells were found in both CD3 i.v.$^-$ (TRM) and CD3 i.v.$^+$ CD3 ex vivo $^+$ (circulating) populations. When analysing the phenotype of DFE$^+$ cells in different compartments we confirmed that in BAL, cells were almost exclusively TEM like after natural infection and post S-FLU

aer. boost (Figure 5.20 B). In TBLN and PBMC, TCM were predominant (77% in TBLN and 46% in PBMC). At 3 weeks post boost, few BAL CD8 were proliferating. I therefore examined whether DFE^+ T cells expressed Ki67 early after challenge. Ki67 was only marginally expressed in $tetramer^+$ cells (2.7%), following the general trend of BAL CD8 T cells. In contrast 42.2% of DFE^+ TBLN cells and 45.4% of DFE^+ PBMC expressed Ki67 (Figure 5.20 C), showing a higher median fluorecent intensity compared to the totality of CD8 T cells . As during influenza infection, in S-FLU immunised pigs DFE^+ BAL cells lacked T-bet and Eomes while these transcription factors were expressed in TBLN. T-bet expression reached 30.6% 4 dpc while Eomes was only slightly upregulated (7.9%). $Tetramer^+$ T cells in PBMC expressed T-bet (55.9%) but minimal levels of Eomes (6.7%) (Figure 5.20 C).

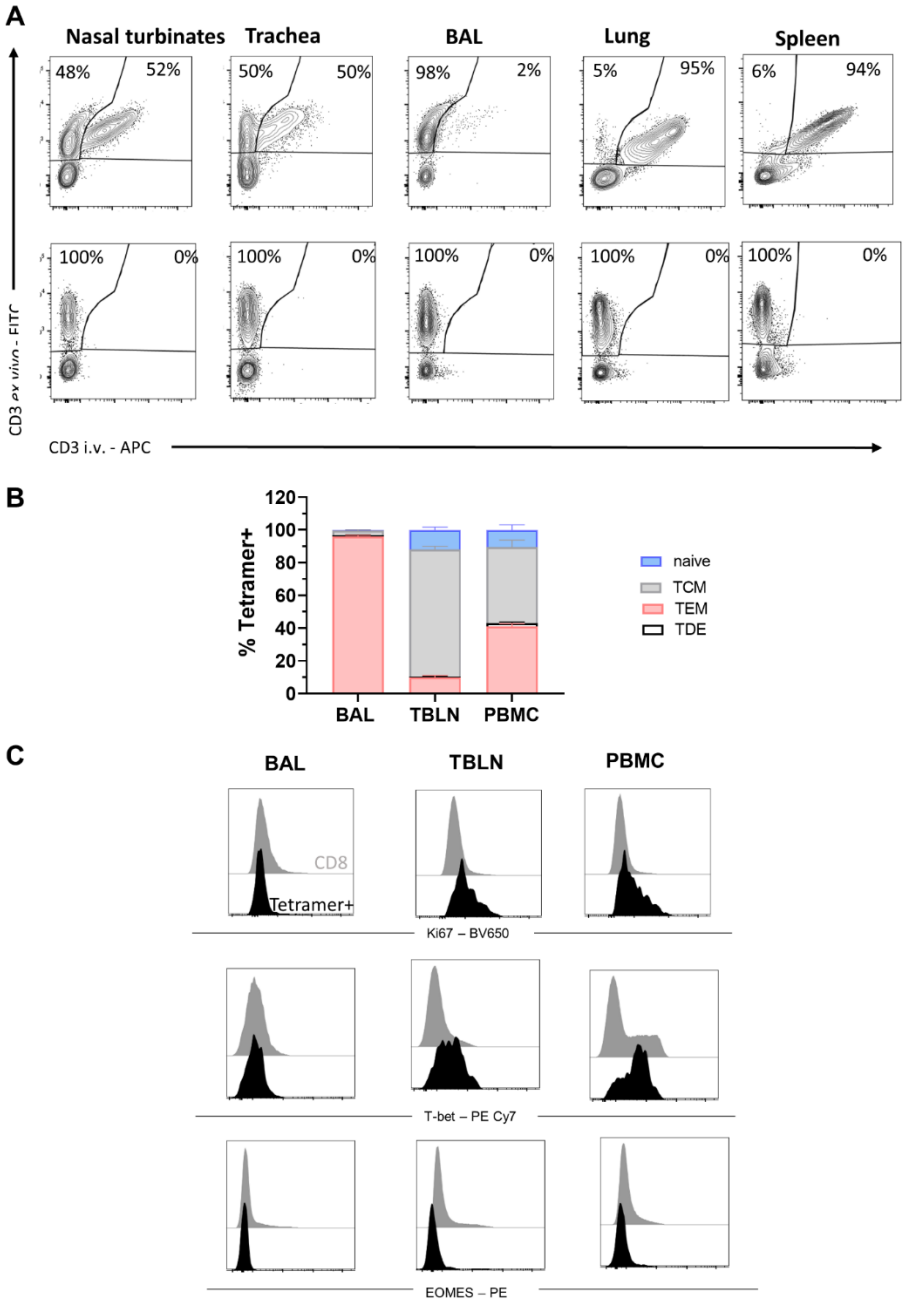

Figure 5.20 **S-FLU SIM: TRM and phenotypic characterisation of DFE$^+$ cells. (A)** Half of the pigs in each group were infused i.v. with CD3 mAb and culled 10 min later. Lymphocytes were then stained *ex vivo* with the same clone of CD3 Ab labelled with FITC. As the infused CD3 does not saturate all

CD3 sites, some cells isolated from the respiratory tract and all splenocytes are double positive (intravascular cells). The top row shows representative FACS plots of infused animal. The bottom row shows staining in animals not infused with CD3 mAb and stained *ex vivo*. The reported proportion of *ex vivo*$^{+}$ and *ex vivo*$^{+}$i.v.$^{+}$ CD3 were calculated from total CD3+. **(B)** CD45RA and CCR7 expression was assessed in BAL, TBLN and PBMC DFE^{+} T cells and proportion of naïve (CD45RA^{+} CCR7^{+}), TDE (CD45RA^{+} CCR7^{-}), TCM (CD45RA^{-}CCR7^{+}) and TEM(CD45RA^{-}CCR7^{-}) reported. **(C)** histograms showing the fluorescence intensity of CD8 (grey) and DFE^{+} cells (black) for Ki67, T-bet and Eomes.

5.5 Discussion

This chapter investigated different strategies to improve the efficacy of S-FLU vaccine in pigs. I aimed to enhance the local and systemic humoral response, since S-FLU administered locally did not induce detectable neutralising Ab in both mice and pigs and does not induce sterile immunity against homologous virus challenge (Morgan et al. 2016; Holzer et al. 2018).

The first approach involved the addition of an HA expressing cassette in the S-FLU backbone, in the form of CLEARFLU. I compared the immune responses generated after S-FLU and CLEARFLU aer. administration in pigs as this delivery route offers several advantages. Pulmonary delivery has been shown to generate cross-reactive T cells and mucosal Ab, associated with protection (Krammer 2019; Lau, Wright, and Subbarao 2012). In addition, local administration has not been linked with vaccine-associated enhanced respiratory diseases (VAERD) as reported for parenterally administered vaccines in pigs (Rajao et al. 2016). Previous studies conducted in our group compared two forms of pulmonary delivery (aer. and i.t.) and showed that aer. delivery was superior to i.t. (Hemmink et al. 2016).

CLEARFLU administered by aer. failed to produce neutralising Ab against HA and inhibitor Ab against NA in pigs, while in mice it elicits high neutralising titres. The lack of neutralising Ab was consistently observed in blood and in the BAL. The high number of tetramers^{+} T cells in the lung of pigs immunised with CLEARFLU indicated that the vaccine administration was successful and low Ab responses could

not be linked to low dosage. Possible causes of the lack of humoral responses might lie in poor immunogenicity of CLEARFLU or weak cell surface expression of HA. The absence of anti-NA neutralising antibodies in pigs could be explained by the reduced abundance of NA on the surface of CLEARFLU. In fact, due to the expression of two different HAs, CLEARFLU has shown a reduced number of NA molecules on its surface (Alain Townsend, personal communication). However, the lack of inhibitory Ab in serum was not observed in mice. In addition, I showed a high frequency of variation within S-FLU immunised group, with 1 animal lacking inhibitory Ab against NA. Increasing the animal numbers might answer the question whether S-FLU is indeed superior to CLEARFLU in generating an anti-NA response.

A second approach adopted to improve immunogenicity was delivering S-FLU systemically by i.m. injection. This route of administration is routinely used in humans and pigs for seasonal influenza vaccines. In previous mouse studies, H7 S-FLU i.p. generated high titre of neutralising Ab in serum (Powell et al. 2019). I therefore studied Ab responses after H7 (A/Netherlands/219/2003) S-FLU administered i.m. H7N9 viruses have been recently classified by the U.S. Centres for Disease Control and Prevention as the highest pandemic potential risk among several other zoonotic influenza viruses (https://www.cdc.gov/flu/pandemic-resources/monitoring/irat-virus-summaries.htm), and the scientific community was urged to develop new vaccines against these viruses. In particular, I chose H7 from A/Netherland/219/2003 as this HA induced the broadest cross reactivity in mice (Powell et al. 2019). In this pig model, H7 S-FLU stimulated a high and cross-reactive Ab response to different H7s and NAs. On the other hand, I detected few tetramer^{+} T cells in circulation. Future work will need to assess in more detail the T cell responses as systemic immunisation might not share the same immunodominant specificity as local immunisation. Furthermore, this study was limited to the investigation of systemic

responses, and it remains unclear whether i.m. delivery of S-FLU can generate local humoral and cellular responses and if the responses in the periphery are protective. A challenge studies will also be needed to investigate the potential risk for VAERD.

As mentioned above, local immune responses are fundamental in heterotypic protection while an hemagglutinin inhibitory (HAI) titre >40 in serum is considered protective by the regulatory agencies (Cox 2013). The pilot study reported here showed that S-FLU i.m. generates strong systemic neutralising responses while when delivered by aer. it elicits high level of antigen-specific T cells locally. How best to achieve both local immune responses and high systemic neutralising titre? To answer this question, I tested a third strategy including simultaneous local (aer.) and systemic (i.m.) immunisation (SIM), previously shown in several model to be protective and induce long lasting immune responses (Uddback et al. 2020; Uddback et al. 2016; Dean et al. 2015; Ronan et al. 2009). I compared, in a challenge experiment, S-FLU administered by aer., i.m. and SIM.

The i.m. group showed a powerful neutralizing Ab response and reduced the viral load and lung pathology. However, cellular responses were weak in this group and strikingly absent in BAL at 4 dpc. Neutralizing antibodies were also absent in BAL, although it is important to note that BAL harvesting causes considerable dilution, so low titres of Ab remain undetected. This indicates that immunisation by i.m. injection fails to develop local responses, as previously reported in mice immunised with the seasonal human inactivated vaccine (Zens, Chen, and Farber 2016b). After challenge, i.m. group did not show signs of VAERD, indicating that S-FLU i.m. administration is safe.

Aer. immunised animals displayed low titres of neutralising Ab in blood and BAL, which did not prevent viral replication in the URT. Gross and histopathology were slightly reduced although not significantly,

while no virus was detected in BAL. I detected powerful CD8 and CD4 responses in BAL and showed that these cells were inaccessible to the circulating Ab. Previous studies using H3N2 S-FLU in pigs administered by aer. showed reduced lung pathology 5 days post heterologous challenge with H1N1pdm09 (Holzer et al. 2018). In the mouse model TRM mediated protection against heterologous influenza challenge (Teijaro et al. 2011; Wu et al. 2014; McMaster et al. 2015). These slightly conflicting data may indicate that, although TRM play a role in protection, in pigs this is not enough to reduce viral replication or abolish lung pathology. It is important to note that in the present study I used Babraham pigs as opposed to the outbred pigs used by Holzer et al, which might have had an effect on the outcome.

The SIM group benefited from the properties of the two immunisations. High serum neutralising Ab were generating in serum together with neutralising Ab in BAL but, in contrast to the i.m. group, high cellular responses were also detected. The SIM pigs had greatly reduced viral replication in the URT and LRT together with reduced lung pathology. T cells isolated from BAL showed high frequencies of cytokine secreting cells and strong cellular responses were recorded in URT and TBLN.

As previously described, SIM regimes have already been investigated in the context of other respiratory diseases. A second strategy, aiming to achieve long lasting local and systemic immunity, has been developed preclinically: prime and pull immunisation. A first dose is administered systemically ("prime") followed by the local administration of an inflammatory or secondary vaccine ("pull"), pulling all circulating T and B cells to the site of infection, where the second immunisation is administered. Prime and pull immunisation was successful for skin or reproductive tract infection, generating protective TRM in these tissues (Mackay et al. 2012; Shin and Iwasaki 2012). On the other hand, systemic administration followed by lung "pull" was less successful in enhancing protection against

respiratory infections (Woodworth et al. 2019; Roces et al. 2019; Britton et al. 2015).. This might be explained by the lack of cognate antigen recognition, fundamental for TRMs generation in the lung (Wakim et al. 2015; McMaster et al. 2018; Uddback et al. 2020). Our SIM strategy may circumvent this issue by administering the antigen to the entire respiratory tract, twice, however future work will need to assess the duration of these protective responses. Uddback and collegues, using an adenovirus expressing influenza nucleoprotein, have demonstrated that SIM immunisation achieved protection lasting up to 8 months in mice (Uddback et al. 2016), showing great potential for this strategy.

Another interesting aspect to consider when choosing different administration routes is the T cell specificity. S-FLU aer. delivery promotes strong local T cells responses, with 2/3 of the NP immunodominant epitopes in common with those generated after infection with the more recent H1N1pdm09. I have shown here that i.m. immunisation failed to produce CD8 T cells specific for the four immunodominant epitopes of S-FLU's NP. Whether this route generates CD8 T cells with different specificity in CD8 T cells or a more dominant CD4 response remains unclear. In an attempt to answer this question, I have stimulated lymphocytes isolated from BAL, spleen PBMC and TBLN with overlapping peptides from HA, NA, NP and M1 and detected the responses by IFNγ ELISpot (data not shown). Due to great variability within each group, it was impossible to identify significant differences in the responses to peptide pools between the different routes. However, it was clear that overall the i.m. route generated weak T cell responses both systemically and locally. I can therefore speculate that for S-FLU the "prime and pull" strategy will be less efficient in eliciting local T cell responses in pigs, due to limited systemic cellular responses in the i.m. group. Another interesting aspect in the dynamic of T cells responses is the different hierarchy of the responses in different tissues. NGK^+ cells dominated in the blood of aer. and SIM animals while being almost absent in TBLN, perhaps indicating a migration

of these cells from local LN to the circulation prior entering to the site of infection. In the RT however IAY$^+$ CD8 T cells represented the biggest population amongst tetramer$^+$ cells. These findings demonstrate the different dynamic of the T cells responses in various tissues and with different immunisation regimes, highlighting the importance of studying the immune responses in local tissues and not only in blood.

In this chapter I have also analysed the generation of TRM after S-FLU aer. immunisation and challenge. Due to limited sample availability and aiming to compare our findings with H1N1pdm09 infection, I focused on studying DFE$^+$ CD8 T cells, as the DFE epitope is 100% conserved between S-FLU and H1N1pdm09 NP. I have shown that T cells in BAL are inaccessible to the infused anti-CD3 mAb consistently in the two experiments, while it was more difficult to identify reliably a TRM population in lung tissues due to its high vasculature and long enzymatic digestion needed for tissue processing. As a positive control, spleen and PBMC were labelled with the infused CD3 Ab as well as *ex vivo*. Interestingly in BAL, three weeks post aer. boost 22.6% of CD8 T cells were DFE$^+$ but only 5% 4 dpc. Conversely, there were higher numbers of TBLN and PBMC DFE$^+$ cells 4 dpc compared to 3 weeks post boost. The expansion of these cells in PBMC and TBLN is tied up with increase expression of Ki67, while this maker was absent in BAL. The phenotype in BAL was stable pre and post challenge, lacking expression of CD45RA and CCR7. There was a rapid increase in the proportion of TCM in TBLN and PBMC after challenge, though the small number of DFE$^+$ cells in PBMC indicates that this observation should be interpreted with caution. As during IAV infection, in S-FLU immunised pigs DFE$^+$ BAL cells lacked T-bet and Eomes while these transcription factors were expressed in TBLN. Tetramer$^+$ T cells in PBMC expressed T-bet at 3 weeks post boost and it increased after challenge (from 23% to 55.9%) with no changes in Eomes expression. Taken together these results suggest that S-FLU

immunisation by aer. elicited a stronger T cell response in BAL compared to influenza infection but the responding T cells had a similar differentiated, non-proliferating phenotype.

In summary, these results suggest that simultaneous aer. and i.m immunisation with S-FLU offers advantages in protection against influenza viruses in pigs. SIM is the best strategy to elicit an excellent systemic Ab response, a correlate of homotypic protection, together with strong local TRM response, indispensable for protection against heterologous challenge.

Chapter 6
General discussion

Although the protective role of TRM against infectious disease has been demonstrated in mice, little is known about their properties in a large animal. This thesis describes the phenotype, generation and transcriptional profile of IAV-specific CD8 TRM in the porcine RT. Inbred Babraham pigs were chosen because of their identifical SLA, which enabled the identification of two novel CD8 epitopes in the NP of H1N1pdm09. Data reported in Chapter 3 showed that NP-specific CD8 T cells can be found in the BAL and lung as early as 6 dpi, presenting a stable phenotype: $CD45RA^{-}CCR7^{-}CD69^{+}$. On the other hand, DFE^{+} BAL cells from 7 dpi significantly differed in gene expression compared to 21 dpi. Although some of the cells at the early time points expressed Ki67, at later time points this proportion is very low and the cells declined in number but not more rapidly than other tissues, indicating that the rate of cell death exceed that of cell division.

The generation of a stable TRM population in the lung is believed to be dependent on local antigen encounter, ensured by local immunisation (Takamura et al. 2016; Zens, Chen, and Farber 2016a). Therefore, vaccine delivery in the RT is likely to be important for the establishment of this protective T cell subset. I studied how best to administer antigen to the RT to generate a TRM population. To do this I characterised the deposition of particles in the RT administered by two different devices targeting the URT (MAD) or able to reach also the LRT (VMNs) (see Chapter 4). Scintigraphic experiments showed that VMNs could homogeneously distribute the formulation to the lung and these results were highly reproducible. I.n. administration with MAD device delivered a significantly high proportion of the dose

to the lung compared to VMN but concentrated to one side of the lung, suggesting that VMN might generate better responses and ultimately more TRM than MAD.

Single-cycle IAV vaccines are safe to be delivered to the lung, where protective TRM can be generated, and represent an alternative to the commercially available LAIV. The single-cycle vaccine candidate S-FLU was previously tested in mice and ferrets, where it protected against lethal challenge and impaired transmission. However, pigs immunised by aer. with S-FLU failed to develop neutralising Ab and stop nasal viral shedding. Therefore, a second generation of S-FLU vaccine, CLEARFLU, was designed to induce the expression of a non-functional HA and broaden the Ab response. As shown in Chapter 5, CLEARFLU delivered by aer. did not generate systemic or local neutralising Ab, despite comparable T cell responses to S-FLU. As a second strategy to improve immunogenicity, I compared aer. delivery of S-FLU, using VMNs, to i.m. injection and a combination of the two (SIM). SIM reduced significantly viral shedding and elicited both local and systemic B and T cell responses, representing the best delivery strategy for S-FLU vaccine.

6.1 T cell responses to influenza

I established for the first time the phenotype of porcine CD8 T cells using similar markers to those used in humans. The distribution of different CD8 T cells subsets across tissues resembles that in humans, validating the translational potential of the pig model. Babraham pigs were chosen to study the responses to H1N1pdm09 because of their identical SLA. The use of inbred animals for IAV research was justified by the finding that Babraham's responses were comparable to those of outbred pigs, (Edmans et al. 2020).

To understand immune responses to IAV it is important that the method of challenge gives similar responses to natural infection. Previous studies in pigs by Khatri et al. combined i.n. and i.t. inoculation while pigs were challenged i.t. by Talker and colleagues (Khatri et al. 2010; Talker et al. 2016). I.t. installation circumvents the URT, site of early viral replication, and Ab and cellular responses. In addition, Talker et al. delivered a high dose (10^7 TCID50/ml) of H1N2 in 15 ml i.t. which resulted in the detection of cellular responses in the lung as early as 4 dpi. Our group has recently compared the immune responses after i.n. H1N1pdm09 experimental challenge with IAV infection acquired after co-housing with experimentally infected pigs (in-contact) (Edmans et al. 2020). I.n. shared similar magnitude and kinetics of viral replication and cellular responses to the in-contact group. In both challenge conditions, T cells responses were first developed at 6 dpi in BAL (Edmans et al. 2020). This showed that i.n. challenge with 10^7 PFU, as performed in Chapter 3, resembles natural in-contact infection. Therefore, the features of porcine TRM described in this chapter are most likely very similar to TRM established during natural infection. It will be interesting to investigate the duration of IAV-specific TRM after natural transmission of the virus and monitor their development after multiple encounters with IAV, as is likely to occur on farms, to prove whether sequential exposures to the virus increases the persistence of this population (Van Braeckel-Budimir et al. 2018).

As shown in Chapter 3, IAV-specific T cells present in the BAL have a TRM phenotype throughout the study. Nevertheless, gene expression changed with genes involved in cytokine production, Th1/Th2 differentiation and the TGFβ pathway highly upregulated at 21 compared to 7 dpi and expression declining at 63 dpi. Future work will need to address the lifespan of porcine TRM beyond 63 dpi. Studies in mice reported that influenza-specific T cells in the lung decayed below the threshold 7 months after infection, leaving mice suceptible to reinfection (Wu et al. 2014). Repeated exposure to influenza viruses

complicates the investigation of the lifespan of human influenza-specific TRM. In addition, asymptomatic infections make it almost impossible to identify reliably the time of last infection. It is also important to note that turnover of memory T cells is different in mice and humans, as shown *in vivo* after deuterium labelling (Akondy et al. 2017), Our group has recently established a protocol for labelling cells *in vivo* using deuterium-rich sugar or water in pigs to analyse turnover of the different porcine T cell subsets, including TRM, and will confirm if these cells are not proliferating at the later time points, as I have shown by the lack of Ki67 expression after 7 dpi.

The study presented in Chapter 3 was limited to CD8 T cells but future work will need to establish if other memory populations (CD4 and B cells) decline with similar kinetics. Neither have I established, as have others in the mouse, whether TRM in mucosal sites contribute to the recirculating pool of memory cells (Fonseca et al. 2020). The data imply but do not prove, that the cells are generated in TBLN and migrate via the blood to mucosal sites in the RT, where a delayed peak response is observed. Murine studies have proved the protective role of TRM against IAV reinfection, however my study was limited to the investigation of the dynamic changes in phenotype and transcriptome of procine TRM. As a proof of concept, FTY720 was administered orally to pigs and leukopenia was found in blood 24 h post-administration and persisted for 4 days. FTY720 treatment of pigs previously exposed with IAV, could be used to prove the contribution of porcine TRM in protection against heterotypic challenge, in the absence of circulating T cells and matching Ab. Such studies will also need to investigate differences in the protection of porcine TRM at different times post IAV first exposure. High numbers of TRM and their activation state correlated with age and a better prognosis after SARS-CoV-2 infection in humans (Szabo et al. 2021). It will also be important to study the phenotype of the T cells in the lung after rechallenge to investigate whether phenotypic features of lung TRM predict the disease outcome in pigs.

Evaluation of protective immune responses in the lung is crucial as severe influenza is caused by viral infection in the LRT and highly pathogenic influenza viruses replicate best in the lung.

The identification of new NP epitopes showed different kinetics for AAV^+ CD8 T cells, peaking at 28 dpi in BAL compared to DFE^+ and VAY^+, which reached their highest percentages at 9 dpi. These findings apparently contrast with parabiosis experiments in mice. Murine studies showed that the successful recruitment of partner CD8 TRM in lung niches occurs when parabiosis is performed early after i.n. IAV infection of both parabiotic animals (6 dpi), suggesting that early migration of circulating IAV-specific CD8 T cells helps establish lung TRM (Takamura et al. 2016). At later time points, circulating CD8 T cells failed to generate TRM. However, it is important to note that this study is limited to CD8 T cells recognising the $NP_{366-375}$ epitope, therefore it does not exclude the possibility that T cells with different epitope-specificity are recruited to the lung with different kinetics. In addition, no difference in phenotype, T-bet and Eomes expression, or proliferative state could justify these dynamics. Future studies on transcriptome and TCR clonality might help further to dissect the differences between the tetramer populations across tissues. Studies in mice demonstrated a change in the immunodominant hierarchy between epitopes of the internal proteins during heterosubtypic challenge (Jenkins et al. 2006; Crowe et al. 2003; La Gruta, Turner, and Doherty 2004; La Gruta et al. 2006; Belz et al. 2000). It will be interesting to study if such differences can also be found between AAV, DFE and VAY epitopes after a second exposure toa different IAV strain. As my work was limited to epitope isolated from NP, future work will need to evaluate other CD8 T cell epitopes to different internal proteins.

6.2 Aerosol and intranasal delivery

Optimal delivery to the RT, essential for lung TRM, is influenced by the device used. Here I have compared the deposition achieved after i.n. instillation using the MAD device and after aer. delivery with two distinct VMNs. This study will inform a future pre-clinical evaluation of novel vaccines candidates, and it contributes to the increasing evidence that the pig is a useful model for human influenza virus research.

Despite generating the largest droplet size (86 μm), the MAD device delivered the highest dose of ^{99m}Tc-DTPA to the lung, used as a surrogate of IAV. This observation can be explained by the high volume administered (1 ml) and the sedation used to image the pigs. Interestingly, pigs challenged with 4 ml containing 10^7 PFU of H1N1pdm09 showed similar viral shedding and immune responses to naturally infected (in-contact) pigs (Edmans et al. 2020). This observation supports the use of the MAD device for IAV administration.

VMNs generated aer. of 3.5 and 4.5 μm diameter, ideal droplet size for lung deposition. Both devices uniformly targeted the lung but deposited a smaller proportion compared to MAD. However, they showed high reproducibility, an ideal characteristic for a vaccine delivery system. It is important to note that 50% of the dose was captured in the masks after aer. delivery (see Chapter 4). Therefore, adjusting the vaccine dose may be required, taking into account the amount not delivered. This implies higher costs, in addition to the price of VMNs, which are expensive devices. An alternative option, currently under development (Dr. Ronan MacLoughlin, personal communication), is to insert a sensor in the VMNs capable of stopping the delivery when the individual is exhaling, limiting the waste of product.

This approach can overcome differences in breathing patterns between individuals and ensure equal delivery of the dose to everyone.

VMNs can deliver 1ml of formulation in around 3 minutes and do not require the assistance of medical personnel. Nevertheless, these devices may need to administer vaccines to a wide range of categories, from infants to children to the elderly. Optimal masks and VMNs combinations will be developed for different age groups, considering that infants are obligatory nose breathers with high breathing frequencies. The study presented in this thesis was performed using piglets of 5 weeks of age, with variable breathing patterns. Nevertheless, VMNs delivered between 25 and 32% of ^{99m}Tc-DTPA to the lung, demonstrating high applicability. In a similar study in humans, six adults received ^{99m}Tc-DTPA by aer. using the same VMN described in this thesis and 33.3 ± 10.4% of the delivered ^{99m}Tc-DTPA dose reached the lung (Dugernier et al. 2017). These results further confirm the value of the pig model; however it will be also important to evaluate the deposition in adult pigs.

I have described the deposition of particles administered by MAD and VMNs devices, but follow-up head-to-head studies are required to assess the immune responses generated by these delivery systems. Early studies in pigs compared the responses generated after i.n. and aer. administration of H1N1pdm09 to those obtained after natural infection (in-contact) (Hemmink et al. 2016). H1N1pm09 delivered by aer. generated stronger systemic responses compared to i.n. administration. It is important to note that this study utilised jet-neb, notoriously less efficient than VMNs. A more recent study compared aer., using VMNs, and i.n. delivery of ChAdOx1 vaccine expressing NP, M1 and NA (Vatzia et al. 2021). Although this comparison was performed after exposure to H1N1pdm09 infection, it showed that aer. was superior to i.n. in boosting the immune responses locally and systemically.

Both i.n. and aer. immunistaion offer several advantages. I.n. delivery is cheap, fast and requires a small volume. On the other hand, aer. administration using VMNs is more expensive, slower and may require a bigger volume. However aer. delivered formulation can more easily reach the circulation, with systemic effects. Mucosal delivery of vaccines may also overcome preexisting immunity to the vaccine's vector (Belyakov et al. 1999). This is highly relevant for widely used viral vectors such as vaccinia virus and adenovirus where pre-existing immunity diminishes their immunogenicity (Saxena et al. 2013). In addition, the existence of a common mucosal immune system comprising gastrointestinal, reproductive, and respiratory mucosa allows the use of MAD and VMNs beyond their application for vaccines for respiratory pathogens., as leukocytes activated in one mucosal barrier disseminate to other mucosal sites. Nasal immunisation generated high level of IgA and IgG Ab in the female reproductive tract mucosa, and this route of administration has been investigated for sexually transmitted pathogens (Rudin et al. 1998). A chlamydia vaccine showed promising results in humans in a prime and pull regime, with i.m. injections followed by i.n. delivery of a subunit vaccines (Abraham et al. 2019). Evaluation of the immunogenicity of aer. delivery of such vaccines should also be performed. Mucosal administration may also be useful when developing vaccines against intracellular pathogens such as HIV, human papilloma virus (HPV), herpes viruses and *M. tuberculosis* which require the activation of multiple arms of the immune system.

6.3 Improving S-FLU immunogenicity

Chapter 5 presented two strategies to enhance Ab response after S-FLU vaccination and ultimately improve protection: CLEARFLU and simultaneous local and systemic administration of S-FLU.

CLEARFLU delivered i.n. and i.p. in mice provided non-sterile immunity to several IAV strains and improved strain-specific neutralising Ab titres for months after vaccination (Holly Sadler, thesis, 2021). However, CLEARFLU delivered by aer. in pigs did not differ from S-FLU, with similar T cell responses and undetectable neutralising Ab levels. Non-neutralising Ab were not evaluated in this study nevertheless, they play an important role in protection. Both human and murine HA-specific non-neutralising mAb protected mice from heterotypic infection by antibody-dependent cellular cytotoxicity and antibody-dependent cellular phagocytosis (Dunand et al. 2016; Ko et al. 2021). Therefore, future studies will need to evaluate the protective efficacy of CLEARFLU in pigs after homologous and heterologous challenge. S-FLU delivered by SIM and i.m, only was able to generate high level of neutralising Ab. Therefore, CLEARFLU should be tested in the future using these different routes. In addition, the presence of 2 different HAs on its surface might improve and broaden the Ab responses to CLEARFLU.

S-FLU delivered i.m. and SIM induced high neutralising Ab titres, however, only pigs immunised by SIM or aer. developed strong T cell responses, detectable both locally and systemically. Most likely differences in antigen presentation between the i.m. and aer. routes are responsible for the differences in the responses. Cellular responses were studied mainly using SLA monomers loaded with CD8 NP epitopes identified previously in S-FLU aer. immunised animals (Tungatt et al. 2018). It is possible that i.m. immunisation induces different specificities, not evaluated by tetramer staining. However, IAV-specific CD8 T cells from i.m. immunised pigs failed to reach the lung and secrete IFNγ, TNF or IL-2 4 dpc, further corroborating the hypothesis that local antigen recognition is essential for the formation of TRM after immunisation.

Similarly, to what was observed after H1N1pdm09 challenge in Chapter 1, the hierarchy of the response to the NP epitopes was different between tissues. Studies of NP-specific CD8 T cells in 8 tissues, highlighted differences in the mucosal tissues compared to LN and blood. TBLN mainly contained DFE^+ and IAV^+ T cells, while the biggest $tetramer^+$ population in blood recognised the NGK epitope. These results indicate the importance of investigating local responses in more detail in the future, in pigs as well as in humans. Human IAV epitopes are normally identified from T cells present in PBMC which may not reflect the abundance present in the lung. In addition, Szabo et al. demonstrated that blood sampling is not indicative of the responses at the site of SARS-CoV-2 infection (Szabo et al. 2021).

Despite increasing evidence on the role of T cells in heterotypic protection, a T cell correlate of protection has not be universally defined. Establishing such a correlate will be indispensable for the pre-clinical evaluation of novel T cell-based vaccine candidates, such as S-FLU. However, where should T cell responses be measured? Protection after LAIV immunisation, from clinical manifestation during a subsequent infection, was reported in infants and young adults when > 100 SFU in 10^6 cells were measured by IFNγ ELISpot in the blood (Forrest et al. 2008). However, mucosal vaccines might elicit local responses without stimulating corresponding detectable systemic T and B cells. My findings align with other human studies suggesting the importance of local immunity and local sampling to best evaluate vaccine efficacy. Nevertheless, sampling the lung is challenging and invasive in humans, therefore, pre-clinical studies in pigs might be essential to assess mucosal responses. Future work will need to define correlates of protection in the pig model. From the pre-clinical testing of S-FLU SIM, it appears that the protection mediated by SIM benefitted from both systemic Ab and local T cells, but a more detailed study of the CD4 T cells and Ab response, including the role of non-neutralising Ab, is required.

During the current COVID-19 pandemic, it has become clear that vaccines against respiratory diseases should reduce viral transmission to naïve individuals and limit lung pathology, responsible for hospitalisations. Recently, S-FLU by aer. was evaluated for its ability to block transmission after heterologous challenge in pigs (Everett et al. 2021). S-FLU immunised animals did not reduce viral shedding and in-contact animals started shedding the virus as early as 2 days post-contact with vaccinated individuals. Interestingly, i.m. immunisation with IIV homologous to the challenge virus reduced viral replication in the vaccinated animals but did not stop transmission to naïve individuals. It is important to note that in this study viral replication was evaluated by quantifying viral RNA by PCR and may not correspond to actual replicating viral particles. Future studies will need to address the heterosubtypic protective potential of S-FLU by SIM and its ability to block transmission.

In conclusion, I have defined the spatial, temporal and molecular dynamics of influenza virus specific CD8 TRM. The porcine RT is anatomically similar and I have demonstrated that the deposition in the lung after aer. delivery was comparable to that in humans. Broadly protective vaccines able to induce long-lasting cross-reactive T cells and Ab responses remain of great interest (Elbahesh et al. 2019). I have established that S-FLU delivered simultaneously i.m. and by aer. conferred the best protection with a high level of local T cell responses, showing promise as a broadly protective vaccine. These results, together with the comparable size of pigs and humans, indicate that the pig is a powerful model for understanding how best to apply vaccines and generate TRM.

6.4 Future perspectives

The tools I established in this thesis will determine the duration of mucosal immunity, the lifespan of TRM, and the role of TRM in protection using FTY720 or cell transfers. In addition, future work will need to explore the differences in the hierarchy of the CD8 responses to the newly identified H1N1pdm09 epitopes. In particular, antigen presentation, MHC affinity, TCR affinity, and clonality should be further investigated as possible critical regulators of the expanded AAV responses. Moreover, it remains unknown if the observed differences in the hierarchy of responses are common to other influenza proteins.

S-FLU by aer. failed to reduce viral shedding in the URT after homologous challenge. Chapter 4 of this thesis highlighted the loss of aerosolised vaccine in the device; therefore increasing the dose will be essential for future vaccination studies. As presented in Chapter 5, pigs received a variable S-FLU nominal dose (10^9 - 10^7 TCID50) depending on vaccine availability. A systematic dose-response analysis will be beneficial for the identification of the optimal dose for S-FLU administration.

Chapter 7 Appendix

Tables

Table 7.1 list of peptides present in each pool of H1N1pmd09 NP tested

P 1	MASQGTKRSYEQMETGGE
	KRSYEQMETGGERQDATE
	METGGERQDATEIRASVG
	RQDATEIRASVGRMIGGI
	IRASVGRMIGGIGRFYIQ
	RMIGGIGRFYIQMCTELK
	GRFYIQMCTELKLSDYDG
	MCTELKLSDYDGRLIQNS
	LSDYDGRLIQNSITIERM
	RLIQNSITIERMVLSAFD
P 2	ITIERMVLSAFDERRNKY
	VLSAFDERRNKYLEEHPS
	ERRNKYLEEHPSAGKDPK
	LEEHPSAGKDPKKTGGPI
	AGKDPKKTGGPIYRRIGG
	KTGGPIYRRIGGKWMREL
	YRRIGGKWMRELILYDKE
	KWMRELILYDKEEIRRVW
	ILYDKEEIRRVWRQANNG
	EIRRVWRQANNGEDATAG
P 3	RQANNGEDATAGLTHIMI
	EDATAGLTHIMIWHSNLN
	LTHIMIWHSNLNDATYQR
	WHSNLNDATYQRTRALVR
	DATYQRTRALVRTGMDPR
	TRALVRTGMDPRMCSLMQ
	TGMDPRMCSLMQGSTLPR

	MCSLMQGSTLPRRSGAAG
	GSTLPRRSGAAGAAVKGV
	RSGAAGAAVKGVGTIAME
P 4	AAVKGVGTIAMELIRMIK
	GTIAMELIRMIKRGINDR
	LIRMIKRGINDRNFWRGE
	RGINDRNFWRGENGRRTR
	NFWRGENGRRTRVAYERM
	NGRRTRVAYERMCNILKG
	VAYERMCNILKGKFQTAA
	CNILKGKFQTAAQRAMMD
	KFQTAAQRAMMDQVRESR
	QRAMMDQVRESRNPGNAE
P 5	QVRESRNPGNAEIEDLIF
	NPGNAEIEDLIFLARSAL
	IEDLIFLARSALILRGSV
	LARSALILRGSVAHKSCL
	ILRGSVAHKSCLPACVYG
	AHKSCLPACVYGLAVASG
	PACVYGLAVASGHDFERE
	LAVASGHDFEREGYSLVG
	HDFEREGYSLVGVDPFKL
	GYSLVGVDPFKLLQNSQV
P 6	VDPFKLLQNSQVVSLMRP
	LQNSQVVSLMRPNENPAH
	VSLMRPNENPAHKSQLVW
	NENPAHKSQLVWMACHSA
	KSQLVWMACHSAAFEDLR
	MACHSAAFEDLRVSSFIR
	AFEDLRVSSFIRGKKVIP
	VSSFIRGKKVIPRGKLST
	GKKVIPRGKLSTRGVQIA
	RGKLSTRGVQIASNENVE
	RGVQIASNENVETMDSNT

P7	SNENVETMDSNTLELRSR
	TMDSNTLELRSRYWAIRT
	LELRSRYWAIRTRSGGNT
	YWAIRTRSGGNTNQQKAS
	RSGGNTNQQKASAGQISV
	NQQKASAGQISVQPTFSV
	AGQISVQPTFSVQRNLPF
	QPTFSVQRNLPFERATVM
	QRNLPFERATVMAAFSGN
P 8	ERATVMAAFSGNNEGRTS
	AAFSGNNEGRTSDMRTEV
	NEGRTSDMRTEVIRMMES
	DMRTEVIRMMESAKPEDL
	IRMMESAKPEDLSFQGRG
	AKPEDLSFQGRGVFELSD
	SFQGRGVFELSDEKATNP
	VFELSDEKATNPIVPSFD
	EKATNPIVPSFDMSNEGS
	IVPSFDMSNEGSYFFGDN
	MSNEGSYFFGDNAEEYDS

Table 7.2 Average percentage of tetramer^{+} CD8 T cells in naïve animals (n=3).

tissue	**tetramer (% of CD8)**		
	AAV	**DFE**	**VAY**
PBMC	0.03	0.03	0.10
TBLN	0.01	0.05	0.13
BAL	0.07	0.03	0.51
lung	0.01	0.12	0.11

spleen	0.05	0.08	0.06
NT	0.09	0.03	0.10
Trachea	0.03	0.10	0.13

Figures

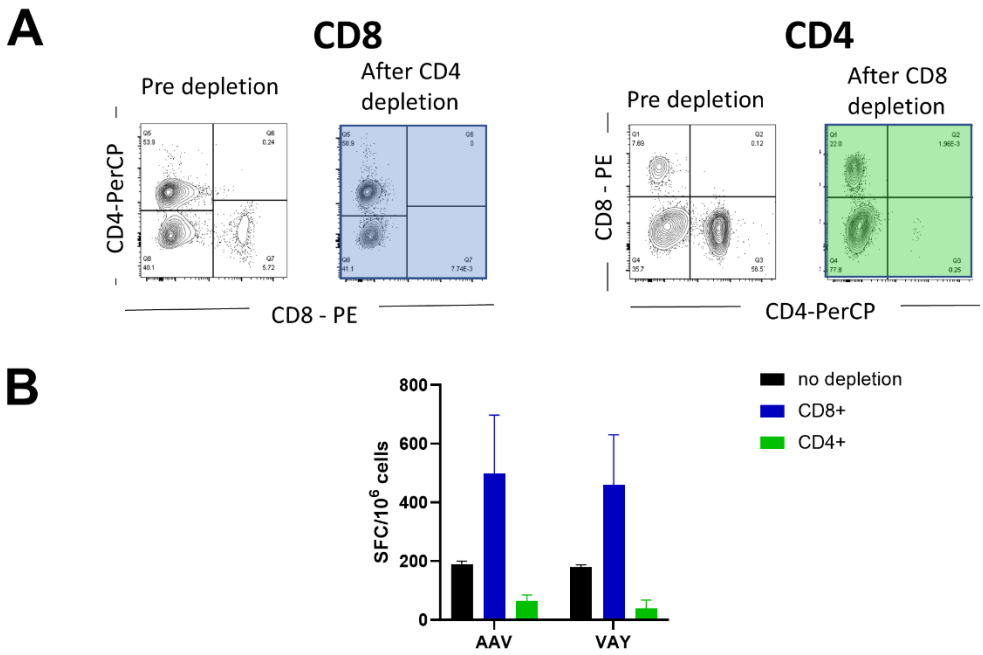

Figure 7.1 **Validation of AAV and VAY as CD8 epitopes**. (A) Cells isolated from TBLN were depleted, using a MS column, from CD4 (left) and CD8 (right) T cells. Representative FACS plot showing the absence of CD4 and CD8 populations. (B) Depleted and undepleted fraction were then inclubated with AAV and VAY peptides and responses assayed by IFNγ ELISpot

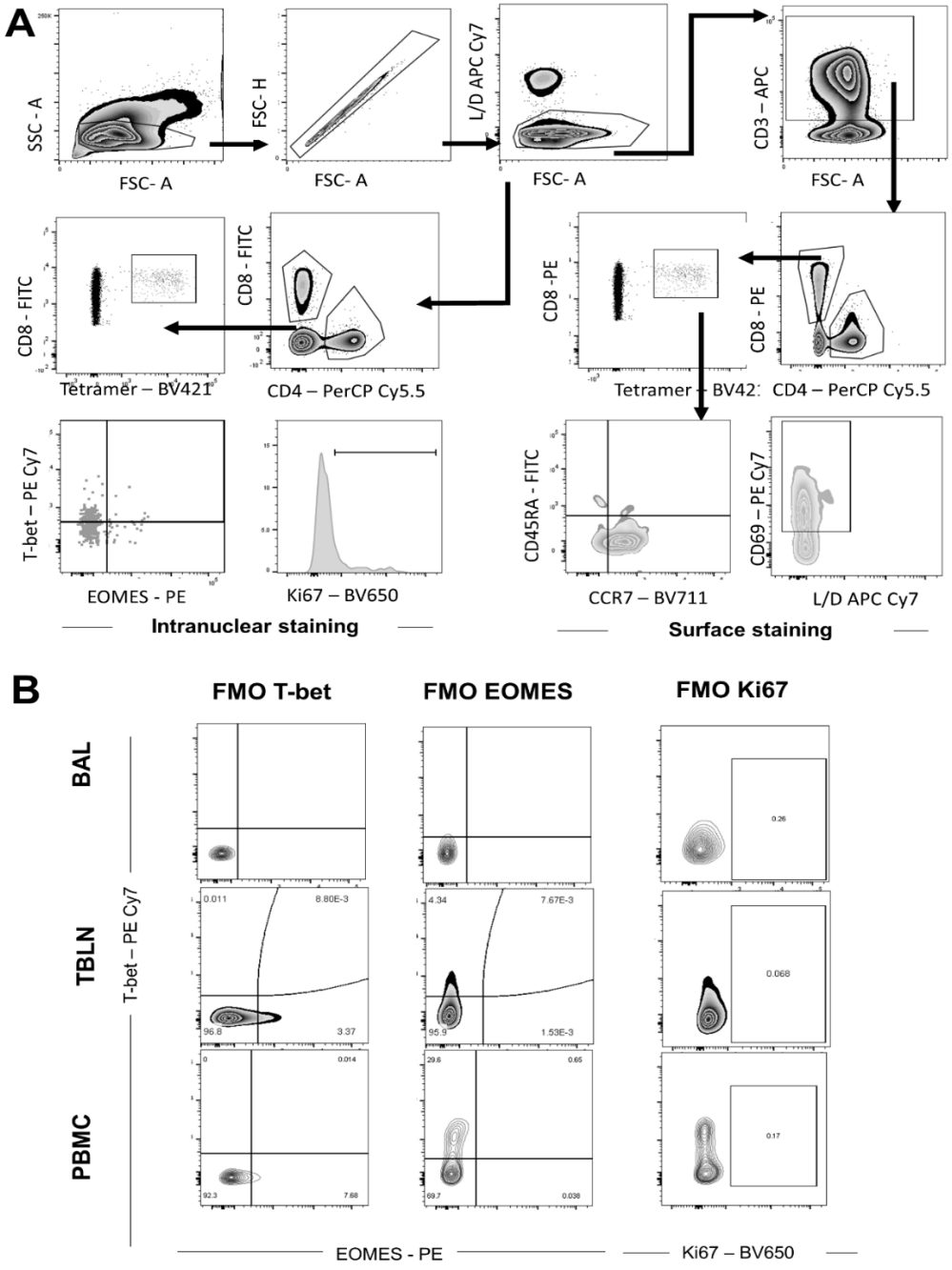

Figure 7.2 **Gating strategy for Chapter 1 and controls. (A)** Representative FACS plots (from PBMC) showing the gating strategy for intranuclear staining (panels on the left) and surface marker staining (on the right.) **(B)** Fluorescence minus one (FMO) controls for transcriptional factors in the different tissues

References

Abraham, S., H. B. Juel, P. Bang, H. M. Cheeseman, R. B. Dohn, T. Cole, M. P. Kristiansen, K. S. Korsholm, D. Lewis, A. W. Olsen, L. R. McFarlane, S. Day, S. Knudsen, K. Moen, M. Ruhwald, I. Kromann, P. Andersen, R. J. Shattock, and F. Follmann. 2019. 'Safety and immunogenicity of the chlamydia vaccine candidate CTH522 adjuvanted with CAF01 liposomes or aluminium hydroxide: a first-in-human, randomised, double-blind, placebo-controlled, phase 1 trial', *Lancet Infect Dis*, 19: 1091-100.

Akondy, R. S., M. Fitch, S. Edupuganti, S. Yang, H. T. Kissick, K. W. Li, B. A. Youngblood, H. A. Abdelsamed, D. J. McGuire, K. W. Cohen, G. Alexe, S. Nagar, M. M. McCausland, S. Gupta, P. Tata, W. N. Haining, M. J. McElrath, D. Zhang, B. Hu, W. J. Greenleaf, J. J. Goronzy, M. J. Mulligan, M. Hellerstein, and R. Ahmed. 2017. 'Origin and differentiation of human memory CD8 T cells after vaccination', *Nature*, 552: 362-67.

Allie, S. R., J. E. Bradley, U. Mudunuru, M. D. Schultz, B. A. Graf, F. E. Lund, and T. D. Randall. 2019. 'The establishment of resident memory B cells in the lung requires local antigen encounter', *Nat Immunol*, 20: 97-108.

Ambrose, C. S., and K. L. Coelingh. 2012. 'Small-particle aerosolization of live attenuated influenza vaccine virus', *J Infect Dis*, 205: 348; author reply 48-9.

Anderson, K. G., K. Mayer-Barber, H. Sung, L. Beura, B. R. James, J. J. Taylor, L. Qunaj, T. S. Griffith, V. Vezys, D. L. Barber, and D. Masopust. 2014. 'Intravascular staining for discrimination of vascular and tissue leukocytes', *Nat Protoc*, 9: 209-22.

Anderson, T. K., J. Chang, Z. W. Arendsee, D. Venkatesh, C. K. Souza, J. B. Kimble, N. S. Lewis, C. T. Davis, and A. L. Vincent. 2021. 'Swine Influenza A Viruses and the Tangled Relationship with Humans', *Cold Spring Harb Perspect Med*, 11.

Arı, A. 2014. 'Jet, Ultrasonic, and Mesh Nebulizers: An Evaluation of Nebulizers for Better Clinical Outcomes', *Eurasian J Pulmonol*, 16: 1-7.

Ariotti, S., M. A. Hogenbirk, F. E. Dijkgraaf, L. L. Visser, M. E. Hoekstra, J. Y. Song, H. Jacobs, J. B. Haanen, and T. N. Schumacher. 2014. 'T cell memory. Skin-resident memory CD8(+) T cells trigger a state of tissue-wide pathogen alert', *Science*, 346: 101-5.

Asahi-Ozaki, Y., T. Yoshikawa, Y. Iwakura, Y. Suzuki, S. Tamura, T. Kurata, and T. Sata. 2004. 'Secretory IgA antibodies provide cross-protection against infection with different strains of influenza B virus', *J Med Virol*, 74: 328-35.

Assarsson, E., H. H. Bui, J. Sidney, Q. Zhang, J. Glenn, C. Oseroff, I. N. Mbawuike, J. Alexander, M. J. Newman, H. Grey, and A. Sette. 2008. 'Immunomic analysis of the repertoire of T-cell specificities for influenza A virus in humans', *J Virol*, 82: 12241-51.

Bahamondez-Canas, T. F., and Z. Cui. 2018. 'Intranasal immunization with dry powder vaccines', *Eur J Pharm Biopharm*, 122: 167-75.

Baratelli, M., L. E. Pedersen, R. Trebbien, L. E. Larsen, G. Jungersen, E. Blanco, J. Nielsen, and M. Montoya. 2017a. 'Identification of cross-reacting T-cell epitopes in structural and non-structural proteins of swine and pandemic H1N1 influenza A virus strains in pigs', *J Gen Virol*, 98: 895-99.

Baratelli, Massimiliano, Lasse Eggers Pedersen, Ramona Trebbien, Lars Erik Larsen, Gregers Jungersen, Esther Blanco, Jens Nielsen, and Maria Montoya. 2017b. 'Identification of cross-reacting T-cell epitopes in structural and non-structural proteins of swine and pandemic H1N1 influenza A virus strains in pigs', *The Journal of General Virology*, 98: 895-99.

Barr, I. G., R. O. Donis, J. M. Katz, J. W. McCauley, T. Odagiri, H. Trusheim, T. F. Tsai, and D. E. Wentworth. 2018. 'Cell culture-derived influenza vaccines in the severe 2017-2018 epidemic season: a step towards improved influenza vaccine effectiveness', *NPJ Vaccines*, 3: 44.

Basak, S., M. Tomana, and R. W. Compans. 1985. 'Sialic acid is incorporated into influenza hemagglutinin glycoproteins in the absence of viral neuraminidase', *Virus Res*, 2: 61-8.

Baudon, E., M. Peyre, M. Peiris, and B. J. Cowling. 2017. 'Epidemiological features of influenza circulation in swine populations: A systematic review and meta-analysis', *PLoS One*, 12: e0179044.

Baz, M., K. Boonnak, M. Paskel, C. Santos, T. Powell, A. Townsend, and K. Subbarao. 2015. 'Nonreplicating Influenza A Virus Vaccines Confer Broad Protection against Lethal Challenge', *MBio*, 6: e01487-15.

Belshe, R. B., K. M. Edwards, T. Vesikari, S. V. Black, R. E. Walker, M. Hultquist, G. Kemble, E. M. Connor, and Caiv- T. Comparative Efficacy Study Group. 2007. 'Live attenuated versus inactivated influenza vaccine in infants and young children', *N Engl J Med*, 356: 685-96.

Belyakov, I. M., B. Moss, W. Strober, and J. A. Berzofsky. 1999. 'Mucosal vaccination overcomes the barrier to recombinant vaccinia immunization caused by preexisting poxvirus immunity', *Proc Natl Acad Sci U S A*, 96: 4512-7.

Belz, G. T., W. Xie, J. D. Altman, and P. C. Doherty. 2000. 'A previously unrecognized H-2D(b)-restricted peptide prominent in the primary influenza A virus-specific CD8(+) T-cell response is much less apparent following secondary challenge', *J Virol*, 74: 3486-93.

Bender, B. S., T. Croghan, L. Zhang, and P. A. Small, Jr. 1992. 'Transgenic mice lacking class I major histocompatibility complex-restricted T cells have delayed viral clearance and increased mortality after influenza virus challenge', *J Exp Med*, 175: 1143-5.

Bennett, G., M. Joyce, E. F. Fernandez, and R. MacLoughlin. 2019. 'Comparison of aerosol delivery across combinations of drug delivery interfaces with and without concurrent high-flow nasal therapy', *Intensive Care Med Exp*, 7: 20.

Berset Convenor, Fwgofacm, M. E. Caristo, F. Ferrara, P. Hardy, M. Oropeza-Moe, and R. Waters. 2021. 'Federation of European Laboratory Animal Science Associations recommendations of best practices for the health management of ruminants and pigs used for scientific and educational purposes', *Lab Anim*, 55: 117-28.

Bertram, E. M., P. Lau, and T. H. Watts. 2002. 'Temporal segregation of 4-1BB versus CD28-mediated costimulation: 4-1BB ligand influences T cell numbers late in the primary response and regulates the size of the T cell memory response following influenza infection', *J Immunol*, 168: 3777-85.

Beverley, P. C., S. Sridhar, A. Lalvani, and E. Z. Tchilian. 2014. 'Harnessing local and systemic immunity for vaccines against tuberculosis', *Mucosal Immunol*, 7: 20-6.

Biddison, W. E., S. Shaw, and D. L. Nelson. 1979. 'Virus specificity of human influenza virus-immune cytotoxic T cells', *J Immunol*, 122: 660-4.

Bikour, M. H., E. Cornaglia, and Y. Elazhary. 1996. 'Evaluation of a protective immunity induced by an inactivated influenza H3N2 vaccine after an intratracheal challenge of pigs', *Can J Vet Res*, 60: 312-4.

Blank, F., M. Wehrli, A. Lehmann, O. Baum, P. Gehr, C. von Garnier, and B. M. Rothen-Rutishauser. 2011. 'Macrophages and dendritic cells express tight junction proteins and exchange particles in an in vitro model of the human airway wall', *Immunobiology*, 216: 86-95.

Bolton, D. L., K. Song, G. D. Tomaras, S. Rao, and M. Roederer. 2017. 'Unique cellular and humoral immunogenicity profiles generated by aerosol, intranasal, or parenteral vaccination in rhesus macaques', *Vaccine*, 35: 639-46.

Braciale, T. J. 1977a. 'Immunologic recognition of influenza virus-infected cells. I. Generation of a virus-strain specific and a cross-reactive subpopulation of cytotoxic T cells in the response to type A influenza viruses of different subtypes', *Cell Immunol*, 33: 423-36.

———. 1977b. 'Immunologic recognition of influenza virus-infected cells. II. Expression of influenza A matrix protein on the infected cell surface and its role in recognition by cross-reactive cytotoxic T cells', *J Exp Med*, 146: 673-89.

Brandenburg, B., W. Koudstaal, J. Goudsmit, V. Klaren, C. Tang, M. V. Bujny, H. J. Korse, T. Kwaks, J. J. Otterstrom, J. Juraszek, A. M. van Oijen, R. Vogels, and R. H. Friesen. 2013. 'Mechanisms of hemagglutinin targeted influenza virus neutralization', *PLoS One*, 8: e80034.

Brinkmann, V., M. D. Davis, C. E. Heise, R. Albert, S. Cottens, R. Hof, C. Bruns, E. Prieschl, T. Baumruker, P. Hiestand, C. A. Foster, M. Zollinger, and K. R. Lynch. 2002. 'The immune modulator FTY720 targets sphingosine 1-phosphate receptors', *J Biol Chem*, 277: 21453-7.

Britton, G., D. C. MacDonald, J. S. Brown, M. K. Collins, and A. L. Goodman. 2015. 'Using a prime and pull approach, lentivector vaccines expressing Ag85A induce immunogenicity but fail to induce protection against Mycobacterium bovis bacillus Calmette-Guerin challenge in mice', *Immunology*, 146: 264-70.

Brown, D. M., S. Lee, L. Garcia-Hernandez Mde, and S. L. Swain. 2012. 'Multifunctional CD4 cells expressing gamma interferon and perforin mediate protection against lethal influenza virus infection', *J Virol*, 86: 6792-803.

Casey, K. A., K. A. Fraser, J. M. Schenkel, A. Moran, M. C. Abt, L. K. Beura, P. J. Lucas, D. Artis, E. J. Wherry, K. Hogquist, V. Vezys, and D. Masopust. 2012. 'Antigen-independent differentiation and maintenance of effector-like resident memory T cells in tissues', *J Immunol*, 188: 4866-75.

Cheng, Y. S. 2014. 'Mechanisms of pharmaceutical aerosol deposition in the respiratory tract', *AAPS PharmSciTech*, 15: 630-40.

Cheuk, S., H. Schlums, I. Gallais Serezal, E. Martini, S. C. Chiang, N. Marquardt, A. Gibbs, E. Detlofsson, A. Introini, M. Forkel, C. Hoog, A. Tjernlund, J. Michaelsson, L. Folkersen, J. Mjosberg, L. Blomqvist, M. Ehrstrom, M. Stahle, Y. T. Bryceson, and L. Eidsmo. 2017. 'CD49a Expression Defines Tissue-Resident CD8(+) T Cells Poised for Cytotoxic Function in Human Skin', *Immunity*, 46: 287-300.

Clements, M. L., R. F. Betts, E. L. Tierney, and B. R. Murphy. 1986. 'Serum and nasal wash antibodies associated with resistance to experimental challenge with influenza A wild-type virus', *J Clin Microbiol*, 24: 157-60.

Couch, R. B., R. L. Atmar, W. A. Keitel, J. M. Quarles, J. Wells, N. Arden, and D. Nino. 2012. 'Randomized comparative study of the serum antihemagglutinin and antineuraminidase antibody responses to six licensed trivalent influenza vaccines', *Vaccine*, 31: 190-5.

Cowling, B. J., S. Ng, E. S. Ma, C. K. Cheng, W. Wai, V. J. Fang, K. H. Chan, D. K. Ip, S. S. Chiu, J. S. Peiris, and G. M. Leung. 2010. 'Protective efficacy of seasonal influenza vaccination against seasonal and pandemic influenza virus infection during 2009 in Hong Kong', *Clin Infect Dis*, 51: 1370-9.

Cox, R. J. 2013. 'Correlates of protection to influenza virus, where do we go from here?', *Hum Vaccin Immunother*, 9: 405-8.

Crotty, S. 2014. 'T follicular helper cell differentiation, function, and roles in disease', *Immunity*, 41: 529-42.

Crowe, C. R., K. Chen, D. A. Pociask, J. F. Alcorn, C. Krivich, R. I. Enelow, T. M. Ross, J. L. Witztum, and J. K. Kolls. 2009. 'Critical role of IL-17RA in immunopathology of influenza infection', *J Immunol*, 183: 5301-10.

Crowe, S. R., S. J. Turner, S. C. Miller, A. D. Roberts, R. A. Rappolo, P. C. Doherty, K. H. Ely, and D. L. Woodland. 2003. 'Differential antigen presentation regulates the changing patterns of CD8+ T cell immunodominance in primary and secondary influenza virus infections', *J Exp Med*, 198: 399-410.

Darrah, P. A., J. J. Zeppa, P. Maiello, J. A. Hackney, M. H. Wadsworth, 2nd, T. K. Hughes, S. Pokkali, P. A. Swanson, 2nd, N. L. Grant, M. A. Rodgers, M. Kamath, C. M. Causgrove, D. J. Laddy, A. Bonavia, D. Casimiro, P. L. Lin, E. Klein, A. G. White, C. A. Scanga, A. K. Shalek, M. Roederer, J. L. Flynn, and R. A. Seder. 2020. 'Prevention of tuberculosis in macaques after intravenous BCG immunization', *Nature*, 577: 95-102.

Davis, S. S. 2001. 'Nasal vaccines', *Adv Drug Deliv Rev*, 51: 21-42.

de Swart, R. L., R. D. de Vries, L. J. Rennick, G. van Amerongen, S. McQuaid, R. J. Verburgh, S. Yuksel, A. de Jong, K. Lemon, D. T. Nguyen, M. Ludlow, Adme Osterhaus, and W. P. Duprex. 2017. 'Needle-free delivery of measles virus vaccine to the lower respiratory tract of non-human primates elicits optimal immunity and protection', *NPJ Vaccines*, 2: 22.

De Vleeschauwer, A., and K. Van Reeth. 2010. 'Prior infection of pigs with swine influenza viruses is a barrier to infection with avian influenza viruses', *Vet Microbiol*, 146: 340-5.

Dean, G. S., D. Clifford, A. O. Whelan, E. Z. Tchilian, P. C. Beverley, F. J. Salguero, Z. Xing, H. M. Vordermeier, and B. Villarreal-Ramos. 2015. 'Protection Induced by Simultaneous Subcutaneous and Endobronchial Vaccination with BCG/BCG and BCG/Adenovirus Expressing Antigen 85A against Mycobacterium bovis in Cattle', *PLoS One*, 10: e0142270.

Demi Brownlie, Inga Rødahl, Renata Varnaite, Hilmir Asgeirsson, Hedvig Glans, Sara Falck-Jones, Sindhu Vangeti, Marcus Buggert, Hans-Gustaf Ljunggren, Jakob Michaëlsson, Sara Gredmark-Russ, Anna Smed-Sörensen, Nicole Marquardt 2021. 'Distinct lung-homing receptor expression and activation profiles on NK cell and T cell subsets in COVID-19 and influenza', *Preprint at Biorxiv*.

Devito, C., J. Hinkula, R. Kaul, L. Lopalco, J. J. Bwayo, F. Plummer, M. Clerici, and K. Broliden. 2000. 'Mucosal and plasma IgA from HIV-exposed seronegative individuals neutralize a primary HIV-1 isolate', *AIDS*, 14: 1917-20.

Dobin, A., C. A. Davis, F. Schlesinger, J. Drenkow, C. Zaleski, S. Jha, P. Batut, M. Chaisson, and T. R. Gingeras. 2013. 'STAR: ultrafast universal RNA-seq aligner', *Bioinformatics*, 29: 15-21.

Dugernier, J., M. Hesse, R. Vanbever, V. Depoortere, J. Roeseler, J. B. Michotte, P. F. Laterre, F. Jamar, and G. Reychler. 2017. 'SPECT-CT Comparison of Lung Deposition using a System combining

a Vibrating-mesh Nebulizer with a Valved Holding Chamber and a Conventional Jet Nebulizer: a Randomized Cross-over Study', *Pharm Res*, 34: 290-300.

Dunand, H. C. J., P. E. Leon, M. Huang, A. Choi, V. Chromikova, I. Y. Ho, G. S. Tan, J. Cruz, A. Hirsh, N. Y. Zheng, C. E. Mullarkey, F. A. Ennis, M. Terajima, J. J. Treanor, D. J. Topham, K. Subbarao, P. Palese, F. Krammer, and P. C. Wilson. 2016. 'Both Neutralizing and Non-Neutralizing Human H7N9 Influenza Vaccine-Induced Monoclonal Antibodies Confer Protection', *Cell Host Microbe*, 19: 800-13.

Edmans, M., A. McNee, E. Porter, E. Vatzia, B. Paudyal, V. Martini, S. Gubbins, O. Francis, R. Harley, A. Thomas, R. Burt, S. Morgan, A. Fuller, A. Sewell, B. Charleston, M. Bailey, and E. Tchilian. 2020. 'Magnitude and Kinetics of T Cell and Antibody Responses During H1N1pdm09 Infection in Inbred Babraham Pigs and Outbred Pigs', *Front Immunol*, 11: 604913.

Ekeruche-Makinde, J., J. J. Miles, H. A. van den Berg, A. Skowera, D. K. Cole, G. Dolton, A. J. Schauenburg, M. P. Tan, J. M. Pentier, S. Llewellyn-Lacey, K. M. Miles, A. M. Bulek, M. Clement, T. Williams, A. Trimby, M. Bailey, P. Rizkallah, J. Rossjohn, M. Peakman, D. A. Price, S. R. Burrows, A. K. Sewell, and L. Wooldridge. 2013. 'Peptide length determines the outcome of TCR/peptide-MHCI engagement', *Blood*, 121: 1112-23.

Ekiert, D. C., A. K. Kashyap, J. Steel, A. Rubrum, G. Bhabha, R. Khayat, J. H. Lee, M. A. Dillon, R. E. O'Neil, A. M. Faynboym, M. Horowitz, L. Horowitz, A. B. Ward, P. Palese, R. Webby, R. A. Lerner, R. R. Bhatt, and I. A. Wilson. 2012. 'Cross-neutralization of influenza A viruses mediated by a single antibody loop', *Nature*, 489: 526-32.

Elbahesh, H., G. Saletti, T. Gerlach, and G. F. Rimmelzwaan. 2019. 'Broadly protective influenza vaccines: design and production platforms', *Curr Opin Virol*, 34: 1-9.

ElHansy, M. H. E., M. E. Boules, A. F. M. El Essawy, M. B. Al-Kholy, M. M. Abdelrahman, A. S. A. Said, R. R. S. Hussein, and M. E. Abdelrahim. 2017. 'Inhaled salbutamol dose delivered by jet nebulizer, vibrating mesh nebulizer and metered dose inhaler with spacer during invasive mechanical ventilation', *Pulm Pharmacol Ther*, 45: 159-63.

Ely, K. H., T. Cookenham, A. D. Roberts, and D. L. Woodland. 2006. 'Memory T cell populations in the lung airways are maintained by continual recruitment', *J Immunol*, 176: 537-43.

Epstein, S. L. 2006. 'Prior H1N1 influenza infection and susceptibility of Cleveland Family Study participants during the H2N2 pandemic of 1957: an experiment of nature', *J Infect Dis*, 193: 49-53.

Epstein, S. L., C. Y. Lo, J. A. Misplon, and J. R. Bennink. 1998. 'Mechanism of protective immunity against influenza virus infection in mice without antibodies', *J Immunol*, 160: 322-7.

European Medical Agency. 2013. 'Fluenz Tetra '. https://www.ema.europa.eu/en/documents/assessment-report/fluenz-tetra-epar-public-assessment-report_en.pdf.

Everett, H. E., P. M. van Diemen, M. Aramouni, A. Ramsay, V. J. Coward, V. Pavot, L. Canini, B. Holzer, S. Morgan, Consortium Dynamics sLoLa, M. E. J. Woolhouse, E. Tchilian, S. M. Brookes, I. H. Brown, B. Charleston, and S. Gilbert. 2021. 'Vaccines That Reduce Viral Shedding Do Not Prevent Transmission of H1N1 Pandemic 2009 Swine Influenza A Virus Infection to Unvaccinated Pigs', *J Virol*, 95.

Eyles, J. E., I. D. Spiers, E. D. Williamson, and H. O. Alpar. 1998. 'Analysis of local and systemic immunological responses after intra-tracheal, intra-nasal and intra-muscular administration of microsphere co-encapsulated Yersinia pestis sub-unit vaccines', *Vaccine*, 16: 2000-9.

Fan, S., Y. Wu, S. Wang, Z. Wang, B. Jiang, Y. Liu, R. Liang, W. Zhou, N. Zhang, and C. Xia. 2016. 'Structural and Biochemical Analyses of Swine Major Histocompatibility Complex Class I Complexes and Prediction of the Epitope Map of Important Influenza A Virus Strains', *J Virol*, 90: 6625-41.

Farber, D. L., N. A. Yudanin, and N. P. Restifo. 2014. 'Human memory T cells: generation, compartmentalization and homeostasis', *Nat Rev Immunol*, 14: 24-35.

Flynn, K. J., G. T. Belz, J. D. Altman, R. Ahmed, D. L. Woodland, and P. C. Doherty. 1998. 'Virus-specific CD8+ T cells in primary and secondary influenza pneumonia', *Immunity*, 8: 683-91.

Fonseca, R., L. K. Beura, C. F. Quarnstrom, H. E. Ghoneim, Y. Fan, C. C. Zebley, M. C. Scott, N. J. Fares-Frederickson, S. Wijeyesinghe, E. A. Thompson, H. Borges da Silva, V. Vezys, B. Youngblood, and D. Masopust. 2020. 'Developmental plasticity allows outside-in immune responses by resident memory T cells', *Nat Immunol*, 21: 412-21.

Food and Agriculture Organization of the United Nations (FAO). 2012. 'H5N1 HPAI Global overview, January-March 2012', Accessed 8th August http://www.fao.org/3/an388e/an388e.pdf.

Food and Drug Administration. 2020. 'Flumist Quadrivalent'. https://www.fda.gov/vaccines-blood-biologics/vaccines/flumist-quadrivalent.

Forberg, H., A. G. Hauge, M. Valheim, F. Garcon, A. Nunez, W. Gerner, K. H. Mair, S. P. Graham, S. M. Brookes, and A. K. Storset. 2014. 'Early responses of natural killer cells in pigs experimentally infected with 2009 pandemic H1N1 influenza A virus', *PLoS One*, 9: e100619.

Forrest, B. D., M. W. Pride, A. J. Dunning, M. R. Capeding, T. Chotpitayasunondh, J. S. Tam, R. Rappaport, J. H. Eldridge, and W. C. Gruber. 2008. 'Correlation of cellular immune responses with protection against culture-confirmed influenza virus in young children', *Clin Vaccine Immunol*, 15: 1042-53.

Forum of International Respiratory Society. 2017. 'The Global Impact of Respiratory Disease'. https://www.who.int/gard/publications/The_Global_Impact_of_Respiratory_Disease.pdf.

Franzoni, G., N. V. Kurkure, D. S. Edgar, H. E. Everett, W. Gerner, K. B. Bodman-Smith, H. R. Crooke, and S. P. Graham. 2013. 'Assessment of the phenotype and functionality of porcine CD8 T cell responses following vaccination with live attenuated classical swine fever virus (CSFV) and virulent CSFV challenge', *Clin Vaccine Immunol*, 20: 1604-16.

Gao, R., B. Cao, Y. Hu, Z. Feng, D. Wang, W. Hu, J. Chen, Z. Jie, H. Qiu, K. Xu, X. Xu, H. Lu, W. Zhu, Z. Gao, N. Xiang, Y. Shen, Z. He, Y. Gu, Z. Zhang, Y. Yang, X. Zhao, L. Zhou, X. Li, S. Zou, Y. Zhang, X. Li, L. Yang, J. Guo, J. Dong, Q. Li, L. Dong, Y. Zhu, T. Bai, S. Wang, P. Hao, W. Yang, Y. Zhang, J. Han, H. Yu, D. Li, G. F. Gao, G. Wu, Y. Wang, Z. Yuan, and Y. Shu. 2013. 'Human infection with a novel avian-origin influenza A (H7N9) virus', *N Engl J Med*, 368: 1888-97.

Gauger, P. C., A. L. Vincent, C. L. Loving, J. N. Henningson, K. M. Lager, B. H. Janke, M. E. Kehrli, Jr., and J. A. Roth. 2012. 'Kinetics of lung lesion development and pro-inflammatory cytokine response in pigs with vaccine-associated enhanced respiratory disease induced by challenge with pandemic (2009) A/H1N1 influenza virus', *Vet Pathol*, 49: 900-12.

Gauger, P. C., A. L. Vincent, C. L. Loving, K. M. Lager, B. H. Janke, M. E. Kehrli, Jr., and J. A. Roth. 2011. 'Enhanced pneumonia and disease in pigs vaccinated with an inactivated human-like (delta-cluster) H1N2 vaccine and challenged with pandemic 2009 H1N1 influenza virus', *Vaccine*, 29: 2712-9.

Gebhardt, T., L. M. Wakim, L. Eidsmo, P. C. Reading, W. R. Heath, and F. R. Carbone. 2009. 'Memory T cells in nonlymphoid tissue that provide enhanced local immunity during infection with herpes simplex virus', *Nat Immunol*, 10: 524-30.

Gehr, P., M. Bachofen, and E. R. Weibel. 1978. 'The normal human lung: ultrastructure and morphometric estimation of diffusion capacity', *Respir Physiol*, 32: 121-40.

Genzow, M., C. Goodell, T. J. Kaiser, W. Johnson, and M. Eichmeyer. 2018. 'Live attenuated influenza virus vaccine reduces virus shedding of newborn piglets in the presence of maternal antibody', *Influenza Other Respir Viruses*, 12: 353-59.

Gerlach, C., J. W. van Heijst, E. Swart, D. Sie, N. Armstrong, R. M. Kerkhoven, D. Zehn, M. J. Bevan, K. Schepers, and T. N. Schumacher. 2010. 'One naive T cell, multiple fates in CD8+ T cell differentiation', *J Exp Med*, 207: 1235-46.

Glennie, N. D., V. A. Yeramilli, D. P. Beiting, S. W. Volk, C. T. Weaver, and P. Scott. 2015. 'Skin-resident memory CD4+ T cells enhance protection against Leishmania major infection', *J Exp Med*, 212: 1405-14.

Graham, M. B., and T. J. Braciale. 1997. 'Resistance to and recovery from lethal influenza virus infection in B lymphocyte-deficient mice', *J Exp Med*, 186: 2063-8.

Grohskopf, L. A., E. Alyanak, K. R. Broder, L. H. Blanton, A. M. Fry, D. B. Jernigan, and R. L. Atmar. 2020. 'Prevention and Control of Seasonal Influenza with Vaccines: Recommendations of the Advisory Committee on Immunization Practices - United States, 2020-21 Influenza Season', *MMWR Recomm Rep*, 69: 1-24.

Gutierrez, A. H., C. Loving, L. Moise, F. E. Terry, S. L. Brockmeier, H. R. Hughes, W. D. Martin, and A. S. De Groot. 2016. 'In Vivo Validation of Predicted and Conserved T Cell Epitopes in a Swine Influenza Model', *PLoS One*, 11: e0159237.

Gutiérrez, Andres H., Crystal Loving, Leonard Moise, Frances E. Terry, Susan L. Brockmeier, Holly R. Hughes, William D. Martin, and Anne S. De Groot. 2016. 'In Vivo Validation of Predicted and Conserved T Cell Epitopes in a Swine Influenza Model', *PLOS ONE*, 11: e0159237-e37.

Gutierrez, K., N. Dicks, W. G. Glanzner, L. B. Agellon, and V. Bordignon. 2015. 'Efficacy of the porcine species in biomedical research', *Front Genet*, 6: 293.

Guvenel, A., A. Jozwik, S. Ascough, S. K. Ung, S. Paterson, M. Kalyan, Z. Gardener, E. Bergstrom, S. Kar, M. S. Habibi, A. Paras, J. Zhu, M. Park, J. Dhariwal, M. Almond, E. H. Wong, A. Sykes, J. Del Rosario, M. B. Trujillo-Torralbo, P. Mallia, J. Sidney, B. Peters, O. M. Kon, A. Sette, S. L. Johnston, P. J. Openshaw, and C. Chiu. 2020. 'Epitope-specific airway-resident CD4+ T cell dynamics during experimental human RSV infection', *J Clin Invest*, 130: 523-38.

Halbur, P. G., L. D. Miller, P. S. Paul, X. J. Meng, E. L. Huffman, and J. J. Andrews. 1995. 'Immunohistochemical identification of porcine reproductive and respiratory syndrome virus (PRRSV) antigen in the heart and lymphoid system of three-week-old colostrum-deprived pigs', *Vet Pathol*, 32: 200-4.

Hao, X., T. S. Kim, and T. J. Braciale. 2008. 'Differential response of respiratory dendritic cell subsets to influenza virus infection', *J Virol*, 82: 4908-19.

Harty, J. T., A. R. Tvinnereim, and D. W. White. 2000. 'CD8+ T cell effector mechanisms in resistance to infection', *Annu Rev Immunol*, 18: 275-308.

Hause, B. M., M. Ducatez, E. A. Collin, Z. Ran, R. Liu, Z. Sheng, A. Armien, B. Kaplan, S. Chakravarty, A. D. Hoppe, R. J. Webby, R. R. Simonson, and F. Li. 2013. 'Isolation of a novel swine influenza

virus from Oklahoma in 2011 which is distantly related to human influenza C viruses', *PLoS Pathog*, 9: e1003176.

Hayashi, Y., M. Okutani, S. Ogawa, T. Tsukahara, and R. Inoue. 2018. 'Generation of anti-porcine CD69 monoclonal antibodies and their usefulness to evaluate early activation of cellular immunity by flow cytometric analysis', *Anim Sci J*, 89: 825-32.

Hayward, A. C., L. Wang, N. Goonetilleke, E. B. Fragaszy, A. Bermingham, A. Copas, O. Dukes, E. R. Millett, I. Nazareth, J. S. Nguyen-Van-Tam, J. M. Watson, M. Zambon, Group Flu Watch, A. M. Johnson, and A. J. McMichael. 2015. 'Natural T Cell-mediated Protection against Seasonal and Pandemic Influenza. Results of the Flu Watch Cohort Study', *Am J Respir Crit Care Med*, 191: 1422-31.

Hayward, S. L., C. D. Scharer, E. K. Cartwright, S. Takamura, Z. T. Li, J. M. Boss, and J. E. Kohlmeier. 2020. 'Environmental cues regulate epigenetic reprogramming of airway-resident memory CD8(+) T cells', *Nat Immunol*, 21: 309-20.

He, X. S., T. H. Holmes, C. Zhang, K. Mahmood, G. W. Kemble, D. B. Lewis, C. L. Dekker, H. B. Greenberg, and A. M. Arvin. 2006. 'Cellular immune responses in children and adults receiving inactivated or live attenuated influenza vaccines', *J Virol*, 80: 11756-66.

Hemmink, J. D., S. B. Morgan, M. Aramouni, H. Everett, F. J. Salguero, L. Canini, E. Porter, M. Chase-Topping, K. Beck, R. M. Loughlin, B. V. Carr, I. H. Brown, M. Bailey, M. Woolhouse, S. M. Brookes, B. Charleston, and E. Tchilian. 2016. 'Distinct immune responses and virus shedding in pigs following aerosol, intra-nasal and contact infection with pandemic swine influenza A virus, A(H1N1)09', *Vet Res*, 47: 103.

Hensel, A., L. A. van Leengoed, M. Szostak, H. Windt, H. Weissenbock, N. Stockhofe-Zurwieden, A. Katinger, M. Stadler, M. Ganter, S. Bunka, R. Pabst, and W. Lubitz. 1996. 'Induction of protective immunity by aerosol or oral application of candidate vaccines in a dose-controlled pig aerosol infection model', *J Biotechnol*, 44: 171-81.

Hertel, S. P., G. Winter, and W. Friess. 2015. 'Protein stability in pulmonary drug delivery via nebulization', *Adv Drug Deliv Rev*, 93: 79-94.

Hibbitts, A., A. M. O'Mahony, E. Forde, L. Nolan, J. Ogier, S. Desgranges, R. Darcy, R. MacLoughlin, C. M. O'Driscoll, and S. A. Cryan. 2014. 'Early-stage development of novel cyclodextrin-siRNA nanocomplexes allows for successful postnebulization transfection of bronchial epithelial cells', *J Aerosol Med Pulm Drug Deliv*, 27: 466-77.

Hodge, L. M., and J. W. Simecka. 2002. 'Role of upper and lower respiratory tract immunity in resistance to Mycoplasma respiratory disease', *J Infect Dis*, 186: 290-4.

Hoft, D. F., E. Babusis, S. Worku, C. T. Spencer, K. Lottenbach, S. M. Truscott, G. Abate, I. G. Sakala, K. M. Edwards, C. B. Creech, M. A. Gerber, D. I. Bernstein, F. Newman, I. Graham, E. L. Anderson, and R. B. Belshe. 2011. 'Live and inactivated influenza vaccines induce similar humoral responses, but only live vaccines induce diverse T-cell responses in young children', *J Infect Dis*, 204: 845-53.

Hogner, K., T. Wolff, S. Pleschka, S. Plog, A. D. Gruber, U. Kalinke, H. D. Walmrath, J. Bodner, S. Gattenlohner, P. Lewe-Schlosser, M. Matrosovich, W. Seeger, J. Lohmeyer, and S. Herold. 2016. 'Correction: Macrophage-expressed IFN-beta Contributes to Apoptotic Alveolar Epithelial Cell Injury in Severe Influenza Virus Pneumonia', *PLoS Pathog*, 12: e1005716.

Holt, P. G. 2000. 'Antigen presentation in the lung', *Am J Respir Crit Care Med*, 162: S151-6.

Holt, P. G., D. H. Strickland, M. E. Wikstrom, and F. L. Jahnsen. 2008. 'Regulation of immunological homeostasis in the respiratory tract', *Nat Rev Immunol*, 8: 142-52.

Holzer, B., V. Martini, M. Edmans, and E. Tchilian. 2019. 'T and B Cell Immune Responses to Influenza Viruses in Pigs', *Front Immunol*, 10: 98.

Holzer, B., S. B. Morgan, V. Martini, R. Sharma, B. Clark, C. Chiu, F. J. Salguero, and E. Tchilian. 2019. 'Immunogenicity and Protective Efficacy of Seasonal Human Live Attenuated Cold-Adapted Influenza Virus Vaccine in Pigs', *Front Immunol*, 10: 2625.

Holzer, B., S. B. Morgan, Y. Matsuoka, M. Edmans, F. J. Salguero, H. Everett, S. M. Brookes, E. Porter, R. MacLoughlin, B. Charleston, K. Subbarao, A. Townsend, and E. Tchilian. 2018. 'Comparison of Heterosubtypic Protection in Ferrets and Pigs Induced by a Single-Cycle Influenza Vaccine', *J Immunol*, 200: 4068-77.

Holzer, B., P. Rijal, A. McNee, B. Paudyal, V. Martini, B. Clark, T. Manjegowda, F. J. Salguero, E. Bessell, J. C. Schwartz, K. Moffat, M. Pedrera, S. P. Graham, A. Noble, M. B. Placido, R. M. La Ragione, W. Mwangi, P. Beverley, J. W. McCauley, R. S. Daniels, J. A. Hammond, A. R. Townsend, and E. Tchilian. 2021. 'Correction: Protective porcine influenza virus-specific monoclonal antibodies recognize similar haemagglutinin epitopes as humans', *PLoS Pathog*, 17: e1009815.

Iborra, S., M. Martinez-Lopez, S. C. Khouili, M. Enamorado, F. J. Cueto, R. Conde-Garrosa, C. Del Fresno, and D. Sancho. 2016. 'Optimal Generation of Tissue-Resident but Not Circulating Memory T Cells during Viral Infection Requires Crosspriming by DNGR-1(+) Dendritic Cells', *Immunity*, 45: 847-60.

International Organization for Standardization. 2013. 'Anaesthetic and respiratory equipment — Nebulizing systems and components (27427:2013)', Accessed 10/07/2020. https://www.iso.org/obp/ui#iso:std:iso:27427:ed-3:v1:en.

Iuliano, A. D., K. M. Roguski, H. H. Chang, D. J. Muscatello, R. Palekar, S. Tempia, C. Cohen, J. M. Gran, D. Schanzer, B. J. Cowling, P. Wu, J. Kyncl, L. W. Ang, M. Park, M. Redlberger-Fritz, H. Yu, L. Espenhain, A. Krishnan, G. Emukule, L. van Asten, S. Pereira da Silva, S. Aungkulanon, U. Buchholz, M. A. Widdowson, J. S. Bresee, and Network Global Seasonal Influenza-associated Mortality Collaborator. 2018. 'Estimates of global seasonal influenza-associated respiratory mortality: a modelling study', *Lancet*, 391: 1285-300.

Iwasaki, A., and P. S. Pillai. 2014. 'Innate immunity to influenza virus infection', *Nat Rev Immunol*, 14: 315-28.

Janke, B. H. 2014. 'Influenza A virus infections in swine: pathogenesis and diagnosis', *Vet Pathol*, 51: 410-26.

Jenkins, M. R., R. Webby, P. C. Doherty, and S. J. Turner. 2006. 'Addition of a prominent epitope affects influenza A virus-specific CD8+ T cell immunodominance hierarchies when antigen is limiting', *J Immunol*, 177: 2917-25.

Jiang, X., R. A. Clark, L. Liu, A. J. Wagers, R. C. Fuhlbrigge, and T. S. Kupper. 2012. 'Skin infection generates non-migratory memory CD8+ T(RM) cells providing global skin immunity', *Nature*, 483: 227-31.

Jin, H., and K. Subbarao. 2014. 'Live attenuated influenza vaccine', *Curr Top Microbiol Immunol*, 386: 181-204.

Jozwik, A., M. S. Habibi, A. Paras, J. Zhu, A. Guvenel, J. Dhariwal, M. Almond, E. H. Wong, A. Sykes, M. Maybeno, J. Del Rosario, M. B. Trujillo-Torralbo, P. Mallia, J. Sidney, B. Peters, O. M.

Kon, A. Sette, S. L. Johnston, P. J. Openshaw, and C. Chiu. 2016. 'Erratum: RSV-specific airway resident memory CD8+ T cells and differential disease severity after experimental human infection', *Nat Commun*, 7: 11011.

Judge, E. P., J. M. Hughes, J. J. Egan, M. Maguire, E. L. Molloy, and S. O'Dea. 2014. 'Anatomy and bronchoscopy of the porcine lung. A model for translational respiratory medicine', *Am J Respir Cell Mol Biol*, 51: 334-43.

Kappes, M. A., M. R. Sandbulte, R. Platt, C. Wang, K. M. Lager, J. N. Henningson, A. Lorusso, A. L. Vincent, C. L. Loving, J. A. Roth, and M. E. Kehrli, Jr. 2012. 'Vaccination with NS1-truncated H3N2 swine influenza virus primes T cells and confers cross-protection against an H1N1 heterosubtypic challenge in pigs', *Vaccine*, 30: 280-8.

Kaser, T. 2021. 'Swine as biomedical animal model for T-cell research-Success and potential for transmittable and non-transmittable human diseases', *Mol Immunol*, 135: 95-115.

Khatri, M., V. Dwivedi, S. Krakowka, C. Manickam, A. Ali, L. Wang, Z. Qin, G. J. Renukaradhya, and C. W. Lee. 2010. 'Swine influenza H1N1 virus induces acute inflammatory immune responses in pig lungs: a potential animal model for human H1N1 influenza virus', *J Virol*, 84: 11210-8.

Khurana, S., C. L. Loving, J. Manischewitz, L. R. King, P. C. Gauger, J. Henningson, A. L. Vincent, and H. Golding. 2013. 'Vaccine-induced anti-HA2 antibodies promote virus fusion and enhance influenza virus respiratory disease', *Sci Transl Med*, 5: 200ra114.

Kitikoon, P., A. L. Vincent, P. C. Gauger, S. N. Schlink, D. O. Bayles, M. R. Gramer, D. Darnell, R. J. Webby, K. M. Lager, S. L. Swenson, and A. Klimov. 2012. 'Pathogenicity and transmission in pigs of the novel A(H3N2)v influenza virus isolated from humans and characterization of swine H3N2 viruses isolated in 2010-2011', *J Virol*, 86: 6804-14.

Klonowski, K. D., K. J. Williams, A. L. Marzo, D. A. Blair, E. G. Lingenheld, and L. Lefrancois. 2004. 'Dynamics of blood-borne CD8 memory T cell migration in vivo', *Immunity*, 20: 551-62.

Ko, Y. A., Y. H. Yu, Y. F. Wu, Y. C. Tseng, C. L. Chen, K. S. Goh, H. Y. Liao, T. H. Chen, T. R. Cheng, A. S. Yang, C. H. Wong, C. Ma, and K. I. Lin. 2021. 'A non-neutralizing antibody broadly protects against influenza virus infection by engaging effector cells', *PLoS Pathog*, 17: e1009724.

Kobasa, D., S. M. Jones, K. Shinya, J. C. Kash, J. Copps, H. Ebihara, Y. Hatta, J. H. Kim, P. Halfmann, M. Hatta, F. Feldmann, J. B. Alimonti, L. Fernando, Y. Li, M. G. Katze, H. Feldmann, and Y. Kawaoka. 2007. 'Aberrant innate immune response in lethal infection of macaques with the 1918 influenza virus', *Nature*, 445: 319-23.

Krammer, F. 2019. 'The human antibody response to influenza A virus infection and vaccination', *Nat Rev Immunol*, 19: 383-97.

Kumar, B. V., W. Ma, M. Miron, T. Granot, R. S. Guyer, D. J. Carpenter, T. Senda, X. Sun, S. H. Ho, H. Lerner, A. L. Friedman, Y. Shen, and D. L. Farber. 2017. 'Human Tissue-Resident Memory T Cells Are Defined by Core Transcriptional and Functional Signatures in Lymphoid and Mucosal Sites', *Cell Rep*, 20: 2921-34.

La Gruta, N. L., K. Kedzierska, K. Pang, R. Webby, M. Davenport, W. Chen, S. J. Turner, and P. C. Doherty. 2006. 'A virus-specific CD8+ T cell immunodominance hierarchy determined by antigen dose and precursor frequencies', *Proc Natl Acad Sci U S A*, 103: 994-9.

La Gruta, N. L., P. G. Thomas, A. I. Webb, M. A. Dunstone, T. Cukalac, P. C. Doherty, A. W. Purcell, J. Rossjohn, and S. J. Turner. 2008. 'Epitope-specific TCRbeta repertoire diversity imparts no

functional advantage on the CD8+ T cell response to cognate viral peptides', *Proc Natl Acad Sci U S A*, 105: 2034-9.

La Gruta, N. L., S. J. Turner, and P. C. Doherty. 2004. 'Hierarchies in cytokine expression profiles for acute and resolving influenza virus-specific CD8+ T cell responses: correlation of cytokine profile and TCR avidity', *J Immunol*, 172: 5553-60.

Lapuente, D., M. Storcksdieck Genannt Bonsmann, A. Maaske, V. Stab, V. Heinecke, K. Watzstedt, R. Hess, A. M. Westendorf, W. Bayer, C. Ehrhardt, and M. Tenbusch. 2018. 'IL-1beta as mucosal vaccine adjuvant: the specific induction of tissue-resident memory T cells improves the heterosubtypic immunity against influenza A viruses', *Mucosal Immunol*, 11: 1265-78.

Larsen, D. L., A. Karasin, F. Zuckermann, and C. W. Olsen. 2000. 'Systemic and mucosal immune responses to H1N1 influenza virus infection in pigs', *Vet Microbiol*, 74: 117-31.

Lau, Y. F., C. Santos, F. J. Torres-Velez, and K. Subbarao. 2011. 'The magnitude of local immunity in the lungs of mice induced by live attenuated influenza vaccines is determined by local viral replication and induction of cytokines', *J Virol*, 85: 76-85.

Lau, Y. F., A. R. Wright, and K. Subbarao. 2012. 'The contribution of systemic and pulmonary immune effectors to vaccine-induced protection from H5N1 influenza virus infection', *J Virol*, 86: 5089-98.

Lee, A. J., and A. A. Ashkar. 2018. 'The Dual Nature of Type I and Type II Interferons', *Front Immunol*, 9: 2061.

Lee, B. W., R. F. Bey, M. J. Baarsch, and M. E. Larson. 1995. 'Class specific antibody response to influenza A H1N1 infection in swine', *Vet Microbiol*, 43: 241-50.

Lee, L. Y., L. A. Ha do, C. Simmons, M. D. de Jong, N. V. Chau, R. Schumacher, Y. C. Peng, A. J. McMichael, J. J. Farrar, G. L. Smith, A. R. Townsend, B. A. Askonas, S. Rowland-Jones, and T. Dong. 2008. 'Memory T cells established by seasonal human influenza A infection cross-react with avian influenza A (H5N1) in healthy individuals', *J Clin Invest*, 118: 3478-90.

Liao, Y., G. K. Smyth, and W. Shi. 2014. 'featureCounts: an efficient general purpose program for assigning sequence reads to genomic features', *Bioinformatics*, 30: 923-30.

Liao, Y., J. Wang, E. J. Jaehnig, Z. Shi, and B. Zhang. 2019. 'WebGestalt 2019: gene set analysis toolkit with revamped UIs and APIs', *Nucleic Acids Res*, 47: W199-W205.

Liew, F. Y., S. M. Russell, G. Appleyard, C. M. Brand, and J. Beale. 1984. 'Cross-protection in mice infected with influenza A virus by the respiratory route is correlated with local IgA antibody rather than serum antibody or cytotoxic T cell reactivity', *Eur J Immunol*, 14: 350-6.

Lim, K., Y. M. Hyun, K. Lambert-Emo, T. Capece, S. Bae, R. Miller, D. J. Topham, and M. Kim. 2015. 'Neutrophil trails guide influenza-specific CD8(+) T cells in the airways', *Science*, 349: aaa4352.

Liu, F., J. L. Whitton, and M. K. Slifka. 2004. 'The rapidity with which virus-specific CD8+ T cells initiate IFN-gamma synthesis increases markedly over the course of infection and correlates with immunodominance', *J Immunol*, 173: 456-62.

Love, M. I., W. Huber, and S. Anders. 2014. 'Moderated estimation of fold change and dispersion for RNA-seq data with DESeq2', *Genome Biol*, 15: 550.

Loving, C. L., K. M. Lager, A. L. Vincent, S. L. Brockmeier, P. C. Gauger, T. K. Anderson, P. Kitikoon, D. R. Perez, and M. E. Kehrli, Jr. 2013. 'Efficacy in pigs of inactivated and live attenuated influenza virus vaccines against infection and transmission of an emerging H3N2 similar to the 2011-2012 H3N2v', *J Virol*, 87: 9895-903.

Loving, C. L., A. L. Vincent, L. Pena, and D. R. Perez. 2012. 'Heightened adaptive immune responses following vaccination with a temperature-sensitive, live-attenuated influenza virus compared to adjuvanted, whole-inactivated virus in pigs', *Vaccine*, 30: 5830-8.

Low, N., A. Bavdekar, L. Jeyaseelan, S. Hirve, K. Ramanathan, N. J. Andrews, N. Shaikh, R. S. Jadi, A. Rajagopal, K. E. Brown, D. Brown, J. B. Fink, O. John, P. Scott, A. X. Riveros-Balta, M. Greco, R. Dhere, P. S. Kulkarni, and A. M. Henao Restrepo. 2015. 'A randomized, controlled trial of an aerosolized vaccine against measles', *N Engl J Med*, 372: 1519-29.

Lund, F. E., and T. D. Randall. 2021. 'Scent of a vaccine', *Science*, 373: 397-99.

Ma, C., and N. Zhang. 2015. 'Transforming growth factor-beta signaling is constantly shaping memory T-cell population', *Proc Natl Acad Sci U S A*, 112: 11013-7.

Maccari, G., J. Robinson, K. Ballingall, L. A. Guethlein, U. Grimholt, J. Kaufman, C. S. Ho, N. G. de Groot, P. Flicek, R. E. Bontrop, J. A. Hammond, and S. G. Marsh. 2017. 'IPD-MHC 2.0: an improved inter-species database for the study of the major histocompatibility complex', *Nucleic Acids Res*, 45: D860-D64.

Mackay, L. K., M. Minnich, N. A. Kragten, Y. Liao, B. Nota, C. Seillet, A. Zaid, K. Man, S. Preston, D. Freestone, A. Braun, E. Wynne-Jones, F. M. Behr, R. Stark, D. G. Pellicci, D. I. Godfrey, G. T. Belz, M. Pellegrini, T. Gebhardt, M. Busslinger, W. Shi, F. R. Carbone, R. A. van Lier, A. Kallies, and K. P. van Gisbergen. 2016. 'Hobit and Blimp1 instruct a universal transcriptional program of tissue residency in lymphocytes', *Science*, 352: 459-63.

Mackay, L. K., A. Rahimpour, J. Z. Ma, N. Collins, A. T. Stock, M. L. Hafon, J. Vega-Ramos, P. Lauzurica, S. N. Mueller, T. Stefanovic, D. C. Tscharke, W. R. Heath, M. Inouye, F. R. Carbone, and T. Gebhardt. 2013. 'The developmental pathway for CD103(+)CD8+ tissue-resident memory T cells of skin', *Nat Immunol*, 14: 1294-301.

Mackay, L. K., A. T. Stock, J. Z. Ma, C. M. Jones, S. J. Kent, S. N. Mueller, W. R. Heath, F. R. Carbone, and T. Gebhardt. 2012. 'Long-lived epithelial immunity by tissue-resident memory T (TRM) cells in the absence of persisting local antigen presentation', *Proc Natl Acad Sci U S A*, 109: 7037-42.

Mancera Gracia, J. C., D. S. Pearce, A. Masic, and M. Balasch. 2020. 'Influenza A Virus in Swine: Epidemiology, Challenges and Vaccination Strategies', *Front Vet Sci*, 7: 647.

Martin, Marcel. 2011. 'Cutadapt Removes Adapter Sequences From High-Throughput Sequencing Reads', *EMBnet*, 17.

Martini, V., M. Hinchcliffe, E. Blackshaw, M. Joyce, A. McNee, P. Beverley, A. Townsend, R. MacLoughlin, and E. Tchilian. 2020. 'Distribution of Droplets and Immune Responses After Aerosol and Intra-Nasal Delivery of Influenza Virus to the Respiratory Tract of Pigs', *Front Immunol*, 11: 594470.

Martini, V., B. Paudyal, T. Chrun, A. McNee, M. Edmans, E. Atangana Maze, B. Clark, A. Nunez, G. Dolton, A. Sewell, P. Beverley, R. MacLoughlin, A. Townsend, and E. Tchilian. 2021. 'Simultaneous Aerosol and Intramuscular Immunization with Influenza Vaccine Induces Powerful Protective Local T Cell and Systemic Antibody Immune Responses in Pigs', *J Immunol*, 206: 652-63.

Masic, Aleksandar, Hyun-Mi Pyo, Shawn Babiuk, and Yan Zhou. 2013. 'An eight-segment swine influenza virus harboring H1 and H3 hemagglutinins is attenuated and protective against H1N1 and H3N2 subtypes in pigs', *Journal of Virology*, 87: 10114 LP-25.

Masopust, D., D. Choo, V. Vezys, E. J. Wherry, J. Duraiswamy, R. Akondy, J. Wang, K. A. Casey, D. L. Barber, K. S. Kawamura, K. A. Fraser, R. J. Webby, V. Brinkmann, E. C. Butcher, K. A. Newell, and R. Ahmed. 2010. 'Dynamic T cell migration program provides resident memory within intestinal epithelium', *J Exp Med*, 207: 553-64.

Masopust, D., J. Jiang, H. Shen, and L. Lefrancois. 2001. 'Direct analysis of the dynamics of the intestinal mucosa CD8 T cell response to systemic virus infection', *J Immunol*, 166: 2348-56.

Masopust, D., and J. M. Schenkel. 2013. 'The integration of T cell migration, differentiation and function', *Nat Rev Immunol*, 13: 309-20.

Masopust, D., V. Vezys, A. L. Marzo, and L. Lefrancois. 2001a. 'Preferential localization of effector memory cells in nonlymphoid tissue', *Science*, 291: 2413-7.

Masopust, D., V. Vezys, E. J. Wherry, D. L. Barber, and R. Ahmed. 2006. 'Cutting edge: gut microenvironment promotes differentiation of a unique memory CD8 T cell population', *J Immunol*, 176: 2079-83.

Masopust, David, Vaiva Vezys, Amanda L. Marzo, and Leo Lefrancois. 2001b. 'Preferential Localization of Effector Memory Cells in Nonlymphoid Tissue', *Science*, 291: 2413-17.

Matrosovich, M., T. Matrosovich, J. Carr, N. A. Roberts, and H. D. Klenk. 2003. 'Overexpression of the alpha-2,6-sialyltransferase in MDCK cells increases influenza virus sensitivity to neuraminidase inhibitors', *J Virol*, 77: 8418-25.

McHeyzer-Williams, M., S. Okitsu, N. Wang, and L. McHeyzer-Williams. 2011. 'Molecular programming of B cell memory', *Nat Rev Immunol*, 12: 24-34.

McKinstry, K. K., T. M. Strutt, Y. Kuang, D. M. Brown, S. Sell, R. W. Dutton, and S. L. Swain. 2012. 'Memory CD4+ T cells protect against influenza through multiple synergizing mechanisms', *J Clin Invest*, 122: 2847-56.

McMaster, S. R., A. N. Wein, P. R. Dunbar, S. L. Hayward, E. K. Cartwright, T. L. Denning, and J. E. Kohlmeier. 2018. 'Pulmonary antigen encounter regulates the establishment of tissue-resident CD8 memory T cells in the lung airways and parenchyma', *Mucosal Immunol*, 11: 1071-78.

McMaster, S. R., J. J. Wilson, H. Wang, and J. E. Kohlmeier. 2015. 'Airway-Resident Memory CD8 T Cells Provide Antigen-Specific Protection against Respiratory Virus Challenge through Rapid IFN-gamma Production', *J Immunol*, 195: 203-9.

McMichael, A. J., and B. A. Askonas. 1978. 'Influenza virus-specific cytotoxic T cells in man; induction and properties of the cytotoxic cell', *Eur J Immunol*, 8: 705-11.

McMichael, A. J., F. M. Gotch, G. R. Noble, and P. A. Beare. 1983. 'Cytotoxic T-cell immunity to influenza', *N Engl J Med*, 309: 13-7.

Medical Advisory Committee of the Immune Deficiency, Foundation, W. T. Shearer, T. A. Fleisher, R. H. Buckley, Z. Ballas, M. Ballow, R. M. Blaese, F. A. Bonilla, M. E. Conley, C. Cunningham-Rundles, A. H. Filipovich, R. Fuleihan, E. W. Gelfand, V. Hernandez-Trujillo, S. M. Holland, R. Hong, H. M. Lederman, H. L. Malech, S. Miles, L. D. Notarangelo, H. D. Ochs, J. S. Orange, J. M. Puck, J. M. Routes, E. R. Stiehm, K. Sullivan, T. Torgerson, and J. Winkelstein. 2014. 'Recommendations for live viral and bacterial vaccines in immunodeficient patients and their close contacts', *J Allergy Clin Immunol*, 133: 961-6.

Mendelson, M., Y. Tekoah, A. Zilka, O. Gershoni-Yahalom, R. Gazit, H. Achdout, N. V. Bovin, T. Meningher, M. Mandelboim, O. Mandelboim, A. David, and A. Porgador. 2010. 'NKp46 O-glycan sequences that are involved in the interaction with hemagglutinin type 1 of influenza virus', *J Virol*, 84: 3789-97.

Minne, A., J. Louahed, S. Mehauden, B. Baras, J. C. Renauld, and R. Vanbever. 2007. 'The delivery site of a monovalent influenza vaccine within the respiratory tract impacts on the immune response', *Immunology*, 122: 316-25.

Miquel-Clopes, A., E. G. Bentley, J. P. Stewart, and S. R. Carding. 2019. 'Mucosal vaccines and technology', *Clin Exp Immunol*, 196: 205-14.

Mohammed, J., L. K. Beura, A. Bobr, B. Astry, B. Chicoine, S. W. Kashem, N. E. Welty, B. Z. Igyarto, S. Wijeyesinghe, E. A. Thompson, C. Matte, L. Bartholin, A. Kaplan, D. Sheppard, A. G. Bridges, W. D. Shlomchik, D. Masopust, and D. H. Kaplan. 2016. 'Stromal cells control the epithelial residence of DCs and memory T cells by regulated activation of TGF-beta', *Nat Immunol*, 17: 414-21.

Mohn, K. G., I. Smith, H. Sjursen, and R. J. Cox. 2018. 'Immune responses after live attenuated influenza vaccination', *Hum Vaccin Immunother*, 14: 571-78.

Monsalvo, A. C., J. P. Batalle, M. F. Lopez, J. C. Krause, J. Klemenc, J. Z. Hernandez, B. Maskin, J. Bugna, C. Rubinstein, L. Aguilar, L. Dalurzo, R. Libster, V. Savy, E. Baumeister, L. Aguilar, G. Cabral, J. Font, L. Solari, K. P. Weller, J. Johnson, M. Echavarria, K. M. Edwards, J. D. Chappell, J. E. Crowe, Jr., J. V. Williams, G. A. Melendi, and F. P. Polack. 2011. 'Severe pandemic 2009 H1N1 influenza disease due to pathogenic immune complexes', *Nat Med*, 17: 195-9.

Morabito, K. M., T. R. Ruckwardt, A. J. Redwood, S. M. Moin, D. A. Price, and B. S. Graham. 2017. 'Intranasal administration of RSV antigen-expressing MCMV elicits robust tissue-resident effector and effector memory CD8+ T cells in the lung', *Mucosal Immunol*, 10: 545-54.

Moreno, S., B. Alvarez, P. Martinez, H. Uenishi, C. Revilla, A. Ezquerra, F. Alonso, and J. Dominguez. 2013. 'Analysis of chemokine receptor CCR7 expression on porcine blood T lymphocytes using a CCL19-Fc fusion protein', *Dev Comp Immunol*, 39: 207-13.

Morgan, S. B., J. D. Hemmink, E. Porter, R. Harley, H. Shelton, M. Aramouni, H. E. Everett, S. M. Brookes, M. Bailey, A. M. Townsend, B. Charleston, and E. Tchilian. 2016. 'Aerosol delivery of a candidate universal influenza vaccine reduces viral load in pigs challenged with pandemic H1N1 virus', *J Immunol*, 196: 5014-23.

Morgan, S. B.; Hemmink, J. D.; Porter, E.; Harley, H.; Holly, H.; Aramouni, M.; Everett, H.E.; Brookes, S.; Bailey, M.; Townsend, A.M.; Charleston, B.; Tchilian, E. 2016. 'Aerosol Delivery of a Candidate Universal Influenza Vaccine Reduces Viral Load in Pigs Challenged with Pandemic H1N1 Virus', *J Immunol*, 196: 5014-23.

Mueller, S. N., T. Gebhardt, F. R. Carbone, and W. R. Heath. 2013. 'Memory T cell subsets, migration patterns, and tissue residence', *Annu Rev Immunol*, 31: 137-61.

Mullarkey, C. E., M. J. Bailey, D. A. Golubeva, G. S. Tan, R. Nachbagauer, W. He, K. E. Novakowski, D. M. Bowdish, M. S. Miller, and P. Palese. 2016. 'Broadly Neutralizing Hemagglutinin Stalk-Specific Antibodies Induce Potent Phagocytosis of Immune Complexes by Neutrophils in an Fc-Dependent Manner', *MBio*, 7.

Murphy, D., W. G. Van Alstine, L. K. Clark, S. Albregts, and K. Knox. 1993. 'Aerosol vaccination of pigs against Mycoplasma hyopneumoniae infection', *Am J Vet Res*, 54: 1874-80.

Nelli, R. K., S. V. Kuchipudi, G. A. White, B. B. Perez, S. P. Dunham, and K. C. Chang. 2010. 'Comparative distribution of human and avian type sialic acid influenza receptors in the pig', *BMC Vet Res*, 6: 4.

Nguyen, T. H., J. L. McAuley, Y. Kim, M. Z. Zheng, N. A. Gherardin, D. I. Godfrey, D. F. Purcell, L. C. Sullivan, G. P. Westall, P. C. Reading, K. Kedzierska, and L. M. Wakim. 2021. 'Influenza, but not SARS-CoV-2, infection induces a rapid interferon response that wanes with age and diminished tissue-resident memory CD8(+) T cells', *Clin Transl Immunology*, 10: e1242.

Peasah, S. K., E. Azziz-Baumgartner, J. Breese, M. I. Meltzer, and M. A. Widdowson. 2013. 'Influenza cost and cost-effectiveness studies globally--a review', *Vaccine*, 31: 5339-48.

Pedersen, L. E., S. O. Breum, U. Riber, L. E. Larsen, and G. Jungersen. 2014a. 'Identification of swine influenza virus epitopes and analysis of multiple specificities expressed by cytotoxic T cell subsets', *Virol J*, 11: 163.

Pedersen, L. E., M. Harndahl, M. Nielsen, J. R. Patch, G. Jungersen, S. Buus, and W. T. Golde. 2013. 'Identification of peptides from foot-and-mouth disease virus structural proteins bound by class I swine leukocyte antigen (SLA) alleles, SLA-1*0401 and SLA-2*0401', *Anim Genet*, 44: 251-8.

Pedersen, Lasse E., Solvej Breum, Ulla Riber, Lars E. Larsen, and Gregers Jungersen. 2014b. 'Identification of swine influenza virus epitopes and analysis of multiple specificities expressed by cytotoxic T cell subsets', *Virology Journal*, 11: 1-5.

Perdomo, C., U. Zedler, A. A. Kuhl, L. Lozza, P. Saikali, L. E. Sander, A. Vogelzang, S. H. Kaufmann, and A. Kupz. 2016. 'Mucosal BCG Vaccination Induces Protective Lung-Resident Memory T Cell Populations against Tuberculosis', *MBio*, 7.

Pizzolla, A., T. H. O. Nguyen, J. M. Smith, A. G. Brooks, K. Kedzieska, W. R. Heath, P. C. Reading, and L. M. Wakim. 2017a. 'Resident memory CD8(+) T cells in the upper respiratory tract prevent pulmonary influenza virus infection', *Sci Immunol*, 2.

———. 2017b. 'Resident memory CD8(+) T cells in the upper respiratory tract prevent pulmonary influenza virus infection', *Sci Immunol*, 2: eaam6970.

Powell, T. J., P. Rijal, R. M. McEwen-Smith, H. Byun, M. Hardwick, L. M. Schimanski, K. A. Huang, R. S. Daniels, and A. R. M. Townsend. 2019. 'A single cycle influenza virus coated in H7 haemagglutinin generates neutralizing antibody responses to haemagglutinin and neuraminidase glycoproteins and protection from heterotypic challenge', *J Gen Virol*, 100: 431-45.

Powell, T. J., J. D. Silk, J. Sharps, E. Fodor, and A. R. Townsend. 2012. 'Pseudotyped influenza A virus as a vaccine for the induction of heterotypic immunity', *J Virol*, 86: 13397-406.

Québec, International Commission on Radiological Protection. 1994. 'Human respiratory tract model for radiological protection. A report of a Task Group of the International Commission on Radiological Protection', *Ann ICRP*, 24: 1-482.

Rajao, D. S., H. Chen, D. R. Perez, M. R. Sandbulte, P. C. Gauger, C. L. Loving, G. D. Shanks, and A. Vincent. 2016. 'Vaccine-associated enhanced respiratory disease is influenced by haemagglutinin and neuraminidase in whole inactivated influenza virus vaccines', *J Gen Virol*, 97: 1489-99.

Rajao, D. S., and A. L. Vincent. 2015. 'Swine as a model for influenza A virus infection and immunity', *ILAR J*, 56: 44-52.

Ran, Z., H. Shen, Y. Lang, E. A. Kolb, N. Turan, L. Zhu, J. Ma, B. Bawa, Q. Liu, H. Liu, M. Quast, G. Sexton, F. Krammer, B. M. Hause, J. Christopher-Hennings, E. A. Nelson, J. Richt, F. Li, and W. Ma. 2015. 'Domestic pigs are susceptible to infection with influenza B viruses', *J Virol*, 89: 4818-26.

Ray, S. J., S. N. Franki, R. H. Pierce, S. Dimitrova, V. Koteliansky, A. G. Sprague, P. C. Doherty, A. R. de Fougerolles, and D. J. Topham. 2004. 'The collagen binding alpha1beta1 integrin VLA-1 regulates CD8 T cell-mediated immune protection against heterologous influenza infection', *Immunity*, 20: 167-79.

Reinhardt, J., A. V. Grishin, H. Oberleithner, and M. J. Caplan. 2000. 'Differential localization of human nongastric H(+)-K(+)-ATPase ATP1AL1 in polarized renal epithelial cells', *Am J Physiol Renal Physiol*, 279: F417-25.

Reutner, K., J. Leitner, A. Mullebner, A. Ladinig, S. E. Essler, J. C. Duvigneau, M. Ritzmann, P. Steinberger, A. Saalmuller, and W. Gerner. 2013. 'CD27 expression discriminates porcine T helper cells with functionally distinct properties', *Vet Res*, 44: 18.

Richt, J. A., P. Lekcharoensuk, K. M. Lager, A. L. Vincent, C. M. Loiacono, B. H. Janke, W. H. Wu, K. J. Yoon, R. J. Webby, A. Solorzano, and A. Garcia-Sastre. 2006. 'Vaccination of pigs against swine influenza viruses by using an NS1-truncated modified live-virus vaccine', *J Virol*, 80: 11009-18.

Roces, C. B., M. T. Hussain, S. T. Schmidt, D. Christensen, and Y. Perrie. 2019. 'Investigating Prime-Pull Vaccination through a Combination of Parenteral Vaccination and Intranasal Boosting', *Vaccines (Basel)*, 8.

Rodgers, B. C., and C. A. Mims. 1982. 'Influenza virus replication in human alveolar macrophages', *J Med Virol*, 9: 177-84.

Rogers, G. N., and J. C. Paulson. 1983. 'Receptor determinants of human and animal influenza virus isolates: differences in receptor specificity of the H3 hemagglutinin based on species of origin', *Virology*, 127: 361-73.

Romero, P., A. Zippelius, I. Kurth, M. J. Pittet, C. Touvrey, E. M. Iancu, P. Corthesy, E. Devevre, D. E. Speiser, and N. Rufer. 2007. 'Four functionally distinct populations of human effector-memory CD8+ T lymphocytes', *J Immunol*, 178: 4112-9.

Ronan, E. O., L. N. Lee, P. C. Beverley, and E. Z. Tchilian. 2009. 'Immunization of mice with a recombinant adenovirus vaccine inhibits the early growth of Mycobacterium tuberculosis after infection', *PLoS One*, 4: e8235.

Ronan, E. O., L. N. Lee, E. Z. Tchilian, and P. C. Beverley. 2010. 'Nasal associated lymphoid tissue (NALT) contributes little to protection against aerosol challenge with Mycobacterium tuberculosis after immunisation with a recombinant adenoviral vaccine', *Vaccine*, 28: 5179-84.

Ross, Gavin J. S. 1990. *Nonlinear estimation* (Springer-Verlag: New York).

Rothkotter, H. J. 2009. 'Anatomical particularities of the porcine immune system--a physician's view', *Dev Comp Immunol*, 33: 267-72.

Rudin, A., E. L. Johansson, C. Bergquist, and J. Holmgren. 1998. 'Differential kinetics and distribution of antibodies in serum and nasal and vaginal secretions after nasal and oral vaccination of humans', *Infect Immun*, 66: 3390-6.

Rufer, N., A. Zippelius, P. Batard, M. J. Pittet, I. Kurth, P. Corthesy, J. C. Cerottini, S. Leyvraz, E. Roosnek, M. Nabholz, and P. Romero. 2003. 'Ex vivo characterization of human CD8+ T subsets with distinct replicative history and partial effector functions', *Blood*, 102: 1779-87.

Saalmuller, A., T. Werner, and V. Fachinger. 2002. 'T-helper cells from naive to committed', *Vet Immunol Immunopathol*, 87: 137-45.

Sabin, A. B. 1983. 'Immunization against measles by aerosol', *Rev Infect Dis*, 5: 514-23.

Sabin, A. B., A. Flores Arechiga, J. Fernandez de Castro, P. Albrecht, J. L. Sever, and I. Shekarchi. 1984. 'Successful immunization of infants with and without maternal antibody by aerosolized measles vaccine. II. Vaccine comparisons and evidence for multiple antibody response', *JAMA*, 251: 2363-71.

Sabin, A. B., A. Flores Arechiga, J. Fernandez de Castro, J. L. Sever, D. L. Madden, I. Shekarchi, and P. Albrecht. 1983. 'Successful immunization of children with and without maternal antibody by aerosolized measles vaccine. I. Different results with undiluted human diploid cell and chick embryo fibroblast vaccines', *JAMA*, 249: 2651-62.

Sakai, S., K. D. Kauffman, J. M. Schenkel, C. C. McBerry, K. D. Mayer-Barber, D. Masopust, and D. L. Barber. 2014. 'Cutting edge: control of Mycobacterium tuberculosis infection by a subset of lung parenchyma-homing CD4 T cells', *J Immunol*, 192: 2965-9.

Salvesen, H. A., and C. B. A. Whitelaw. 2021. 'Current and prospective control strategies of influenza A virus in swine', *Porcine Health Manag*, 7: 23.

Santosuosso, M., S. McCormick, X. Zhang, A. Zganiacz, and Z. Xing. 2006. 'Intranasal boosting with an adenovirus-vectored vaccine markedly enhances protection by parenteral Mycobacterium bovis BCG immunization against pulmonary tuberculosis', *Infect Immun*, 74: 4634-43.

Sathaliyawala, T., M. Kubota, N. Yudanin, D. Turner, P. Camp, J. J. Thome, K. L. Bickham, H. Lerner, M. Goldstein, M. Sykes, T. Kato, and D. L. Farber. 2013. 'Distribution and compartmentalization of human circulating and tissue-resident memory T cell subsets', *Immunity*, 38: 187-97.

Satti, I., J. Meyer, S. A. Harris, Z. R. Manjaly Thomas, K. Griffiths, R. D. Antrobus, R. Rowland, R. L. Ramon, M. Smith, S. Sheehan, H. Bettinson, and H. McShane. 2014. 'Safety and immunogenicity of a candidate tuberculosis vaccine MVA85A delivered by aerosol in BCG-vaccinated healthy adults: a phase 1, double-blind, randomised controlled trial', *Lancet Infect Dis*, 14: 939-46.

Saxena, M., T. T. H. Van, F. J. Baird, P. J. Coloe, and P. M. Smooker. 2013. 'Pre-existing immunity against vaccine vectors--friend or foe?', *Microbiology (Reading)*, 159: 1-11.

Schenkel, J. M., K. A. Fraser, V. Vezys, and D. Masopust. 2013. 'Sensing and alarm function of resident memory CD8(+) T cells', *Nat Immunol*, 14: 509-13.

Schmidt, A., and D. Lapuente. 2021. 'T Cell Immunity against Influenza: The Long Way from Animal Models Towards a Real-Life Universal Flu Vaccine', *Viruses*, 13.

Schoettler, N., C. L. Hrusch, K. M. Blaine, A. I. Sperling, and C. Ober. 2019. 'Transcriptional programming and T cell receptor repertoires distinguish human lung and lymph node memory T cells', *Commun Biol*, 2: 411.

Schulman, J. L., and E. D. Kilbourne. 1965. 'Induction of Partial Specific Heterotypic Immunity in Mice by a Single Infection with Influenza a Virus', *J Bacteriol*, 89: 170-4.

Schwartz, J. C., J. D. Hemmink, S. P. Graham, E. Tchilian, B. Charleston, S. E. Hammer, C. S. Ho, and J. A. Hammond. 2018. 'The major histocompatibility complex homozygous inbred Babraham pig as a resource for veterinary and translational medicine', *HLA*.

Shin, H., and A. Iwasaki. 2012. 'A vaccine strategy that protects against genital herpes by establishing local memory T cells', *Nature*, 491: 463-7.

Signer, E. N., A. J. Jeffreys, S. Licence, R. Miller, P. Byrd, and R. Binns. 1999. 'DNA profiling reveals remarkably low genetic variability in a herd of SLA homozygous pigs', *Res Vet Sci*, 67: 207-11.

Slepushkin, A. N. 1959. 'The effect of a previous attack of A1 influenza on susceptibility to A2 virus during the 1957 outbreak', *Bull World Health Organ*, 20: 297-301.
Slutter, B., N. Van Braeckel-Budimir, G. Abboud, S. M. Varga, S. Salek-Ardakani, and J. T. Harty. 2017. 'Dynamics of influenza-induced lung-resident memory T cells underlie waning heterosubtypic immunity', *Sci Immunol*, 2: eaag2031.
Smith, J. H., M. Papania, D. Knaus, P. Brooks, D. L. Haas, R. Mair, J. Barry, S. M. Tompkins, and R. A. Tripp. 2012. 'Nebulized live-attenuated influenza vaccine provides protection in ferrets at a reduced dose', *Vaccine*, 30: 3026-33.
Smith, T., A. Heger, and I. Sudbery. 2017. 'UMI-tools: modeling sequencing errors in Unique Molecular Identifiers to improve quantification accuracy', *Genome Res*, 27: 491-99.
Snyder, M. E., M. O. Finlayson, T. J. Connors, P. Dogra, T. Senda, E. Bush, D. Carpenter, C. Marboe, L. Benvenuto, L. Shah, H. Robbins, J. L. Hook, M. Sykes, F. D'Ovidio, M. Bacchetta, J. R. Sonett, D. J. Lederer, S. Arcasoy, P. A. Sims, and D. L. Farber. 2019. 'Generation and persistence of human tissue-resident memory T cells in lung transplantation', *Sci Immunol*, 4.
Song, K., D. L. Bolton, C. J. Wei, R. L. Wilson, J. V. Camp, S. Bao, J. J. Mattapallil, L. A. Herzenberg, L. A. Herzenberg, C. A. Andrews, J. C. Sadoff, J. Goudsmit, M. G. Pau, R. A. Seder, P. A. Kozlowski, G. J. Nabel, M. Roederer, and S. S. Rao. 2010. 'Genetic immunization in the lung induces potent local and systemic immune responses', *Proc Natl Acad Sci U S A*, 107: 22213-8.
Sonoguchi, T., H. Naito, M. Hara, Y. Takeuchi, and H. Fukumi. 1985. 'Cross-subtype protection in humans during sequential, overlapping, and/or concurrent epidemics caused by H3N2 and H1N1 influenza viruses', *J Infect Dis*, 151: 81-8.
Sridhar, S. 2016. 'Heterosubtypic T-Cell Immunity to Influenza in Humans: Challenges for Universal T-Cell Influenza Vaccines', *Front Immunol*, 7: 195.
Sridhar, S., S. Begom, A. Bermingham, K. Hoschler, W. Adamson, W. Carman, T. Bean, W. Barclay, J. J. Deeks, and A. Lalvani. 2013. 'Cellular immune correlates of protection against symptomatic pandemic influenza', *Nat Med*, 19: 1305-12.
Stahl, W. R. 1967. 'Scaling of respiratory variables in mammals', *J Appl Physiol*, 22: 453-60.
Stein-Streilein, J., M. Bennett, D. Mann, and V. Kumar. 1983. 'Natural killer cells in mouse lung: surface phenotype, target preference, and response to local influenza virus infection', *J Immunol*, 131: 2699-704.
Steinert, E. M., J. M. Schenkel, K. A. Fraser, L. K. Beura, L. S. Manlove, B. Z. Igyarto, P. J. Southern, and D. Masopust. 2015. 'Quantifying Memory CD8 T Cells Reveals Regionalization of Immunosurveillance', *Cell*, 161: 737-49.
Sterlin, D., A. Mathian, M. Miyara, A. Mohr, F. Anna, L. Claer, P. Quentric, J. Fadlallah, H. Devilliers, P. Ghillani, C. Gunn, R. Hockett, S. Mudumba, A. Guihot, C. E. Luyt, J. Mayaux, A. Beurton, S. Fourati, T. Bruel, O. Schwartz, J. M. Lacorte, H. Yssel, C. Parizot, K. Dorgham, P. Charneau, Z. Amoura, and G. Gorochov. 2021. 'IgA dominates the early neutralizing antibody response to SARS-CoV-2', *Sci Transl Med*, 13.
Su, W., J. Sun, K. Shimizu, and K. Kadota. 2019. 'TCC-GUI: a Shiny-based application for differential expression analysis of RNA-Seq count data', *BMC Res Notes*, 12: 133.
Szabo, P. A., P. Dogra, J. I. Gray, S. B. Wells, T. J. Connors, S. P. Weisberg, I. Krupska, R. Matsumoto, M. M. L. Poon, E. Idzikowski, S. E. Morris, C. Pasin, A. J. Yates, A. Ku, M. Chait, J. Davis-Porada, X. V. Guo, J. Zhou, M. Steinle, S. Mackay, A. Saqi, M. R. Baldwin, P. A. Sims, and D.

L. Farber. 2021. 'Longitudinal profiling of respiratory and systemic immune responses reveals myeloid cell-driven lung inflammation in severe COVID-19', *Immunity*, 54: 797-814 e6.

Szabo, P. A., M. Miron, and D. L. Farber. 2019. 'Location, location, location: Tissue resident memory T cells in mice and humans', *Sci Immunol*, 4.

Takamura, S., H. Yagi, Y. Hakata, C. Motozono, S. R. McMaster, T. Masumoto, M. Fujisawa, T. Chikaishi, J. Komeda, J. Itoh, M. Umemura, A. Kyusai, M. Tomura, T. Nakayama, D. L. Woodland, J. E. Kohlmeier, and M. Miyazawa. 2016. 'Specific niches for lung-resident memory CD8+ T cells at the site of tissue regeneration enable CD69-independent maintenance', *J Exp Med*, 213: 3057-73.

Talker, S. C., T. Kaser, K. Reutner, C. Sedlak, K. H. Mair, H. Koinig, R. Graage, M. Viehmann, E. Klingler, A. Ladinig, M. Ritzmann, A. Saalmuller, and W. Gerner. 2013. 'Phenotypic maturation of porcine NK- and T-cell subsets', *Dev Comp Immunol*, 40: 51-68.

Talker, S. C., M. Stadler, H. C. Koinig, K. H. Mair, I. M. Rodriguez-Gomez, R. Graage, R. Zell, R. Durrwald, E. Starick, T. Harder, H. Weissenbock, B. Lamp, S. E. Hammer, A. Ladinig, A. Saalmuller, and W. Gerner. 2016. 'Influenza A Virus Infection in Pigs Attracts Multifunctional and Cross-Reactive T Cells to the Lung', *J Virol*, 90: 9364-82.

Tannock, G. A., J. A. Paul, and R. D. Barry. 1984. 'Relative immunogenicity of the cold-adapted influenza virus A/Ann Arbor/6/60 (A/AA/6/60-ca), recombinants of A/AA/6/60-ca, and parental strains with similar surface antigens', *Infect Immun*, 43: 457-62.

Taylor, P. M., and B. A. Askonas. 1986. 'Influenza nucleoprotein-specific cytotoxic T-cell clones are protective in vivo', *Immunology*, 58: 417-20.

Tchilian, E., and B. Holzer. 2017. 'Harnessing Local Immunity for an Effective Universal Swine Influenza Vaccine', *Viruses*, 9.

Tchilian, E. Z., E. O. Ronan, C. de Lara, L. N. Lee, K. L. Franken, M. H. Vordermeier, T. H. Ottenhoff, and P. C. Beverley. 2011. 'Simultaneous immunization against tuberculosis', *PLoS One*, 6: e27477.

Team, R Core. 2020. 'R: A Language and Environment for Statistical Computing'.

Teijaro, J. R., D. Turner, Q. Pham, E. J. Wherry, L. Lefrancois, and D. L. Farber. 2011. 'Cutting edge: Tissue-retentive lung memory CD4 T cells mediate optimal protection to respiratory virus infection', *J Immunol*, 187: 5510-4.

Teleflex. 'Intranasal Mucosal Atomization Device', Accessed 09/09. https://www.teleflex.com/usa/en/product-areas/anesthesia/atomization/mad-nasal-device/AN_ATM_Anesthesia-MAD-Nasal-User-Guide_MC_MC-001925_Rev1.pdf.

Thom, J. T., T. C. Weber, S. M. Walton, N. Torti, and A. Oxenius. 2015. 'The Salivary Gland Acts as a Sink for Tissue-Resident Memory CD8(+) T Cells, Facilitating Protection from Local Cytomegalovirus Infection', *Cell Rep*, 13: 1125-36.

Thomas, P. G., S. A. Brown, M. Y. Morris, W. Yue, J. So, C. Reynolds, R. J. Webby, and P. C. Doherty. 2010. 'Physiological numbers of CD4+ T cells generate weak recall responses following influenza virus challenge', *J Immunol*, 184: 1721-7.

Thomas, P. G., P. Dash, J. R. Aldridge, Jr., A. H. Ellebedy, C. Reynolds, A. J. Funk, W. J. Martin, M. Lamkanfi, R. J. Webby, K. L. Boyd, P. C. Doherty, and T. D. Kanneganti. 2009. 'The intracellular sensor NLRP3 mediates key innate and healing responses to influenza A virus via the regulation of caspase-1', *Immunity*, 30: 566-75.

Thome, J. J., N. Yudanin, Y. Ohmura, M. Kubota, B. Grinshpun, T. Sathaliyawala, T. Kato, H. Lerner, Y. Shen, and D. L. Farber. 2014. 'Spatial map of human T cell compartmentalization and maintenance over decades of life', *Cell*, 159: 814-28.

Thompson, W. W., L. Comanor, and D. K. Shay. 2006. 'Epidemiology of seasonal influenza: use of surveillance data and statistical models to estimate the burden of disease', *J Infect Dis*, 194 Suppl 2: S82-91.

Tong, S., X. Zhu, Y. Li, M. Shi, J. Zhang, M. Bourgeois, H. Yang, X. Chen, S. Recuenco, J. Gomez, L. M. Chen, A. Johnson, Y. Tao, C. Dreyfus, W. Yu, R. McBride, P. J. Carney, A. T. Gilbert, J. Chang, Z. Guo, C. T. Davis, J. C. Paulson, J. Stevens, C. E. Rupprecht, E. C. Holmes, I. A. Wilson, and R. O. Donis. 2013. 'New world bats harbor diverse influenza A viruses', *PLoS Pathog*, 9: e1003657.

Torremorell, M., M. Allerson, C. Corzo, A. Diaz, and M. Gramer. 2012. 'Transmission of influenza A virus in pigs', *Transbound Emerg Dis*, 59 Suppl 1: 68-84.

Townsend, A. R., J. Bastin, K. Gould, and G. G. Brownlee. 1986. 'Cytotoxic T lymphocytes recognize influenza haemagglutinin that lacks a signal sequence', *Nature*, 324: 575-7.

Townsend, A. R., F. M. Gotch, and J. Davey. 1985. 'Cytotoxic T cells recognize fragments of the influenza nucleoprotein', *Cell*, 42: 457-67.

Townsend, A. R., J. Rothbard, F. M. Gotch, G. Bahadur, D. Wraith, and A. J. McMichael. 1986. 'The epitopes of influenza nucleoprotein recognized by cytotoxic T lymphocytes can be defined with short synthetic peptides. ', *J Immunol*, 176: 5141-50.

Trebbien, R., L. E. Larsen, and B. M. Viuff. 2011. 'Distribution of sialic acid receptors and influenza A virus of avian and swine origin in experimentally infected pigs', *Virol J*, 8: 434.

Tse, S. W., A. J. Radtke, D. A. Espinosa, I. A. Cockburn, and F. Zavala. 2014. 'The chemokine receptor CXCR6 is required for the maintenance of liver memory CD8(+) T cells specific for infectious pathogens', *J Infect Dis*, 210: 1508-16.

Tumpey, T. M., A. Garcia-Sastre, J. K. Taubenberger, P. Palese, D. E. Swayne, M. J. Pantin-Jackwood, S. Schultz-Cherry, A. Solorzano, N. Van Rooijen, J. M. Katz, and C. F. Basler. 2005. 'Pathogenicity of influenza viruses with genes from the 1918 pandemic virus: functional roles of alveolar macrophages and neutrophils in limiting virus replication and mortality in mice', *J Virol*, 79: 14933-44.

Tungatt, K., G. Dolton, S. B. Morgan, M. Attaf, A. Fuller, T. Whalley, J. D. Hemmink, E. Porter, B. Szomolay, M. Montoya, J. A. Hammond, J. J. Miles, D. K. Cole, A. Townsend, M. Bailey, P. J. Rizkallah, B. Charleston, E. Tchilian, and A. K. Sewell. 2018. 'Induction of influenza-specific local CD8 T-cells in the respiratory tract after aerosol delivery of vaccine antigen or virus in the Babraham inbred pig', *PLoS Pathog*, 14: e1007017.

Turner, D. L., K. L. Bickham, J. J. Thome, C. Y. Kim, F. D'Ovidio, E. J. Wherry, and D. L. Farber. 2014. 'Lung niches for the generation and maintenance of tissue-resident memory T cells', *Mucosal Immunol*, 7: 501-10.

Uddback, I., E. K. Cartwright, A. S. Scholler, A. N. Wein, S. L. Hayward, J. Lobby, S. Takamura, A. R. Thomsen, J. E. Kohlmeier, and J. P. Christensen. 2020. 'Long-term maintenance of lung resident memory T cells is mediated by persistent antigen', *Mucosal Immunol*.

Uddback, I. E., L. M. Pedersen, S. R. Pedersen, M. A. Steffensen, P. J. Holst, A. R. Thomsen, and J. P. Christensen. 2016. 'Combined local and systemic immunization is essential for durable T-cell mediated heterosubtypic immunity against influenza A virus', *Sci Rep*, 6: 20137.

Van Braeckel-Budimir, N., S. M. Varga, V. P. Badovinac, and J. T. Harty. 2018. 'Repeated Antigen Exposure Extends the Durability of Influenza-Specific Lung-Resident Memory CD8(+) T Cells and Heterosubtypic Immunity', *Cell Rep*, 24: 3374-82 e3.

Van Poucke, S. G., J. M. Nicholls, H. J. Nauwynck, and K. Van Reeth. 2010. 'Replication of avian, human and swine influenza viruses in porcine respiratory explants and association with sialic acid distribution', *Virol J*, 7: 38.

Van Reeth, K., D. Braeckmans, E. Cox, S. Van Borm, T. van den Berg, B. Goddeeris, and A. De Vleeschauwer. 2009. 'Prior infection with an H1N1 swine influenza virus partially protects pigs against a low pathogenic H5N1 avian influenza virus', *Vaccine*, 27: 6330-9.

Vatzia, E.; , E.; Allen, T.; Manjegowda, S.; Morris, A.; McNee, V.; Martini, R.; Kaliath, M.; Ulaszewska, A.; Boyd, B.; Pauday, V.; Carr, T.; Chrun, E.; Maze, R.; MacLoughlin, P.; van Diemen, H.; Everett, T.; Lambe, S.; Gilbert, and E.. Tchilian. 2021. 'Respiratory and intramuscular immunization with ChAdOx2 NPM1-NA induces distinct immune responses in H1N1pdm09 pre-exposed pigs', *Research Square*.

Vidana, B., J. Martinez, P. Martinez-Orellana, L. Garcia Migura, M. Montoya, J. Martorell, and N. Majo. 2014. 'Heterogeneous pathological outcomes after experimental pH1N1 influenza infection in ferrets correlate with viral replication and host immune responses in the lung', *Vet Res*, 45: 85.

Vigano, S., R. Banga, F. Bellanger, C. Pellaton, A. Farina, D. Comte, A. Harari, and M. Perreau. 2014. 'CD160-associated CD8 T-cell functional impairment is independent of PD-1 expression', *PLoS Pathog*, 10: e1004380.

Vijaykrishna, D., L. L. Poon, H. C. Zhu, S. K. Ma, O. T. Li, C. L. Cheung, G. J. Smith, J. S. Peiris, and Y. Guan. 2010. 'Reassortment of pandemic H1N1/2009 influenza A virus in swine', *Science*, 328: 1529.

Villegas, P., and S. H. Kleven. 1976. 'Aerosol vaccination against Newcastle disease. II. Effect of vaccine diluents', *Avian Dis*, 20: 260-7.

Vincent, A. L., W. Ma, K. M. Lager, B. H. Janke, and J. A. Richt. 2008. 'Swine influenza viruses a North American perspective', *Adv Virus Res*, 72: 127-54.

Vincent, A. L., W. Ma, K. M. Lager, J. A. Richt, B. H. Janke, M. R. Sandbulte, P. C. Gauger, C. L. Loving, R. J. Webby, and A. Garcia-Sastre. 2012. 'Live attenuated influenza vaccine provides superior protection from heterologous infection in pigs with maternal antibodies without inducing vaccine-associated enhanced respiratory disease', *J Virol*, 86: 10597-605.

Wakim, L. M., J. Smith, I. Caminschi, M. H. Lahoud, and J. A. Villadangos. 2015. 'Antibody-targeted vaccination to lung dendritic cells generates tissue-resident memory CD8 T cells that are highly protective against influenza virus infection', *Mucosal Immunol*, 8: 1060-71.

Wakim, L. M., A. Woodward-Davis, and M. J. Bevan. 2010. 'Memory T cells persisting within the brain after local infection show functional adaptations to their tissue of residence', *Proc Natl Acad Sci U S A*, 107: 17872-9.

Wakim, L. M., A. Woodward-Davis, R. Liu, Y. Hu, J. Villadangos, G. Smyth, and M. J. Bevan. 2012. 'The molecular signature of tissue resident memory CD8 T cells isolated from the brain', *J Immunol*, 189: 3462-71.

Wang, D., L. Yang, W. Zhu, Y. Zhang, S. Zou, H. Bo, R. Gao, J. Dong, W. Huang, J. Guo, Z. Li, X. Zhao, X. Li, L. Xin, J. Zhou, T. Chen, L. Dong, H. Wei, X. Li, L. Liu, J. Tang, Y. Lan, J. Yang,

and Y. Shu. 2016. 'Two Outbreak Sources of Influenza A (H7N9) Viruses Have Been Established in China', *J Virol*, 90: 5561-73.

Wang, X., H. Jiang, P. Wu, T. M. Uyeki, L. Feng, S. Lai, L. Wang, X. Huo, K. Xu, E. Chen, X. Wang, J. He, M. Kang, R. Zhang, J. Zhang, J. Wu, S. Hu, H. Zhang, X. Liu, W. Fu, J. Ou, S. Wu, Y. Qin, Z. Zhang, Y. Shi, J. Zhang, J. Artois, V. J. Fang, H. Zhu, Y. Guan, M. Gilbert, P. W. Horby, G. M. Leung, G. F. Gao, B. J. Cowling, and H. Yu. 2017. 'Epidemiology of avian influenza A H7N9 virus in human beings across five epidemics in mainland China, 2013-17: an epidemiological study of laboratory-confirmed case series', *Lancet Infect Dis*, 17: 822-32.

Wei, C. J., M. C. Crank, J. Shiver, B. S. Graham, J. R. Mascola, and G. J. Nabel. 2020. 'Author Correction: Next-generation influenza vaccines: opportunities and challenges', *Nat Rev Drug Discov*, 19: 427.

Wiley, J. A., R. J. Hogan, D. L. Woodland, and A. G. Harmsen. 2001. 'Antigen-specific CD8(+) T cells persist in the upper respiratory tract following influenza virus infection', *J Immunol*, 167: 3293-9.

Wilk, M. M., A. Misiak, R. M. McManus, A. C. Allen, M. A. Lynch, and K. H. G. Mills. 2017. 'Lung CD4 Tissue-Resident Memory T Cells Mediate Adaptive Immunity Induced by Previous Infection of Mice with Bordetella pertussis', *J Immunol*, 199: 233-43.

Wilkinson, T. M., C. K. Li, C. S. Chui, A. K. Huang, M. Perkins, J. C. Liebner, R. Lambkin-Williams, A. Gilbert, J. Oxford, B. Nicholas, K. J. Staples, T. Dong, D. C. Douek, A. J. McMichael, and X. N. Xu. 2012. 'Preexisting influenza-specific CD4+ T cells correlate with disease protection against influenza challenge in humans', *Nat Med*, 18: 274-80.

Woodworth, J. S., D. Christensen, J. P. Cassidy, E. M. Agger, R. Mortensen, and P. Andersen. 2019. 'Mucosal boosting of H56:CAF01 immunization promotes lung-localized T cells and an accelerated pulmonary response to Mycobacterium tuberculosis infection without enhancing vaccine protection', *Mucosal Immunol*, 12: 816-26.

World Health Organisation. 2021. 'Avian Influenza Weekly Update Number 805', Accessed 25 August 2021. https://www.who.int/docs/default-source/wpro---documents/emergency/surveillance/avian-influenza/ai-20210813.pdf?sfvrsn=30d65594_157.

Wrammert, J., D. Koutsonanos, G. M. Li, S. Edupuganti, J. Sui, M. Morrissey, M. McCausland, I. Skountzou, M. Hornig, W. I. Lipkin, A. Mehta, B. Razavi, C. Del Rio, N. Y. Zheng, J. H. Lee, M. Huang, Z. Ali, K. Kaur, S. Andrews, R. R. Amara, Y. Wang, S. R. Das, C. D. O'Donnell, J. W. Yewdell, K. Subbarao, W. A. Marasco, M. J. Mulligan, R. Compans, R. Ahmed, and P. C. Wilson. 2011. 'Broadly cross-reactive antibodies dominate the human B cell response against 2009 pandemic H1N1 influenza virus infection', *J Exp Med*, 208: 181-93.

Wu, T., Y. Hu, Y. T. Lee, K. R. Bouchard, A. Benechet, K. Khanna, and L. S. Cauley. 2014. 'Lung-resident memory CD8 T cells (TRM) are indispensable for optimal cross-protection against pulmonary virus infection', *J Leukoc Biol*, 95: 215-24.

Yap, K. L., G. L. Ada, and I. F. McKenzie. 1978. 'Transfer of specific cytotoxic T lymphocytes protects mice inoculated with influenza virus', *Nature*, 273: 238-9.

Yoshizawa, A., K. Bi, D. B. Keskin, G. Zhang, B. Reinhold, and E. L. Reinherz. 2018. 'TCR-pMHC encounter differentially regulates transcriptomes of tissue-resident CD8 T cells', *Eur J Immunol*, 48: 128-50.

Yu, X., T. Tsibane, P. A. McGraw, F. S. House, C. J. Keefer, M. D. Hicar, T. M. Tumpey, C. Pappas, L. A. Perrone, O. Martinez, J. Stevens, I. A. Wilson, P. V. Aguilar, E. L. Altschuler, C. F. Basler,

and J. E. Crowe, Jr. 2008. 'Neutralizing antibodies derived from the B cells of 1918 influenza pandemic survivors', *Nature*, 455: 532-6.

Zens, K. D., J. K. Chen, and D. L. Farber. 2016a. 'Vaccine-generated lung tissue-resident memory T cells provide heterosubtypic protection to influenza infection', *JCI Insight*, 1: e85832.

———. 2016b. 'Vaccine-generated lung tissue-resident memory T cells provide heterosubtypic protection to influenza infection', *JCI Insight*, 1.

Zhang, N., and M. J. Bevan. 2013. 'Transforming growth factor-beta signaling controls the formation and maintenance of gut-resident memory T cells by regulating migration and retention', *Immunity*, 39: 687-96.

Zhou, B., V. A. Meliopoulos, W. Wang, X. Lin, K. M. Stucker, R. A. Halpin, T. B. Stockwell, S. Schultz-Cherry, and D. E. Wentworth. 2016. 'Reversion of Cold-Adapted Live Attenuated Influenza Vaccine into a Pathogenic Virus', *J Virol*, 90: 8454-63.